Dendritic Rhodium Catalyst Precursors For

The Hydroformylation of Olefins

Cody Williams

University of Cape Town

February 2018

Dendritic Rhodium Catalyst Precursors For

The Hydroformylation of Olefins

by

Cody Williams

Dissertation presented for the degree

Masters by Dissertation

Supervisors: **Associate Professor Gregory S. Smith (UCT)**

Professor Selwyn F. Mapolie (SU)

Department of Chemistry
University of Cape Town
Rondebosch, 7701
Cape Town

February 2018

Plagiarism Declaration

I know the meaning of plagiarism and declare that all of the work in the document, **"Dendritic Rhodium Catalyst Precursors for the Hydroformylation of Olefins",** is my own work and to the best of my knowledge has never been submitted for examination for any degree at any university. All sources of information are cited and fully referenced at the end of each chapter.

SIGNATURE: Signed by candidate

Cody Williams

DATE: 19/02/2018

Acknowledgements

First and foremost, I would like to express my sincere gratitude and appreciation to Assoc. Prof. Gregory Smith and Prof. Selwyn Mapolie, for their invaluable guidance, encouragement and constructive criticism. I thank them for motivating me to approach challenges from different perspectives which allowed me to expand my thinking process in research and in life, for this I am forever indebted.

My gratitude extends to the various collaborators and their respective research groups who hosted me, namely Indian collaborator Prof. Raj. Kumar Joshi (Malaviya National Institute for Technology) and French collaborators Prof. Sebastian Tilloy, Dr. Michel Ferreira and Prof. Eric Monflier (Université de catalyse, Artois). Furthermore a special thanks to Dr. Hervé Bricout, Jerome Leblond and Kévin Cousin for their guidance with respect to the hydroformylation and hydroaminomethylation of long-chain substrates.

I would like to acknowledge Mrs Deirdre Brooks for the administrative work and noteworthy encouragement throughout this degree. Further thanks extend to the UCT analytical staff, namely Mr. Pete Roberts for running 2D-NMR experiments, Dr. Hong Su for single-crystal X-ray diffraction studies and Mr. Gianpierro Benincasa for recording elemental analysis data. A special thanks to Dr. Marietjie Stander (University of Stellenbosch) and Dr. Johan Hachani (University of Artois) for running the ESI-MS and MALDI-TOF-MS experiments respectively.

I wish to express my heartfelt thanks to my friends and colleagues, Diteboho Ramarou, Laaiqah Rylands, Marwaan Rylands and Shakeela Sayed for useful discussions. A special thanks to the members of the Organometallic Research group (UCT and US) for helpful discussions and assistance. My sincere gratitude is extended to my mentors and friends, Dr. Preshen Govender, Dr. Tameryn Stringer, Mr. Dylan Giffard and Mr. Shepherd Siangwata, for guidance, encouragement, fruitful discussion and most importantly friendship over the last few years.

Financial support was provided by the National Research Foundation-Department of Science and technology, c*change, University of Cape Town and the Harry Crossley Foundation.

Lastly, I would like to thank my family and friends for their unrivalled support for this landmark in my life. A special thanks to my friends Jody and Robin for their continuous support and inspiration throughout my university career. To my family, especially Beverly, Margaret, Desiree and Shaun, I thank them for the inspiration, love and stupendous support throughout this journey. This dissertation is an ode to you for all your trust bestowed upon me.

"A journey of a thousand miles begins with a single step"

Lao Tzu

Abstract

The hydroformylation reaction is the transition-metal catalysed addition of CO/H_2 to olefins, resulting in linear and/or branched aldehydes. This reaction is in accordance with Green Chemistry principles, as it operates with 100% atom efficiency and uses renewable feedstocks such as olefins from the Fischer-Tropsch process. Rhodium is the metal of choice when designing catalysts for hydroformylation, owing to its good catalytic activity under mild reaction conditions. The strategy of appending bulky ligands has often been employed to enhance catalytic activity and selectivity. Dendritic wedges are promising to the field of catalysis, as one branch may possess multiple surface terminal groups and the other branch may consist of a mononuclear metal centre. This method differs to classical approaches whereby multinuclear effects are explored to enhance the catalyst activity. The purpose of this study was to synthesize and characterise a series of Fréchet dendrons bearing rhodium Schiff-base moieties at the focal point, and investigate their potential as catalyst precursors in the hydroformylation of olefins.

A series of Fréchet dendrons with methyl ester groups at the periphery were prepared. The *N,O*-salicylaldimine and *N,P*-iminophosphine Schiff-base ligands were synthesized and consequently coupled to the Fréchet dendrons to yield a new class of Fréchet dendrons with *N,O*-salicylaldimine or *N,P*-iminophosphine ligands at the focal point. Complexes of these ligands were synthesized to form a new series of neutral rhodium(I) metallodendrons.

Complexation of the *N,O*-salicylaldimine Fréchet dendrons with the metal-precursor $[Rh(\mu\text{-}Cl)(\eta^2\text{:}\eta^2\text{-}COD)]_2$ (where COD = 1,5-cyclooctadiene) afforded the Rh(I)-COD metallodendrons. The Rh(I)-COD metallodendrons were reacted under a carbon monoxide atmosphere to yield a new series of dicarbonyl Rh(I) metallodendrons. The bridge splitting reaction between the *N,P*-iminophosphine Fréchet dendrons and $[Rh(\mu\text{-}Cl)(CO)_2]_2$ afforded the carbonyl-chloride Rh(I) metallodendrons.

The Fréchet dendron ligands and rhodium metallodendrons were fully characterised using an array of spectroscopic (^1H, $^{13}C\{^1H\}$, $^{31}P\{^1H\}$ NMR, FT-IR spectroscopy) and analytical (elemental analysis and mass spectrometry) techniques. Single crystal X-ray diffraction confirmed the proposed molecular structure and square-planar geometry around the metal

centre for the zeroth generation analogues of the *N,O*-salicylaldimine and *N,P*-iminophosphine rhodium metallodendrons.

The Rh(I) Schiff-base metallodendrons were applied as catalyst precursors in the hydroformylation of various olefins. All of the catalyst precursors were active in the hydroformylation of 1-octene. The *N,O*-salicylaldimine metallodendrons displayed good to excellent conversion (78 – 100%), good chemoselectivity (66 – 95%) and moderate regioselectivity (51 – 67%). In contrast, the *N,P*-iminophosphine metallodendrons displayed low conversion (4 – 8%), good chemoselectivity (76 – 80%) and good regioselectivity (64 – 68%) under the hydroformylation conditions. Notably, the increase in dendron size (G_0 – G_2) resulted in an increase in the chemoselectivity towards aldehydes.

Hydroformylation reactions were conducted using various olefin substrates. These include 1-octene, styrene, 7-tetradecene, methyl oleate, triolein, *D*-limonene and *R*-citronellal. The model precursor was active in the hydroformylation of these substrates. More importantly, conversions obtained were promising for styrene (100%), *D*-limonene (90%), 1-octene (86%), methyl oleate (78%), 7-tetradecene (73%) and triolein (52%). The regioselectivity for the internal olefins ranged between 85 – 98%. These results are particularly promising for tandem-catalytic processes. Mercury drop experiments performed on the zeroth generation analogues of the *N,O*-salicylaldimine-COD, *N,O*-salicylaldimine-dicarbonyl and *N,P*-iminophosphine chloro-carbonyl rhodium(I) metallodendrons displayed suppressed activity in the presence of mercury.

Conference/Symposia Contributions

1. **Poster Presentation:** Cody Williams, Michel Ferreira, Eric Monflier, Selwyn F. Mapolie and Gregory S. Smith, *Hydroaminomethylation using Rhodium Catalysts: Towards Biodiesel with Biocidal Properties,* presented at the Catalysis Society of South Africa Annual Conference, Johannesburg, South Africa, **2017.**

2. **Poster Presentation:** Cody Williams, Michel Ferreira, Eric Monflier, Selwyn F. Mapolie and Gregory S. Smith, *Rhodium Mononuclear Dendrons as Catalyst Precursors for the Hydroformylation of Olefins,* presented at the Modern Trends in Dendrimer Chemistry and Applications Conference, Moscow, Russia, **2017.**

3. **Poster Presentation:** Cody Williams, Selwyn F. Mapolie and Gregory S. Smith, *Dendritic Rhodium Catalyst Precursors for the Aqueous Hydroformylation of 1-Octene,* presented at the 10th Annual Science Postgraduate Symposium, Cape Town, South Africa, **2017.**

4. Poster Presentation: Poster Presentation: Cody Williams, Selwyn F. Mapolie and Gregory S. Smith, *Rhodium Carboxylate Catalyst Precursors for Aqueous Biphasic Hydroformylation of 1-Octene,* presented at the Catalysis Society of South Africa annual Conference, Durban, South Africa, **2016.**

Abbreviations, Symbols and Units

°	Degree(s)
δ	Chemical shift
2D	Two-dimensional
18-C-6	18-Crown-6
°C	Degrees Celsius
Å	Angstrom(s)
v/v %	Percent by volume
acac	Acetylacetone
appd	apparent doublet
apps	apparent singlet
appt	apparent triplet
Ar	Aromatic or aryl
ATR	Attenuated total reflectance
br	Broad signal (NMR)
$^{13}C\{^{1}H\}$	Proton decoupled carbon-13
cat.	Catalyst
cm^{-1}	Wavenumbers (reciprocal centimetres)
COD	1,5-Cyclooctadiene
COSY	Correlation spectroscopy
Cy	Dicyclohexyl
d	Doublet
dd	Doublet of doublets
DAB	1,4-Diaminobutane
DCM	Dichloromethane
EA	Elemental analysis
EI	Electron impact
eq.	Equivalent(s)
ESI	Electrospray ionisation
FT-IR	Fourier transform infrared spectroscopy
g	Gram(s)
GC	Gas chromatography
^{1}H	Proton
HAM	Hydroaminomethylation
HMBC	Heteronuclear multiple bond correlation
hr	Hour(s)
HR	High resolution
HSQC	Heteronuclear single quantum correlation

Hz	Hertz
i	*ipso*; *iso*
***i*-Pr**	*iso*-Propyl
IR	Infrared
J	Coupling constant
kV	Kilovolt(s)
m	Multiplet (NMR); medium intensity (IR); *meta*
MALDI-TOF	Matrix-assisted desorption/ionization-time of flight
MHz	Megahertz
mL	Millilitre(s)
mol	Mole(s)
mmol	Millimole(s)
MP	Melting Point
MS	Mass spectrometry
m/z	Mass to charge ratio
n	normal
NHC	N-heterocylic carbene
NMR	Nuclear magnetic resonance
ORTEP	Oak Ridge Thermal Ellipsoid Plot
o	*ortho*
p	*Para*
$^{31}P\{^{1}H\}$	Proton decoupled phosphorous-31
PAMAM	Poly(amidoamine)
Pet. Ether	Petroleum ether
PGM	Platinum Group Metal
Ph	Phenyl
PPI	Poly(propyleneimine)
ppm	Parts per million
q	Quartet
RCH/RP	Ruhrchemie/Rhône-Poulenc
RT	Room temperature
s	Singlet (NMR); strong intensity (IR)
SD	Standard deviation
SHOP	Shell higher olefin process
syngas	Synthesis gas
t	Triplet

td	Triplet of doublets
THF	Tetrahydrofuran
TOF	Turnover frequency
TPPTS	Triphenylphosphine trisulfonate
TRIS	Tris-2-(aminoethyl)amine
vs	Versus
w	Weak intensity (IR)
XRD	X-ray diffraction

Table of Contents

Chapter 1

Advances in the Use of Dendritic Molecules for Hydroformylation

1.1 Introduction

The use of transition metal catalysts is pivotal to both industry and academia, as it provides efficient and sustainable pathways for organic syntheses and processes.[1] Catalysts are ubiquitous in the chemical industry, whereby their applications ranges from pharmaceuticals to polymers to petroleum industries. Over 90% of industrial process utilises catalysts, indicating the vital importance of research in this field.[2] The ability of catalysts to reduce the time, waste and energy constraints of these reactions have allowed for an effective green solution to the large scale manufacturing of compounds. Furthermore, the ability of catalysts to maximise the selectivity and output of reactions makes this field attractive to industry. The acknowledgement of catalysis by virtue of the Nobel Prizes heralds its importance in the scientific and industrial communities. Selected examples are described in Table 1.1.

Table 1.1 *Examples of Nobel laureates and their recognised work in catalysis.*

Authors	Title	Year
K. Ziegler and G. Natta	Application of Catalysis in Polymer Synthesis	1963
G. Wilkinson and E.O Fischer	Chemistry of Organometallic Sandwich Compounds	1973
W.S Knowles, R. Noyori and K.B Sharpless	Asymmetric Hydrogenation and Oxidation Reactions	2001
Y. Chauvin, R.H Grubbs and R.R Schrock	Catalysed Metathesis	2005
E. Negishi, R.F Heck and A. Suzuki	Palladium-Catalysed Reactions in Organic Synthesis	2010

Economical, ecological and safer catalytic alternatives are highly sought after as alternatives to the classical stoichiometric methodologies.[3-5] The implementation of sustainable syntheses has evolved into a key aspect of modern organic synthesis. Green Chemistry incorporates solutions to various difficulties faced in chemistry, namely waste generation, hazardous processes, and energy demanding technologies (Figure 1.1). Most notably, catalysis intertwines with the Green Chemistry principles as it provides solutions to conforming to these principles.[6]

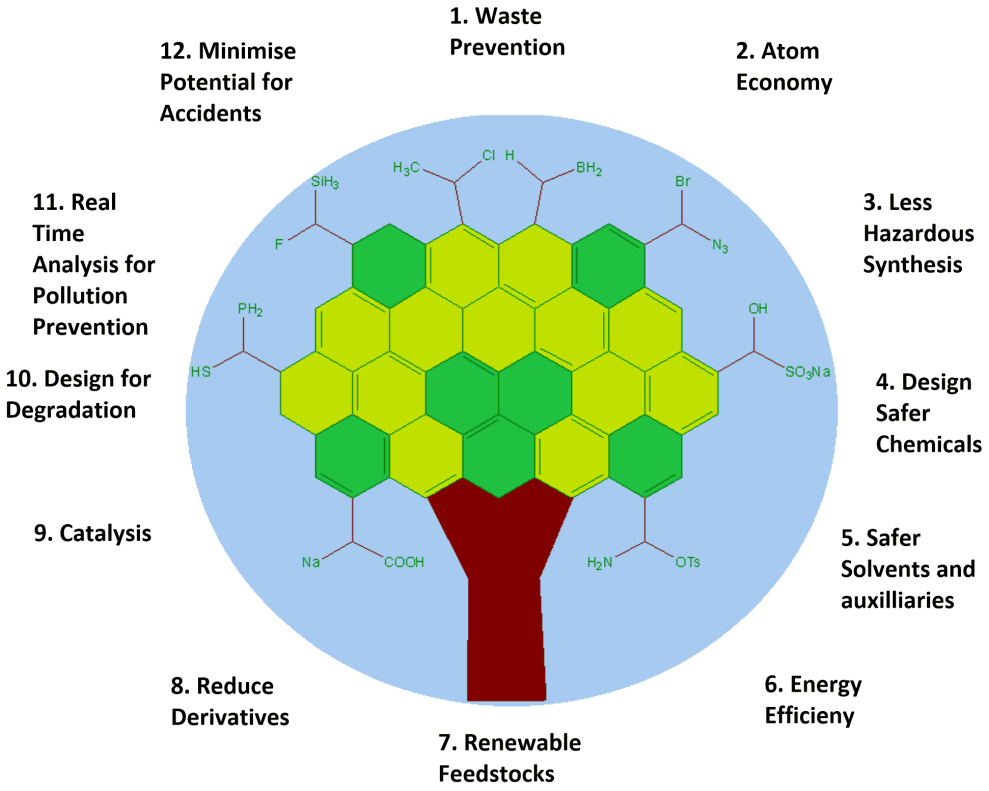

Figure 1.1. *The twelve Green Chemistry principles.*[2, 6]

Developing efficient and sustainable processes poses various challenges to industry as it often requires a paradigm shift with regards to infrastructure and methodologies. However, the concept of Green Chemistry aims to develop more environmentally friendly processes and syntheses for industry and academia. The crux of these principles is the use of highly effective catalysts in combination with the choice of benign and environmentally friendly solvents.[1, 2]

In conjunction with Green Chemistry principles, the refinement of existing catalysts is needed to enhance properties such as recyclability, selectivity and substrate conversion under mild conditions. Homogeneous and heterogeneous catalytic reactions are the major classes of reactions in this field, hence greener and cleaner synthetic analogues of catalysts are constantly researched and improved.

1.2 Catalysis

One of the fundamental pillars of Green Chemistry is catalysis. Catalysis offers a plethora of benefits with respect to lower energy requirements, the use of catalytic amounts

of materials, increased selectivity, minimized processing and separating processes which amounts to the use of less toxic material.[2] There are two major forms of catalysis, namely homogeneous and heterogeneous catalysis.

1.2.1 Heterogeneous Catalysis

Heterogeneous catalysis occurs whereby the phase of the catalyst and reactants are different. The use of heterogeneous catalysts are widely used in industry due to their simple separation protocol and their superior stability.[4] However their activity, stability and reproducibility is hampered by its multiphasic nature.[3, 7] Most research in this field focuses on the use of polymer supported catalysts.[7, 8] The separation of high boiling point products and reactants from non-volatile catalysts has limited the commercialisation of these systems.[9]

1.2.2 Homogeneous Catalysis

Homogeneous-based catalysis has both catalyst and reactants in the same phase. Transition-metal-based homogeneous catalysts have progressed in the field and are characterised by their superior activity, selectivity and manner in which they operate with high atom efficiency.[10] The homogeneity of the reaction denies any mass transfer restrictions, which is a common problem identified with heterogeneous catalysis. Problems associated with monophasic media include product separation, catalyst recovery and toxicity of organic solvents. Hence, the main objective is to transform the research catalyst into an industrial operating catalyst.[11]

The recycling of a catalyst is essential, as most transition metals involved are costly and/or toxic. Their recovery and recyclability proffers greater turnover numbers and produce less toxic waste, making them environmentally and economically viable.[11] A proposed solution to the above-mentioned problems is to link the advantages of both homogeneous and heterogeneous catalysis, by addressing the issues of catalyst recovery and product separation. Biphasic media is described as one potential solution to the disadvantages displayed by heterogeneous and homogeneous catalytic systems.

1.3 Biphasic Systems

The biphasic system is seen as the solution to bridging the gap between heterogeneous and homogeneous catalysts. These systems involve the immobilisation of homogeneous catalysts, while still maintaining its catalytic efficiency.[8, 12-15] The immobilisation of catalysts have been reported using dendrimers, silica, polymers, cyclodextrins and activated carbons.[8, 11, 14-20] The primary objective of immobilisation is to overcome the problem associated with catalyst recovery and recyclability. This approach is commonly referred to as 'heterogenizing the homogeneous catalyst'.

Biphasic systems consist of two immiscible liquids in the same reaction vessel.[21, 22] Biphasic catalysis is homogeneous, as it fulfils all the requirements for homogeneously catalysed reactions.[23] The catalyst is entirely heterogeneous in comparison to the reactants, however upon sufficient heat and pressure, the reaction becomes homogeneous.[24] The cooling of the reaction mixture results in the separation of phases, with the catalyst and products in different phases. This process maintains the high catalytic activity associated with homogeneous catalysis and incorporates the facile separation associated with heterogeneous catalysis.[21, 24] Biphasic systems include, thermo-regulated phase transfer systems,[25-28] fluorous biphasic catalysts,[22, 29-32] ionic liquid/supercritical fluid mixtures,[33-38] CO_2 phase switchable systems and aqueous biphasic systems.[39-42] The most studied and industrially relevant process is undoubtedly aqueous biphasic systems, as it incorporates the economic and environmental benefits of catalysis.

1.3.1 Aqueous Biphasic Systems

Aqueous biphasic catalytic systems consist of two immiscible phases, namely aqueous and organic layers. The catalyst applied in the reaction is water-soluble and remains in the aqueous layer. The reactants and reaction products are ideally organic, and remain in the organic phase.[43] Green Chemistry principles state that reactions which use no solvent are ideal. However, solvents which are readily available, odourless, non-flammable, non-toxic and most importantly environmentally friendly are highly sought after.[44-46] The characteristics described above correlates to the properties of water, which signifies its importance as a solvent choice. The immiscibility of water with organic solvents results in facile separation, making it ideal for biphasic catalysis (Figure 1.2).

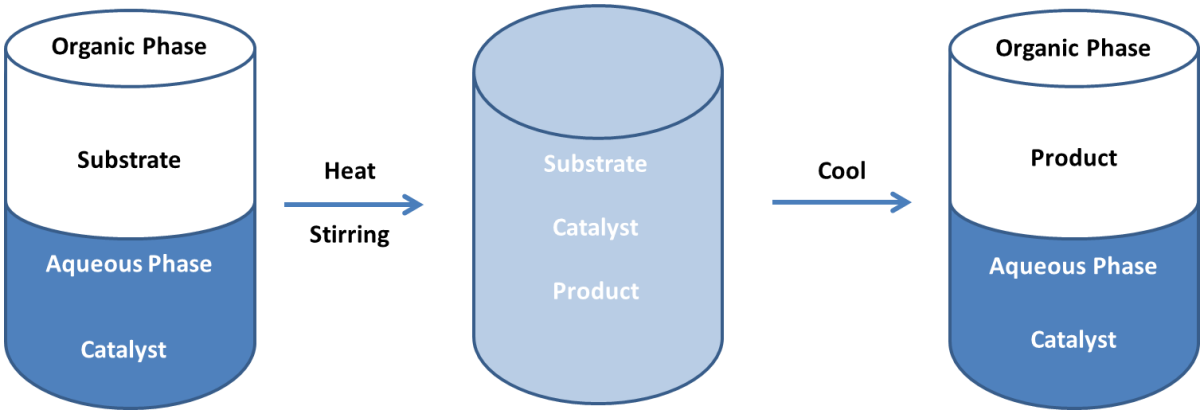

Figure 1.2. *Aqueous biphasic catalysis illustration.*[21]

Many organometallic complexes are insoluble in water, thus placing emphasis on the design of ligands to immobilize the catalyst in the aqueous layer. By obtaining improved solubility, the probability of the catalyst transferring to the organic phase is reduced. Thus, the study of surface-active ligands, micelle's, counter-ions, co-solvents, co-ligands and surfactants are well documented.[16, 42, 47, 48] Furthermore, the immobilisation of these complexes have been reported as a means to enhance selectivity and activity with electronic effects, as well as reducing catalyst leaching into the organic phase. Literature bodes a variety of ligands containing sulfonates, however the use of carboxylates is not as prevalent. These selected examples of carboxylates are succinctly displayed in **Table 1.2**.[49]

Table 1.2. *A summary of carboxylate based ligands and their application and relevance to catalysis, as adapted from Shaugnhessy.[49] (Ph – phenyl, Cy – dicyclohexyl-, Me – methyl, i-Pr – iso-propyl).*

Ligand	Application	Ligand	Application
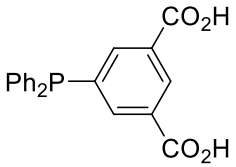	Synthesis[50]	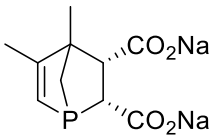	Synthesis[51]
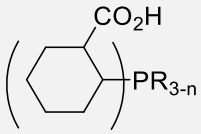 **n = 1, R = Ph** **n = 1, R = Cy** **n = 2, R = Ph** **n = 2, R = Cy**	Synthesis[52]	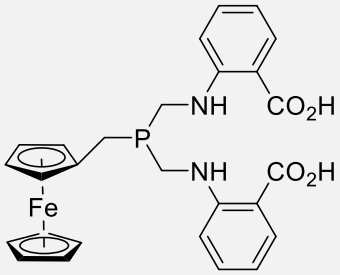	Synthesis[53]
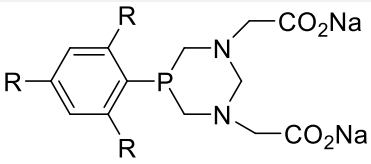 **R = H** **R = Me** **R = *i*-Pr**	Synthesis[54]	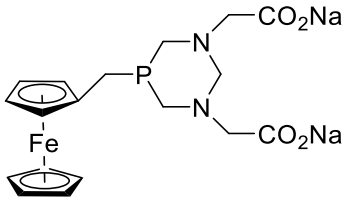	Synthesis[53]
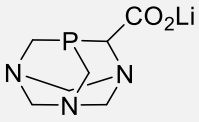	Synthesis[55]	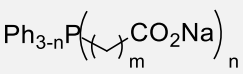 m = 1-7; n = 1-3	Synthesis[56, 57] Hydrogenation[58]
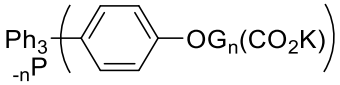	Suzuki-Miyaura[59]	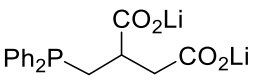	Hydroformylation[60]
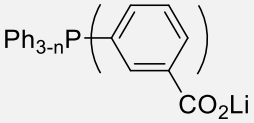	Heck[61] Rh-catalysed coupling[62, 63]	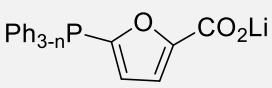	Hydroformylation[64] Hydrogenation[64]

In catalytic reactions the bonds between ligand and metal is frequently broken and reformed.[38] This process can cause the breaking away of the catalyst from the support, resulting in the dissolving of the catalyst into the organic phase.[38] The catalyst needs to be sufficiently hydrophilic to minimise catalyst leaching. This is an important property as noted by the increased development of methodologies to include hydrophilic ligands to the metal catalytic centre.

1.4 Hydroformylation

The use of transition metal catalysts for hydroformylation is a significant methodology for the formation of C-C bonds. This process converts inexpensive feedstocks to industrially relevant aldehydes, holding applications in both detergent and fine chemical streams.[48, 65] The hydroformylation reaction is the transition-metal catalysed addition of CO and H_2 to olefins to form linear and/or branched aldehydes.[66, 67] This reaction is chemoselective whereby either aldehydes or alcohols can be formed. A refinement of the steric and electronic effects allows the reaction to proceed regioselectively (Scheme 1.1), as the possibility of both linear and branched products may be formed.

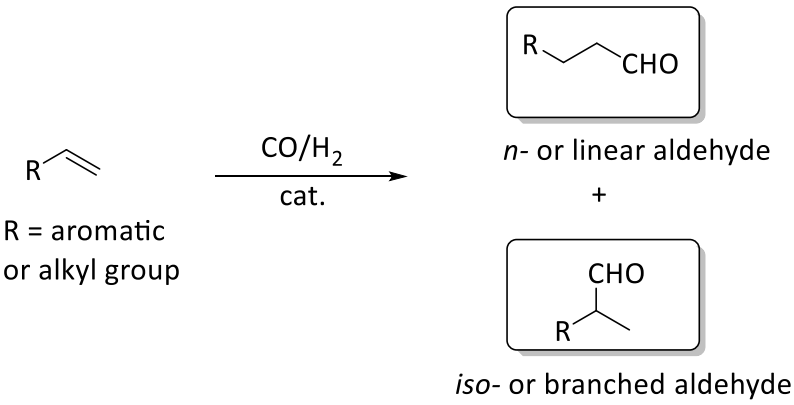

Scheme 1.1. *Hydroformylation reaction to form linear and/or branched aldehydes.*

The hydroformylation reaction was discovered in 1938 by Otto Roelen, and coined this reaction as the "oxo" process. This discovery was annotated through the studies on the oxygenated side products of the cobalt-catalysed Fischer-Tropsch reaction.[67] Further industry examples includes the monosulfonated triphenylphosphine palladium complex, which was used by the Kuraray company in the synthesis of nonane-1,9-diol.[68]

Olefin hydroformylation has the ability to produce side reactions, some of these include the hydrogenation of olefins to form the alkane or the hydrogenation of aldehydes to form alcohols. The main product, aldehydes, are important feedstocks to the pharmaceutical, fragrance and agrochemical industries.[69] With suitable modification, aldehydes can be converted into amines, carboxylic acids, acetals and diols, which all serve as building blocks to more complex and economically desirable molecules.[3]

The first industrial application of the hydroformylation reaction utilised the cobalt catalyst, namely $H[Co(CO)_4]$.[70] This catalyst required high temperatures and pressures to obtain economically viable selectivity of the product. The catalyst was unstable due to ligand loss, hence higher pressures were used to avoid degradation. These catalysts were not ideal as they predominantly formed cobalt clusters in the reaction. Furthermore the active species was relatively volatile, making the separation of products and reactants quite challenging, as the catalyst needed to be separated by chemical decobaltation before distillation.[71] This process involves the oxidation of the cobalt catalysts to yield an aqueous solution containing cobalt(II) ions. The crude products can then be separated by a simple phase separation. These catalysts primarily favoured isomerisation towards internal olefins and the hydrogenation to alcohols.[71]

A refinement of the original cobalt catalyst by displacing a CO group for a PR_3 group (R = aryl or alkyl), increased the thermal stability of these complexes. This allowed for the distillation of the crude reaction products without any significant catalyst decomposition being observed. The bulkier nature of the phosphine imparted a bias of selectivity towards linear hydroformylated products. However, the increased electron density around the metal centre favours the oxidative addition of dihydrogen, and consequently leads to the favouring of hydrogenated linear alcohols. The main disadvantage of these catalysts is the high temperature and pressures that these catalysts operate at.[71]

Studies by Wilkinson and co-workers on the $[RhCl(PPh_3)_3]$ catalysed hydroformylation under mild conditions showed increased catalytic efficiency and improved selectivity.[72] More importantly, these catalysts operate under much milder conditions, which is in alignment with Green Chemistry principles. Thus, rhodium-based catalytic complexes have received

widespread attention as homogeneous catalysts and it forms the basis for most hydroformylation catalytic studies to date.[18, 37, 68, 72-74]

1.4.1 Mechanism of Rhodium Catalysed Hydroformylation

The bulk of hydroformylation reactions utilises rhodium-based catalysts, as these show enhanced activity and selectivity in comparison to other transition metals, namely cobalt, iridium, ruthenium and platinum.[8, 48, 75]

The mechanism of the rhodium catalysed reaction (Scheme 1.2), is widely reported in literature.[12, 41, 67, 72, 76-78] The cycle is initiated by the formation of an unsaturated 16-electron rhodium hydrido-complex (**i**). The complex co-ordinates to the olefin (η-2) to form a five co-ordinate intermediate (**ii**). A migratory insertion of the olefin yields two regioisomeric Rh-alkyl intermediates, namely the linear (**iii**) and branched (**iv**) intermediates. The linear intermediate is formed *via* the anti-Markovnikov addition of the hydride moiety, whereby the branched is formed by the comparative Markovnikov addition. The consequent addition of CO (**v**) to the unsaturated four co-ordinate complex yields compound (**vi**). The oxidative addition of hydrogen (**vii**) allows for the formation of (**viii**), which undergoes a reductive elimination to yield an aldehyde (**A** or **B**). The transition metal catalyst is regenerated simultaneously to form (**i**). The regioselectivity (addition of hydride) is dictated by pH and the electronic and steric constraints of the ligands. The chemoselectivity to aldehydes and regioselectivity towards linear aldehydes can be refined by altering the pressure, temperature, solvent, ligands and immobilisation support.[38, 68]

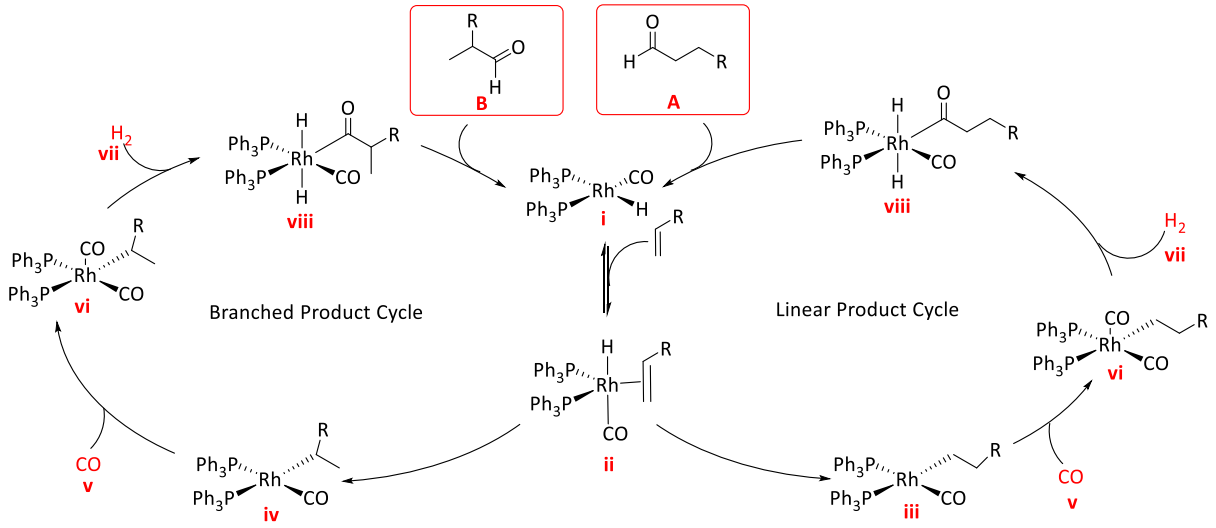

Scheme 1.2. *Rhodium catalytic cycle to form branched and linear aldehydes.*[68, 76]

Despite the advantageous activity and selectivity rhodium offers, the high cost of the metal and inadequate recycling methods makes the catalyst undesirable for industry. Alternatively better and more effective processes are required to combat these problems. Therefore, the incorporation of a biphasic system with water-soluble rhodium catalysts pilots advances in applied homogeneous catalysis.[43]

1.4.2 Hydroformylation In Aqueous Biphasic Media

The use of aqueous biphasic systems has received extensive plaudits in literature as it combines key Green Chemistry principles and commercial industry requirements.[48, 79, 80] The retention of the catalyst in the aqueous phase and the products in an alternative phase is an elegant method to recycle the catalyst, this method has been extensively studied.[79, 81, 82] The hydroformylation in aqueous reaction media was discovered in the 1970's by Emile Kuntz at Rhône-Poulenc (RP) and later commercialised by Ruhrchemie (RCH).[81] Hence, this technique is referred to as the Ruhrchemie/Rhône-Poulenc 'oxo' process.[81] This process is currently called the OXEA process and makes use of a tri-sulfonated water-soluble rhodium catalyst (Figure 1.3).[81] The alkene and hydroformylated alkene exists in a separate phase to that of the catalysts (aqueous) which results in facile separation.

Currently, over 800 000 tonnes of propene and butene is produced per year using the OXEA process.[83] Although the results are highly effective, the process is not effective for higher

olefins due to the poor solubility and mass transfer limitations of these substrates in water at higher temperature and pressures.

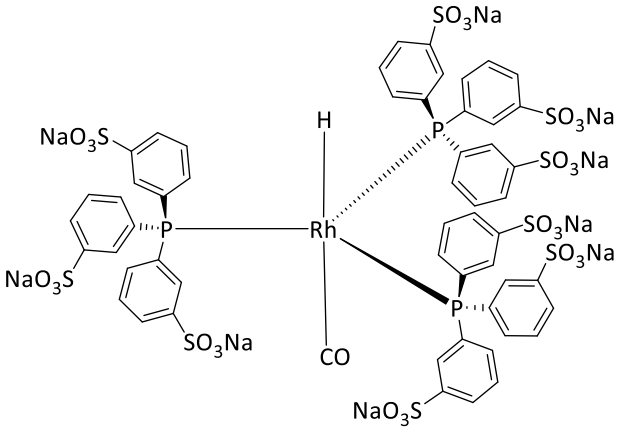

Figure 1.3. *Trisulfonated water-soluble rhodium catalyst, TPPTS, used in the OXEA process.*

To combat these problems a myriad of methods have been attempted, these include surfactants, polymers, co-solvents, amphiphilic molecules, thermomorphic solvents, dispersed particles and supramolecular receptors.[26, 73, 84-86] Thus, with the variety of methodologies, only a few have been successful in catalyst recyclability while still maintaining good activity, thus emphasizing the complexity of this challenge.[83]

1.4.3 Cyclodextrins Application In Aqueous Biphasic Media

A highly successful approach lies in the use of supramolecular receptors, namely cyclodextrins.[84] Cyclodextrins (CDs) are macromolecular oligomers, which consists of 1,4-linked α-glucopyranose units joined in a cyclic array (Figure 1.4).[87] The seminal work by Alper in 1980's on CDs have prompted the extensive studies of cyclodextrin in aqueous organic catalysis.[88] These studies ranges from the mass transfer effect of CDs, importance of CD structure and degree of substitution, CD dimers used to combat long-alkyl chain substrates and its use of CDs in micellar interfacial catalysis.[83]

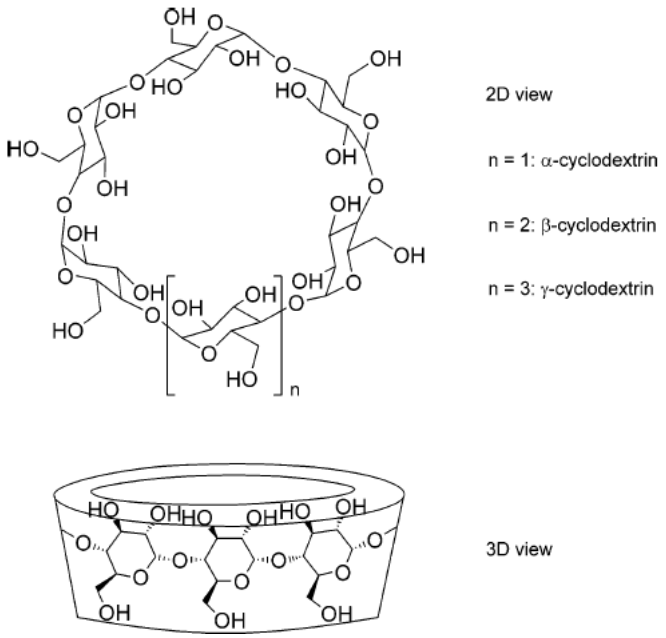

Figure 1.4. *2D and 3D representation of cyclodextrin.*[84]

Catalyst design aims to maximise factors such as stability, turnover number, separation and solubility.[2] The aqueous solubility is dictated by ligand modification, namely by adding hydrophilic groups to the complex.[89] These ligands are generally polar and the most popular ligands are sulfonates, phosphonates, carboxylates, hydroxyl and quaternary ammonium groups. It should be noted that the catalysis occurs at the interface for longer chain olefins. Polar ligands can partition into the aqueous phase, which allows for increased activity due to the reduced mass transfer limitations. However, the minor lipophilic nature of the catalytic scaffold causes leaching into the organic phase. Dendrimers offer a possibility to immobilize the catalyst in order for it to possess certain properties which are not possible in the monomeric case.[90] This positive influence is called the dendritic effect. In the context of hydroformylation, this effect describes the increase of catalytic activity and/or decrease of catalyst leaching as the dendritic generation increases.

1.5 Metallodendrimers

Dendrimers have become increasingly popular, whereby applications in pharmaceutical, petrochemical and material science are well researched.[14, 91-94] The term dendrimer is a conjunction of two Greek words, namely “dendros” meaning “tree” or “branch” and “meros” meaning “part” in Greek.[95] With the subsequent addition of a

transition metal to the dendritic scaffold, the molecule is referred to as a metallodendrimer. Dendrimers differ from polymers as the formers' architecture can be synthetically controlled. Furthermore, the location and amount of catalytic sites within dendrimers can be selectively modified.[96-98] Recent developments are focused on the molecular design of these tree-like structures, and more importantly on altering the electrostatic environment whereby the weak interactions can be controlled, in order to modulate chemical and physical properties of the dendrimer.[96]

The generic dendrimer representation displays four key areas, as shown in Figure 1.5. These are i) void spaces, ii) central core, iii) interior branching units which can expand into various generations [G*n*] and iv) surface terminal groups which allows for suitable modification.[99]

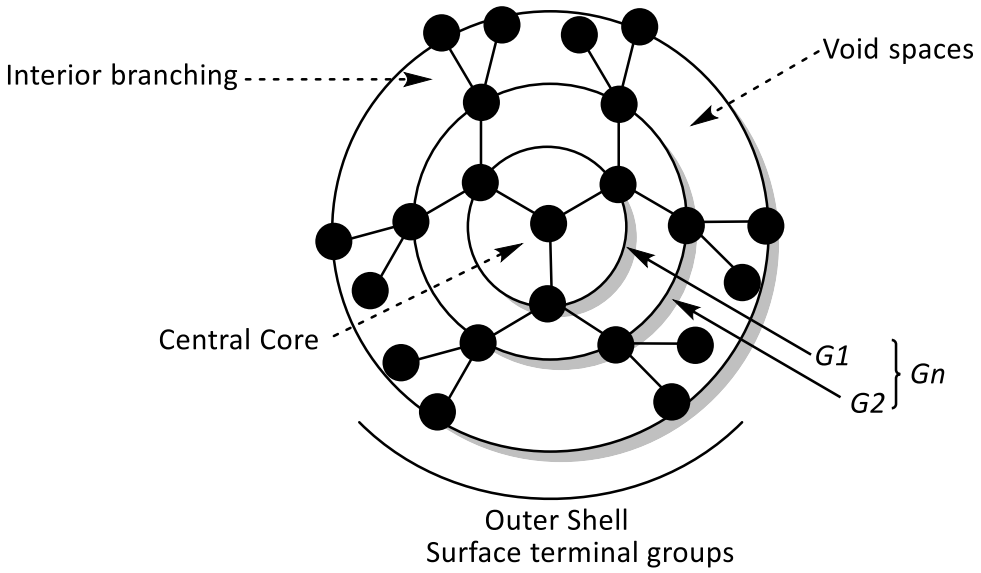

Figure 1.5. *Structural representation of a metallodendrimer.*[99]

The properties of dendrimers are primarily dictated by the functionality of the terminal moieties. These can be altered to enhance water solubility with the addition of charged or hydrophilic groups. This feat can be manipulated to enhance characteristics which are highly sought after in catalysis and medicinal chemistry. Dendrimers are classified according to their synthetic pathway and generation number, G*n*.

The characteristic of dendrimers to possess multiple functionalities may allow it to possess multiple properties in a single molecule.[90] *Janus* dendrimers consists of two dendritic

segments, each possessing a different functionality at the termini (Figure 1.6).[100] This characteristic allows for one segment to possess hydrophilic properties, which will promote water solubility. The other segment could be bound to numerous catalytic metal centres to exercise a co-operative enhancement of multinuclear transition metal catalysts.[100, 101] A fundamental understanding of the structural nuances is required to manipulate dendrimers and construct molecules with extensive applications. Therefore, key methodologies that enable variations to the various topologies would be highly advantageous. With extended applications of *Janus* dendrimers, the synthesis and purification of these compounds become extremely challenging.

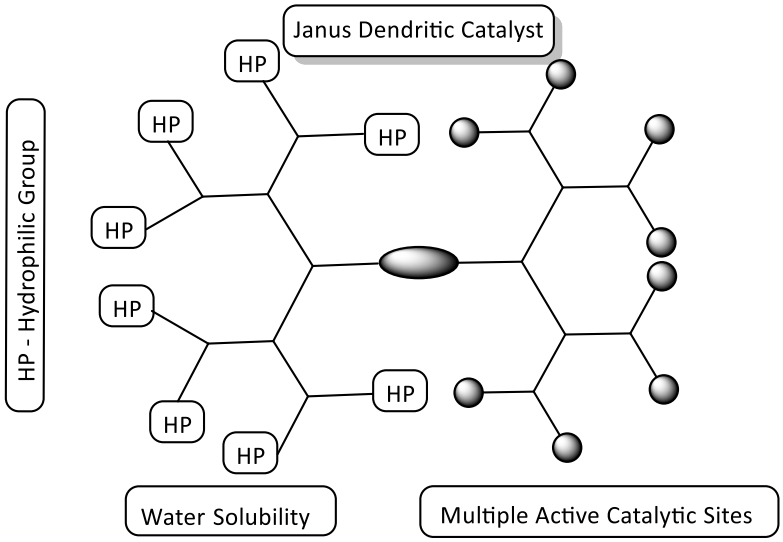

Figure 1.6. *A schematic of an aqueous biphasic "Janus" dendritic catalyst.*[100]

1.5.1 Synthetic Routes for Dendrimers

Dendrimer synthesis has developed since its inception, and focus has been honed into the improvement of dendrimer design and synthesis. Historically, the first synthesis of a dendrimer was reported in 1978 by Vögtle and co-workers, as depicted in Scheme 1.3.[102] Initially referred to as cascade molecules, these structures were used to encapsulate smaller molecules.[95]

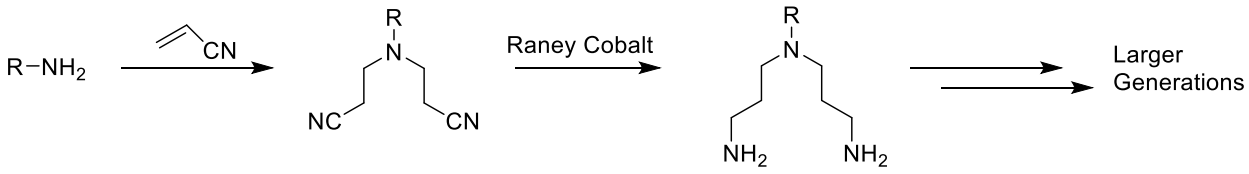

Scheme 1.3. *Vögtle's seminal work on the formation low generation branched diamines.*[102]

Vögtle's seminal work was elaborated into a poly(propylene imine) derivative (PPI), which have multiple applications in the field of catalysis, material science and biology.[95, 102, 103] These dendrimers consist of polyalkylamine functionalities, with each amine group serving as a potential branching point. These diaminobutane-cored systems (DAB) are formed from the Michael addition of acrylonitrile with a 1,4-diaminobutane to yield the corresponding branched nitrile system. A reduction using the Raney cobalt catalyst yields the reactive amine. Hence, a repetition of these transformations leads to the construction of larger generations, as displayed in Scheme 1.4.[92, 95, 104]

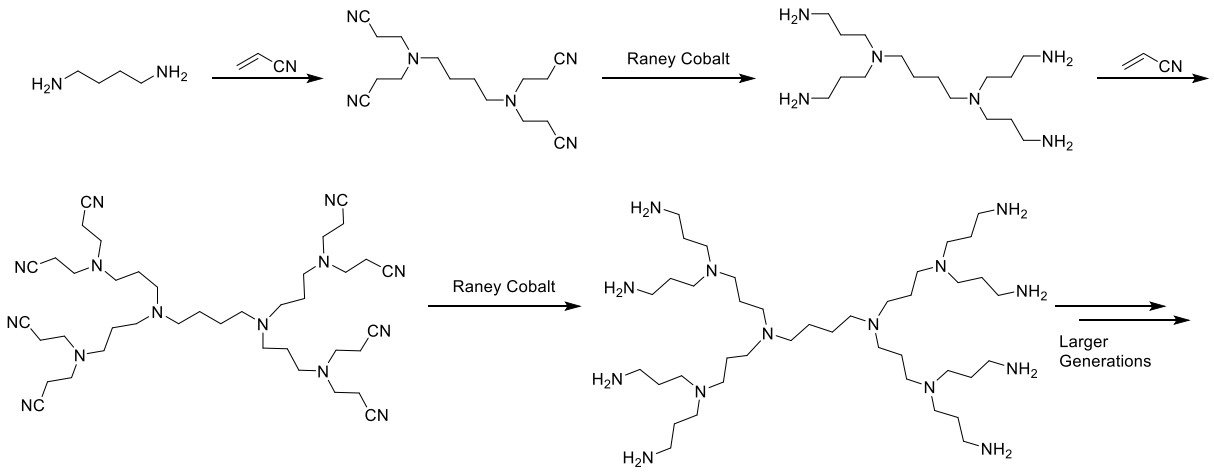

Scheme 1.4. *The stepwise divergent synthesis of the (poly)propylene imine dendrimer.*[103]

There are namely two main synthetic methodologies for dendrimer synthesis, divergent and convergent routes, as indicated in Scheme 1.5. The divergent method is built stepwise from the core and is grown outwards through an iterative synthetic strategy.[105] There are two types of divergent strategies, as discussed by Tomalia and co-workers.[20, 106] A linear genealogically directed synthesis (L-GDS) is the construction of a linear molecule, with synthetic methodology similar to that of protein/peptide synthesis.[95] The amplified

genealogically directed synthesis (A-GDS) is the construction of a multi-pronged system, which branches out into one direction.[95]

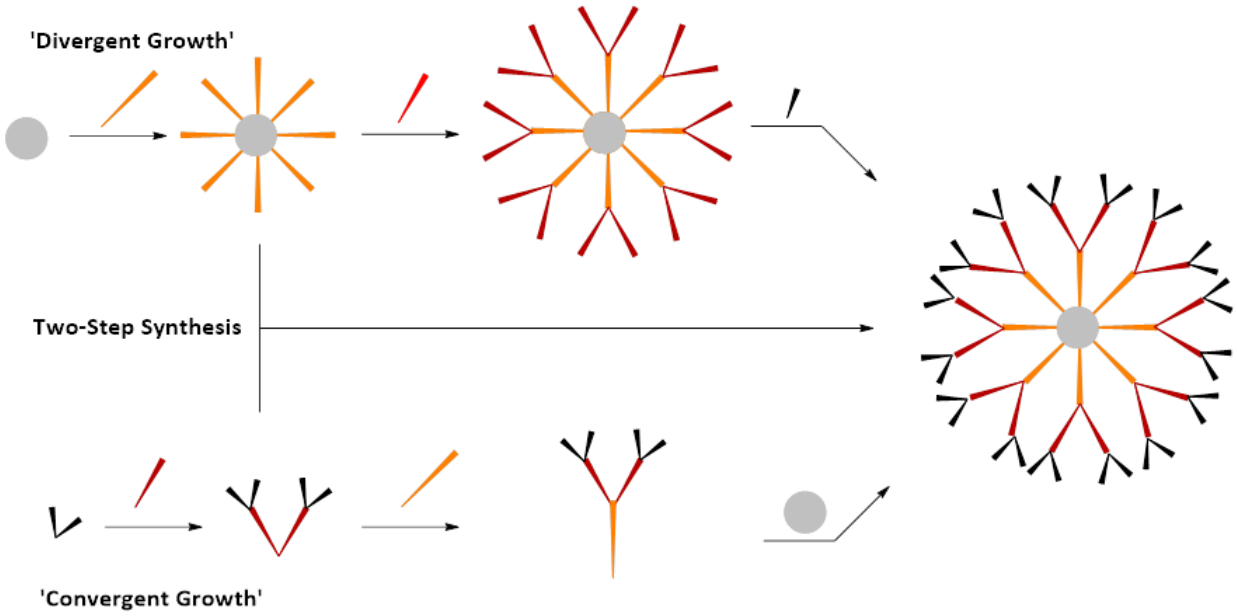

Scheme 1.5. *The divergent, convergent and two-step (combination of divergent and convergent approaches) synthetic pathways for the formation of dendrimers.*

The divergent method was elaborated from Vögtle's seminal work and discovered independently by Tomalia and Newkome in 1985. Tomalia focused on the synthesis of poly(amidoamine) (PAMAM) based macromolecules, which has become the landmark in the dendrimer field. The starburst compound formed, PAMAM, consists of polyamide branches with amino motifs at the periphery. This cascade moiety was later coined by Tomalia as dendrimers, and since has obtained widespread use.[4, 92-94, 103, 105, 107] The PAMAM-based cascade dendrimer allowed for the incorporation of smaller molecules into a larger macromolecular motif.[92, 103] The dendrimer was obtained *via* the 1,4 conjugate addition of ammonia with methyl acrylate. Amidation of the methyl ester was conducted using 1,2-ethylene diamine to regenerate the reactive primary amine, as shown in Scheme 1.6.

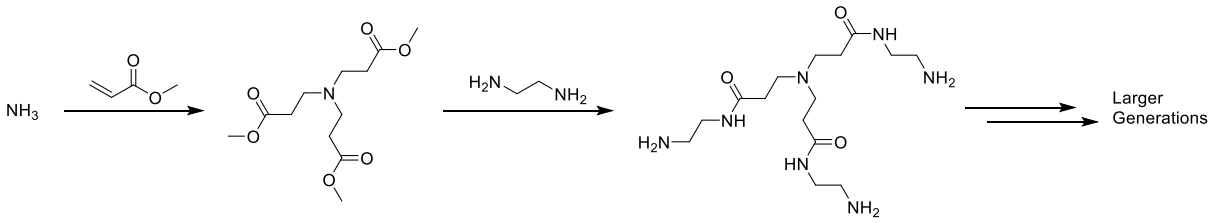

Scheme 1.6. *Overall synthetic scheme for the synthesis of PAMAM dendrimers.*

Conversely the methodology proposed by Newkome and co-workers involved arborescent motifs with work specialised on molecules possessing two-directional spherical cascades, with application as unimolecular micelles.[91, 92] As depicted in Scheme 1.7, these tree shaped molecules were synthesized *via* the two-step nucleophilic substitution-amidation procedure.[91]

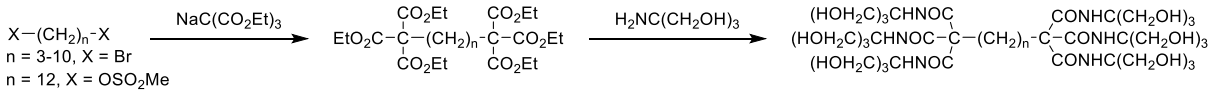

Scheme 1.7. *Newkome's synthetic strategy to form cascade molecules, defined as arborals.*

An alternative synthetic route for the construction of dendrimers is the stepwise growth from the periphery leading to the core.[105] This approach was discovered in 1990 by Hawker and Fréchet and has since been coined as the convergent method. Their work on polybenzylether dendrons allows for control of the nature and placement of surface terminal groups (Scheme 1.8). The synthetic scheme shows a coupling of benzyl bromide to the reactive 3,5-dihydroxybenzyl alcohol core, *via* the Williamson-ether reaction. A conversion of the benzylic alcohol to the bromide was obtained utilising the Appel reaction. The iterative reaction of the bromido-Fréchet dendrons with 3,5-dihydroxybenzyl alcohol allows for the construction of larger generations.

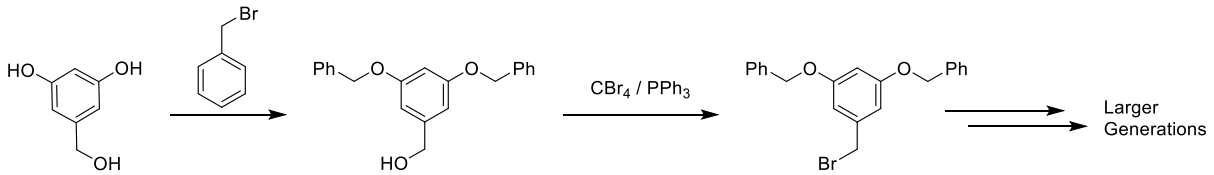

Scheme 1.8. *Hawker and Fréchet's convergent synthetic strategy.*

These synthetic methods each have distinct characteristics associated to them. Structural nuances have produced pronounced effects regarding dendrimers. This has motivated for the use of different cores and surface terminal groups. The use of multivalent phosphorus as the dendritic core has been implemented by Majoral and Caminade, thus paving way for dendrimers with new found properties and applications.[90, 95, 105] Similarly with the introduction of green chemistry principles in synthesis, new methods which are highly selective and high yielding are sought after. These transformations in the dendrimer field includes Astruc's azide-alkyne cycloadditions,[1, 94, 108-110] Malkoch and Badi's thiol-ene and thio-lactone coupling,[111, 112] and Percec's self-assembly of macromolecules to name a few.[113]

Table 1.3. *Selected differences between the divergent and convergent synthetic approaches.*

	Divergent Synthesis	**Convergent approach**
Larger Generation (>G_4)	Surface defects, Polydispersity	Steric constraints
Synthesis	Excess reagents	Synthetically challenging
	Exponential growth at each step (n^2)	Dendrons possess much slower growth (n x 2)
	Reactive functionalities increase	More structural control, better purification
	Increase of the molecular weight exponentially, slower reaction kinetics	Time consuming synthesis, difficult and expensive.
Core	Structurally inert core, however fixed.	Flexibility of the core, as the incorporation is the final step.

The most important aspect of dendrimer synthesis is obtaining the highest possible yield, irrespective of the synthetic strategy.[98] Low yields results in a polydispersity for the divergent strategy and loss of starting material for the convergent strategy, with these differences summarised in Table 1.3.[98] From a synthesis aspect, classical methodologies are applied, due to the iterative procedure of dendrimer construction.

Various synthetic methods allow for a variety of dendrimer motifs, each bearing different shapes and morphologies. These allow for different complexation modes to the metal, leading to numerous topologies of dendrimers available in literature.[104]

1.5.2 Topologies of Metal-Based Dendrimers

Metallodendritic scaffolds vary with respect to the position of the metal ion, as described in Figure 1.7. Each scaffold aims to enhance specified properties of the metallodendrimer. Since the landmark work by Tomalia, Newkome and Fréchet, an array of different dendrimers have been synthesized, with application in both catalysis and bio-medical field.

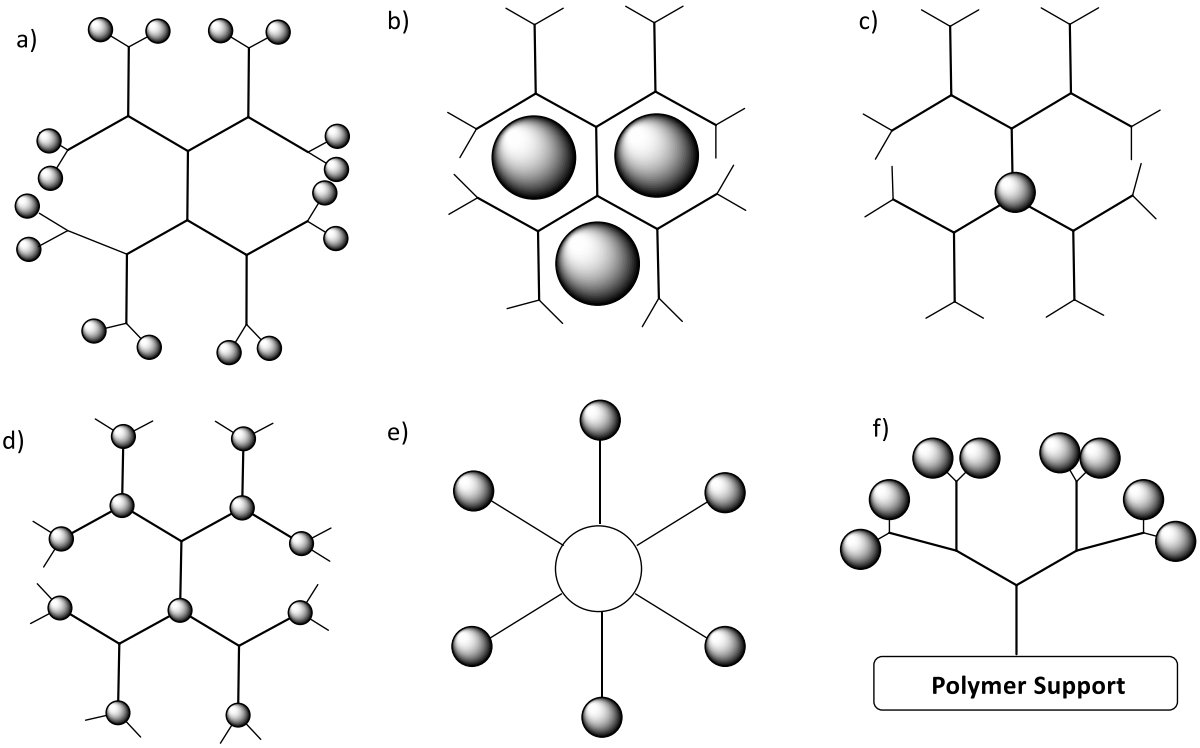

Figure 1.7. *Topologies associated with metallodendrimers.[107] The figure shows the active metal centre situated at the: Termini **(a)**, Void spaces **(b)**, Nodal core **(c)**, Interstitial branches **(d)**. The star-shaped dendrimer **(e)**, and polymer supported dendrimer **(f)**, has the active metal centres at the periphery. The former is primarily used for catalysis and the latter incorporates the use of a polymer support for immobilisation and recyclability.*

The dendrimer with metals located on the periphery are the most popular, due to the ease of complexation as the final step. This dendritic class is primarily used for catalysis and

medicinal applications, as depicted in Figure 1.8.[92]

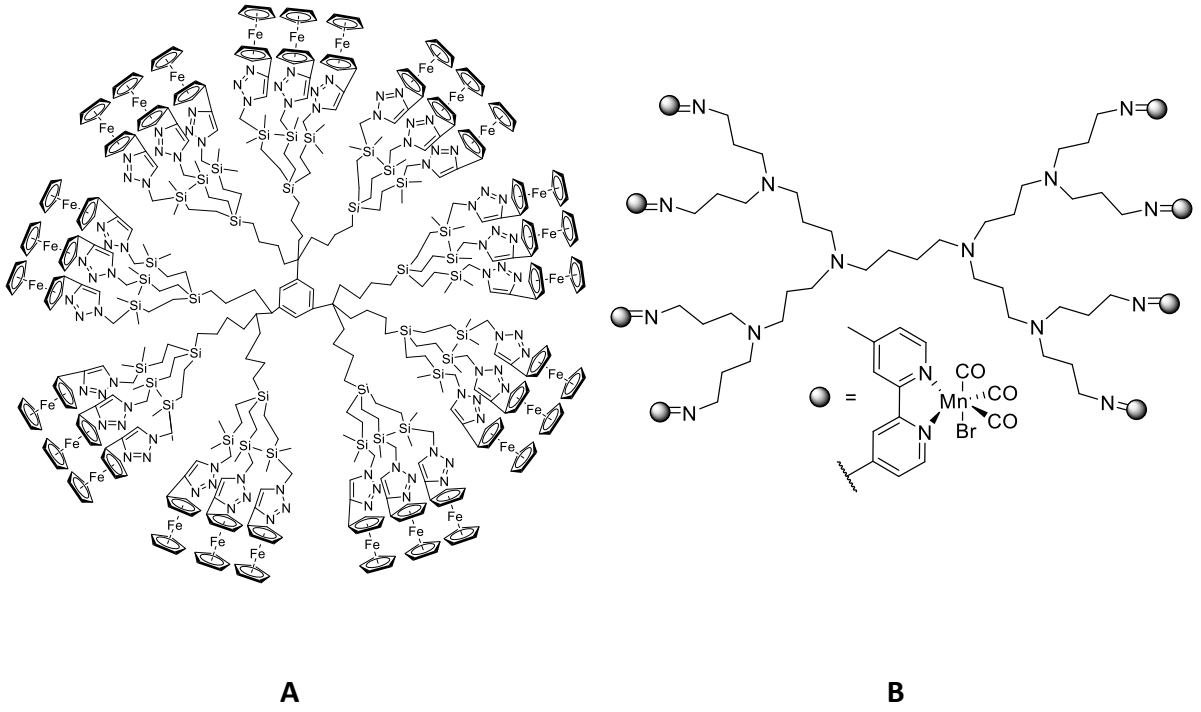

Figure 1.8. *Literature examples of organometallic dendrimers with the metal located at the periphery.* ***A*** *depicts Astruc's ferrocene terminated dendrimer used as a nanoparticle stabilizer,[94] in comparison to* ***B****, Smith and Govender's manganese terminated PPI scaffold, used as a photoCORM.[114]*

The encapsulation of catalysts inside the dendrimer encourages steric shielding and stabilization of the active site.[91, 104] Core modified dendrimers (Figure 1.9) can mimic enzyme behaviour as they offer substrate binding opportunities.[91, 104] Predominantly these metallodendrimers consist of a porphyrin core and are constructed using a convergent approach. The encapsulating moiety of the dendrimer can influence the microenvironment around the metal centre.

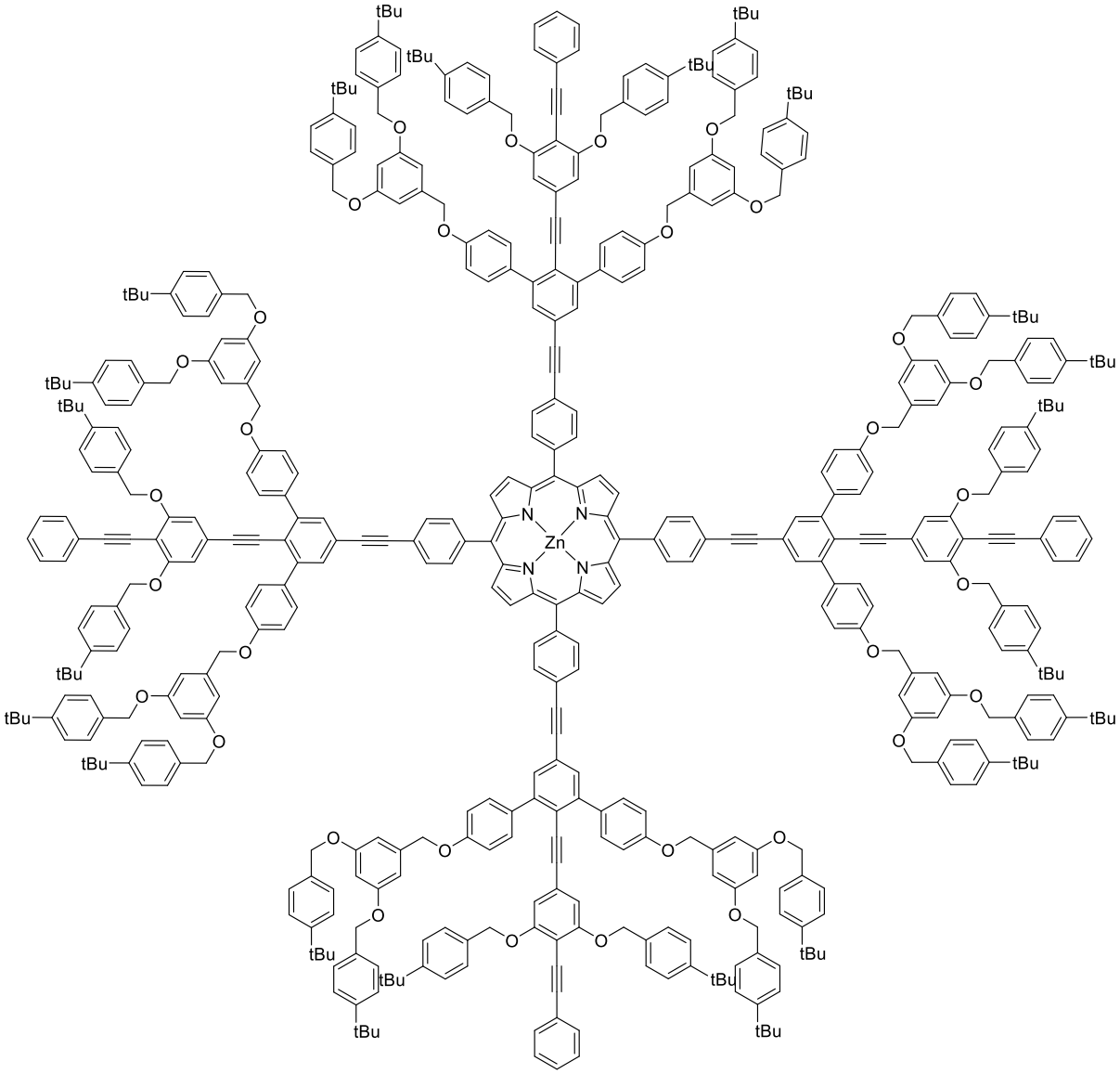

Figure 1.9. *Zinc-incorporated metallodendrimer, resembling a core-modified metallodendrimer.*[91]

The incorporation of metals into void spaces allows for applications in host-guest supramolecular chemistry and medicinal chemistry.[92, 103] These dendrimers were synthesized by Newkome (Figure 1.10), and were obtained *via* the site-specific attachment of a metal centre to form these piperazine complexes. The topology of this type of dendrimer is generally rare, as the site of co-ordination needs to be controlled.[91]

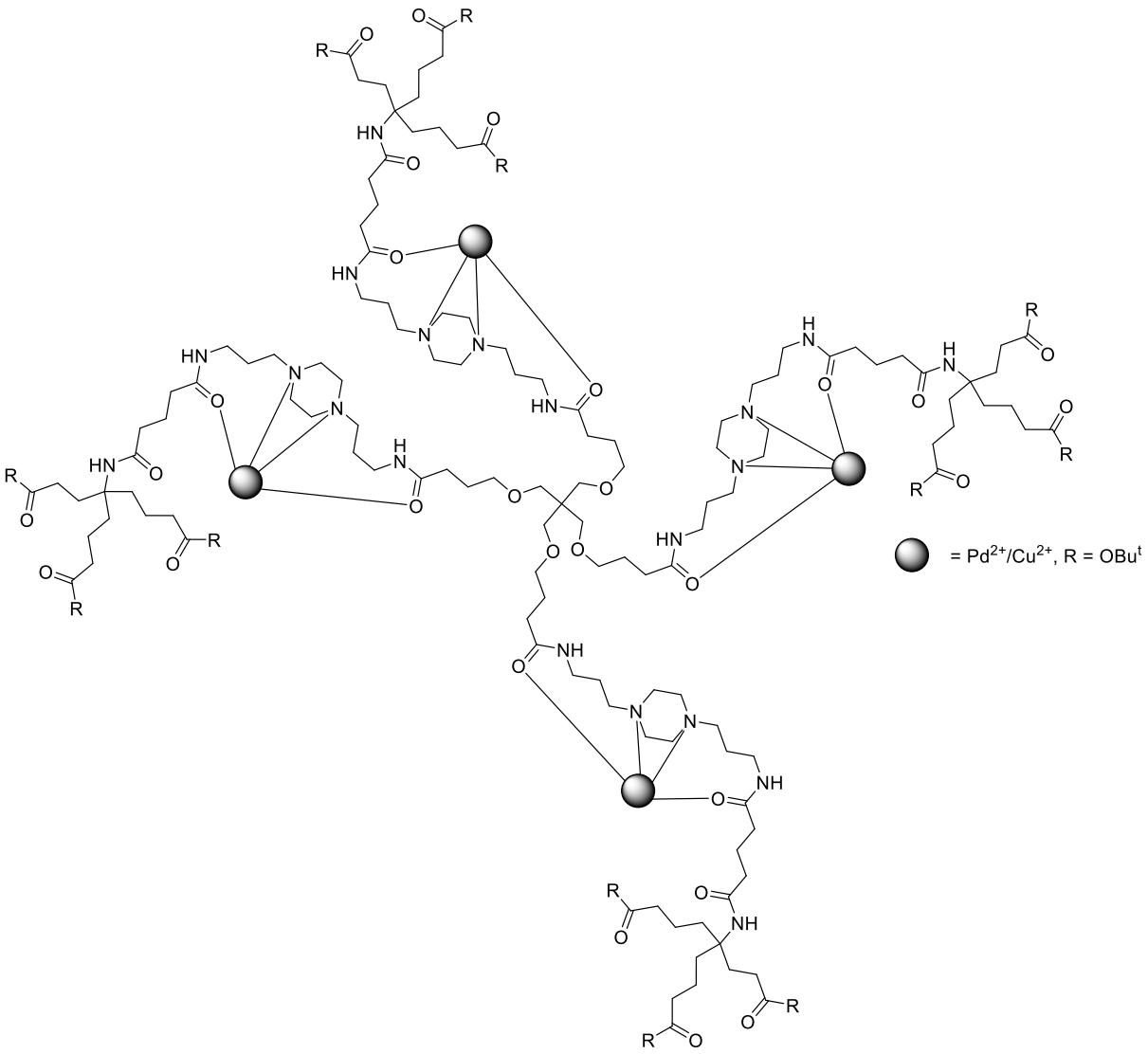

Figure 1.10. *The palladium and copper piperazine metallodendritic complexes formed by Newkome, via the site specific inclusion of these metal complexes.*[91]

Notable applications of metallodendritic catalysts include hydroformylation,[9, 14, 73, 85, 115-118] Suzuki, Mizoroki-Heck and Sonogashira cross-coupling,[31, 119] metathesis,[92, 93] Knoevenagel and Aldol condensations[120-123] and hydrogenation reactions.[40, 75, 100, 124-126]

1.6 Metallodendrimers As Catalysts

Since the early 1990's, dendritic catalysts have been refined and novel discoveries of applications have been observed.[92, 127] Notably, the incorporation of metal catalysts onto the periphery or interior cavities of dendrimers allowed for significant control on the catalytic activity and solubility.[92] The metallodendritic catalysts found were on the

nano-scale, which allowed for facile separation with respect to precipitation, ultra-centrifugation or ultra-filtration using zeolites or membranes.[10, 22, 107, 128] The use of metallodendrimers for multiphasic catalysis has been widely reported in literature. [73, 94]

The pioneers of metallodendritic homogeneous catalysts, van Koten and van Leeuwen, synthesized carbosilane dendrimers used as supports for homogeneous catalysts (Scheme 1.9).[1, 4] These were applied to the Kharasch addition of polyhalogenated alkanes to alkenes. Similarly, dendrimers can be altered to perform in multiphasic media as the peripheral groups are functionally tunable.[73] Further work done by van Leeuwen showed that the use of star shaped catalysts reduced the amount of catalytic fouling in comparison to the mononuclear species.

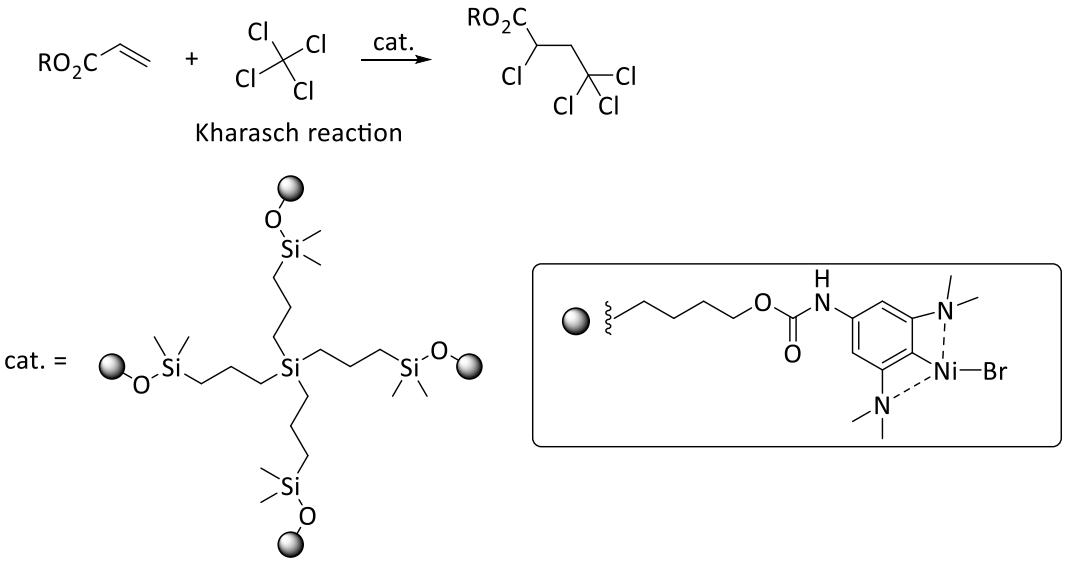

Scheme 1.9. *van Kotens metallodendrimer, which catalyses the Kharasch addition of polyhalogenoalkanes to olefin moieties.*[129]

The first discovery of a positive dendritic effect and catalyst recovery was noted by Reetz *et al*.[4] The increased multinuclearity resulted in improved catalytic activity and efficiency, this effect is noted as the positive dendritic effect. Their work was based on a diaminobutane (DAB) dendrimer with dimethyl diphosphine palladium complexes at the periphery. Their work sparked an interest in the field of catalysis as common problems encountered with homogeneous catalysis were being addressed.

Rhodium(I) catalysts are mostly studied for hydroformylation and hydrogenation reactions due to their superior catalytic activity.[92] Hence, their incorporation in dendrimers may allow for the development of novel catalytic metallodendritic systems. It is within our interest to explore applications of metallodendrimers in hydroformylation.

1.6.1 Metallodendrimers As Hydroformylation Catalysts

The Ruhrchemie/Rhône-Poulenc or 'oxo' process is undoubtedly the most important application of aqueous biphasic catalysis.[4, 68, 130] The hydroformylation reaction is a convenient method in preparing functionalized olefins. Recent developments aim to refine catalytic systems to bridge the gap between homogeneous and heterogeneous systems. This idealised system should be highly recyclable and maintain a high catalytic efficiency.[14]

Rhodium (I) catalysts are mostly studied for hydroformylation reactions, and their popularity is widely recognised across literature.[14, 37, 65, 118] The seminal work by Reetz and co-workers utilised a rhodium-diphosphine terminated polypropyleneimine dendrimer for the hydroformylation reaction.[131] Their work was later expanded by Cole-Hamilton with the use of an oligomeric silsesquioxane-cored G_1 dendrimer, which consisted of sixteen triphenylphosphine arms (Figure 1.11).[132] This scaffold was loaded with a [Rh(acac)(CO_2)] precursor and subsequently used as pre-catalysts for the hydroformylation of propen-1-ol.[38]

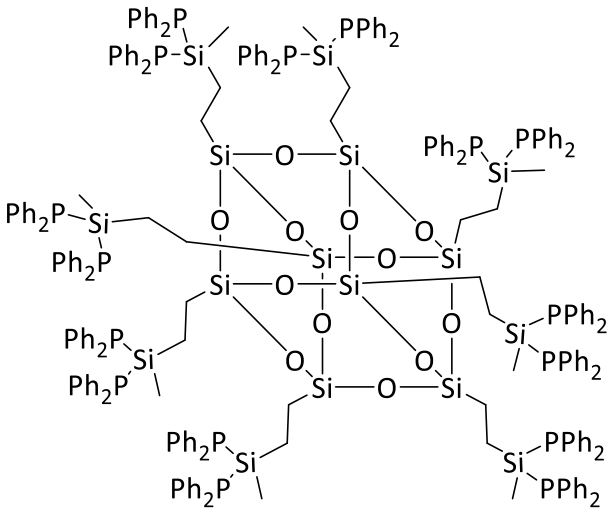

Figure 1.11. *Polyhedral oligomeric silsesquioxane (POSS) core synthesized by Cole-Hamilton and co-workers.*[38]

Studies by Alper and Arya reported on the use of dendritic wedges (G_0 to G_3) anchored to an amide-based resin, in an effort to simplify the separation procedure.[9, 14, 116] These complexes have been used for the hydroformylation of styrene, and their catalyst was separated by filtration. An evaluation of their results showed that their catalyst maintained excellent conversion (>98% across 5 cycles) and good selectivity's towards branched aldehydes. Their studies showed that their discrete metallo-dendronised catalyst displayed high reactivity, with this being attributed to the well exposed ligands on the periphery.[9, 14, 38, 116]

Although separation is facile, the activity is hampered due to the heterogeneous nature of dendronised resins. Homogeneous systems, such as Cole-Hamilton's POSS catalysts, was used in the monophasic hydroformylation, however no recyclability was reported. Moreover, a methodology to bridge homogeneous and heterogeneous systems is highly sought after. The use of aqueous biphasic systems for metallodendrimers provides insight to approach a new frontier in aqueous organometallic reactions.

1.6.2 Metallodendrimers as Hydroformylation Catalysts in Aqueous Biphasic Media

Water-soluble dendritic catalysts were synthesized in an attempt to increase the recyclability of the reaction and to limit any catalyst leaching. Xi and co-workers synthesized water-soluble monodentate G_3 metallodendrimers with a PAMAM scaffold.[85] These contained surface termini groups varying from phosphines to sulfonates. The rhodium metal was added *in situ*, hence no discrete metal complexes were formed. These were applied as aqueous-biphasic hydroformylation catalysts to styrene and 1-octene. Predominantly branched aldehydes were obtained for styrene as expected. However for the hydroformylation of 1-octene, an *n:iso* ratio of 1:2 was obtained. This study produced positive results with respect to reduced leaching of the catalysts in the organic phase in comparison to the TPPTS compound. The metallodendritic catalysts were separated from the product phase, however no recycling experiments were performed.[85] Furthermore the TON ranged between 0.93 – 24.57 h^{-1} for 1-octene and 0.83 – 10.53 for styrene. These values reported are not desirable for transforming the research catalyst into an industrial operating catalyst.

Furthermore Smith and co-workers synthesized a DAB-based and TRIS-based sulfonate dendrimer/macromolecule.[21] The ligands were found to be water-soluble and hygroscopic. No discrete metal complexes were formed, thus an *in situ* rhodium catalyst was formed and

applied in the hydroformylation of 1-octene. The dendrimers displayed consistent chemo- and regioselectivity across the various systems. Furthermore recyclability studies showed that the catalysts exhibited good recyclability over 5 cycles, however rhodium leaching occurred and this resulted in an average of 6% loss of conversion per cycle.[21] Moreover, with this field being in its infancy further insight and understanding is required for the improvement of these systems.

1.7 Rationale for the Current Study

In South Africa, substrates for the hydroformylation are readily available, as these products are a result of the Fischer-Tropsch processes at SASOL or available as plant extracts from sunflower and citrus industries. With the abundance of platinum group metals in this region, it is important to catalytically convert these inexpensive feedstocks to industrially and economically promising compounds. With the implementation of greener and cleaner synthetic routes in industrial synthesis, it is important to be mindful and pro-active regarding the impact of chemistry on the environment. Therefore the introduction of a greener, recyclable and efficient catalysts are paramount for the future of industrial syntheses.

In context of this work and to the best of our knowledge, no literature has been reported on discrete organometallic dendrons used for the hydroformylation of long chain olefins. These organometallic complexes formed are novel, and provides a different perspective of dendrimer synthesis. Very few examples exist of mononuclear dendritic wedges, thus providing further motivation for the synthesis and application of these metallodendrons.

1.8 Aims and Objectives

1.8.1 General Aims

As discussed in this chapter, the lack of reports on discrete metallodendritic wedges applied in the hydroformylation reaction may be interesting to investigate. Hence, the aims of the project were:

- To synthesise and characterise a series of Fréchet dendrons bearing Schiff-bases at the focal point.
- The respective ligands were complexed rhodium to afford discrete Rh(I) Fréchet metallodendrons bearing *N,O*-salicylaldimine or *N,P*-iminophosphine moieties at the focal point
- To evaluate the rhodium(I) catalyst precursors for the hydroformylation of various olefins.

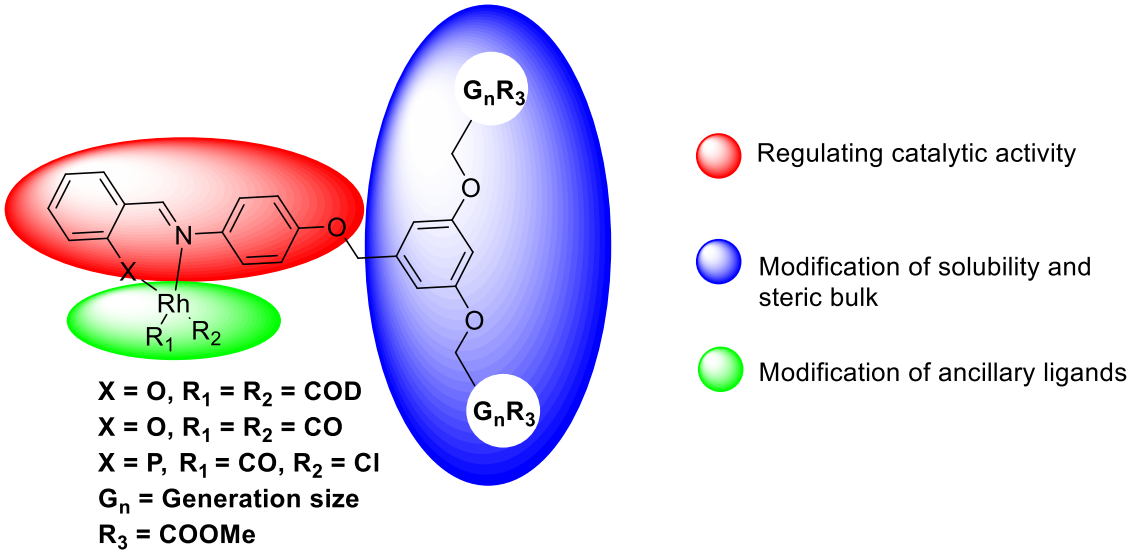

Figure 1.12. *The general schematic for the hydroformylation catalyst consisting of a dendritic wedge.*

1.8.2 Specific Objectives

1. The synthesis of zeroth-, first- and second-generation Fréchet-type dendrimers bearing a methyl ester functional group at the periphery (Scheme 1.10).

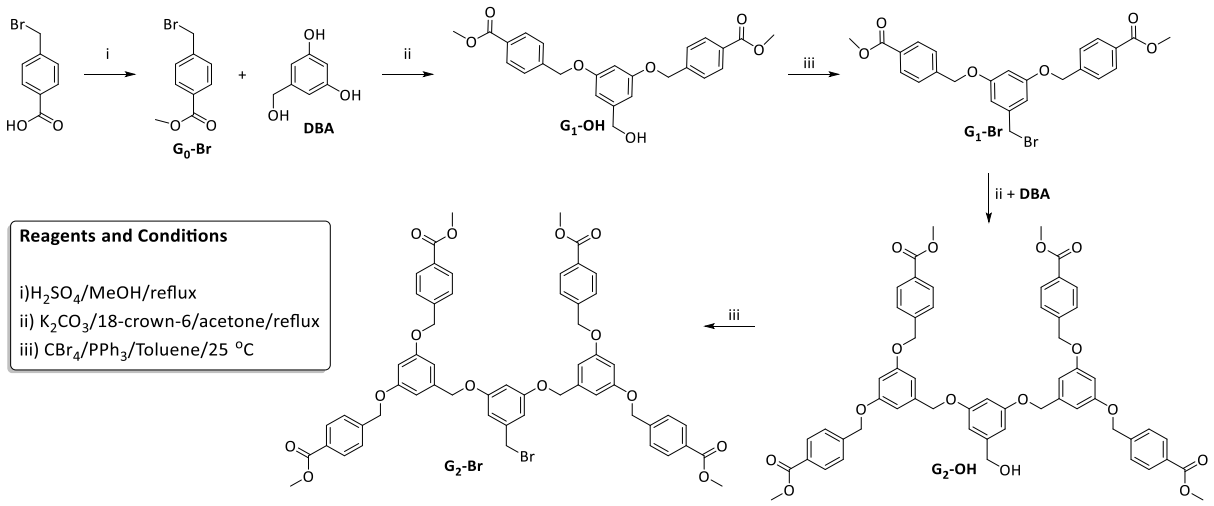

Scheme 1.10. *The synthetic scheme for Fréchet dendritic wedges, with varying generation sizes and reactive core functionalities.*

2. To prepare a series of Fréchet dendrons with Schiff-base moieties at the focal point. The focal point varies between *N,O*-salicylaldimine and *N,P*-iminophosphine ligands. (Scheme 1.11)

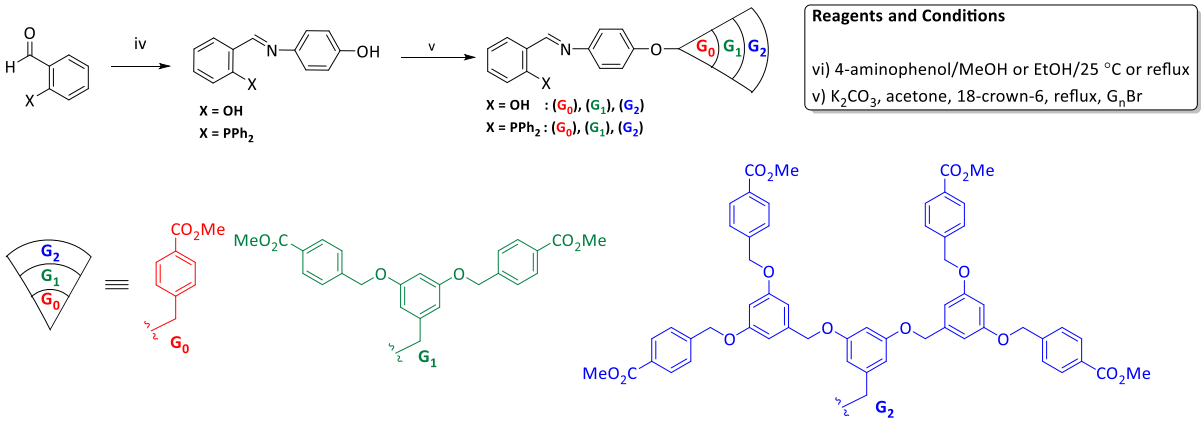

Scheme 1.11. *Synthesis of Fréchet dendrons bearing Schiff-bases at the focal point.*

3. Using the ligands outlined in Scheme 1.11, rhodium is complexed to the Fréchet ligands to yield discrete Fréchet metallodendrons with rhodium(I) cyclooctadiene (*N,O*), dicarbonyl (*N,O*) or chloro-carbonyl (*N,P*) complexes at the focal point (Scheme 1.12).

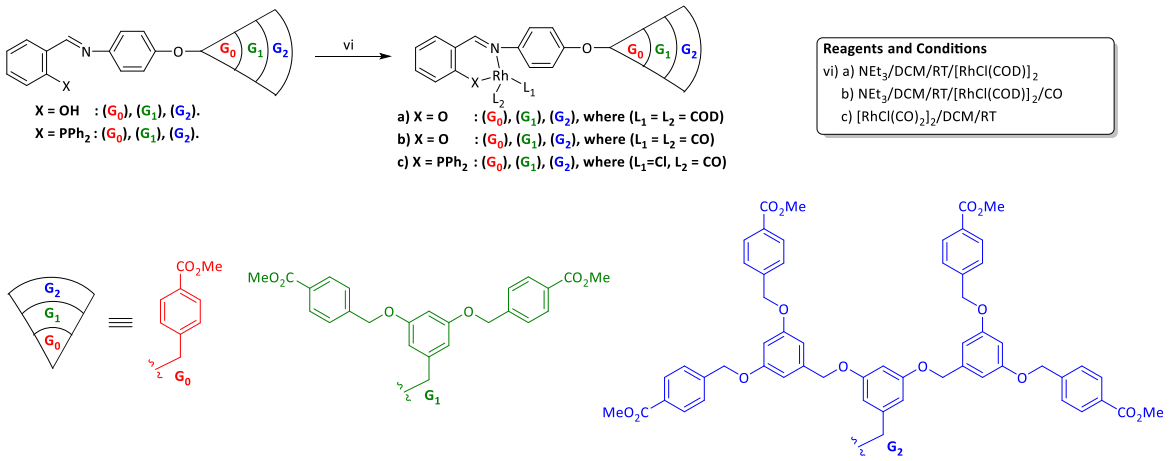

Scheme 1.12. *Synthetic outline for the formation of discrete organometallic dendrimers, each bearing different ancillary ligands.*

4. All of the compounds were characterised using various spectroscopic and analytical techniques, these include Nuclear Magnetic Resonance spectroscopy (NMR), Fourier Transform - Infrared spectroscopy (FT-IR), Elemental Analysis (EA), Electrospray Ionisation (ESI), Electron Impact (EI) or Matrix-assisted Laser Desorption/Ionisation (MALDI) mass spectrometry. Single crystal X-ray diffraction (XRD) analysis was used on single crystals to provide further evidence of the molecular structure for the isolated ligands and complexes.

5. The rhodium catalyst precursors were tested as catalysts for the hydroformylation of 1-octene, styrene, 7-tetradecene, methyl oleate, triolein, *D*-limonene and *R*-citronellal in organic monophasic media (Scheme 1.13). The conditions have been optimised by varying the syngas pressure and temperature. The hydroformylated products were quantified using GC-FID or NMR spectroscopy.

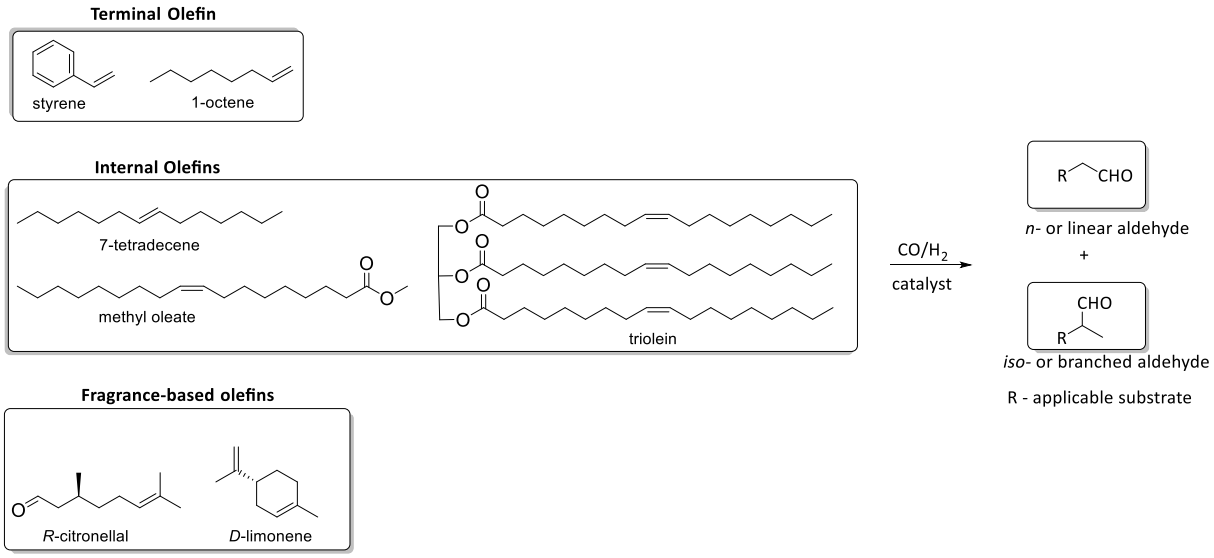

Scheme 1.13. *Hydroformylation reaction scheme which varies the substrate, these are namely, 1-octene, styrene, 7-tetradecene, methyl oleate, triolein, R-citronellal, D-limonene.*

1.9 References

1. R. J. Detz, S. A. Heras, R. de Gelder, P. W. N. M. van Leeuwen, H. Hiemstra, J. N. H. Reek and J. H. van Maarseveen, *Org. Lett.*, 2006, **8**, 3227-3230.
2. P. T. Anastas, M. M. Kirchhoff and T. C. Williamson, *Appl. Catal., A*, 2001, **221**, 3-13.
3. L. C. Matsinha, PhD thesis, University of Cape Town, 2015.
4. E. de Jesus and J. C. Flores, *Ind. Eng. Chem. Res.*, 2008, **47**, 7968-7981.
5. G. Centi, P. Ciambelli, S. Perathoner and P. Russo, *Catal. Today*, 2002, **75**, 3-15.
6. P. T. Anastas, L. B. Bartlett, M. M. Kirchhoff and T. C. Williamson, *Catal. Today*, 2000, **55**, 11-22.
7. B. C. Makhubela, PhD thesis, University of Cape Town, 2012.
8. B. C. Makhubela, A. Jardine and G. S. Smith, *Green Chem.*, 2012, **14**, 338-347.
9. P. Arya, N. V. Rao, J. Singkhonrat, H. Alper, S. C. Bourque and L. E. Manzer, *J. Org. Chem.*, 2000, **65**, 1881-1885.
10. H. P. Dijkstra, G. P. M. van Klink and G. van Koten, *Acc. Chem. Res.*, 2002, **35**, 798-810.
11. R. van de Coevering, R. J. M. Klein Gebbink and G. van Koten, *Prog. Polym. Sci.*, 2005, **30**, 474-490.
12. A. Behr, Y. Brunsch and A. Lux, *Tetrahedron Lett.*, 2012, **53**, 2680-2683.

13. S. Siangwata, MSc dissertation, University of Cape Town, 2015.
14. S. C. Bourque, F. Maltais, W. Xiao, O. Tardif, H. Alper, P. Arya and L. E. Manzer, *J. Am. Chem. Soc.*, 1999, **121**, 3035-3038.
15. S. Hübner, J. G. de Vries and V. Farina, *Adv. Synth. Catal.*, 2016, **358**, 3-25.
16. M. Elard, J. Denis, M. Ferreira, H. Bricout, D. Landy, S. Tilloy and E. Monflier, *Catal. Today*, 2015, **247**, 47-54.
17. N. Guo, L. Li and T. J. Marks, *J. Am. Chem. Soc.*, 2004, **126**, 6542-6543.
18. L. C. Sudding, P. Chellan, P. Govender and G. S. Smith, *J. Inorg. Organomet. Polym. Mater.*, 2015, **25**, 457-465.
19. J. M. J. Fréchet, *Science*, 1994, **263**, 1710.
20. D. A. Tomalia, H. Baker, J. Dewald, M. Hall, G. Kallos, S. Martin, J. Roeck, J. Ryder and P. Smith, *Polym. J. (Tokyo, Jpn.)*, 1985, **17**, 117-132.
21. E. B. Hager, B. C. Makhubela and G. S. Smith, *Dalton Trans.*, 2012, **41**, 13927-13935.
22. L. Maqeda, MSc dissertation, University of Cape Town, 2014.
23. O. Wachsen, K. Himmler and B. Cornils, *Catal. Today*, 1998, **42**, 373-379.
24. S. Siangwata, N. Baartzes, B. C. E. Makhubela and G. S. Smith, *J. Organomet. Chem.*, 2015, **796**, 26-32.
25. H. Azoui, K. Baczko, S. Cassel and C. Larpent, *Green Chem.*, 2008, **10**, 1197-1203.
26. R. Chen, X. Liu and Z. Jin, *J. Organomet. Chem.*, 1998, **571**, 201-204.
27. C. Liu, X. Li and Z. Jin, *Catal. Today*, 2015, **247**, 82-89.
28. Y. Zeng, Y. Wang, J. Jiang and Z. Jin, *Catal. Commun.*, 2012, **19**, 70-73.
29. J. A. Gladysz and D. P. Curran, *Tetrahedron*, 2002, **58**, 3823-3825.
30. E. G. Hope and A. M. Stuart, *J. Fluorine Chem.*, 1999, **100**, 75-83.
31. C. C. Tzschucke, C. Markert, H. Glatz and W. Bannwarth, *Angew. Chem., Int. Ed. Engl.*, 2002, **41**, 4500-4503.
32. I. T. Horváth and J. Rábai, *Science*, 1994, **266**, 72-75.
33. J. Dupont, R. F. de Souza and P. A. Suarez, *Chem. Rev*, 2002, **102**, 3667-3692.
34. T. J. Geldbach and P. J. Dyson, *J. Am. Chem. Soc.*, 2004, **126**, 8114-8115.
35. P. Wasserscheid and W. Keim, *Angew. Chem., Int. Ed. Engl.*, 2000, **39**, 3772-3789.
36. T. Welton, *Chem. Rev*, 1999, **99**, 2071-2084.
37. D. Koch and W. Leitner, *J. Am. Chem. Soc.*, 1998, **120**, 13398-13404.
38. D. J. Cole-Hamilton, *Science*, 2003, **299**, 1702-1706.

39. L. C. Matsinha, S. F. Mapolie and G. S. Smith, *Dalton Trans.*, 2015, **44**, 1240-1248.
40. S. Paganelli, O. Piccolo, P. Pontini, R. Tassini and V. D. Rathod, *Catal. Today*, 2015, **247**, 64-69.
41. S. K. Sharma and R. V. Jasra, *Catal. Today*, 2015, **247**, 70-81.
42. Q. Zhang, S. Zhang and Y. Deng, *Green Chem.*, 2011, **13**, 2619.
43. C. W. Kohlpaintner, R. W. Fischer and B. Cornils, *Appl. Catal., A*, 2001, **221**, 219-225.
44. B. Cornils, *Top. Curr. Chem*, 1999, **206**, 133-152.
45. B. Cornils, *J. Mol. Catal. A: Chem*, 1999, **143**, 1-10.
46. B. Cornils and E. Wiebus, *Recl.: J. R. Neth. Chem. Soc*, 1996, **115**, 211-&.
47. F. Heshmatpour, R. Abazari and S. Balalaie, *Tetrahedron*, 2012, **68**, 3001-3011.
48. P. J. Baricelli, M. Rodriguez, L. G. Melean, M. Modrono Alonso, M. Borusiak, M. Rosales, B. Gonzalez, K. C. B. de Oliveira, E. V. Gusevskaya and E. N. dos Santos, *Appl. Catal., A*, 2015, **490**, 163-169.
49. K. H. Shaughnessy, *Chem. Rev*, 2009, **109**, 643-710.
50. M. Hingst, M. Tepper and O. Stelzer, *Eur. J. Inorg. Chem.*, 1998, **1998**, 73-82.
51. F. Mercier and F. Mathey, *J. Organomet. Chem.*, 1993, **462**, 103-106.
52. D. J. Brauer, K. W. Kottsieper, T. Nickel, O. Stelzer and W. S. Sheldrick, *Eur. J. Inorg. Chem.*, 2001, **2001**, 1251-1259.
53. A. A. Karasik, R. N. Naumov, R. Sommer, O. G. Sinyashin and E. Hey-Hawkins, *Polyhedron*, 2002, **21**, 2251-2256.
54. A. A. Karasik, I. O. Georgiev, O. G. Sinyashin and E. Hey-Hawkins, *Polyhedron*, 2000, **19**, 1455-1459.
55. G. W. Wong, W.-C. Lee and B. J. Frost, *Inorg. Chem.*, 2008, **47**, 612-620.
56. M. Rauhut, I. Hechenbleikner, H. A. Currier, F. Schaefer and V. Wystrach, *J. Am. Chem. Soc.*, 1959, **81**, 1103-1107.
57. K. Issleib and G. Thomas, *Eur. J. Inorg. Chem.*, 1960, **93**, 803-808.
58. D. C. Mudalige and G. Rempel, *J. Mol. Catal. A: Chem*, 1997, **116**, 309-316.
59. H. Hattori, K.-i. Fujita, T. Muraki and A. Sakaba, *Tetrahedron Lett.*, 2007, **48**, 6817-6820.
60. G. Fremy, Y. Castanet, R. Grzybek, E. Monflier, A. Mortreux, A. M. Trzeciak and J. J. Ziolkowski, *J. Organomet. Chem.*, 1995, **505**, 11-16.

61. R. Amengual, E. Genin, V. Michelet, M. Savignac and J. P. Genêt, *Adv. Synth. Catal.*, 2002, **344**, 393-398.
62. R. Amengual, V. Michelet and J.-P. Genêt, *Tetrahedron Lett.*, 2002, **43**, 5905-5908.
63. E. Genin, R. Amengual, V. Michelet, M. Savignac, A. Jutand, L. Neuville and J. P. Genêt, *Adv. Synth. Catal.*, 2004, **346**, 1733-1741.
64. F. Eymery, P. Burattin, F. Mathey and P. Savignac, *Eur. J. Org. Chem.*, 2000, **2000**, 2425-2431.
65. J. Pospech, I. Fleischer, R. Franke, S. Buchholz and M. Beller, *Angew. Chem., Int. Ed. Engl.*, 2013, **52**, 2852-2872.
66. H. Fu, M. Yuan, H. Chen, R. Li and X. Li, *Chin. J. Catal.*, 2010, **31**, 251-260.
67. R. Franke, D. Selent and A. Borner, *Chem. Rev*, 2012, **112**, 5675-5732.
68. A. Buhling, J. W. Elgersma, S. Nkrumah, P. C. J. Kamer and P. van Leeuwen, *J. Chem. Soc., Dalton Trans.*, 1996, **10**, 2143-2154.
69. G. T. Whiteker and C. J. Cobley, in *Organometallics as Catalysts in the Fine Chemical Industry*, eds. M. Beller and H. U. Blaser, 2012, vol. 42, pp. 35-46.
70. A. Chalk and J. Harrod, *Adv. Organomet. Chem.*, 1968, **6**, 119-170.
71. S. L. Desset, PhD thesis, University of St. Andrews, 2009.
72. D. Evans, J. A. Osborn and G. Wilkinson, *J. Am. Chem. Soc.*, 1968, **90**, 3133-3142.
73. B. C. Makhubela, A. M. Jardine, G. Westman and G. S. Smith, *Dalton Trans.*, 2012, **41**, 10715-10723.
74. L. C. Sudding, R. Payne, P. Govender, F. Edafe, C. M. Clavel, P. J. Dyson, B. Therrien and G. S. Smith, *J. Organomet. Chem.*, 2014, **774**, 79-85.
75. A. A. Dabbawala, H. C. Bajaj, H. Bricout and E. Monflier, *Catal. Sci. Technol.*, 2012, **2**, 2273-2278.
76. S. Gladiali, J. C. Bayón and C. Claver, *Tetrahedron: Asymmetry*, 1995, **6**, 1453-1474.
77. A. M. Trzeciak and J. J. Ziolkowski, *Coord. Chem. Rev.*, 1999, **192**, 883-900.
78. C. De, R. Saha, S. K. Ghosh, A. Ghosh, K. Mukherjee, S. S. Bhattacharyya and B. Saha, *Res. Chem. Intermed.*, 2013, **39**, 3463-3474.
79. L. Obrecht, P. C. J. Kamer and W. Laan, *Catal. Sci. Technol.*, 2013, **3**, 541-551.
80. Q. R. Peng, Y. Yang, C. J. Wang, X. L. Liao and Y. Z. Yuan, *Catal. Lett.*, 2003, **88**, 219-225.
81. C. W. Kohlpaintner, R. W. Fischer and B. Cornils, *Appl. Catal., A*, 2001, **221**, 219-225.

82. T. Vanbésien, A. Sayede, E. Monflier and F. Hapiot, *Catal. Sci. Technol.*, 2016, **6**, 3064-3073.

83. F. Hapiot, S. Menuel, H. Bricout, S. Tilloy and E. Monflier, *Appl. Organomet. Chem.*, 2015, **29**, 580-587.

84. F. Hapiot, S. Tilloy and E. Monflier, *Chem. Rev*, 2006, **106**, 767-781.

85. A. Gong, Q. Fan, Y. Chen, H. Liu, C. Chen and F. Xi, *J. Mol. Catal. A: Chem*, 2000, **159**, 225-232.

86. N. Pinault and D. W. Bruce, *Coord. Chem. Rev.*, 2003, **241**, 1-25.

87. H. Bricout, F. Hapiot, A. Ponchel, S. Tilloy and E. Monflier, *Sustainability*, 2009, **1**, 924-945.

88. H. A. Zahalka, K. Januszkiewicz and H. Alper, *J. Mol. Catal.*, 1986, **35**, 249-253.

89. A. A. Dabbawala, H. C. Bajaj, H. Bricout and E. Monflier, *Appl. Catal., A*, 2012, **413**, 273-279.

90. A.-M. Caminade, R. Laurent, B. Delavaux-Nicot and J.-P. Majoral, *New J. Chem.*, 2012, **36**, 217-226.

91. G. R. Newkome, E. He and C. N. Moorefield, *Chem. Rev*, 1999, **99**, 1689-1746.

92. D. Astruc, E. Boisselier and C. Omelas, *Chem. Rev*, 2010, **110**, 1857-1959.

93. D. Astruc and F. Chardac, *Chem. Rev*, 2001, **101**, 2991-3023.

94. D. Astruc, R. Ciganda, C. Deraedt, S. Gatard, L. Liang, N. Li, C. Ornelas, A. Rapakousiou, J. Ruiz, D. Wang, Y. Wang and P. Zhao, *Synlett*, 2015, **26**, 1437-1449.

95. U. Boas, J. B. Christensen and P. M. H. Heegaard, *J. Mater. Chem.*, 2006, **16**, 3785.

96. C. Cordovilla, S. Coco, P. Espinet and B. Donnio, *J. Am. Chem. Soc.*, 2010, **132**, 1424-1431.

97. M. A. Hearshaw and J. R. Moss, *Chem. Commun.*, 1999, 1-8.

98. C. Gorman, *Adv. Mater.*, 1998, **10**, 295-309.

99. S. El Kazzouli, N. El Brahmi, S. Mignani, M. Bousmina, M. Zablocka and J.-P. Majoral, *Curr. Med. Chem.*, 2012, **19**, 4995-5010.

100. J. Liu, Y. Feng, B. Ma, Y.-M. He and Q.-H. Fan, *Eur. J. Org. Chem.*, 2012, **2012**, 6737-6744.

101. S. W. S. Choy, M. J. Page, M. Bhadbhade and B. A. Messerle, *Organometallics*, 2013, **32**, 4726-4729.

102. E. Buhleier, W. Wehner and F. Vögtle, *Chem. Informationsdienst*, 1978, **9**.

103. A. W. Bosman, H. M. Janssen and E. W. Meijer, *Chem. Rev.*, 1999, **99**, 1665-1688.
104. A. Caminade, C. O. Turrin, R. Laurent, A. Ouali and B. Delavaux-Nicot, *Dendrimers - Towards Catalytic, Material and Biomedical Uses*, John Wiley & Sons, Toulouse, France, 2011.
105. J.-P. Majoral and A.-M. Caminade, *Chem. Rev. (Washington, DC, U. S.)*, 1999, **99**, 845-880.
106. D. A. Tomalia, A. M. Naylor and W. A. Goddard, *Angew. Chem., Int. Ed.*, 1990, **29**, 138-175.
107. D. Méry and D. Astruc, *Coord. Chem. Rev.*, 2006, **250**, 1965-1979.
108. H. C. Kolb, M. Finn and K. B. Sharpless, *Angew. Chem., Int. Ed.*, 2001, **40**, 2004-2021.
109. F. P. V. Paoloni, S. Kelling, J. Huang and S. R. Elliott, *Adv. Funct. Mater.*, 2011, **21**, 372-379.
110. L. Liang and D. Astruc, *Coord. Chem. Rev.*, 2011, **255**, 2933-2945.
111. N. U. Kaya, F. E. Du Prez and N. Badi, *Macromol. Chem. Phys.*, 2017, 1600575.
112. A. Carlmark, C. Hawker, A. Hult and M. Malkoch, *Chem. Soc. Rev.*, 2009, **38**, 352-362.
113. B. M. Rosen, C. J. Wilson, D. A. Wilson, M. Peterca, M. R. Imam and V. Percec, *Chem. Rev*, 2009, **109**, 6275-6540.
114. P. Govender, PhD thesis, University of Cape Town, 2014.
115. N. Antonels, MSc dissertation, University of Cape Town, 2010.
116. P. Arya, P. Gautam, N. Venugopal Rao, H. Alper, S. C. Bourque and L. E. Manzer, *J. Am. Chem. Soc.*, 2001, **123**, 2889-2890.
117. D. de Groot, P. G. Emmerink, C. Coucke, J. N. Reek, P. C. Kamer and P. W. van Leeuwen, *Inorg. Chem. Commun.*, 2000, **3**, 711-713.
118. S.-M. Lu and H. Alper, *J. Am. Chem. Soc.*, 2003, **125**, 13126-13131.
119. J. Liu, Y. Feng, Y. He, N. Yang and Q.-H. Fan, *New J. Chem.*, 2012, **36**, 380-385.
120. Y.-H. Tang, A. Ya-Ting Huang, P.-Y. Chen, H.-T. Chen and C.-L. Kao, *Curr. Pharm. Des.*, 2011, **17**, 2308-2330.
121. O. Bourrier and A. K. Kakkar, *Macromol. Symp.*, 2004, **209**, 97-118.
122. V. Rodionov, H. Gao, S. Scroggins, D. A. Unruh, A.-J. Avestro and J. M. Fréchet, *J. Am. Chem. Soc.*, 2010, **132**, 2570-2572.
123. R. Kreiter, A. W. Kleij, R. J. K. Gebbink and G. van Koten, in *Dendrimers IV*, Springer, 2001, pp. 163-199.

124. A. Berger, R. J. K. Gebbink and G. van Koten, in *Dendrimer Catalysis*, Springer, 2006, pp. 1-38.

125. F. Wang, H. Liu, L. Cun, J. Zhu, J. Deng and Y. Jiang, *J. Org. Chem.*, 2005, **70**, 9424-9429.

126. M. Guerrero, N. T. T. Chau, S. Noel, A. Denicourt-Nowicki, F. Hapiot, A. Roucoux, E. Monflier and K. Philippot, *Curr. Org. Chem.*, 2013, **17**, 364-399.

127. G. S. Smith and S. F. Mapolie, *J. Mol. Catal. A: Chem*, 2004, **213**, 187-192.

128. L. Ropartz, K. J. Haxton, D. F. Foster, R. E. Morris, A. M. Z. Slawin and D. J. Cole-Hamilton, *J. Chem. Soc., Dalton Trans.*, 2002, 4323.

129. J. W. Knapen, A. W. van der Made, J. C. de Wilde, P. W. van Leeuwen, P. Wijkens, D. M. Grove and G. van Koten, *Nature*, 1994, **372**, 659-663.

130. A. Buhling, P. C. J. Kamer, P. van Leeuwen and J. W. Elgersma, *J. Mol. Catal. A: Chem*, 1997, **116**, 297-308.

131. M. T. Reetz, G. Lohmer and R. Schwickardi, *Angew. Chem., Int. Ed. Engl.*, 1997, **36**, 1526-1529.

132. L. c. Ropartz, R. E. Morris, D. F. Foster and D. J. Cole-Hamilton, *J. Mol. Catal. A: Chem*, 2002, **182**, 99-105.

Chapter 2

Synthesis and Characterisation of *N,O*-salicylaldimine and *N,P*-iminophosphine Fréchet Dendrons

2.1 Introduction

In the current era, the demand for highly specific materials is increasing at an alarming rate. These materials should be easily functionalised to address an array of utilitarian applications. Polymers form one class of macromolecules which addresses these factors, as it is evident that differences in the architecture can influence the properties of the polymer.[1] Although polymers are well explored,[2-4] the lack of control on the synthesis of polymers does not allow for the efficient tailoring of these structures to suit desired applications.[5] The polydisperse nature of polymers often has reproducibility and characterisation issues, which makes the study of catalytic events more challenging.[1, 6, 7] An alternative is to focus on a class of branched macromolecules, namely dendrimers. Dendrimer synthesis has evolved since the seminal work by Vögtle (cascade molecules),[8, 9] Newkome (arborals)[10-13] Tomalia (polyamidoamine)[4, 6, 14, 15] and Fréchet (poly-benzylether),[16] as it often described as the bridging the gap between polymer science and advanced organic chemistry.[1]

As discussed in Chapter 1, some of the popular dendritic architectures include polyamidoamines (PAMAM),[4, 6, 14, 15] polycarbosilanes,[17-19] poly(propyleneimine) (PPI)[10-13] and specific to this chapter, polybenzyl ethers (Fréchet-type)[16] dendrimers.

Fréchet dendrimers (Scheme 1.8, Chapter 1) are constructed using the convergent method. These individual Fréchet dendrons were synthesized with the specific functional groups (examples include carboxylates,[20] alkyl chains[21] and benzyl groups[16]), and consequently coupled to the core synthon.[1] These Fréchet dendritic systems require an activation/deactivation step for the construction of larger generations. This method of convergent dendrimer synthesis is advantageous over the divergent method, as the dendrimer growth is more efficiently monitored and controlled.[1]

One of the most attractive characteristics of this construction is the preparation of bifunctional dendrimers, whereby the dendrons coupled possesses different functional groups and inherently a combination of several properties within a single molecule is observed (Figure 2.1).[22] One downfall of this synthetic sequence is in the final coupling step, whereby the bulky nature of these dendrons often requires a suitable spacer due to the steric hindrance of these Fréchet dendrons.[1, 20] A unique alternative to overcoming the final coupling step is to utilise the suitable Fréchet dendron and couple this to another molecule via an orthogonal synthesis.

This construction of asymmetric dendrimers yields macromolecules with different properties.[23] The functionalisation of these Fréchet dendrons can potentially produce Janus (co-dendrimers) dendrimers, hybrid dendrimers or importantly asymmetrical core-functionalised dendrons (Figure 2.1).[22, 24-26] The latter is formed whereby a smaller molecule is coupled to the larger Fréchet dendron. Selected examples of asymmetric dendrimers/dendrons include Parrott's bis(pyridyl)amine polyester dendron,[27] Hawker's hybrid polybenzyl ether dendrimer[20] and Liu's Janus-type chiral diphosphane dendrimer respectively (Figure 2.1).[28]

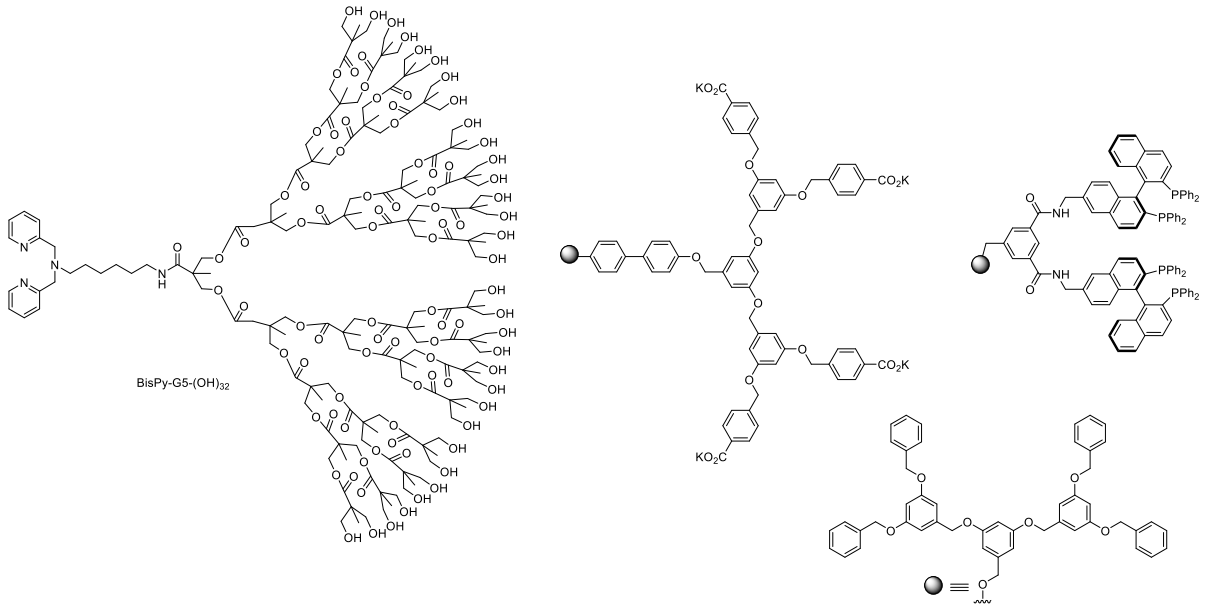

Figure 2.1. *Selected examples of asymmetric dendritic ligands and wedges.*[20, 27, 28]

Parrott's bis(pyridyl)amine polyester dendron[27] and Liu's Janus-type chiral diphosphane dendrimer[28] are interesting synthons, as these molecules can act as ligands for the incorporation of metals. The resultant metallodendrimers formed may offer advanced properties and applications. These include but are not limited to luminescence probes (lasers, light sensors, display),[29, 30] nanoparticle stabilizers,[31] electrode surfaces,[31, 32] contrast agents for NMR,[29, 32] redox active switches,[31] molecular nanobatteries,[33] sensors (ion detection, gas sensing),[29, 34] and in context of this work, transition-metal catalysts.[31]

One method to prepare a well-defined and monodisperse metallodendrimer is to include a high-affinity rhodium ligand at the core of the dendrimer, which allows for the site-specific complexation of the rhodium metal.[35-39] This structural property ensures that complexation is highly facile and limits the generation of polydisperse species which is a common challenge in metallodendrimer synthesis.[23, 40] This site-isolation within the core of dendrimers is a well-known technique.[5]

The use of hemilabile ligands have been well documented, one promising example is the use of Schiff-base ligands. Schiff-bases are formed via condensation between an aldehyde or ketone and amine to form imines. These imines can differ in denticity, however in the context of the hydroformylation reaction, bidentate complexes are favoured due to the chelation with rhodium to form stable 5 or 6-membered rhodacycles. Imines are versatile as

the electronic and steric effects can be altered to suit the desired application. Furthermore these ligands display good stability which is highly favourable for catalytic reactions.[41-45]

As an extension to our previous work on Schiff-base Rh(I) complexes,[41-43, 46-51] we aimed to immobilise the respective Schiff-bases to the suitable Fréchet dendron. It was envisaged that this combination of the dendron and Schiff-base will allow for the modulation of electronic and steric effects. Furthermore the incorporation of the dendritic synthon allows for potential in ultrafiltration separation techniques.

To the best of our knowledge, Fréchet dendrons with Schiff-bases at the focal point have not been reported, which prompted us to explore these Schiff-base dendrons. Since very little research has been done on dendritic wedges in catalysis, this chapter focuses on the synthesis and characterisation of Fréchet and Schiff-base dendrons. These were characterised using ^{1}H, $^{13}C\{^{1}H\}$, $^{31}P\{^{1}H\}$, ^{1}H-^{1}H correlation spectroscopy (COSY), heteronuclear single quantum coherence (HSQC), heteronuclear multiple quantum coherence (HMBC) nuclear magnetic resonance (NMR) spectroscopy, infrared (IR) spectroscopy, mass spectrometry and elemental analysis.

2.2 Protection of peripheral dendrons

2.2.1 Synthesis

The synthesis of 4-(bromomethyl) methyl benzoate (**2.1**) was conducted using modified literature procedures (Scheme 2.1).[52, 53] Esterification was carried out by reacting 4-(Bromomethyl)benzoic acid with methanol in the presence of concentrated sulfuric acid to afford compound **2.1** as a yellow oil in excellent yields (91%).

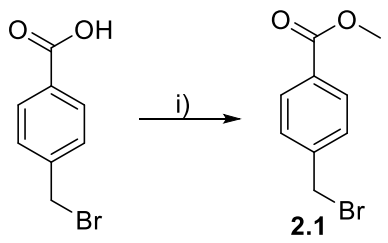

Scheme 2.1. *The Fischer-esterification of 4-(bromomethyl)benzoic acid to 4-(bromomethyl) methyl benzoate (**2.1**). Reagents and conditions: i) MeOH, H_2SO_4 (conc.), reflux, 5 hours.*

The Fischer-esterification is a Lewis or Brønstead acid-catalyzed reaction between a carboxylic acid and alcohol to form the respective ester (Scheme 2.2). The addition of the acid catalyst (H_2SO_4) enhances the electrophilicity of the carbonyl carbon. This is followed by a nucleophilic attack of the alcohol to form a tetrahedral intermediate. A tautomerism occurs whereby one of the hydroxyl groups is eliminated to yield the ester as well as water as a by-product.[52]

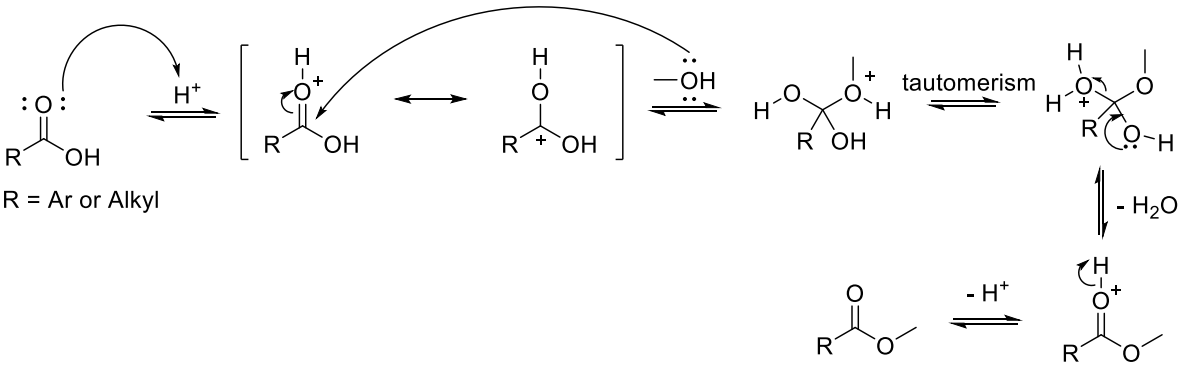

Scheme 2.2. *The proposed general mechanism for the Fischer esterification of aromatic carboxylic acids.*[54]

2.2.2 Characterisation

The methyl ester (**2.1**) was characterised using ^{1}H NMR, $^{13}C\{^{1}H\}$ NMR, infrared (IR) spectroscopy, elemental analysis (C and H) and electron impact mass spectrometry (EI-MS).

2.2.2.1 ^{1}H and $^{13}C\{^{1}H\}$ NMR spectroscopy

The analysis of the ^{1}H NMR spectra of compound **2.1** confirms the successful synthesis of the proposed structure. The ^{1}H NMR spectrum of the ester **2.1** displays an AA'BB' quartet between δ_H 8.01 and 7.45 ppm (Figure 2.2), which corresponds to the *para*-substituted aryl system. The introduction of a new methyl singlet was observed at δ_H 3.91 ppm which integrates for three protons, thus providing evidence of successful esterification. The $^{13}C\{^{1}H\}$ NMR spectrum displays a new signal at δ_C 32.30 ppm which is indicative of a methoxy carbon atom. A total of seven signals were observed in the $^{13}C\{^{1}H\}$ NMR spectrum which correlates to the proposed structure and with literature.[52]

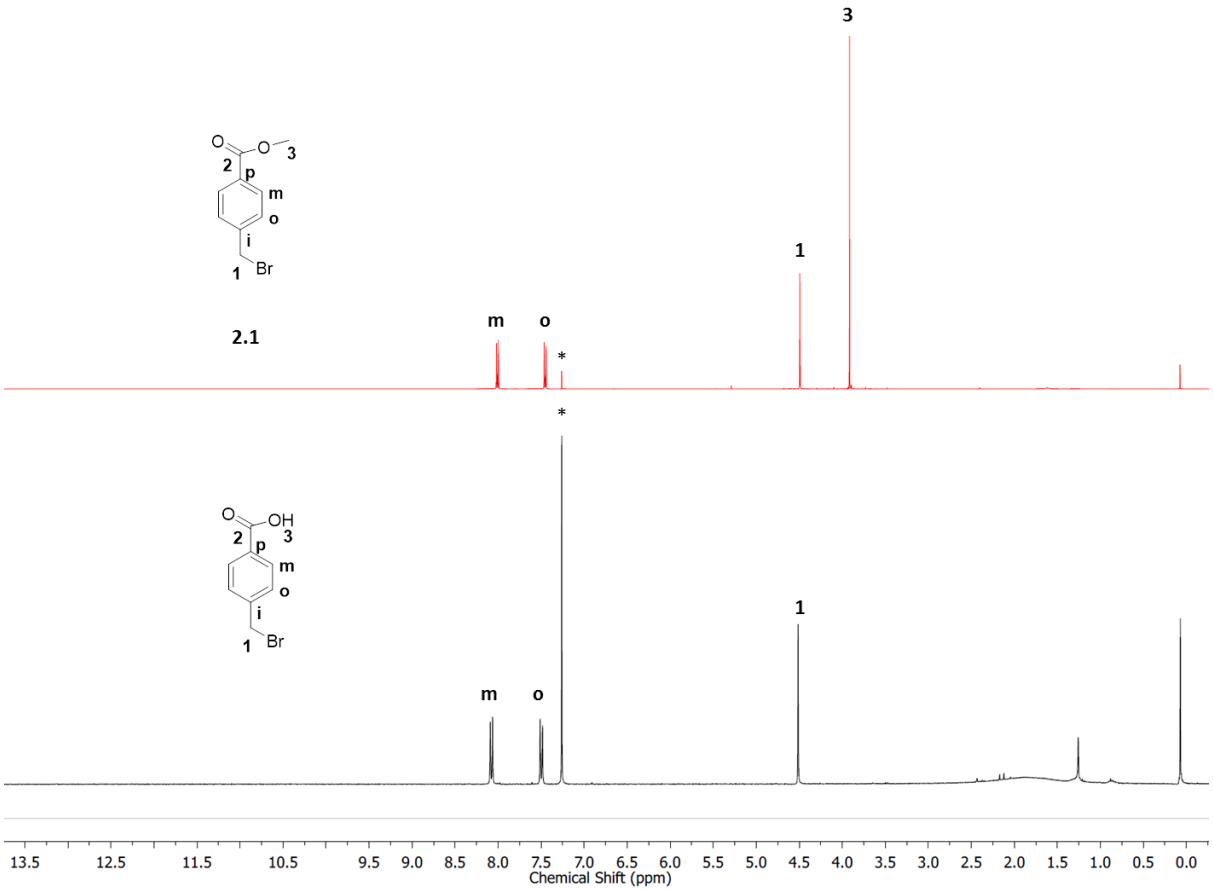

Figure 2.2. *Stacked ^{1}H NMR spectra for 4-(bromomethyl)benzoic acid and compound* ***2.1.*** *The spectra was recorded in $CDCl_3$ (* - $CDCl_3$).*

2.2.2.2 Infrared spectroscopy

Infrared analysis of 4-(bromomethyl)benzoic acid displays a *v*(O-H) and *v*(C=O) signal at 2972 and 1684 cm^{-1} respectively. The absence of the *v*(O-H) signal and shift of the *v*(C=O) signal to 1716 cm^{-1} was observed upon successful esterification. The shift of the carbonyl absorption band to higher wavenumber is attributed to the inductive nature of the methoxy group into the carbonyl signal, which strengthens the C=O bond and shifts the absorption band to higher wavenumbers.

2.2.2.3 Mass Spectrometry and Elemental Analysis

Compound **2.1** was evaluated using electron impact mass spectrometry (EI-MS) to confirm the molecular weight of the product. A base peak was observed at *m/z* 148.96, this corresponds to the $[M\text{-}Br]^+$ fragment. A molecular ion peak was observed at *m/z* 227.90 which corresponds to the $[^{79}M]^+$ parent ion. Furthermore an additional peak of equal

intensity was observed at *m/z* 229.00 which corresponds to the $[^{81}M]^+$ fragment. This phenomenon is consistent for compounds containing a bromido-group.[16] The elemental analysis obtained is within acceptable limits for the expected compound.

2.3 Fréchet Dendrons

2.3.1 Synthesis of Fréchet dendrons with hydroxyl groups at the focal point

A series of Fréchet dendrons (**2.2** and **2.4**) bearing an hydroxyl group at the focal point were synthesized following modified literature methods (Scheme 2.3).[16, 20] The dendritic bromides (**2.1** and **2.3**) were reacted with the monomer unit, 3,5-dihydroxybenzyl alcohol, under standard Williamson-ether conditions employing potassium carbonate as the base and 18-crown-6 as the phase transfer catalyst in refluxing acetone to afford dendrons **2.2** and **2.4** respectively. To drive the reaction to full functionalisation, excess dendritic bromides (1.05 – 1.25 equivalents per phenolic group) were utilised.

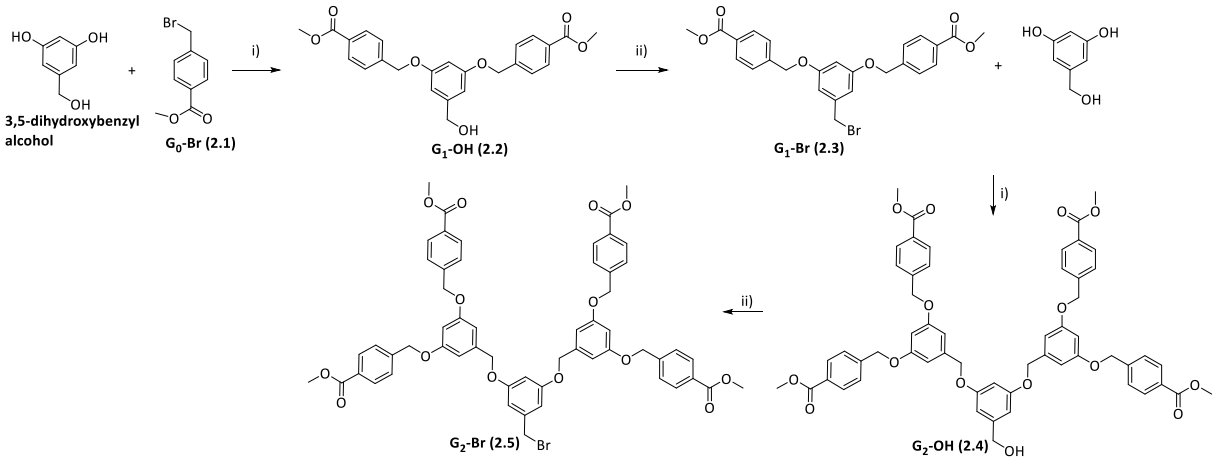

Scheme 2.3. *Synthesis of the methyl ester poly-benzylether dendrons (**2.1 – 2.5**). Reagents and conditions: (i) Williamson-ether synthesis – K_2CO_3/18-crown-6/acetone/reflux/24 hours; (ii) Appel synthesis – CBr_4/PPh_3/toluene/25 °C/0.5 hours.*

The Williamson-ether reaction is the nucleophilic substitution reaction between an alcohol and an organohalide in the presence of a base to form ethers. In the context of Fréchet dendrimer synthesis, the mechanism is based on the reaction between the appropriate

phenol and benzyl bromide in the presence of a suitable base (Scheme 2.4). The deprotonation of the phenol by potassium carbonate forms the respective phenoxide. The phenoxide displays poor solubility in organic media, hence 18-crown-6 (a cryptand, used to solvate metal cations) is used to encapsulate the potassium cation which enhances the nucleophilicity and solubility of the phenoxide. The nucleophilic attack of the phenoxide on the benzylic carbon proceeds in a S_N2 manner to yield the resultant dendrons **2.2** and **2.4**. Note that this reaction was used to synthesize larger generations of the Fréchet dendrons.

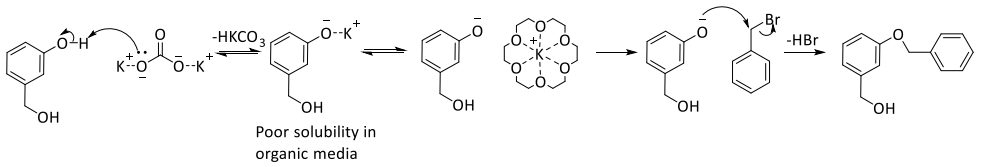

Scheme 2.4. *Proposed mechanism of the Williamson-ether alkylation of phenols and benzylic bromides.*[16]

The dendrons **2.2** and **2.4** were isolated as white powders in good yields (86 – 87%). Compounds **2.2** and **2.4** were soluble in most organic solvents, namely acetone, ethyl acetate, methanol, toluene, dimethyl sulfoxide and chloroform.

2.3.2 Characterisation

2.3.2.1 ^{1}H and $^{13}C\{^{1}H\}$ NMR spectroscopy

The NMR spectrum for compounds **2.2** and **2.4** were recorded in $CDCl_3$. In the ^{1}H NMR spectra of compounds **2.2** and **2.4**, the terminal *para*-substituted aryl ring displays an AA'BB' quartet between δ_H 7.45 – 7.49 and δ_H 8.03 – 8.06 ppm with coupling constants of $^{3}J_{HH}$ = 8.6 Hz respectively. The internal aryl ether protons were observed between δ_H 6.45 – 6.64 ppm. These protons appear as a doublet (2H) and triplet (1H) with a coupling constant of $^{4}J_{HH}$ = 2.30 Hz, as expected for the *meta*-substituted aryl system. The proton resonance denoted as H_p (Figure 2.3, *vide infra*) was used as a diagnostic proton for the elucidation of larger generation dendrons, as this proton integrates for 1H across the dendron series (G_1 and G_2). The unique signals in the region between δ_H 4.20 and 5.20 ppm were assigned to the methylene proton resonances. A downfield shift was observed between the G_n-Br (**2.1** and **2.3**) precursor and the alkylated product (**2.2** and **2.4**) from δ_H 4.49 – 4.64 for the G_1-OH

(**2.2**) dendron and 4.37 – 4.60 ppm for the G_2-OH (**2.4**) dendron. This shift was attributed to the more electron-withdrawing character of the aryl ether group in comparison to the bromide moiety. The methoxy proton resonance (–O**CH$_3$**) was observed at δ_H 3.94 ppm and integrates for 6H and 12H for the G_1-OH (**2.2**) and G_2-OH (**2.4**) dendrons respectively. In comparison to the starting material, the absence of the phenol proton (Ar-O**H**) resonance indicates that dialkylation was observed. Furthermore, the integration of the proton resonances is consistent with the proposed structures and confirms the successful synthesis of compounds **2.2** and **2.4**.

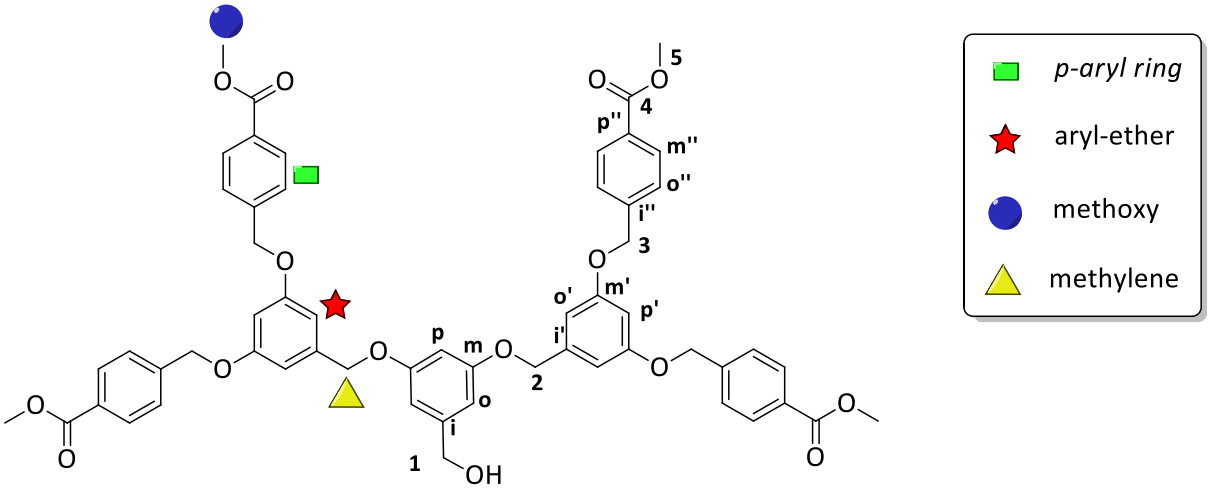

Figure 2.3. *Molecular structure and assignment for the diagnostic carbon and proton signals for the G2-OH (**2.4**) dendron.*

There were distinct differences observed when comparing the ^{1}H NMR spectra between the G_1-OH (**2.2**) and G_2-OH (**2.4**) dendrons. Peak broadening was observed for larger generations, which is due to the reduced tumbling of the larger macromolecule in solution.[20] For larger generation dendrons (**2.4**), three additional peaks are observed. Two new aryl ether peaks are observed between δ_H 6.52 – 6.68 ppm and an additional methylene peak is observed at δ_H 4.96 ppm for compound **2.4**, which corresponds well with literature.[20]

The $^{13}C\{^{1}H\}$ NMR spectra displays the expected number of peaks for both generations (**2.2** and **2.4**, Scheme 2.3). The methylene (C_1, C_2 and C_3) and methoxy (C_5) signals are observed between δ_C 51 – 70 ppm. The aryl ether methine carbon signals (C_o, C_p, $C_{o'}$, $C_{p'}$) are observed between δ_C 101 – 109 ppm. The terminal *para*-substituted methine carbon signals ($C_{m''}$ and $C_{o''}$) are observed between δ_C 126 – 131 ppm. The carbon resonances for the quaternary carbons are observed between δ_C 138 – 168 ppm. The carbon signals were assigned using HSQC and HMBC 2D-NMR spectroscopic techniques. The numbers of carbon signals are consistent with the proposed structures **2.2** and **2.4**. Furthermore the NMR spectroscopic data is in agreement with literature.[20]

2.3.2.2 Infrared spectroscopy

Infrared spectroscopy was used to assist in the characterisation of the dendrons. No phenolic vibrations *v*(ArO-H) were observed at 3150 cm^{-1} attesting to successful dialkylation to afford compounds **2.2** and **2.4**. The presence of a broad band at 3508 cm^{-1} is indicative of the *v*(O-H) vibration. Furthermore the ester *v*(C=O) absorption band at 1720 cm^{-1} confirms the presence of the ester moiety.[20]

2.3.2.3 Mass Spectrometry and Elemental Analysis

Mass spectrometry was conducted for compounds **2.2** (EI-MS) and **2.4** (MALDI-TOF-MS). A molecular ion peak was observed at *m/z* 436.2 which corresponds to the $[M]^+$ fragment for compound **2.2**. Due to the larger molecular weight of compound **2.4**, matrix-assisted laser desorption/ionisation time-of-flight mass spectrometry (MALDI-TOF-MS) was used elucidate the proposed structure. A peak was observed at *m/z* 999.4, which corresponds to the sodium adduct of the proposed structure, $[M + Na]^+$. The elemental analysis for compounds **2.2** and **2.4** are in agreement with the calculated values. Thus, the characterisation obtained further corroborates the synthesis of the proposed structures **2.2** and **2.4**.

2.3.3. Activation of the Fréchet Dendrons *via* the Appel synthesis

2.3.3.1 Synthesis

The first and second generation dendrons bearing a bromide at the focal point (**2.3** and **2.5** respectively) were synthesized using known methods.[16, 20] The G_1-OH (**2.2**) and G_2-OH (**2.4**) dendrons were activated to the G_1-Br (**2.3**) and G_2-Br (**2.5**) dendrons via the Appel reaction (Scheme 2.3). The reaction converts alcohols into the corresponding halides in the presence of halophosphonium salts (Scheme 2.5). Initially the Appel salt is formed by the nucleophilic attack of triphenylphosphine on the carbon atom of carbon tetrabromide. The resulting carbanion ($-CBr_3$) is stabilized inductively by the three bromide groups. This carbanion acts as a base to deprotonate the hydroxyl group, and in turn enhances the nucleophilicity of the hydroxide formed. The attack of the hydroxide group on the bromophosphonium ion ($Br-PPh_3$) results in the release of the bromide anion. The bromide anion attacks the resonance stabilized oxophosphonium carbon in an S_N2 manner to yield the product and consequently releases triphenylphosphine oxide as a by-product.

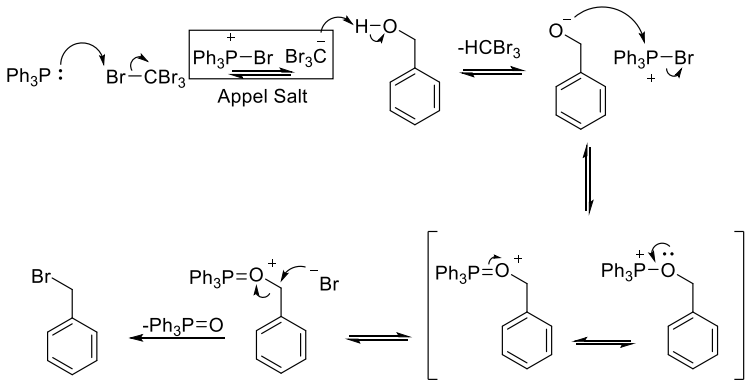

Scheme 2.5. *Proposed mechanism for the bromination of benzylic alcohols via the Appel reaction.*[16]

The G_1-Br (**2.3**) and G_2-Br (**2.5**) dendrons were isolated as white powders in excellent yields (90 – 92%). Compounds **2.3** and **2.5** are readily soluble in most organic solvents such as dichloromethane, toluene, acetone, dimethyl sulfoxide, and tetrahydrofuran. Notably the dendrons are sparingly soluble in methanol.

2.3.4 Characterisation

2.3.4.1 ^{1}H and $^{13}C\{^{1}H\}$ NMR spectroscopy

The ^{1}H NMR spectroscopic analyses of the 1st and 2nd generation dendrons (**2.3** and **2.5** respectively) were similar to that of their precursors (**2.2** and **2.4** respectively). The distinct differences includes the absence of the –O**H** proton signal at 5.17 ppm in d^{6}-DMSO, indicating successful functional group conversion. Further evidence is the shift of the methylene proton resonance (C**H$_2$**-OH) from δ_H 4.37 to 4.64 ppm, indicative of the conversion from the CH_2-OH to the CH_2-Br moiety (C_1, Figure 2.3). The chemical shift and magnitude of the shift correlates with literature.[20] The integration of the proton resonances were consistent with the proposed structures. Four distinct regions are visible in the stacked ^{1}H NMR spectra for compounds **2.1** – **2.5** (Figure 2.4). These are namely the *para*-substituted aryl ring δ_H (7.25 – 8.25 ppm), aryl-ether δ_H (6.25 – 6.75 ppm), methylene δ_H (4.25 – 5.25 ppm) and methoxy δ_H (3.92 ppm) regions. The AA'BB' quartet occurs between δ_H 7.30 – 8.10 ppm, these protons show a gable effect, which is indicative of a *para*-substituted aryl system. The aryl-ether core displays proton resonances between δ_H 6.30 – 6.80 ppm, these are inherently absent for compound **2.1**. The benzylic methylene proton resonances appear between δ_H 4.10 and 5.20 ppm. Each generation size (**2.1** – **2.5**) has a distinct number for aryl-ether and methylene proton resonances, these are displayed in Table 2.1.

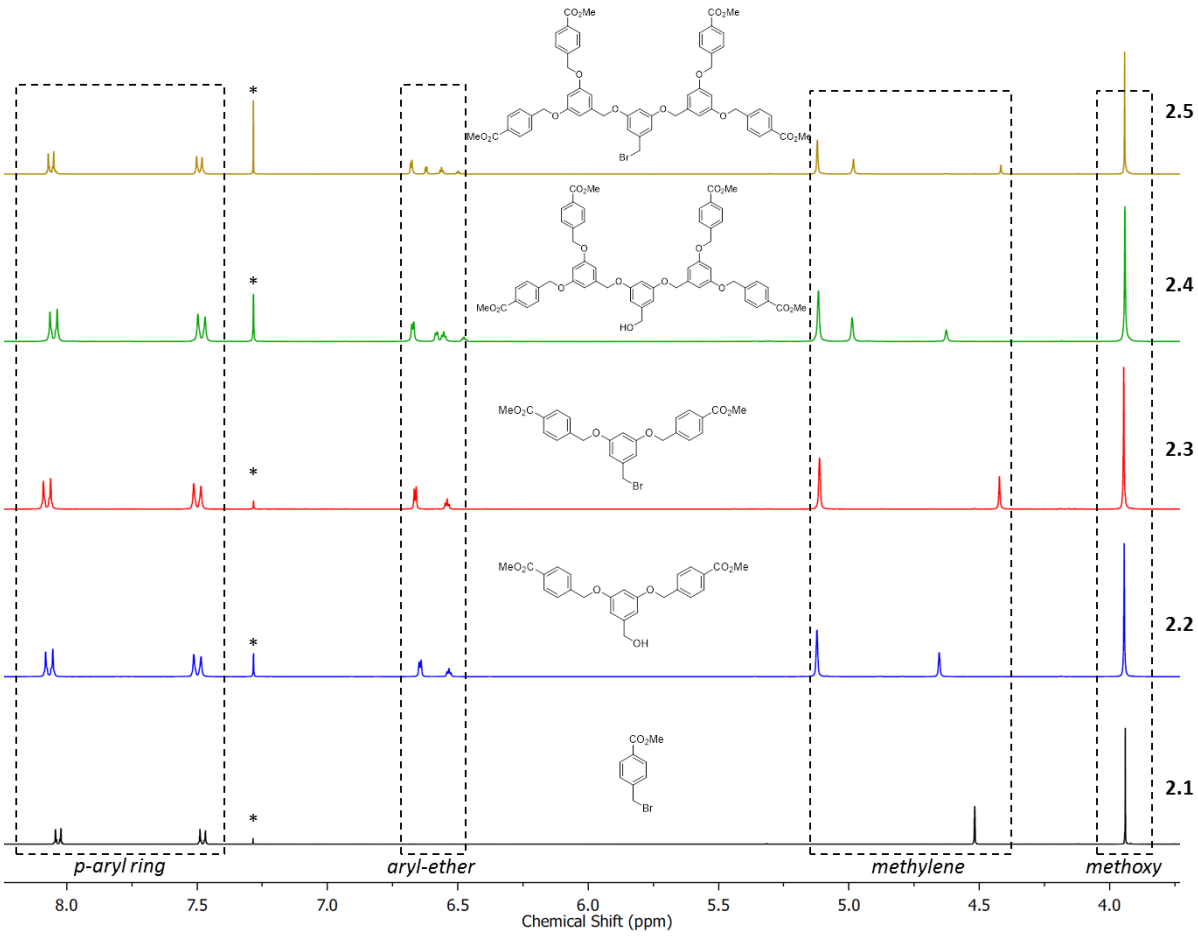

Figure 2.4. *^{1}H NMR spectra for the Fréchet dendron series **2.1 – 2.5** in $CDCl_3$. (* - $CDCl_3$). Refer to Figure 2.3 to distinguish between the p-aryl, aryl ether, methylene and methoxy proton signals.*

Table 2.1. *The distinct number of aryl-ether and methylene signals per Fréchet dendron.*

Compound	Generation number	Aryl-ether protons	Methylene signals
2.1	0	0	1
2.2 and 2.3	1	2	2
2.4 and 2.5	2	4	3
G_n	n	n x 2	n + 1

More importantly, as the generation size is increased, no significant changes are experienced in solution, which implies that these dendrons are stable and the conformations are comparable.

2.3.2.2 Infrared Spectroscopy

The G_1-Br and G_2-Br dendrons (**2.3** and **2.5** respectively) were recorded in solid state using attenuated total reflection (ATR) sampling technique. The absence of the absorption band *v*(O-H) at 3508 cm^{-1} suggests the successful functional group conversion. Similarly to compounds **2.2** and **2.4**, the characteristic *v*(C=O) signals were observed at 1720 cm^{-1}.

2.3.2.3 Mass Spectrometry and Elemental Analysis

Mass spectrometry was conducted using either ESI-MS or MALDI-TOF-MS in both positive and negative modes. For the G_1-Br (**2.3**) and G_2-Br (**2.5**) dendrons, sodium and potassium adducts of the parent ion was observed in both cases (Figure 2.5). The isotopic adducts, $[^{79}M + Na]^+$ and $[^{81}M + Na]^+$, were observed in a 1:1 ratio, this phenomenon is indicative of a bromide-containing substrate whereby the isotopes exist in approximately a 1:1 ratio. Elemental analysis was obtained for the Fréchet dendrons **2.3** and **2.5**, and the experimental data is in agreement with the calculated values.

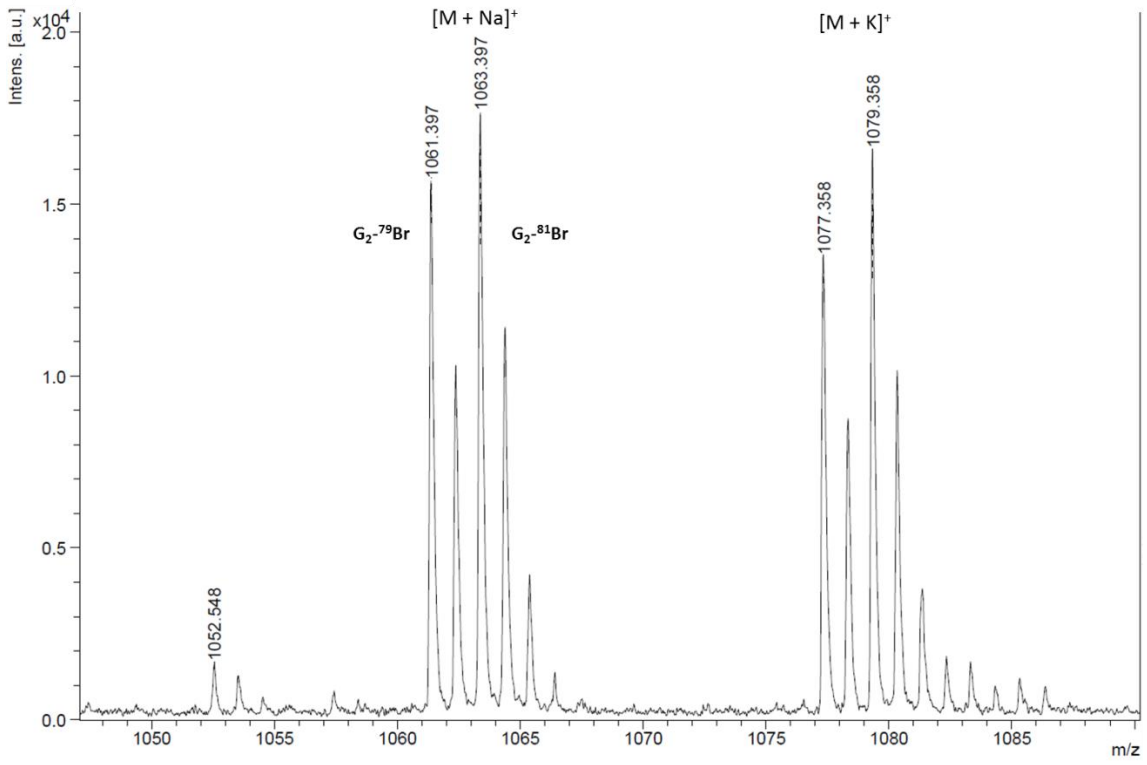

Figure 2.5. *MALDI-TOF-MS spectrum conducted in positive mode (+ve) for compound* ***2.5.*** *Importantly note that both sodium and potassium adducts were observed for compound* ***2.5*** *in the positive mode.*

2.4 Schiff-Base Ligands

2.4.1 Synthesis

The Schiff-base ligands **2.6** and **2.7** were synthesized using modified literature methods (Scheme 2.6).[55, 56] Salicylaldehyde or 2-diphenylphosphinobenzaldehyde was reacted with 4-aminophenol via a Schiff base condensation reaction to afford the respective imine products **2.6** and **2.7** respectively.

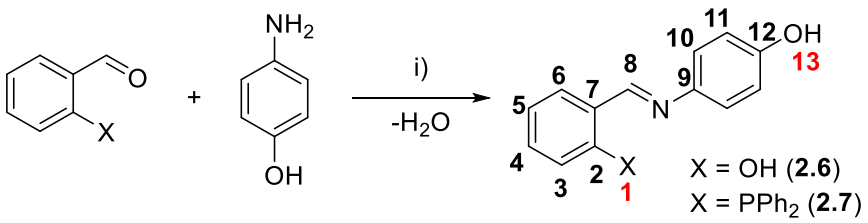

Scheme 2.6. *Synthesis of Schiff-base ligands* ***2.6*** *and* ***2.7****. Conditions and reagents: i) EtOH, reflux, 4 hours.*

The nucleophilic aryl amine attacks the electrophilic formyl carbon (Scheme 2.7). The tetrahedral intermediate formed is followed by the elimination of water to yield the conjugated aromatic imine. Generally the reaction is promoted in the presence of an acid, however the resultant conjugation and inherent product stability drives the reaction to form aryl imines.

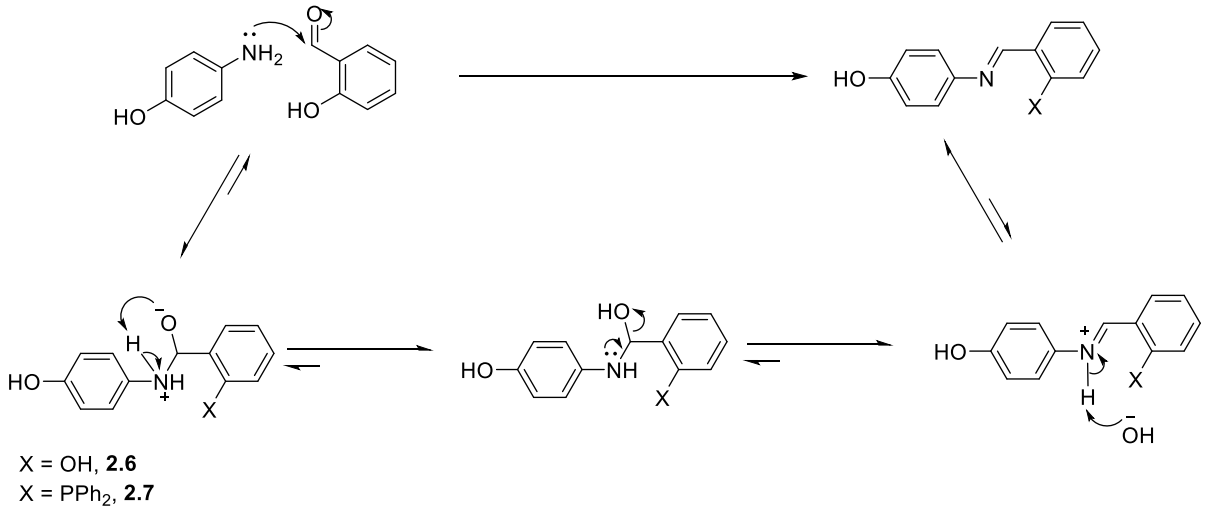

X = OH, **2.6**
X = PPh_2, **2.7**

Scheme 2.7. *The reaction mechanism of the Schiff-base condensation reaction to form compounds **2.6** and **2.7**.*[55, 57]

The Schiff-base products **2.6** and **2.7** were isolated as orange and yellow block-like crystals respectively in high yields (81 – 94%).

2.4.2 Characterisation

2.4.2.1 ^{1}H, $^{13}C\{^{1}H\}$ and $^{31}P\{^{1}H\}$ NMR spectroscopy

The ^{1}H and $^{13}C\{^{1}H\}$ NMR spectra were recorded in $CDCl_3$. These were compared to literature and are well in agreement.[55, 56] The ^{1}H NMR spectra of **2.6** and **2.7** shows a distinct upfield shift of the aldehyde (C**H**O) proton resonance δ_H (10.26 – 10.55) to the imine (C**H**N) proton resonance δ_H (8.59 – 9.08) for compounds **2.6** and **2.7** respectively. The aryl protons for the 4-aminophenol spin system are observed in the region of δ_H 6.85 – 7.24 ppm, these are observed as a doublet pair ($^{3}J_{HH}$ = 8.8), which is expected for a *para*-substituted aryl ring. This AA'BB' quartet displays the corresponding gable effect which is commonly observed for *para*-substituted aryl rings.[55, 56]A downfield shift was observed for protons H_{10} (Scheme 2.6),

with this shift being attributed to the electron withdrawing nature of the imine. Furthermore the absence of the broad amine proton signal (-N**H$_2$**) at δ_H 4.35 ppm suggests successful Schiff-base formation. In the COSY spectrum of compound **2.6**, the imine signal (H_8, Scheme 2.6) at δ_H 8.59 ppm couples with proton H_6 on the salicylaldimine moiety, thus further attesting to the correct assignment of compound **2.6**.

The ^{1}H NMR spectrum of compound **2.7** displays the imine proton resonance as a doublet. This observation is attributed to the through space coupling to the spin active ^{31}P atom.[56] To confirm whether the coupling is through bonds or through space, the phosphine oxide was synthesized for compound **2.7** (Figure 2.6). Upon oxidation, the lone pair of the phosphorous atom is unable to couple to the imine. This results in the imine proton being observed as a singlet. This observation confirms that the coupling is through space and not through bonds. Further evidence of the condensation reaction for compound **2.7** includes the shift of the phosphorous signal in the ^{31}P{^{1}H} NMR from δ_P -11.70 to δ_P -13.24 ppm. This shift is comparable to literature for similar compounds.[56]

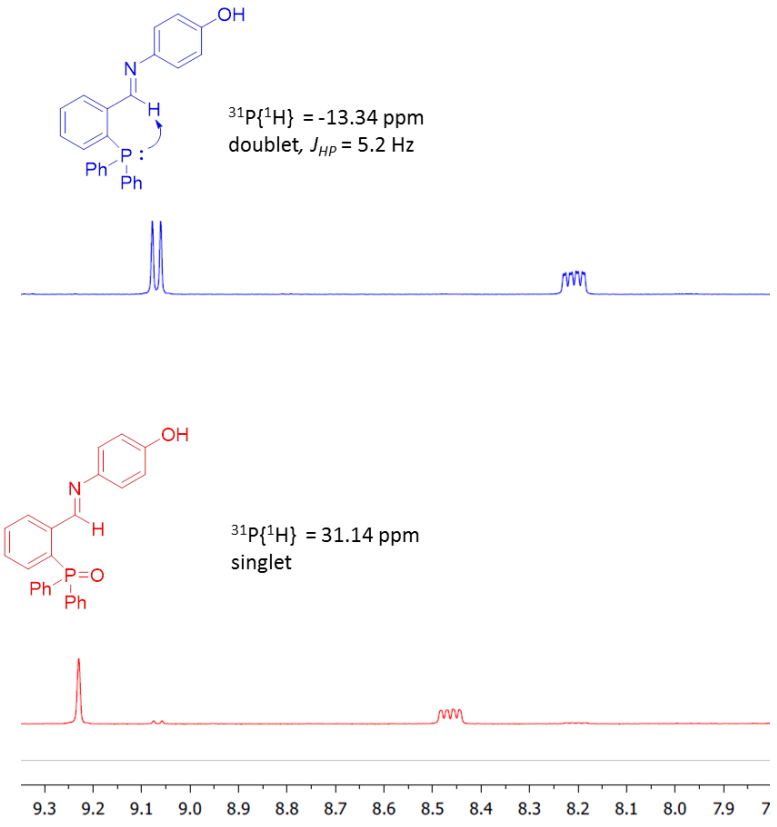

Figure 2.6. *Stacked ^{1}H NMR spectra which displays the through space coupling of phosphorous to the imine proton. The ^{1}H NMR spectra were recorded in $CDCl_3$.*

In the $^{13}C\{^{1}H\}$ NMR spectrum, the number of peaks correlates to that of the proposed compounds **2.6** and **2.7**. The signals for the imine carbon atoms (H**C**=N) are assigned between δ_C 156 – 161 ppm (Table 2.2). The phenolic (**C**OH) carbon resonances were observed between δ_C 154 – 161 ppm. Furthermore the methine carbon (C=**C**H) resonances for the *para*-aminophenol moiety are observed between δ_C 115 – 122 ppm. With respect to compound **2.7**, the phosphorous atom is 100% abundant (spin of ½), hence this atom can couple to neighbouring carbon atoms in the $^{13}C\{^{1}H\}$ spectrum. Therefore all carbon atoms within 4 bonds of the phosphorous atom were observed as a doublet (J_{PC}). The coupling constants for $^{1}J_{CP}$, $^{2}J_{CP}$, $^{3}J_{CP}$ and $^{4}J_{CP}$ were observed and were elucidated to be 17 Hz, 20 Hz, 15 Hz and 4 Hz respectively. These coupling constants corresponds to literature for structurally similar *N,P*-iminophosphine compounds.[56, 58]

Table 2.2. *Selected spectroscopic and analytical data for the Schiff bases **2.6** and **2.7**.*

Compound	^{1}H NMR (imine) [ppm][a]	$^{13}C\{^{1}H\}$ NMR (imine) [ppm][a]	IR (imine) [cm^{-1}][b]	EI-MS [*m/z*][c]
2.6	8.59	160.70	1615	213.01
2.7	9.08	156.88	1615	381.00

[a] Recorded in $CDCl_3$

[b] Recorded in solid state

[c] $[M]^+$

2.4.2.2 Infrared Spectroscopy

The absorption band for the aldehyde signals *v*(C=O) were observed at 1661 cm^{-1} and 1696 cm^{-1} for salicylaldehyde and 2-diphenylphosphinobenzaldehyde respectively. Upon condensation, the imine moiety appears as an intense absorption band at 1615 cm^{-1} for compounds **2.6** and **2.7**. The phenolic *v*(O-H) band was observed between 3200 – 3050 cm^{-1} for compounds **2.6** and **2.7**. Compound **2.6** can potentially tautomerise from the

hydroxyimine to the ketoamine (Scheme 2.8). The amine *v*(N-H, ≈ 3300 cm^{-1}) and carbonyl *v*(C=O, ≈ 1700 cm^{-1}) absorption bands were not observed in IR spectroscopy for compound **2.6**.[59]

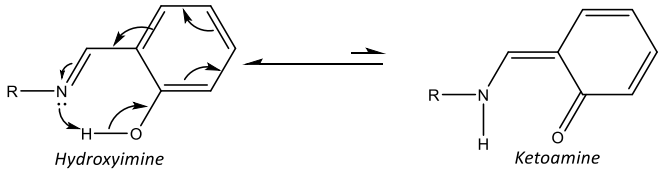

Scheme 2.8. *Proposed tautomerism for the N,O-salicylaldimine Schiff bases.*[60]

2.4.2.3 Mass Spectrometry and Elemental Analysis

Compounds **2.6** and **2.7** were analysed using electron impact mass spectrometry. Base peaks were observed at 213.01 and 381.00 (*m/z*) respectively, which corresponds to the parent ion, $[M]^+$. Similarly, the elemental analysis data obtained is in agreement with the calculated values and are within acceptable limits.

2.5 Schiff Base Dendrons

2.5.1 Synthesis

The Schiff-base ligands (**2.6** and **2.7**) were immobilised with the bromide-Fréchet dendrons (**2.1, 2.3** and **2.5**) *via* the Williamson ether synthesis. This yielded a new class of Fréchet dendrons with Schiff bases at the focal point (**2.8** – **2.13**, Scheme 2.9).

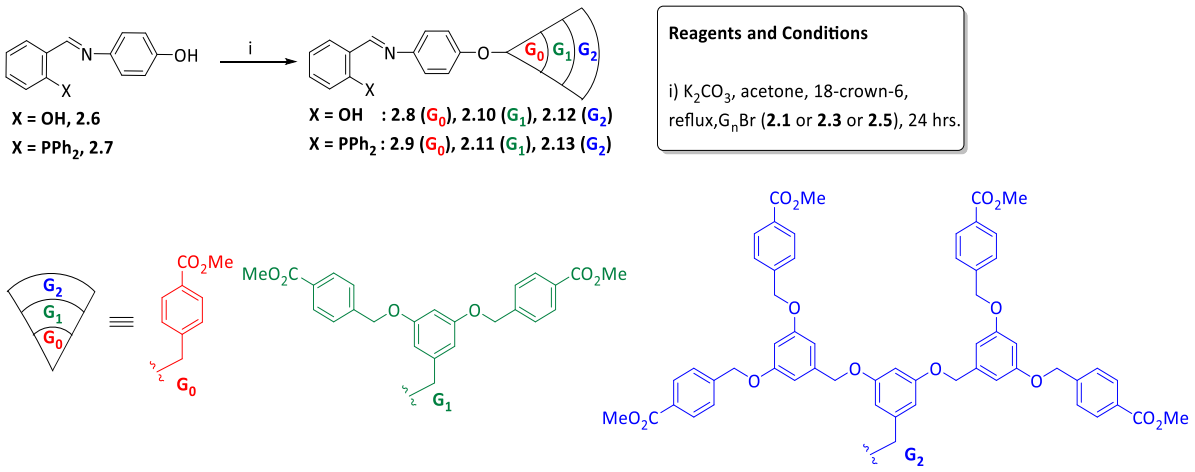

Scheme 2.9. *Synthesis of the Schiff-base dendrons **2.8** – **2.13**. i) 18-C-6 (cat.)/K_2CO_3/acetone/reflux/18 – 48 hours.*

The Schiff-base dendron products (**2.8** – **2.13**) were isolated as either yellow crystalline solids (**2.8** and **2.9**) or as yellow powders (**2.10** – **2.13**) in high yields (85 – 96%). The compounds **2.8** – **2.13** had similar solubility in comparison to the Fréchet dendron precursors (**2.1**, **2.3** and **2.5**). More importantly, the G_1 and G_2 Schiff base dendrons (**2.10** – **2.13**) were poorly soluble in methanol. This property was useful for the purification of larger generations. The compounds **2.8** – **2.13** display good thermal stability with melting points ranging between 130 – 161 °C.

2.5.2 Characterisation

2.5.2.1 ^{1}H , $^{13}C\{^{1}H\}$ and $^{31}P\{^{1}H\}$ NMR spectroscopy

The Williamson-ether coupling can take place at two sites (Figure 2.7, OH-1 or OH-13) for compound **2.6**. The ^{1}H NMR spectrum of compound **2.6** displays two broad signals at δ_H 13.41 and 9.66 ppm, these are assigned to proton **1** and **13** respectively. The ^{1}H NMR of the product (**2.8, 2.10** and **2.12**) shows one broad phenolic signal between δ_H 13.23 – 13.26 ppm. This signal integrates in a 1:1 ratio with the imine, which suggests that the Williamson-ether synthesis had occurred at one site exclusively, hence the reaction proceeds with 100% regioselectivity.

To confirm the site of alkylation, literature and prediction software were used to identify molecules which had similar electronics and structures (Figure 2.7). The data depicted in Figure 2.7, shows predicted and literature values for the phenolic protons (Ar-O**H**) of structurally similar *N,O*-salicylaldimine ligands.[61, 62] The presence of the broad signal between δ_H 13.23 – 13.26 ppm indicates that alkylation had occurred at position 13 (Figure 2.7).[61, 62] Notably excess equivalents of the benzylic bromide and longer reaction times were used to evaluate whether any alkylation was possible at position 1 (Figure 2.7), however alkylation at position 13 was exclusive.

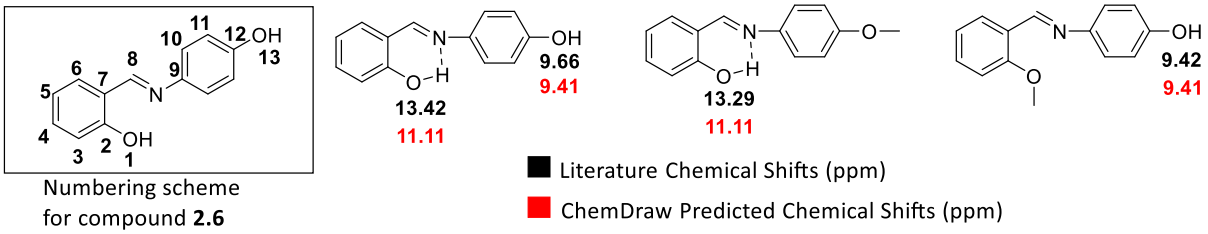

Figure 2.7. *Experimental and Chemdraw predicted chemical shifts for selected N,O-salicylaldimines.*[61, 62] *The experimental and literature chemical shifts were calculated or recorded in d*[6]*-dmso.*

The ^{1}H and $^{13}C\{^{1}H\}$ NMR were recorded in either $CDCl_3$ or d_6-DMSO. The ^{1}H NMR spectra was useful to determine the alkylation mode for compounds **2.8** – **2.13** (Figure 2.7). From ^{1}H NMR, no phenolic signal (-OH) was observed at δ_H 9.66 ppm, which is indicative of the successful Williamson-ether reaction (Compound **2.10**, Figure 2.8). Furthermore a shift of the bromo-methylene signal was observed (H_{13}, Figure 2.8), which indicates that the nucleophilic attack had occurred at the reactive benzylic position. A small shift was observed for the imine signal which indicates that there is no significant effect of the dendron on the electronics of the aryl imine. The integration of compounds **2.8** – **2.13** correlate to that of the proposed compounds.

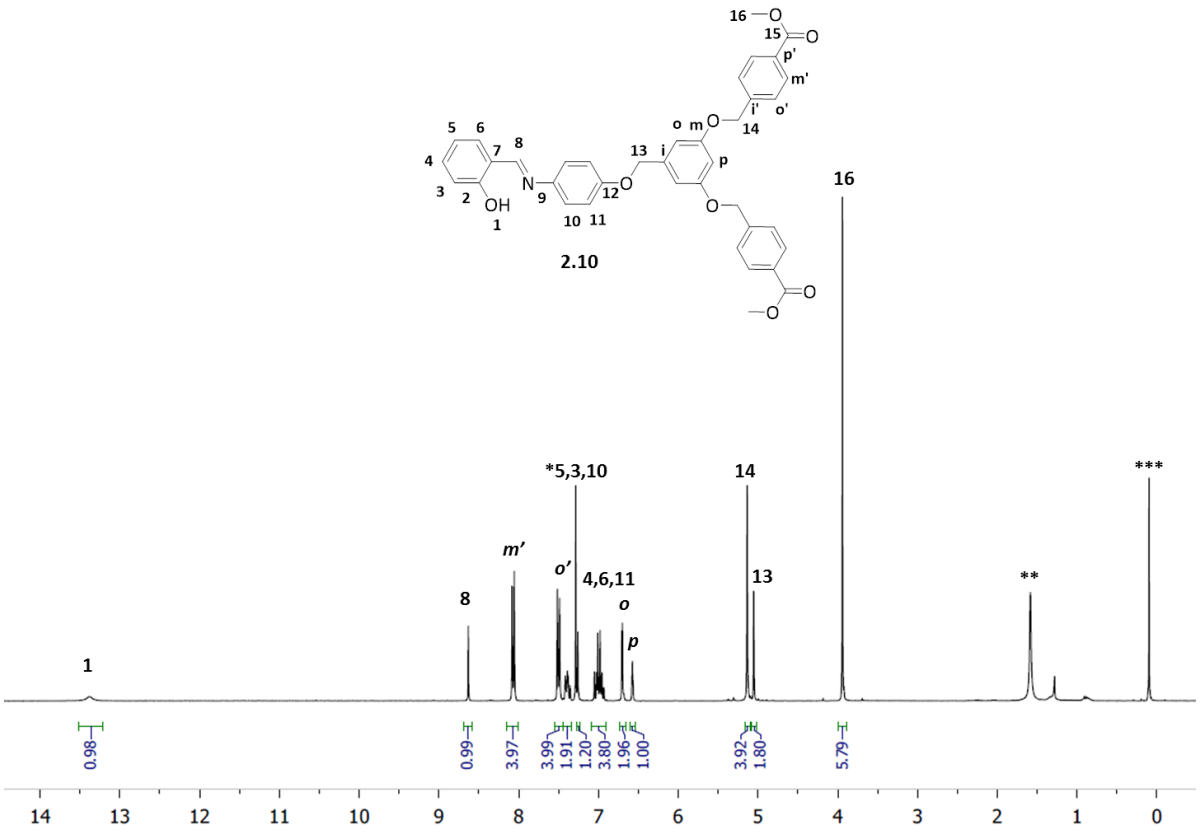

Figure 2.8. *Representative structure for Fréchet dendrons with N,O-salicylaldimine at the focal point, namely compound* ***2.10****. The* ^{1}*H NMR was recorded in* $CDCl_3$*. Importantly note that the integration obtained matches that for the expected compound. (*, ** and *** denotes* $CDCl_3$*,* H_2O *and TMS respectively).*

A comparison across the dendron series (**2.8, 2.10** and **2.12**) is depicted by the stacked ^{1}H NMR spectra (Figure 2.9, *vide infra*). The regions of significant interest are the methylene region between δ_H 4.75 – 5.75 ppm (-CH_2, Figure 2.9) and the aryl-ether region δ_H 6.30 – 6.80 ppm. Notably an increase in generation size results in a similar effect as displayed in Figure 2.4. Peak broadening was observed for compound **2.12**, which is expected due to the overlap of aryl-ether protons and inherent reduced tumbling of the macromolecule in solution as indicated by ^{1}H NMR spectroscopy.

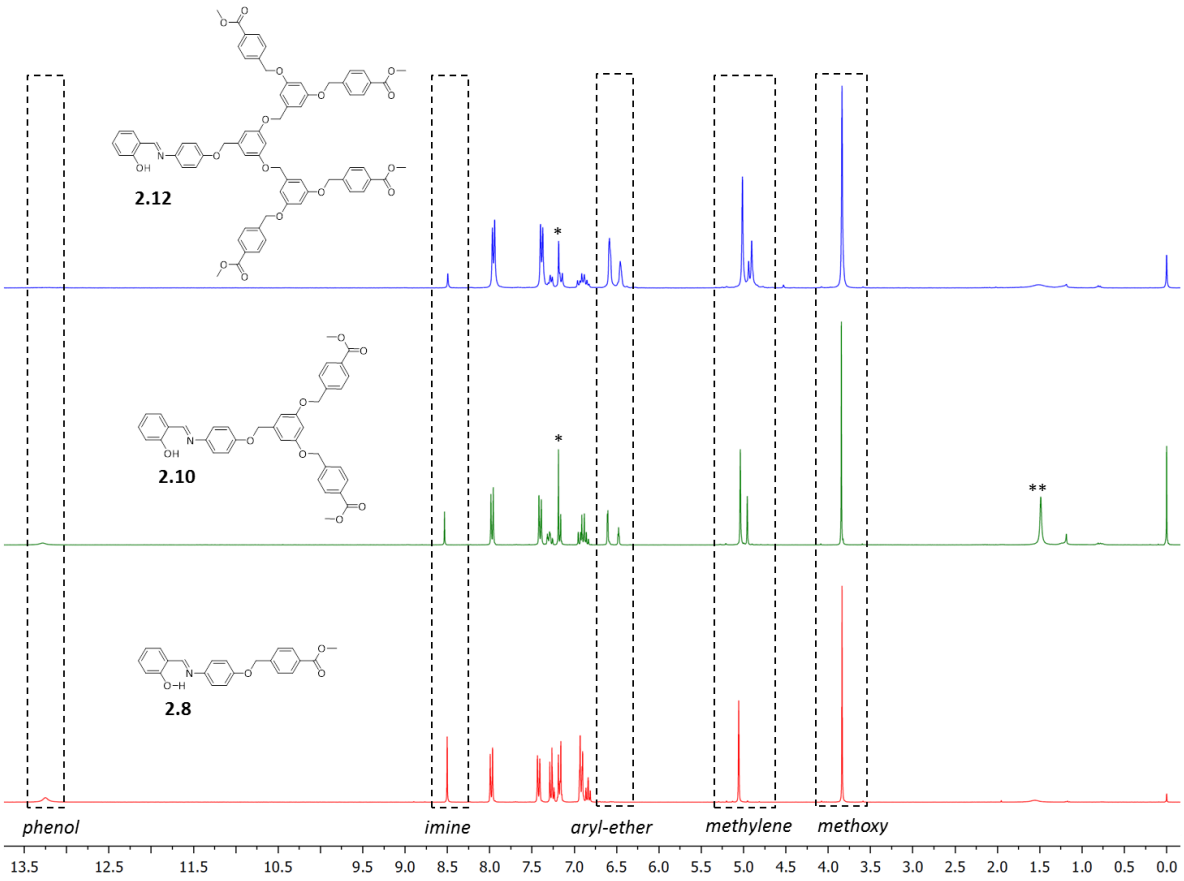

Figure 2.9. *Stacked ^{1}H NMR spectra for compound **2.8, 2.10** and **2.12** respectively. Note the region between δ_H 4.75 – 5.75 ppm for the methylene proton resonances and δ_H 6.30 – 6.80 ppm for the aryl-ether proton resonances. The spectra for **2.8, 2.10** and **2.12** were recorded in $CDCl_3$ (* - $CDCl_3$, ** - H_2O).*

In the ^{13}C NMR spectrum for compounds **2.8** – **2.13**, the number of carbons resonances correlates to the proposed structures. Chemical shifts of selected imine signals are tabulated (Table 2.3). Similar trends were observed in the $^{13}C\{^{1}H\}$ spectra for *N,O*-salicylaldimine moiety of **2.6** and the *N,O*-salicylaldimine moiety of the Schiff-base dendrons (**2.8, 2.10** and **2.12**). This observation further suggests that the dendron has a small effect on the electronics of the Schiff-base moiety. The Schiff-base dendrons (**2.8**-**2.13**) and bromido-Fréchet dendrons (**2.1**, **2.3** and **2.5**) display similar chemical shifts for the dendron moiety, except for the bromo-methylene carbon which displays a chemical shift difference of $\Delta\delta_C \approx 18$ ppm upon the successful Williamson-ether synthesis.

Table 2.3. *Selected spectroscopic and analytical data of the Schiff-base dendrons **2.8** – **2.13**.*

Schiff-Base Dendron	^{1}H NMR (imine) [ppm][a]	$^{13}C\{^{1}H\}$ NMR (imine) [ppm][a]	^{1}H NMR (Ar-O<u>H</u>) [ppm][a]	$^{31}P\{^{1}H\}$ NMR [ppm][a]	IR (imine) [cm^{-1}][b]	MS ($[M]^{+}$) [*m/z*][c]
2.8	8.53	161.06	13.25	-	1617	361.13[c]
2.10	8.51	159.66	13.26	-	1617	632.10[d]
2.12	8.49	160.71	13.26	-	1617	1172.59[e]
2.9	9.11	157.30	-	-13.25	1613	529.04[c]
2.11	9.09	156.65	-	-13.26	1611	799.86[e]
2.13	9.08	156.97	-	-13.29	1611	1340.43[e]

[a] Recorded in $CDCl_3$

[b] Recorded in solid state (ATR)

[c] EI-MS

[d] ESI-MS (+ve mode)

[e] MALDi-TOF-MS (+ve mode)

HMBC (heteronuclear multiple bond correlation) spectroscopy is a useful tool to observe correlations between carbons and protons separated by 2 – 4 bonds (note that one-bond correlations are suppressed, namely HSQC – heteronuclear single quantum coherence). The successful Williamson-ether immobilisation of Schiff-bases with Fréchet dendrons was confirmed using HMBC, whereby a correlation was observed between the key methylene (1-CH_2, Figure 2.10) and carbon-12 (C_{12}, Figure 2.10) resonance signals. Figure 2.10, clearly depicts a cross-peak for this correlation, thus providing further evidence for the successful amalgamation of Fréchet dendrons and the Schiff-base synthons.

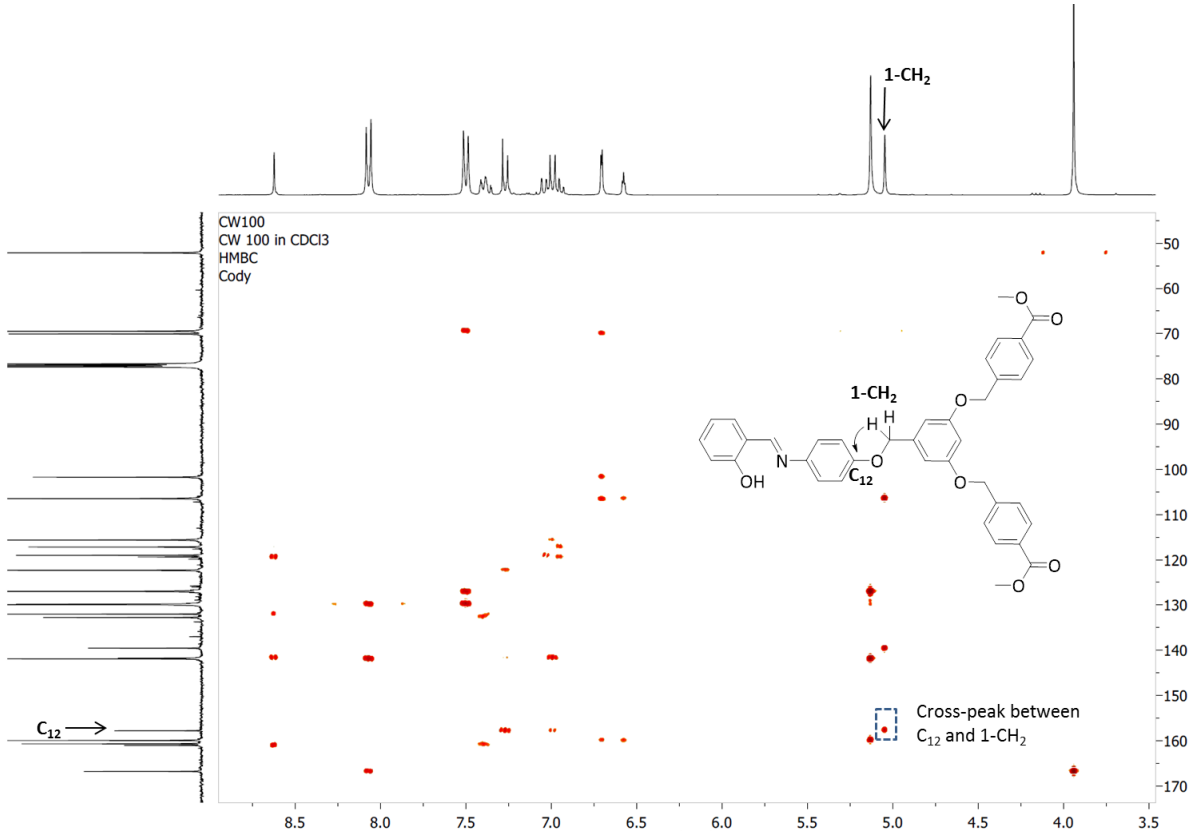

Figure 2.10. *The 2D NMR (HMBC) for* ***2.11****, which displays through bond coupling of the Fréchet dendron moiety and the respective Schiff-base.*

A similar trend iss observed for the *N,P*-iminophosphine dendrons (**2.9, 2.11** and **2.13**) in both ^{1}H and ^{13}C{^{1}H} NMR spectroscopy (Table 2.3, *vide supra*). A small shift of the imine signal (doublet, $^{3}J_{CP}$ ≈ 21.8 Hz) is observed upon successful alkylation. Compounds **2.9, 2.11** and **2.13** were characterised using ^{31}P{^{1}H} NMR spectroscopy, as shown in Table 2.3. A single resonance is observed in the ^{31}P{^{1}H} NMR spectrum at δ_P -13.25, -13.26 and -13.26 ppm for compounds **2.9, 2.11** and **2.13** respectively, thus attesting to the presence of a single phosphorous species. The compounds display good stability in air with negligible oxidation observed for these phosphorous ligands. The integration of the proton resonance correlates to the proposed compounds, further attesting to the successful formation of products **2.8** – **2.13.**

2.5.2.2 Infrared Spectroscopy

The absorption band for the imine moiety *v*(C=N) is observed in the IR spectra for compounds **2.8** – **2.13**. This *v*(C=N) vibration appears as an intense absorption band

between 1611 – 1617 cm^{-1}. The absence of the phenolic band *v*(O-H) at ≈3200 cm^{-1} suggests successful alkylation and further corroborates the ^{1}H NMR spectroscopic evidence.

2.5.2.3 Mass Spectrometry and Elemental Analysis

Compounds **2.8** – **2.13** were analysed using mass spectrometry. Compounds **2.8** and **2.9** were analysed using EI-MS. A molecular ion is observed at *m/z* 361.13 and *m/z* 529.04 for compounds **2.8** and **2.9** respectively. Compound **2.10** was analysed using HR-ESI-MS (+ve mode) whereby a *m/z* of 632.22 is observed, this corresponds to the $[M+H]^{+}$ adduct. For the larger dendrons **2.11** – **2.13**, MALDI-TOF-MS (+ve mode) was used to confirm the successful product formation. The parent ion $[M]^{+}$ is observed for these dendrons at *m/z* 799.86, 1172.59 and 1340.43 for compounds **2.11, 2.12** and **2.13** respectively. The elemental analysis obtained is in agreement with the calculated values and are within acceptable limits.

2.5.2.4 Single Crystal X-Ray Diffraction

Single crystal XRD is a useful method to confirm the molecular structures of proposed compounds. Single crystals of **2.8** (Figure 2.11) were obtained by slow diffusion of petroleum ether into a concentrated solution of the compound dissolved in dichloromethane.

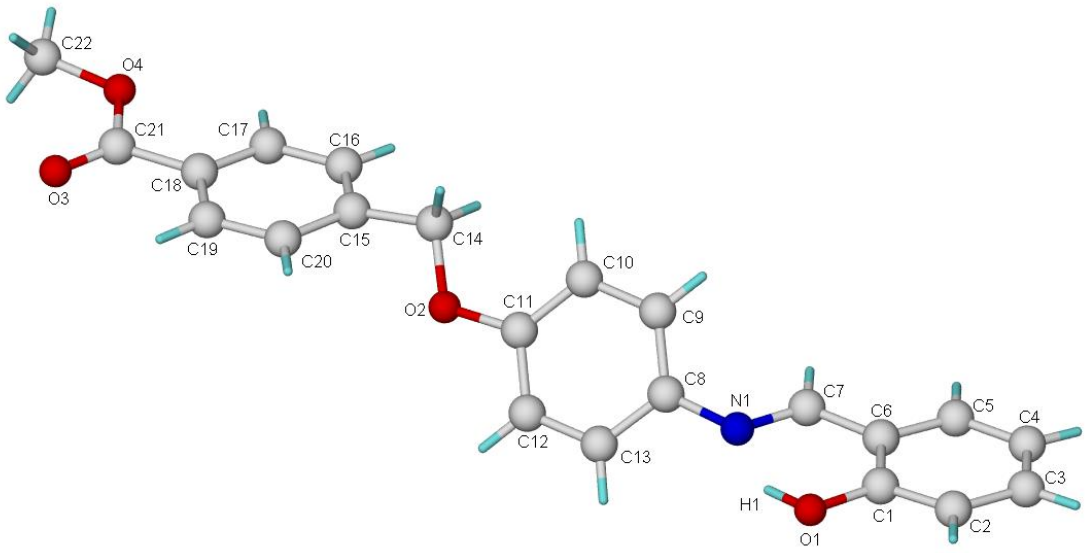

Figure 2.11. *Ball and stick representation of compound* ***2.8****.*

The compound **2.8** crystallizes in the orthorhombic space group, *Pna*2_1, with six molecules present per unit cell (Figure 2.11). The torsion angle about the imine bond is observed to be 175°, thus confirming the *trans*-configuration of the imine in the solid state. This observation is consistent for structurally similar compounds obtained by Smith and co-workers.[43, 46, 63] The bond length (N1-C7, 1.28 Å) and angle (N1-C7-H7, 119(3)°) around the imine bond ($C=N_{imine}$) is comparable to structurally similar Schiff-base *N,O*-salicylaldimine ligands reported in literature (Table 2.4).[47,55,46] Importantly, an intramolecular O1-H1···N1 hydrogen bond (H1···N1 distance = 1.78(1) Å, O1-H1···N1 angle = 147(6)°) is observed for the ligand **2.8**.[46, 55] These observations are consistent for structurally similar Schiff-base compounds.[46, 55]The full crystallographic details are described in Table 5.1, Chapter 5.

Table 2.4. *Selected crystallographic data for compound* ***2.8.***

Selected Bond Lengths	**Interatomic distances (Å)**
O1-H1	0.92(3)
$N1_{imine}$-C7	1.288(3)
H7-C7	0.950
O1-H1-----$N1_{imine}$	1.78(1)
Selected Bond Angles	**Angles (°)**
H1-O1-C1	108(2)
C1-C6-C7	121.4(2)
C6-C7-$N1_{imine}$	121.5(2)
H7-C7-$N1_{imine}$	119.3(2)
O1-H1···$N1_{imine}$	147(6)

The correlation between the proposed structure and spectroscopic and analytical results concludes that the desired compounds **2.1** – **2.13** were successfully synthesized.

2.6 Overall Summary

A series of Fréchet dendrons (**2.1** – **2.5**), Schiff-bases (**2.6** and **2.7**), *N,O*-salicylaldimine (**2.8, 2.10** and **2.12**) and *N,P*-iminophosphine (**2.9, 2.11** and **2.13**) dendrons were successfully synthesized and isolated in good yields. Compounds **2.1** – **2.13** were characterised using an array of spectroscopic and analytical techniques and the compounds are stable at room temperature. ^{1}H, $^{13}C\{^{1}H\}$, $^{31}P\{^{1}H\}$ NMR spectroscopy, infrared spectroscopy, mass spectrometry (positive-ion mode) and elemental analysis were predominantly used to correctly elucidate the structures of the products (**2.1** – **2.13**). The regioselectivity of the Williamson-ether synthesis for compounds **2.8, 2.10** and **2.12** were confirmed using ^{1}H NMR and HMBC NMR spectroscopy. The Williamson-ether reaction was highly regioselective towards the proposed products **2.8**, **2.10** and **2.12**, with 100% regioselectivity observed. Single crystal XRD was used as a tool to confirm the molecular structure **2.8** in the solid state. The bond lengths and angles for the imine moiety was consistent for structurally similar Schiff-base *N,O*-salicylaldimine ligands reported in literature. [47,55,46] Furthermore 2D NMR experiments (COSY, HSQC, HMBC) were used to correctly assign proton and carbon resonances and correlations for compounds **2.1** – **2.13**. The ligands **2.1** – **2.13** were complexed with the suitable rhodium precursors to form the respective Rh(I) Schiff-base dendrons, these are discussed in the following Chapter.

2.7 References

1. A. Carlmark, C. Hawker, A. Hult and M. Malkoch, *Chem. Soc. Rev.*, 2009, **38**, 352-362.
2. G. I. Dzhardimalieva and I. E. Uflyand, *Dalton Trans.*, 2017, **46**, 10139-10176.
3. V. Rodionov, H. Gao, S. Scroggins, D. A. Unruh, A.-J. Avestro and J. M. Fréchet, *J. Am. Chem. Soc.*, 2010, **132**, 2570-2572.
4. D. A. Tomalia, H. Baker, J. Dewald, M. Hall, G. Kallos, S. Martin, J. Roeck, J. Ryder and P. Smith, *Polym. J. (Tokyo, Jpn.)*, 1985, **17**, 117-132.
5. M. C. Parrott, E. B. Marchington, J. F. Valliant and A. Adronov, *J. Am. Chem. Soc.*, 2005, **127**, 12081.

6. D. A. Tomalia, *Aldrichim. Acta*, 2004, **37**, 39-57.
7. S.-H. Hwang and G. R. Newkome, in *Frontiers in Transition Metal-Containing Polymers*, eds. A. S. Abd-El-Aziz and I. Manners, John Wiley & Sons, Inc., New York, 2007, vol. 10, pp. 399-438.
8. E. Buhleir, W. Wehner and F. Vögtle, *Chem. Informationsdienst*, 1978, **155**, 158.
9. A. Belser, A. von Zelewski, M. Frank, C. Seel, F. Vögtle, L. de Cola, F. Barigelletti and V. Balzani, *J. Am. Chem. Soc.*, 1993, **115**, 4076.
10. G. R. Newkome, Z. Yao, G. R. Baker and V. K. Gupta, *J. Org. Chem.*, 1985, **50**, 2003.
11. G. R. Newkome, G. R. Baker, M. J. Saunders, P. S. Russo, V. K. Gupta, Z. K. Yao, J. E. Miller and K. J. Buillon, *Chem. Commun.*, 1986, **22**, 752.
12. G. R. Newkome, Z. q. Yao, J. R. Baker, G. A. Gupta, P. S. Russo and M. J. Saunders, *J. Am. Chem. Soc.*, 1986, **108**, 849.
13. G. R. Newkome, G. R. Baker, S. Arai, P. S. Russop, K. J. Theriot, C. N. Moorefield, L. E. Rogers, J. E. Miller, T. R. Lieux, M. E. Murray, B. Phillips and L. Pascal, *J. Am. Chem. Soc.*, 1990, **112**, 8458.
14. D. A. Tomalia, H. Baker, J. Dewald, M. Hall, G. Kallos, S. Martin, J. Roeck, J. Ryder and P. Smith, *Polym. J.*, 1985, **17**, 117.
15. D. A. Tomalia, V. B. Berry, M. Hall and D. M. Hedstrand, *Macromolecules*, 1987, **20**, 1164.
16. C. J. Hawker and J. M. J. Fréchet, *J. Am. Chem. Soc*, 1990, **112**, 7638-7647.
17. L. c. Ropartz, R. E. Morris, D. F. Foster and D. J. Cole-Hamilton, *J. Mol. Catal. A: Chem*, 2002, **182**, 99-105.
18. A. W. Kleij, R. A. Gossage, R. J. Klein Gebbink, N. Brinkmann, E. J. Reijerse, U. Kragl, M. Lutz, A. L. Spek and G. van Koten, *J. Am. Chem. Soc.*, 2000, **122**, 12112-12124.
19. D. de Groot, P. G. Emmerink, C. Coucke, J. N. Reek, P. C. Kamer and P. W. van Leeuwen, *Inorg. Chem. Commun.*, 2000, **3**, 711-713.
20. C. J. Hawker, K. L. Wooley and J. M. J. Fréchet, *J. Am. Chem. Soc*, 1993, **115**, 4375-4376.
21. M. A. Hearshaw and J. R. Moss, *Chem. Commun.*, 1999, 1-8.
22. A.-M. Caminade, R. Laurent, B. Delavaux-Nicot and J.-P. Majoral, *New J. Chem.*, 2012, **36**, 217-226.
23. U. Boas, J. B. Christensen and P. M. H. Heegaard, *J. Mater. Chem.*, 2006, **16**, 3785.

24. J. Liu, Y. Feng, Y. He, N. Yang and Q.-H. Fan, *New J. Chem.*, 2012, **36**, 380-385.
25. K. Onitsuka and S. Takahashi, *Top. Curr. Chem*, 2003, **228**, 39-63.
26. M. Tristany, R. Laurent, H. Dib, L. Gonsalvi, M. Peruzzini, J.-P. Majoral and A.-M. Caminade, *Inorg. Chim. Acta*, 2014, **409**, 121-126.
27. M. C. Parrot, S. R. Benhabbour, C. Saab, J. A. Lemon, S. Parker, J. F. Valliant and A. Andrianoov, *J. Am. Chem. Soc.*, 2009, **131**, 2906.
28. J. Liu, Y. Feng, B. Ma, Y.-M. He and Q.-H. Fan, *Eur. J. Org. Chem.*, 2012, **2012**, 6737-6744.
29. S.-H. Hwang, C. D. Shreiner, C. N. Moorefield and G. R. Newkome, *New J. Chem.*, 2007, **31**, 1192-1217.
30. O. A. Bozdemir, S. Erbas-Cakmak, O. O. Ekiz, A. Dana and E. U. Akkaya, *Angew. Chem. Int. Ed.*, 2011, **50**, 10907-10912.
31. H. Gu, R. Ciganda, S. Gatard, F. Lu, P. Zhao, J. Ruiz and D. Astruc, *J. Organomet. Chem.*, 2016, **813**, 95-102.
32. B. M. Rosen, C. J. Wilson, D. A. Wilson, M. Peterca, M. R. Imam and V. Percec, *Chem. Rev.*, 2009, **109**, 6275-6540.
33. D. Astruc, E. Boisselier and C. Ornelas, *Chem. Rev.*, 2010, **110**, 1857-1959.
34. P. A. Chase, R. J. M. K. Gebbink and G. van Koten, *J. Organomet. Chem.*, 2004, **689**, 4016-4054.
35. I. Cuadrado, M. Morán, C. M. Casado, B. Alonso and J. Losada, *Coord. Chem. Rev.*, 1999, **193**, 395-445.
36. G. R. Newkome, E. He and C. N. Moorefield, *Chem. Rev*, 1999, **99**, 1689-1746.
37. E. C. Constable, *Chem. Commun.*, 1997, 1073-1080.
38. C. Gorman, *Adv. Mater.*, 1998, **10**, 295-309.
39. I. Angurell, O. Rossell and M. Seco, *Inorg. Chim. Acta*, 2014, **409**, 2-11.
40. S. Svenson and D. A. Tomalia, *Adv Drug Deliv Rev*, 2005, **57**, 2106-2129.
41. S. Siangwata, S. Chulu, C. L. Oliver and G. S. Smith, *Appl. Organomet. Chem.*, 2017, **31**, e3593-n/a.
42. S. Siangwata, N. Baartzes, B. C. E. Makhubela and G. S. Smith, *J. Organomet. Chem.*, 2015, **796**, 26-32.
43. L. C. Matsinha, S. F. Mapolie and G. S. Smith, *Dalton Trans.*, 2015, **44**, 1240-1248.

44. M. M. Mogorosi, T. Mahamo, J. R. Moss, S. F. Mapolie, J. C. Slootweg, K. Lammertsma and G. S. Smith, *J. Organomet. Chem.*, 2011, **696**, 3585-3592.
45. G. S. Smith and S. F. Mapolie, *J. Mol. Catal. A: Chem*, 2004, **213**, 187-192.
46. P. Govender, S. Ngubane, B. Therrien and G. S. Smith, *J. Organomet. Chem.*, 2017, **848**, 281-287.
47. L. C. Matsinha, P. Malatji, A. T. Hutton, G. A. Venter, S. F. Mapolie and G. S. Smith, *Eur. J. Inorg. Chem.*, 2013, **2013**, 4318-4328.
48. L. Maqeda, B. C. E. Makhubela and G. S. Smith, *Polyhedron*, 2015, **91**, 128-135.
49. E. B. Hager, B. C. Makhubela and G. S. Smith, *Dalton Trans.*, 2012, **41**, 13927-13935.
50. B. C. Makhubela, A. M. Jardine, G. Westman and G. S. Smith, *Dalton Trans.*, 2012, **41**, 10715-10723.
51. B. C. Makhubela, A. Jardine and G. S. Smith, *Green Chem.*, 2012, **14**, 338-347.
52. N. Zydziak, C. M. Preuss, V. Winkler, M. Bruns, C. Hübner and C. Barner-Kowollik, *Macromol. Rapid Commun.*, 2013, **34**, 672-680.
53. A. C. Pauly and P. Theato, *J. Polym. Sci., Part A: Polym. Chem.*, 2011, **49**, 211-224.
54. V. Theodorou, K. Skobridis, A. G. Tzakos and V. Ragoussis, *Tetrahedron Lett.*, 2007, **48**, 8230-8233.
55. S. A. Elroby, S. Aboud, S. G. Aziz and R. Hilal, *J. Struct. Chem.*, 2015, **56**, 414-427.
56. M. Koprowski, R.-M. Sebastian, V. Maraval, M. Zablocka, V. Cadierno, B. Donnadieu, A. Igau, A. Caminade and J.-P. Majoral, *Organometallics*, 2002, **21**, 4680-4687.
57. E. Cordes and W. Jencks, *J. Am. Chem. Soc.*, 1962, **84**, 832-837.
58. C. A. Ghilardi, S. Midollini, S. Moneti, A. Orlandini and G. Scapacci, *J. Chem. Soc., Dalton Trans.*, 1992, **23**, 3371-3376.
59. P. Govender, PhD thesis, University of Cape Town, 2014.
60. H. H. Freedman, *J. Am. Chem. Soc.*, 1961, **83**, 2900-2905.
61. S. Misra, K. B. Pandeya, A. K. Tiwari, A. Z. Ali, T. Saradamani, S. B. Agawane and K. Madhusudana, *Med. Chem. Res.*, 2011, **20**, 1431-1437.
62. G. Ceyhan, M. Köse, M. Tümer and İ. Demirtaş, *Spectrochim. Acta, Part A*, 2015, **149**, 731-743.
63. I. Cassells, MSc dissertation, University of Cape Town, 2017.

Chapter 3

Synthesis and Characterisation of Neutral Rh(I) complexes based on *N,O*-salicylaldimine and *N,P*-iminophosphine Fréchet Dendrons

3.1 Introduction

The inception of dendrimers in the 1970's has stimulated interest into the study and synthesis of these versatile structures.[1] The structural variation of dendrimers allows for a plethora of applications. These are predominantly used in catalytic, sensing and biomedical spheres.[2-7] The increased technological advances have initiated the demand for highly specific materials with highly controlled molecular architectures. One formidable means of constructing materials with advanced applications is to introduce a metal with known properties. An important synthon to immobilise metals are dendrimers. More importantly, this approach subsequently yields a new class of macromolecules, namely metallodendrimers. This metal-dendrimer relationship offers a niche of new materials, which emanates from the synergistic effect between metal and dendrimer. These effects are often attributed to their cooperativity, steric control, recyclability and site isolation. Since the seminal work by Balzani and Newkome on metallodendrimers in the 1990's, a myriad of metallodendrimers and organometallic dendrimers were discovered, thus opening new vistas in chemistry.[8, 9]

The architectural design and synthetic strategies for the construction of metallodendrimers have led to an array of topologies.[4, 10] These are namely interstitial, peripheral-, and core-

functionalised metallodendrimers.[4] The synthesis and applications of these architectures have been subject to extensive reviews.[2, 11-13] In the context of this work, core-functionalised organometallic dendrimers are of particular importance, as these structures are often less explored due to drawbacks associated with the synthesis and purification of these dendrons.[14, 15] More importantly, there is a lack of literature on dendrons with transition metals at the focal point. Selected examples include Parrot's high generation polyester dendrons containing a rhenium bis(pyridyl)amine moiety at the core used as precursors for radiolabelling studies, de la Mata's water-soluble carbosilane dendrons containing ferrocene at the focal point used as anti-bacterial agents and Gómez-Sal's Fréchet-type palladium-dendrimers containing bis-(pyrazolyl) methane ligands at the core used as Heck cross-coupling catalyst precursors (Figure 3.1).[16-18]

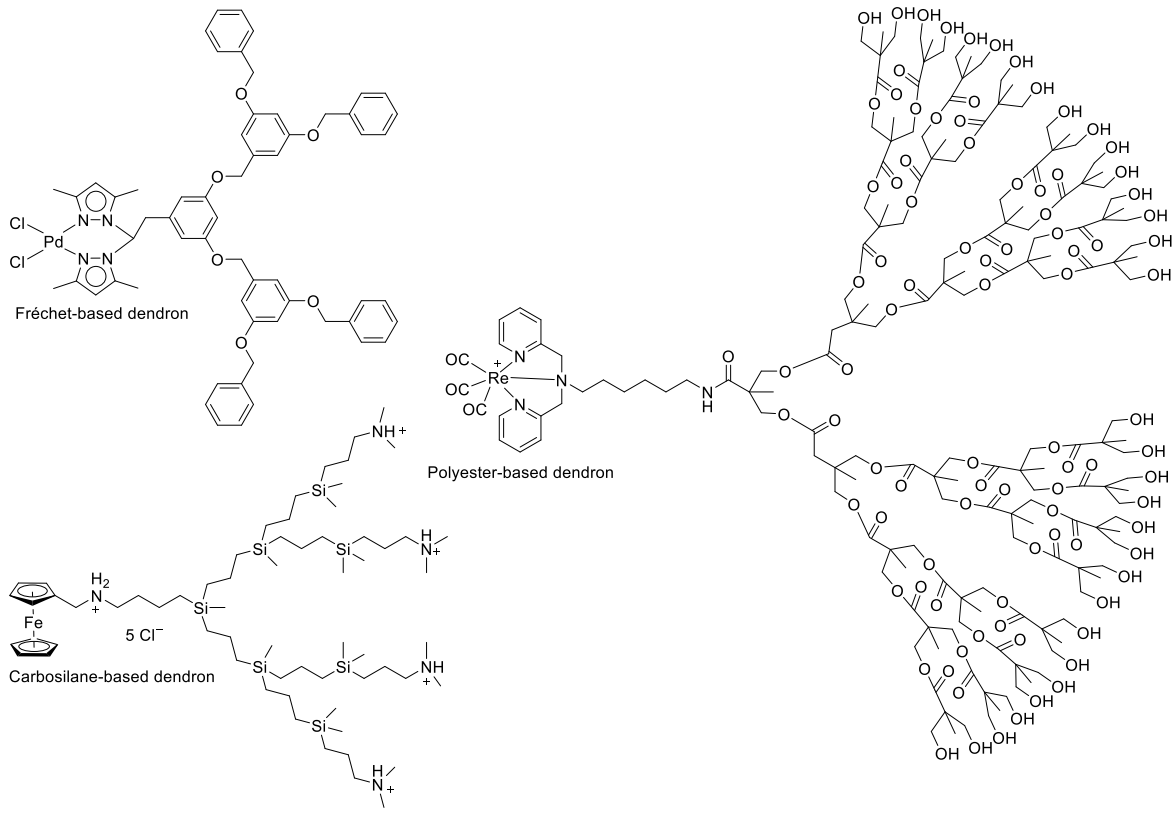

Figure 3.1. *Selected examples of dendrons bearing transition metals at the focal point. These include Gómez-Sal's Fréchet-type palladium-dendrimers, de la Mata's ferrocenyl carbosilane dendrons and Parrot's rhenium polyester dendron.* [16-18]

The lack of literature on the synthesis of discrete rhodium(I) organometallic dendrons has motivated the study of these complexes. Furthermore, the catalytic applications of these

architectures are limited. More importantly, there are no reports of dendrons with metals at the core being used in the hydroformylation reaction.

Most scaffolds utilised in the hydroformylation reaction are based on DAB-PPI, PAMAM or carbosilane scaffolds, with the metals located on the periphery or interior cavities of these dendritic architectures.[19, 20] Most dendrimers used for hydroformylation reactions are anchored to insoluble supports, thus the activity and selectivity of the catalysts are hampered due to the heterogeneous nature of the catalysts (Figure 3.2).[21-25] Selected examples include Arya's dendritic arms anchored to amide-resin beads, Ropartz's carbosilane dendrons bearing a polyhedral silsesquioxane core, Bourque's PAMAM dendrons containing silica-gel particles at the core and Hager's water-soluble DAB-PPI-*N,O*-salicylaldimine dendrimer.[21, 22, 25, 26] More importantly, Ropartz, Bourque and Hager formed the discrete metallodendrimers *in situ,* as noted in Figure 3.2 by the addition of the appropriate rhodium dimer.[21, 23-26]

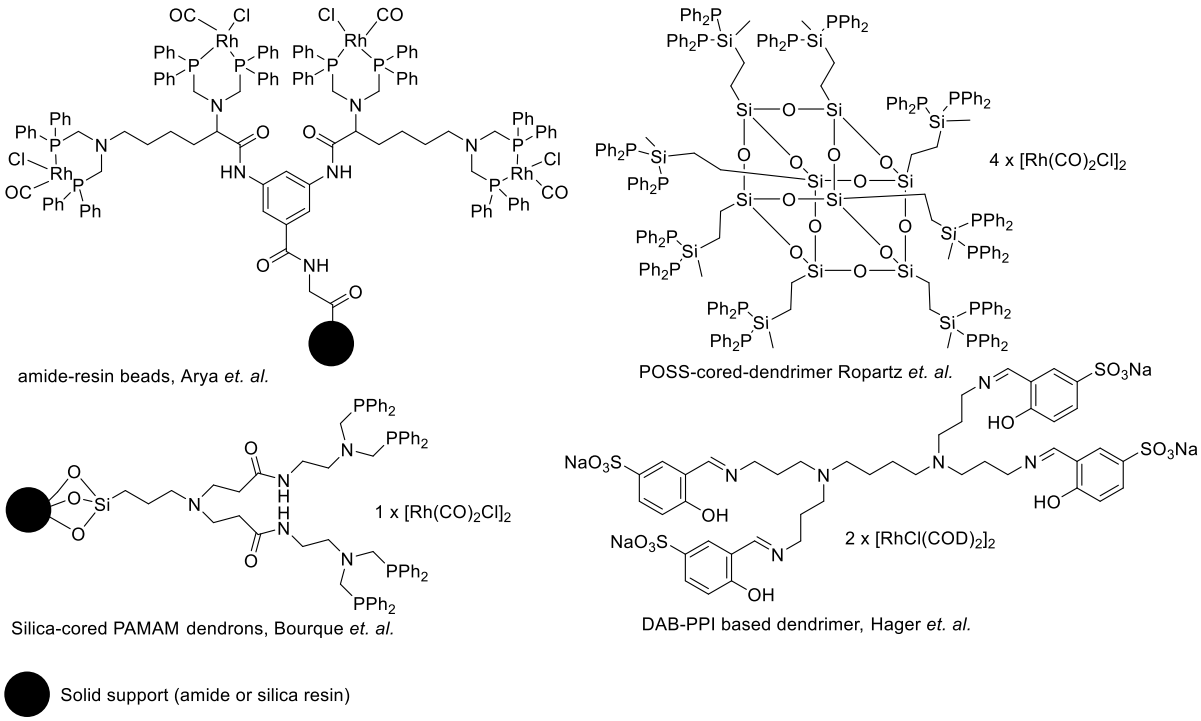

Figure 3.2. *Selected examples of dendritic catalysts used in hydroformylation reactions.*[21, 23-26]

To the best of our knowledge, no work has been reported using the Fréchet-type dendritic scaffolds with rhodium at the focal point in the hydroformylation reaction. This Chapter

describes the synthesis and characterisation of novel rhodium(I) organometallic dendrons. An array of analytical and spectroscopic techniques was conducted for structural elucidation of the proposed structures. The application of these dendrons in the hydroformylation of olefins is discussed in Chapter 4.

3.2 Rhodium(I) 1,5-Cyclooctadiene *N,O*-salicylaldimine Organometallic Dendrons

3.2.1 Synthesis

The synthesis of the rhodium 1,5-cyclooctadiene (COD) *N,O*-salicylaldimine organometallic dendrons **3.1** – **3.3** involved two reactions (Scheme 3.1). Firstly, the preparation of the $[Rh(\mu\text{-}Cl)COD]_2$ metal dimer was accomplished following a modified literature method.[27, 28] Complexes **3.1** – **3.3** were synthesized by reacting the appropriate *N,O*-salicylaldimine ligand (**2.9, 2.11,** or **2.13**) in the presence of triethylamine (to deprotonate the phenolic group) and the $[Rh(\mu\text{-}Cl)COD]_2$ dimer. The *N,O*-salicylaldimine Rh(I) organometallic dendron complexes **3.1** – **3.3** were afforded as yellow powders in high yields (79 – 88 %).[29]

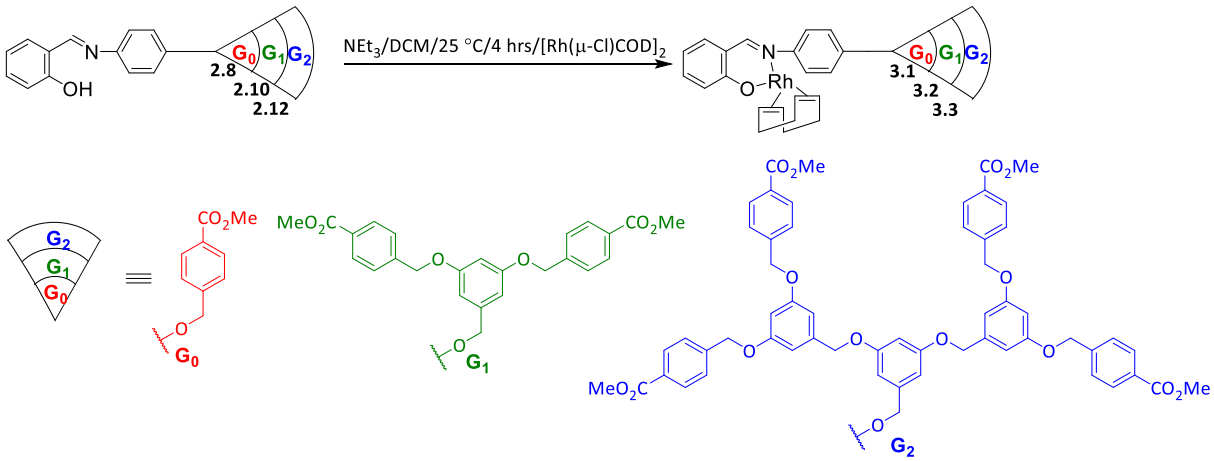

Scheme 3.1. *Synthesis of the N,O-salicylaldimine Rh(I) metallodendron complexes (**3.1** – **3.3**) bearing COD as an auxiliary ligand.*

3.2.2 Characterisation

3.2.2.1 ^{1}H and $^{13}C\{^{1}H\}$ NMR spectroscopy

The ^{1}H and $^{13}C\{^{1}H\}$ NMR spectra were recorded in $CDCl_3$ across the dendron series **3.1** – **3.3**. The mode of co-ordination and structural integrity was confirmed using ^{1}H NMR spectroscopy (Figure 3.3). The upfield shift of the imine proton (**H**-C=N) resonance is observed from δ_H 8.53 ppm (**2.9**) to δ_H 7.97 ppm (**3.1**). Furthermore the imine proton resonance (**H**-C=N) of complexes **3.1** and **3.2** are observed as a doublet with a coupling constant of 1.7 Hz ($^{3}J_{RhH}$). This is attributed to the coupling of the imine proton (**H**-C=N) to the spin active ^{103}Rh centre (100% natural abundance, nuclear spin of ½). This is observed for **3.1** and **3.2**, however the macromolecular nature of **3.3** shows peak broadening, hence the signal is observed as an apparent singlet. In comparison to the ligands, **2.8**, **2.10** and **2.12**, no phenolic proton signal between δ_H 13.25 – 13.26 ppm was observed for the resultant complexes **3.1** – **3.3**, which confirms the deprotonation and subsequent bidentate co-ordination mode of the Rh(I) metal. The aryl protons for the Schiff-base moiety (H_3, H_4, H_5, H_6, H_{10} and H_{11}, Figure 3.3) display minute shifts, these being attributed to the electronic influences upon co-ordination of the metal. The methylene (-C**H$_2$**) and methoxy (-OC**H$_3$**) proton signals are evident in their diagnostic regions (3.8 – 5.3 ppm) as noted for the ligands **2.8, 2.10** and **2.12**.

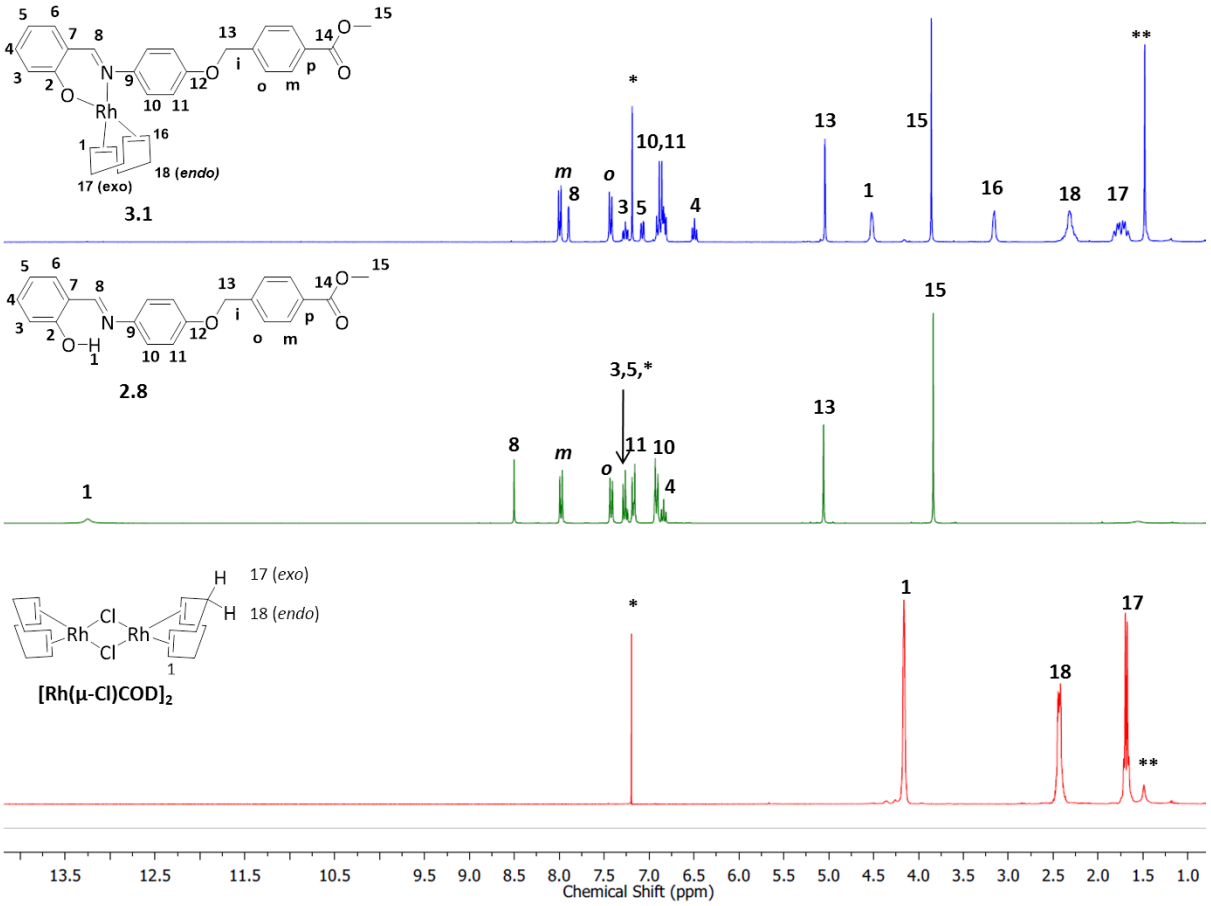

Figure 3.3. *Stacked ^{1}H NMR spectra for the $[Rh(\mu\text{-}Cl)COD]_2$ dimer, ligand **2.8** and complex **3.1** respectively. The ^{1}H NMR spectra were recorded in $CDCl_3$ (*$CDCl_3$, **H_2O).*

Key evidence of successful co-ordination is the presence of the olefinic (H_1 and H_{16}) and methylene (H_{17} and H_{18}) proton signals of the COD moiety (δ_H 1.5 – 4.5 ppm, Figure 3.3). The integration of these signals correlates to that of the proposed structures **3.1** – **3.3**. Complexes **3.1** – **3.3** display four distinct signals for the COD motif. Splitting of the olefinic COD proton resonances are observed, these are attributed to the *trans* effect induced by the chelating *N,O*-salicylaldimine ligand (Figure 3.3).[30-32] The proton resonance at δ_H 4.60 ppm (Figure 3.4, H_1) is assigned the olefinic protons *trans* to the imine nitrogen whilst the signal at δ_H 3.23 ppm (Figure 3.4, H_{16}) is assigned to the protons *trans* to the phenolic oxygen. This phenomenon is consistent with structurally similar *N,O*-chelating-Rh(I) complexes.[30-32]

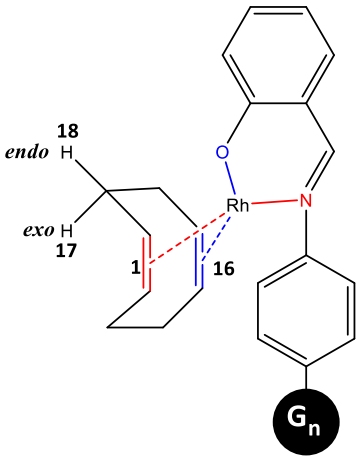

Figure 3.4. *Representative structure depicting the trans-N-olefinic (red), trans-O-olefinic (blue), exo and endo methylene protons, see Scheme 3.1 for G_n.*[31]

The methylene resonances for the COD moiety are chemically non-equivalent (Figure 3.4, H_{17} and H_{18}), which results in the splitting pattern of the methylene proton resonance. In aromatic π-systems, a non-uniform magnetic field is observed. Once a magnetic field is applied to the electrons in π-aromatic systems, non-uniformity is induced *via* magnetic anisotropic effects resulting in the change in chemical shifts for these resonances.[30] Hence the *exo* and *endo* methylene proton signals are observed at δ_H 1.81 and 2.31 ppm respectively.

$^{13}C\{^1H\}$ NMR spectroscopy was a useful technique for the structural elucidation of complexes **3.1** – **3.3**. The presence of methylene carbon signals of COD are observed between δ_C 29.13 – 31.59 ppm across the dendron series (**3.1** – **3.3**, Table 3.1, *vide infra*). The olefinic COD signals (C_1 and C_{16}, Figure 3.4) are observed between δ_C 73.01 – 84.90 ppm (Table 3.1). The multiplicity of these carbon resonances are doublets, due to the coupling between rhodium and carbon ($^1J_{RhC}$, Table 3.1). The coupling constants are 12.3 Hz (C_1, Figure 3.4) and 14.1 Hz (C_{16}, Figure 3.4) respectively. These differ to the $[Rh(\mu\text{-}Cl)COD]_2$ dimer whereby one doublet is observed for the olefinic carbons (δ_C 78.83 ppm, $^1J_{RhC}$ = 13.9 Hz) and one singlet for the aliphatic methylene signal (δ_C 31.03 ppm). This correlation is consistent with structurally similar *N,O*-salicylaldimine complexes in literature.[30, 32]

Table 3.1. *^{1}H and ^{13}C resonances for the COD protons across the dendron series, **3.1 – 3.3.***

Complex	^{1}H NMR [ppm][a]	^{1}H NMR [ppm][a,b]	$^{13}C\{^{1}H\}$ NMR [ppm][a]	$^{13}C\{^{1}H\}$ NMR [ppm][a,c]
	HC-COD$_{exo}$	*N*-Rh-**CH$_2$** (*trans*)	**C**H$_2$-COD	*N*-Rh-**C**H$_2$ (*trans*)
	HC-COD$_{endo}$	*O*-Rh-**CH$_2$** (*trans*)	**C**H$_2$-COD	*O*-Rh-**C**H$_2$ (*trans*)
3.1	1.81	4.60	29.20	84.90 (12.3 Hz)
	2.38	3.23	31.59	73.02 (14.1 Hz)
3.2	1.81	4.59	29.17	84.84 (12.0 Hz)
	2.37	3.23	31.52	73.05 (14.1 Hz)
3.3	1.80	4.59	29.13	84.79 (12.1 Hz)
	2.39	3.23	31.48	73.01 (13.9 Hz)

[a] Recorded in $CDCl_3$

[b] CH_2 *trans* to donor atom

[c] (d, $^{1}J_{Rh\text{-}C}$)

Shading denotes exo COD protons where applicable. Non-shaded denotes endo COD protons in contrast.

In the $^{13}C\{^{1}H\}$ spectrum of complex **3.1** (Figure 3.5), signals of the aryl protons of the Schiff-base moiety displays distinct shifts for C_8 (from δ_C 161 to 166 ppm) and C_2 (from δ_C 161 to 167 ppm), which further confirms bidentate coordination to the imine nitrogen and phenolic oxygen. These chemical shifts are similar for complexes **3.2** (G_1) and **3.3** (G_2). The resonances for the aromatic carbons are present between 114 – 168 ppm. The methylene

(-**C**H_2) and methoxy (-O**C**H_3) carbon resonances for complexes **3.1** – **3.3** were observed between δ_C 51 – 70 ppm. The ^{1}H and $^{13}C\{^1H\}$ NMR spectra obtained are in agreement with the proposed structures.

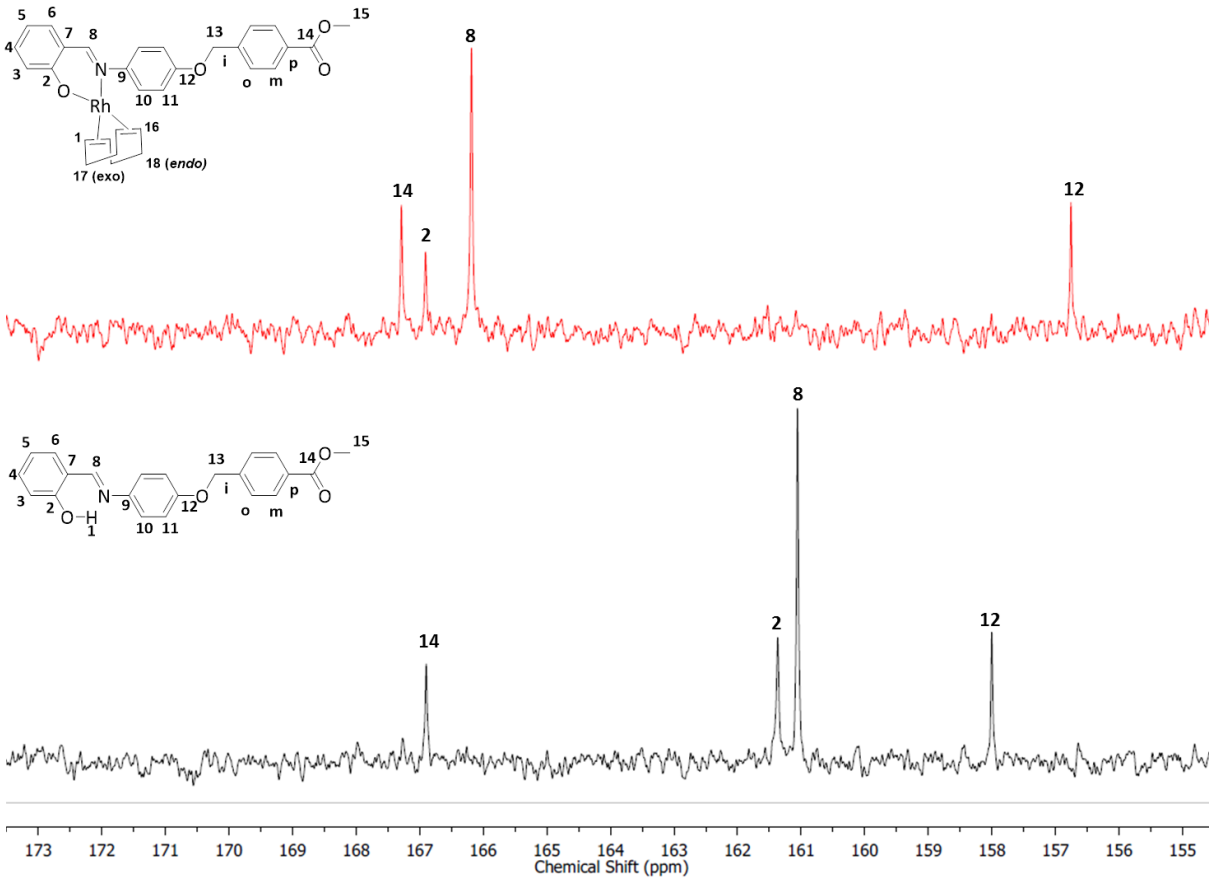

Figure 3.5. *$^{13}C\{^1H\}$ NMR spectra for the comparison between ligand **2.8** and complex **3.1** in $CDCl_3$. The chemical shift region magnified is between δ_C 155 – 173 ppm, note the important resonance shifts for C_2 and C_8 from ligand **2.8** to complex **3.1**.*

Variable temperature ^{1}H NMR spectroscopy was employed on complexes **3.1** – **3.3**, as it is known from literature that these systems may undergo conformational changes in solution due to the hemilability of the ligand.[30] A common observation is the ring-opening of 5-membered *N,O*-salicylaldimine chelates. These ring-opening reactions of the five-membered *N,O*-salicylaldimine chelate might occur, thus resulting in the rapid exchange on the NMR time scale and fluxional behaviour of the complex. To understand the stability of complexes **3.1** – **3.3**, variable temperature ^{1}H NMR was conducted in $CDCl_3$, at 30 °C, 40 °C and 50 °C (Figure 3.6). Importantly, no coalescence is observed for the olefinic or aliphatic

protons of the COD moiety, which suggests that the complexes and more importantly the rhodacycles are stable in $CDCl_3$ at the temperatures tested. The complexes **3.1** – **3.3** are poorly soluble in deuterated dimethylsulfoxide and methanol, hence experiments could not be conducted at temperatures higher than 50 °C.

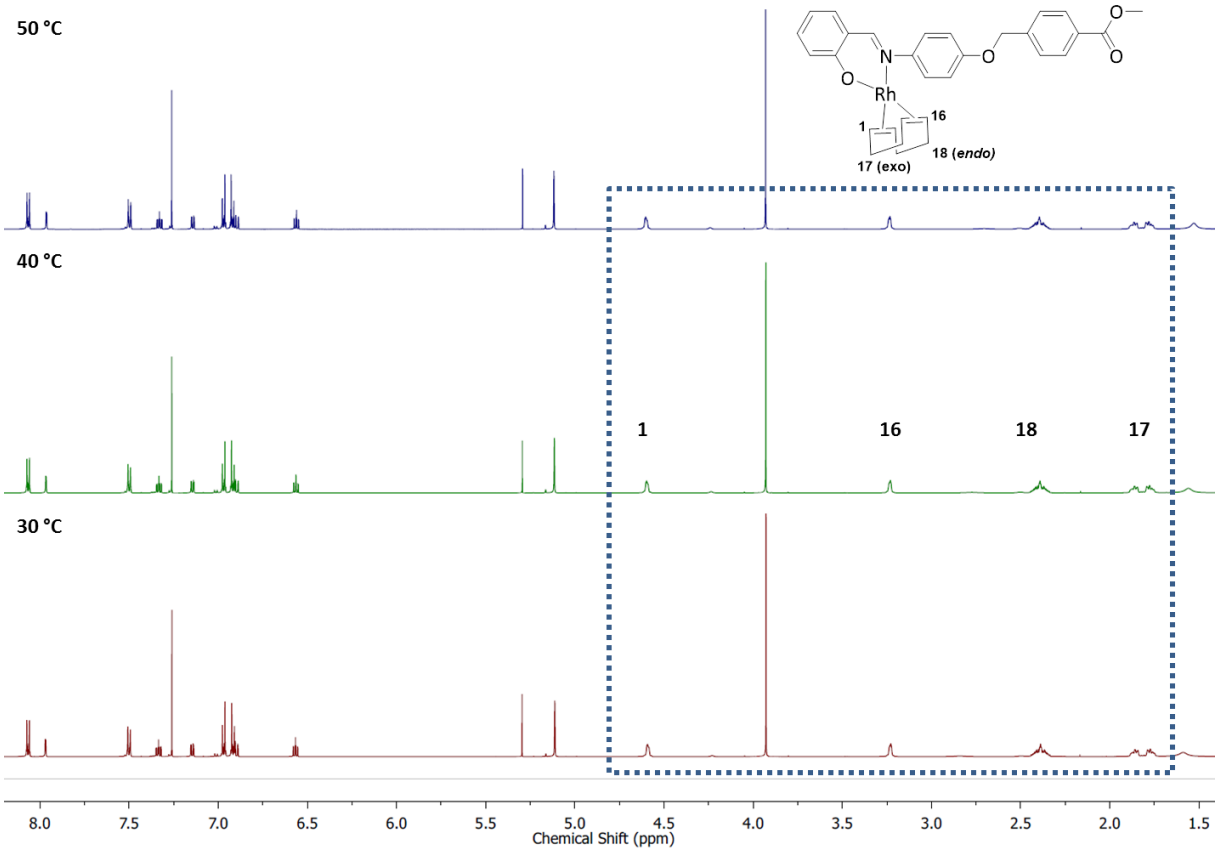

Figure 3.6. *Stacked ^1H NMR spectra of **3.1** ($CDCl_3$) at 30, 40 and 50 °C respectively. The selected COD protons 1, 16, 17, and 18 are labelled in this figure.*

3.2.2 Infrared spectroscopy

The complexes, **3.1** – **3.3** display shifts in their spectra for the ν(C=N) band to lower wavenumbers compared to the ligands (Figure 3.7). The shift from the free ligand **2.8, 2.10** and **2.12** (1617 cm^{-1}) to the complexes **3.1** – **3.3** (1605 – 1609 cm^{-1}) provides further evidence of successful co-ordination to the imine nitrogen (Figure 3.7). The lower wavenumber suggests the weakening of the C=N bond and synergistically, the metal nitrogen bond is strengthened *via* a back-bonding of the rhodium metal into the anti-bonding nitrogen orbital (π*). This reduces the order of the nitrogen bond and subsequently results in the lowering of the wavenumber, as observed in Figure 3.7. These observations

suggest the bidentate coordination of the rhodium metal to the *N,O* atoms of the salicylaldimine moiety of compounds **2.8, 2.10** and **2.12**. In addition, similar trends are observed for the metal complexes **3.2** and **3.3.** The results are in agreement with literature for structurally similar *N,O*-salicylaldimine Rh(I) complexes.[32, 33]

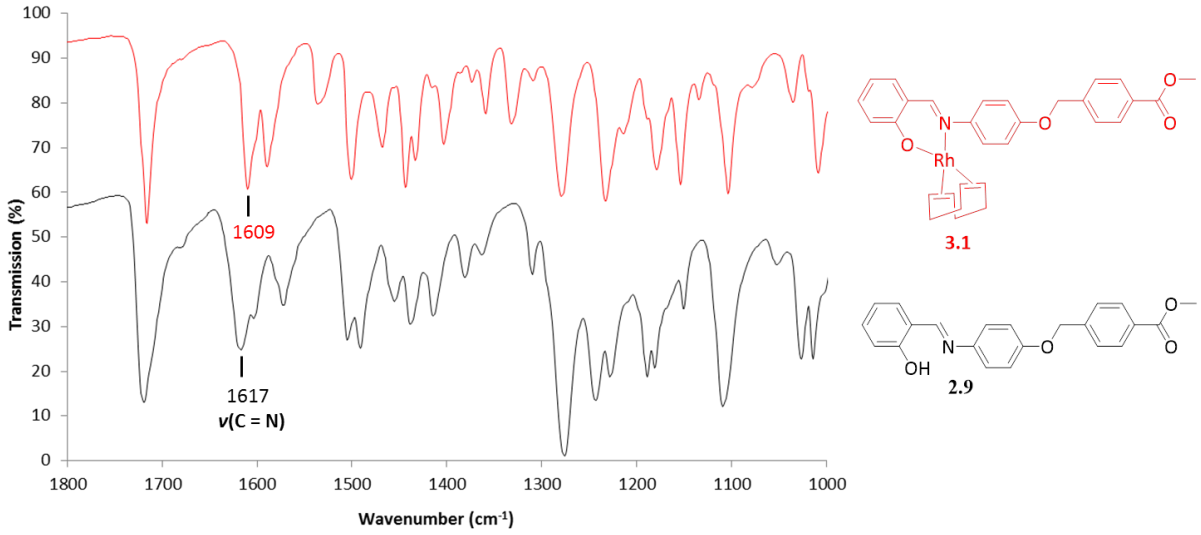

Figure 3.7. *The stacked IR spectra for ligand **2.8** and complex **3.1,** which shows the diagnostic imine absorbance region (1600 – 1645 cm^{-1}).*

3.2.3 Mass Spectrometry and Elemental Analysis

Elemental analysis was used to confirm the purity of these organometallic dendrons **3.1** – **3.3**. Initially, the elemental analysis for complex **3.1** and **3.2** were outside acceptable limits. However recalculation of the C, H and N percentages obtained for complex **3.1** and **3.2** with the inclusion of water (work-up solvent, observed in the ^{1}H NMR spectrum), resulted in percentages within acceptable limits. This phenomenon is commonly observed for dendrimers functionalised with inorganic and organic synthons, whereby the entrapment of solvents and/or salts is encapsulated within the dendritic framework.[29, 34] The elemental analysis of complex **3.3** is in agreement with the calculated values.

The EI-MS (**3.1**), ESI-MS (**3.2**) and MALDI-TOF-MS (**3.3**) spectra of the respective complexes further confirmed the synthesis of the proposed structures. The analysis of the mass spectrum of complex **3.1** displays a molecular ion peak at *m/z* 571.0999 and a base peak at *m/z* 212.0335, with the latter assigned to the [M-Rh-COD]$^{+}$ fragment. Mass spectrometry experiments (ESI) conducted in the positive mode displays a [M-Rh-COD]$^{+}$ fragment for

complex **3.2** (*m/z* 632.2287) whilst the MALDI-TOF-MS analysis of **3.3,** displays a molecular ion, $[M]^+$ (*m/z* 1382.5970) (Figure 3.8). Notably, a distinct fragmentation pattern is observed for complex **3.3**. Figure 3.8 displays the major fragments for **3.3**, these include the $[M\text{-}Rh\text{-}COD]^+$, $[M\text{-}COD]^+$ and $[M]^+$ fragments. The mass spectrometry results correlate with the calculated values for complexes **3.1** – **3.3**.

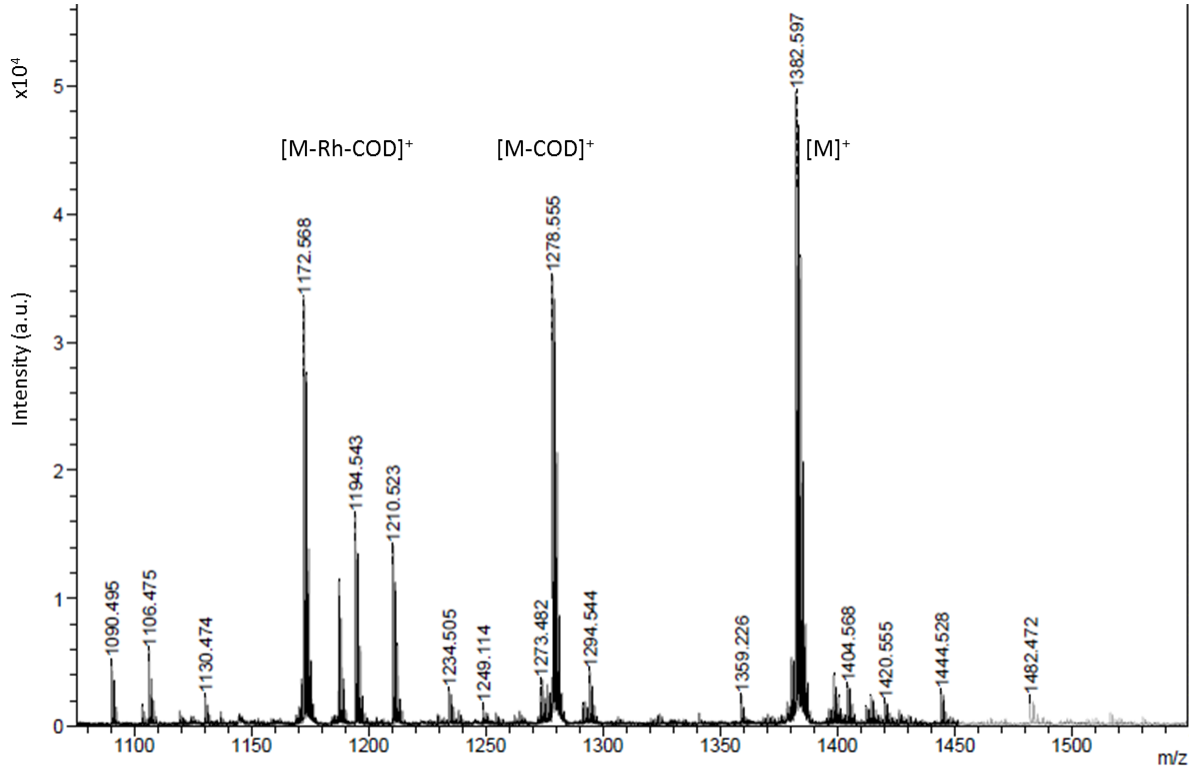

Figure 3.8. *MALDI-TOF-MS spectrum conducted in positive mode for complex **3.3**. Notably, a distinct fragmentation pattern is observed, these are indicated as $[M\text{-}Rh\text{-}COD]^+$, $[M\text{-}COD]^+$ and $[M]^+$ fragments.*

3.2.4 Single Crystal X-Ray Diffraction

Single crystal X-ray diffraction was used to further confirm the co-ordination mode of the proposed structure, complex **3.1** (Figure 3.9, *vide infra*). Single crystals were obtained for **3.1** *via* a slow diffusion of petroleum ether into a concentrated dichloromethane solution of the complex. The compound crystallizes in the monoclinic $P2_1/c$ space group. Four molecules per unit cell were observed. Furthermore the imine bonds were found to be *anti* to the aryl moieties, as indicated by the torsion angles around the imine bond (176°), this is comparable to structurally-similar structures.[33]

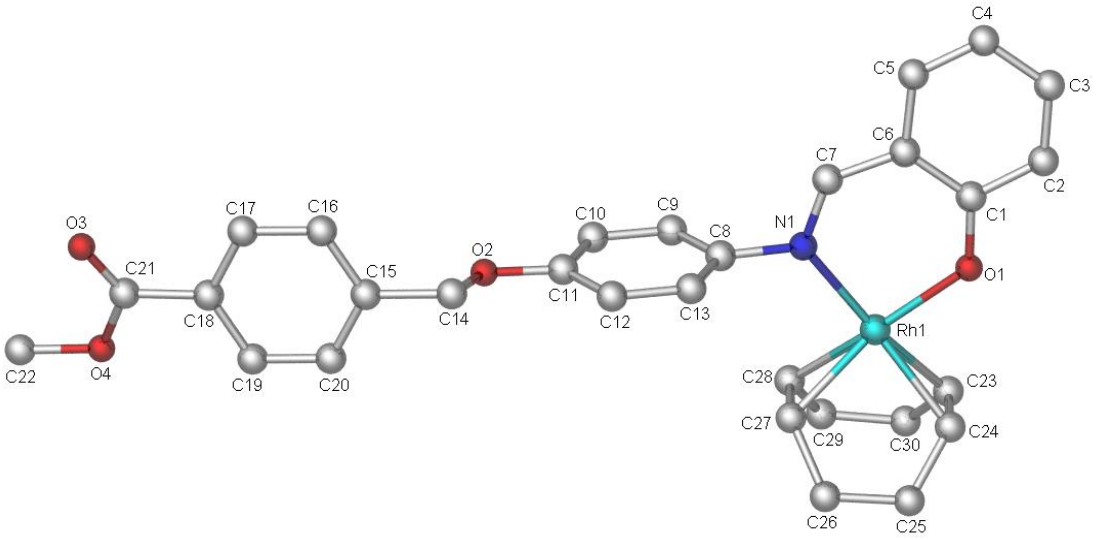

Figure 3.9. *Ball and stick representation of **3.1**. Note hydrogen atoms are omitted for clarity. Selected atoms are labelled for referral in Table 3.2.*

The molecular structure of complex **3.1** shows a square-planar geometry at the rhodium metal centre. The rhodium metal is co-ordinated to the COD moiety in an *(η^2:η^2)* manner and to the *N,O*-chelating ligand in a bidentate fashion (Figure 3.9). The bond angles between the metal centre and the *N,O*-salicylaldimine moiety are between 81 – 94° (Table 3.2, *vide infra*), this is similar to structurally-analogous compounds reported, and further confirms the square-planar geometry at the metal centre.[30, 33] The formation of a six-membered chelate ring imposes distortion around the rhodium atom. The distortion is evident with the O1-Rh1-C27 angle (161°), which is smaller than the expected value of 180°.

In comparison to the precursor compound **2.8**, the torsion angle about the imine bond is 177° (176° for the ligand **2.8**). An increase in the imine bond length (N1-C7, Δ 0.015 Å) is observed, as expected upon coordination of the metal to the imine nitrogen. This is due to the synergistic effect as the metal nitrogen bond is strengthened and the resultant imine bond (C=N) is weakened. This observation is in line with the IR spectroscopic analysis, as the lower wavenumber (lengthening of the C=N bond) is observed for the imine bond *v*(C=N) upon coordination to the complex **3.1**. Selected bond lengths and angles are summarised in Table 3.2. The full crystallographic data and structure refinement parameters can be found in Table 5.2, Chapter 5.

Table 3.2. *Selected crystallographic information for complex* ***3.1****, atom labels are defined in Figure 3.9.*

Selected Bond Lengths	**Interatomic distances (Å)**
Rh1-N1	2.074(2)
Rh1-O1	2.036(2)
Rh1-C23	2.139(3)
Rh1-C24	2.117(3)
Rh1-C27	2.134(3)
Rh1-C28	2.114(3)
Selected Bond Angles	**Angles (°)**
N1-Rh1-O1	90.80(8)
N1-Rh1-C27	94.20(1)
O1-Rh1-C23	87.60(9)
O1-Rh1-C24	86.49(9)
C24-Rh1-C27	81.80(1)
C24-Rh1-C28	94.10(1)

Based on the correlation between the analytical and spectroscopic data with the proposed structures, it can be concluded that complexes **3.1** – **3.3** were successfully synthesized and characterised.

3.3 Rhodium(I) Dicarbonyl *N,O*-salicylaldimine Organometallic Dendrons

3.3.1 Synthesis

The synthesis of the dicarbonyl Rh(I) organometallic dendrons, **3.4** – **3.6** were synthesized using a modified literature method (Scheme 3.2).[35] The COD moiety is readily displaced in the presence carbon monoxide (1 bar).[36-38] This observation is common for trispyrazolyl, pyridyl, *N*-heterocyclic carbene (NHC) and biphosphine Rh(I) complexes,[35, 38-40] however, to the best of our knowledge, the formation of dicarbonyl *N,O*-salicylaldimine complexes have not been reported. Thus, under higher pressures of syngas, it is presumed that the dicarbonyl Rh(I) complexes would form.[39, 41] The unpublished work by Mapolie and co-workers looked at the high pressure NMR studies on *N,O*-bidentate Rh(I) complexes which contains COD as a co-ligand.[42] The result of this study shows that at 75 °C and 30 bar (syngas), the COD moiety is displaced, as observed for the non-coordinated COD moiety in ^{1}H NMR spectra. Furthermore, no rhodium hydride is observed, which suggests that the dicarbonyl rhodium complex is the most stable catalytic species under the conditions tested. It is suggested that the rhodium hydride species is short-lived therefore this is not observed in the ^{1}H NMR spectra. More importantly, the dicarbonyl complexes **3.4** – **3.6** could potentially be much more structurally similar to the presumed active catalyst in comparison to the rhodium COD counterparts **3.1** – **3.3**.[39, 41]

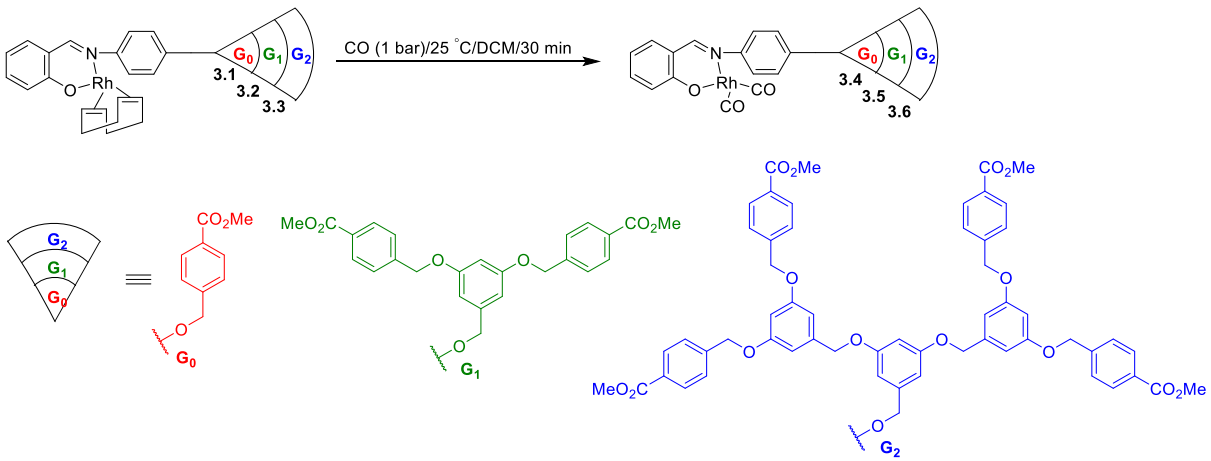

Scheme 3.2. *Synthesis of N,O-salicylaldimine Rh(I) metallodendron complexes bearing two carbonyls (CO) as auxiliary ligands (**3.4** – **3.6**).*

The dicarbonyl Rh(I) dendrons, **3.4** – **3.6** (Scheme 3.2) were synthesized by exposing a solution of **3.1** – **3.3** in dichloromethane to an atmosphere of CO (1 bar). The complexes **3.4** – **3.6** were isolated as orange, red and yellow powders respectively in excellent yields (95 – 99%).

3.3.2 Characterisation

3.3.2.1 ^{1}H and $^{13}C\{^{1}H\}$ NMR spectroscopy

The ^{1}H and $^{13}C\{^{1}H\}$ NMR spectra of complexes **3.4** – **3.6** were recorded in $CDCl_3$. The ^{1}H NMR spectra of **3.4** – **3.6** displays a distinct downfield shift for the imine proton resonance from δ_H 7.96 – 7.97 to 8.16 – 8.17 ppm (Figure 3.10). This observation suggests that carbon monoxide is a better π-acceptor than the *N,O*-salicylaldimine moiety. The imine is observed as a doublet ($^{3}J_{RhH}$ = 1.6 Hz), further attesting to the co-ordination of rhodium to the imine nitrogen. Similar to complexes **3.1** – **3.3**, the aromatic proton resonances occur between δ_H 6.54 – 8.11 ppm, methylene (-C**H$_2$**) proton signals between δ_H 5.00 – 5.40 ppm and the methoxy (-OC**H$_3$**) proton signal at δ_H 3.83 ppm (Figure 3.10).

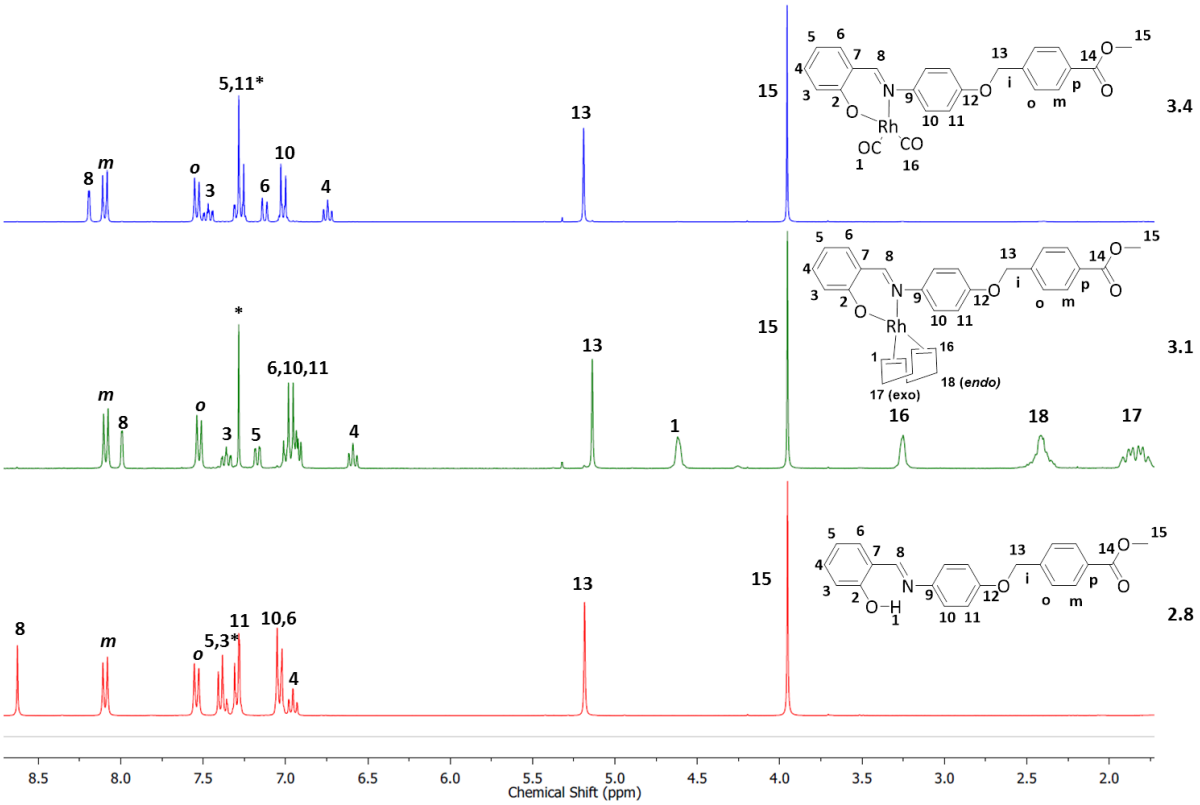

Figure 3.10. *Stacked ^{1}H NMR spectra for compounds **2.8, 3.1** and **3.4** respectively recorded in $CDCl_3$ (*$CDCl_3$).*

The successful co-ordination of carbon monoxide is attributed to the absence of the 1,5-cyclooctadiene proton resonances. The $^{13}C\{^{1}H\}$ NMR spectrum of complex **3.4** displays two sets of doublets between δ_C 183 – 185 ppm (Figure 3.11, *vide infra*). These are attributed to the co-ordinated carbonyl carbon atoms which couple to the spin active ^{103}Rh centre. The splitting is due to the *trans* effect observed in square-planar *N,O*-systems, which were similarly observed for complexes **3.1** – **3.3**.[30] As expected, no COD signals are observed in the $^{13}C\{^{1}H\}$ NMR spectra, further attesting to the successful synthesis of **3.4** – **3.6**. The COSY spectrum of complexes **3.4** – **3.6** shows the correlation of the imine proton resonance (H_8, $\delta_H \approx 8.1$ ppm) with proton signal of H_6 (Figure 3.10), thus confirming the correct assignment.

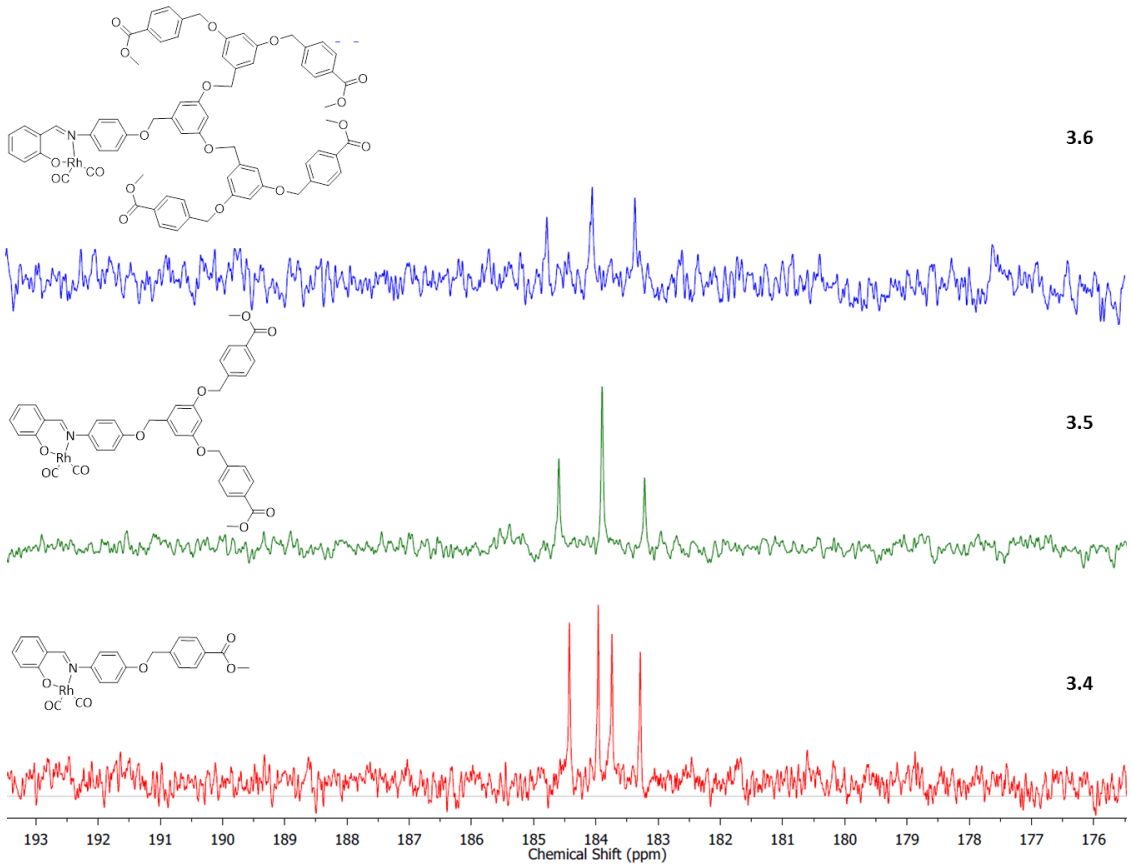

Figure 3.11. *Stacked $^{13}C\{^{1}H\}$ NMR spectra of complexes **3.4 – 3.6** in $CDCl_3$, which displays the diagnostic carbonyl signals between δ_C 185 – 183 ppm.*

Similarly to complexes **3.1** – **3.3**, the aromatic proton resonances for complexes **3.4** – **3.6** occur between δ_H 6.4 – 8.1 ppm, methylene (-C**H**$_2$) protons between δ_H 4.8 – 5.1 ppm and methoxy (-OC**H**$_3$) signal at δ_H 3.8 ppm (Figure 3.12). The spectra of the dendron series **3.4** – **3.6** displays no significant changes in the *N,O*-salicylaldimine moiety. The distinct differences are the number of aryl-ether and methylene (-C**H**$_2$) proton resonances (Figure 3.12). Furthermore the integration of the proton resonances are consistent with the proposed structures. The ^{1}H and $^{13}C\{^{1}H\}$ NMR data obtained is in agreement with the proposed complexes **3.4** – **3.6**.

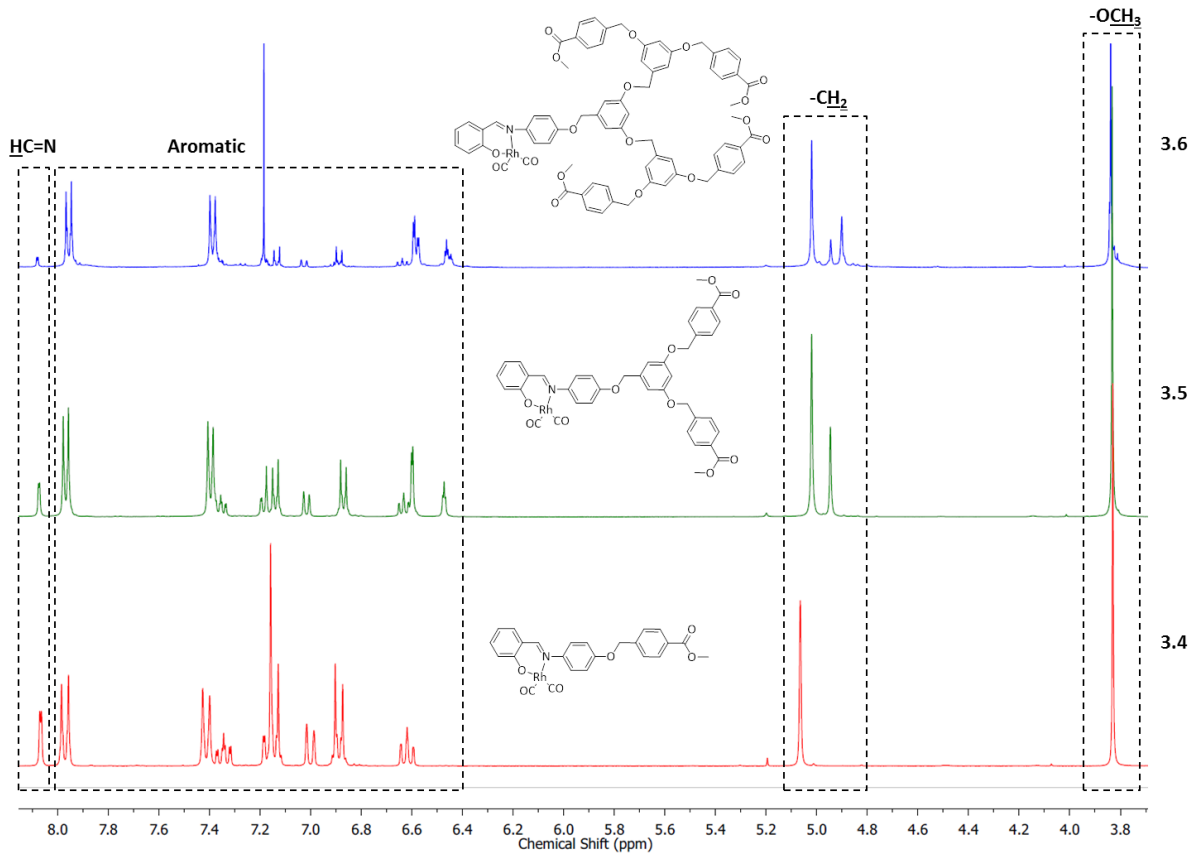

Figure 3.12. *Stacked ^{1}H NMR spectra for complexes **3.4 – 3.6**, showing the diagnostic protons for the zeroth (**3.4**), first (**3.5**) and second (**3.6**) generations respectively. A similar trend was observed for complexes **3.1 – 3.3**, hence this figure is a representative to depict differences across the dendron series. ^{1}H NMR spectra of complexes **3.4 – 3.6** were recorded in $CDCl_3$.*

3.3.2.2 Infrared spectroscopy

Carbonyl complexes of rhodium with *N*-donor ligands can form terminal or bridging carbonyls as reported by Dzik *et. al.*[40, 43] This is of particular importance as bridging carbonyls are defined as a "dead end" species in carbonylation catalytic reactions.[40, 43] It is noted that similar Rh(I) complexes containing *N*-donors behave differently in the solid and solution states, whereby the complex displays bridging carbonyls in the solid state and terminal carbonyls in solution state.[40, 43] This observation was particularly interesting and prompted the analysis of complexes **3.4** – **3.6** as pure solids using FT-IR spectroscopy and in solution state (DCM) to confirm the structural integrity of the complexes.

The IR spectra of complexes **3.4** – **3.6** displays two characteristic carbonyl absorption bands at *v*(C≡O) ≈2070 and ≈2000 cm^{-1} (Figure 3.13). These are attributed to the C≡O stretches and are in the diagnostic region for terminal carbonyls. These stretching vibrations are comparable to similar rhodium dicarbonyl complexes reported.[35, 38-40] A shift to higher wavenumbers (≈1605 to ≈1611 cm^{-1}) was observed for the imine absorption band *v*(C=N), which suggests a strengthening of the *v*(C=N) imine bond. The carbonyl is a better π-acceptor than the COD moiety. Hence upon coordination of the carbonyl motifs, more electron density is present on the rhodium centre, however the better π-accepting ability of the carbonyl moiety results in a back-donation of the electrons from the metal to the π^*-orbitals of the carbonyl ligand. This synergistic interaction results in a weaker *v*(Rh-N) metal-nitrogen bond and stronger *v*(C=N) bond. The shortening of the *v*(C=N) bond is observed as a shift to higher wavenumbers in the IR spectrum of complex **3.4** (Figure 3.13).

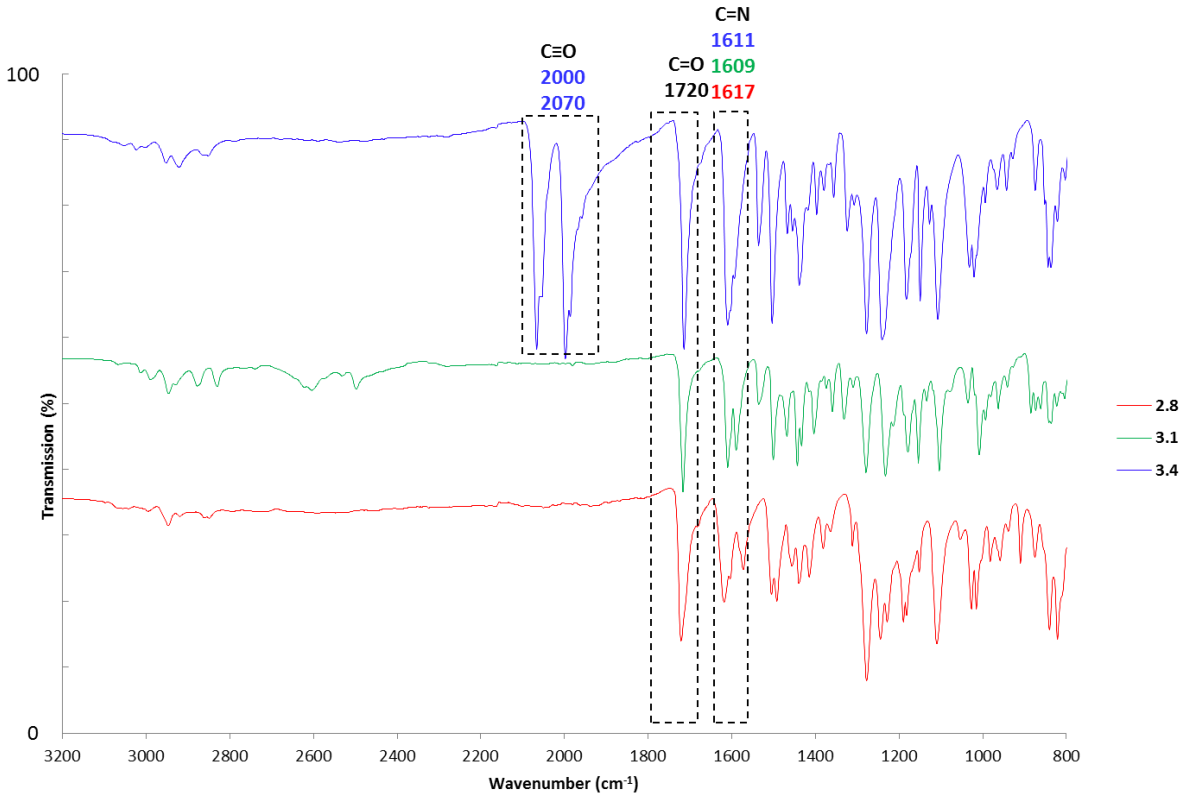

Figure 3.13. *The stacked IR spectra of compounds **2.8** (Ligand), **3.1** (COD complex) and **3.4** ($(CO)_2$ complex). Importantly, note the shifts of the imine (C=N) bands as well as the introduction of the carbonyl bands (C≡O). The sample was recorded in solid state (ATR).*

3.3.2.3 Mass Spectrometry and Elemental Analysis

HR-ESI mass spectrometry was used to further confirm the structural integrity of the organometallic dendrons **3.4** – **3.6**. The molecular ion peak $[M]^+$ is observed for the respective complexes **3.4** – **3.6** (Table 3.3). These are *m/z* 520.0323, 790.1157 and 1330.3027 for complexes **3.4** – **3.6** respectively. As expected, $[M\text{-}CO_2]^+$ and $[M\text{-}Rh\text{-}CO_2]^+$ fragments are observed in all complexes, with the former attributed to the decarbonylation of complexes **3.4** – **3.6.** The elemental analysis results are consistent with the proposed structures of complexes **3.4** – **3.6.**

3.3.2.4 Single Crystal X-Ray Diffraction (XRD)

A molecular structure was obtained for complex **3.4** (Figure 3.14) to confirm its structural integrity. Single crystals of complex **3.4** were obtained *via* slow evaporation of a concentrated solution of complex **3.4** in dichloromethane.

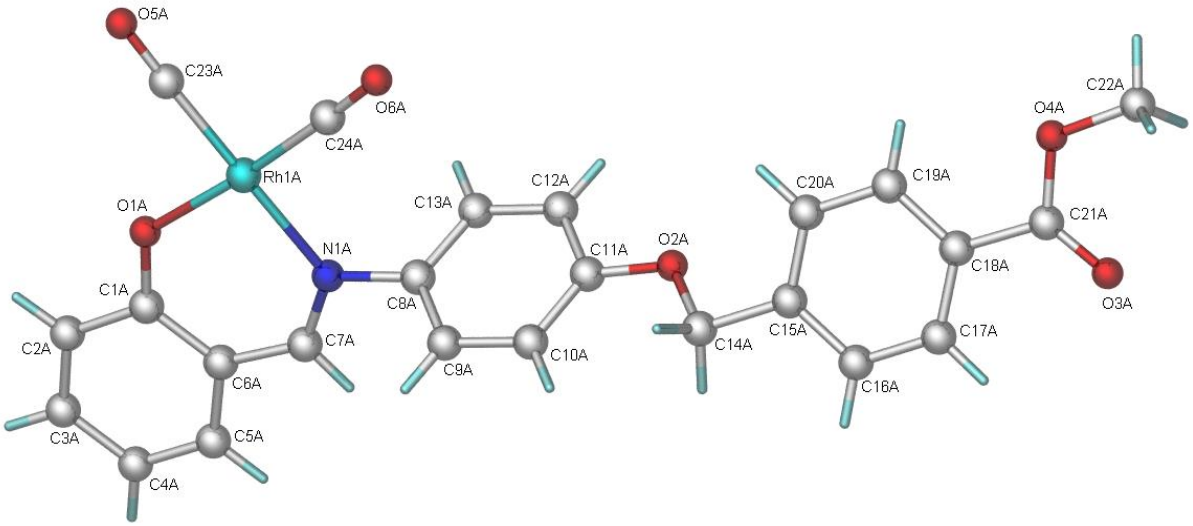

Figure 3.14. *Ball and stick representation of complex **3.4**. Selected atoms are labelled for referral in Table 3.3.*

Complex **3.4**, like the precursors **3.1**, crystallizes in the $P2_1/c$ space group. A total of 8 molecules per unit cell are observed for complex **3.4**. Notably bond angles between the metal centre are between 87 to 94°, thus confirming the square-planar arrangement around the metal centre.[30, 33] The bond angle between O1-Rh1-C24 is 175.5° (1), which is lower than the expected value of 180° for a square-planar complex (Table 3.3). Similarly to complex **3.1**, this distortion is caused by the six-membered chelate ring formed upon successful

complexation. The geometry, bond length and angles are comparable to structurally similar *N,O*-salicylaldimine Rh(I) complexes.[30, 32, 33, 44] The packing arrangement of complex **3.4** displays a pi-pi interaction between the rhodium atoms of two separate molecules, which is observed for structurally similar complexes.[30] This was not however observed in complex **3.1**, which is due to the bulky 1,5-cyclooctadiene ligand which inhibits the π···π stacking between the metal atoms. This observation has been reported in literature for structurally similar complexes.[35]

The comparison of the crystallographic data for complex **3.1** and **3.4** revealed similar bond lengths and angles about the salicylaldimine moiety. A slight shortening of the imine (C=N) bond is observed from 1.303 Å to 1.298 Å, this supports the conclusions from the IR spectroscopic analysis of complex **3.4**. This further suggests that CO is a better π-acceptor than the *N,O*-salicylaldimine ligand. A small change was observed in the chelation angle (N-Rh-O, Table 3.3) from 90.08° to 90.34°, which suggests the chelate is unaffected by the change in co-ligand [COD vs $(CO)_2$]. Selected bond lengths and angles are summarised in Table 3.3. The full crystallographic data and structure refinement parameters of complex **3.4** can be found in Table 5.2, Chapter 5.

Table 3.3. *Selected crystallographic information for complex* ***3.4.***

Selected Bond Lengths	**Interatomic distances (Å)**
Rh1A-N1A	2.067(3)
Rh1A-O1A	2.016(2)
Rh1A-C23A	1.877(5)
Rh1A-C24A	1.853(4)
O5A-C23A	1.127(6)
O6A-C24A	1.141(5)
C21A-O3A	1.208(2)
Selected Bond Angles	**Angles (°)**
N1A-Rh1A-O1A	90.34(1)
N1A-Rh1A-C24A	94.1(2)
N1A-Rh1A-C23A	175.8(2)
O1A-Rh1A-C23A	87.8(2)
O1A-Rh1A-C24A	175.5(1)
O5A-C23A-Rh1A	178.3(4)
O6A-C24A-Rh1A	177.1(4)

3.4 Rhodium(I) Chloro-Carbonyl *N,P*-iminophosphine Organometallic Dendrons

3.4.1 Synthesis

The synthesis of the chloro-carbonyl containing Rh(I) organometallic dendrons **3.7** – **3.9** involved two reactions (Scheme 3.3). The first reaction is the preparation of the $[Rh(\mu\text{-}Cl)(CO)_2]_2$ metal dimer which was employed using modified literature procedures.[45] This $[Rh(\mu\text{-}Cl)(CO)_2]_2$ dimer was reacted with the appropriate *N,P*-iminophosphine dendron **2.9, 2.11** or **2.13** *via* a bridge splitting reaction to form the complexes **3.7** – **3.9** (Scheme 3.3) respectively. The complexes **3.7** – **3.9** were isolated as orange solids in excellent yields (92 – 96%).

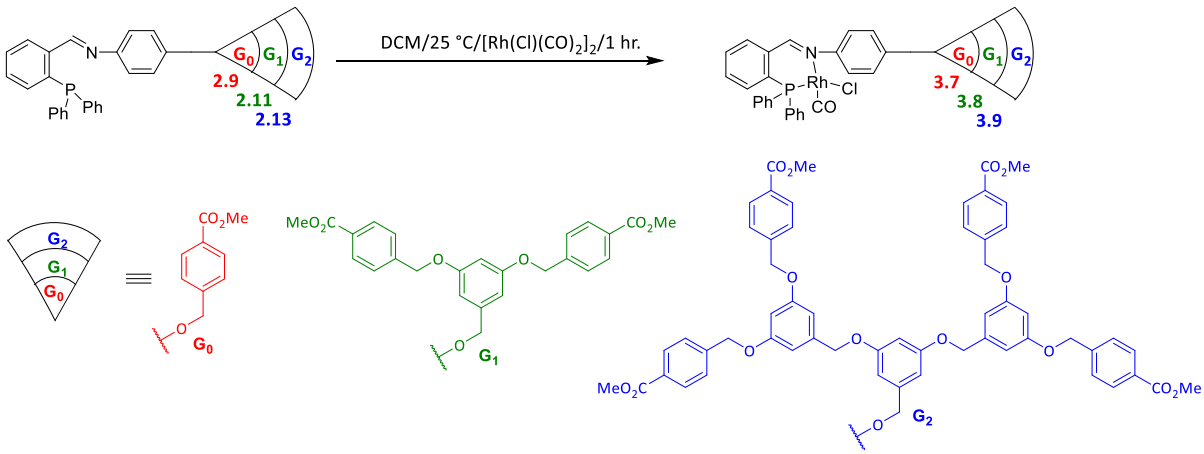

Scheme 3.3. *Synthesis of the N,P-iminophosphine Rh(I) metallodendron complexes bearing the carbonyl cis to the phosphine (**3.7** – **3.9**).*

3.4.2 Characterisation

3.4.2.1 ^{1}H, $^{13}C\{^{1}H\}$ and $^{31}P\{^{1}H\}$ NMR spectroscopy

The ^{1}H NMR spectra of complexes **3.7** – **3.9** displays a shift from δ_H 9.11 ppm to 8.02 – 8.05 ppm for the imine proton (**H**C=N) upon complexation. The magnitude of the shift is comparable to structurally similar *N,P*-iminophosphine Rh(I) complexes.[46-48] The multiplicity of the imine (**H**C=N) proton resonance could not be observed due to overlap with the aromatic dendritic proton resonances. The shift of the imine signal further confirms successful complexation to the imine nitrogen. The proton signals for the methylene (-C**H$_2$**),

methoxy (-OC**H$_3$**) and aryl-ether protons (Fréchet dendron) of the dendritic core occur at similar chemical shifts to those of the *N,P*-iminophosphine dendron ligands **2.9, 2.11** and **2.13**.

The bidentate coordination mode was confirmed using $^{31}P\{^1H\}$ NMR spectroscopy, as a downfield shift is observed from δ_P -13.2 to 48.5 ppm (Figure 3.15). The $^{31}P\{^1H\}$ NMR spectra shows a doublet with a coupling constant of 165 Hz ($^1J_{RhP}$) for complexes **3.7** – **3.9**, this is comparable to structurally similar compounds reported in literature.[46, 47] The presence of one doublet for complexes **3.7** – **3.9** attests to the formation of a single isomer for the complexes, whereby the carbonyl is *cis* to the phosphorous atom. The magnitude of the coupling constant and the chemical shift for complexes **3.7** – **3.9** are comparable for structurally similar *cis*-isomers (carbonyl *cis* to phosphorous) reported in literature.[46, 48, 49] Partial oxidation (4 – 7%) of the complex was observed to the phosphine oxide of the ligand. This was realised within 2 hours of running the $^{31}P\{^1H\}$ NMR of complexes **3.7** – **3.9**. Hence the complexes were not stable in solution and were stored as solids under an inert atmosphere.

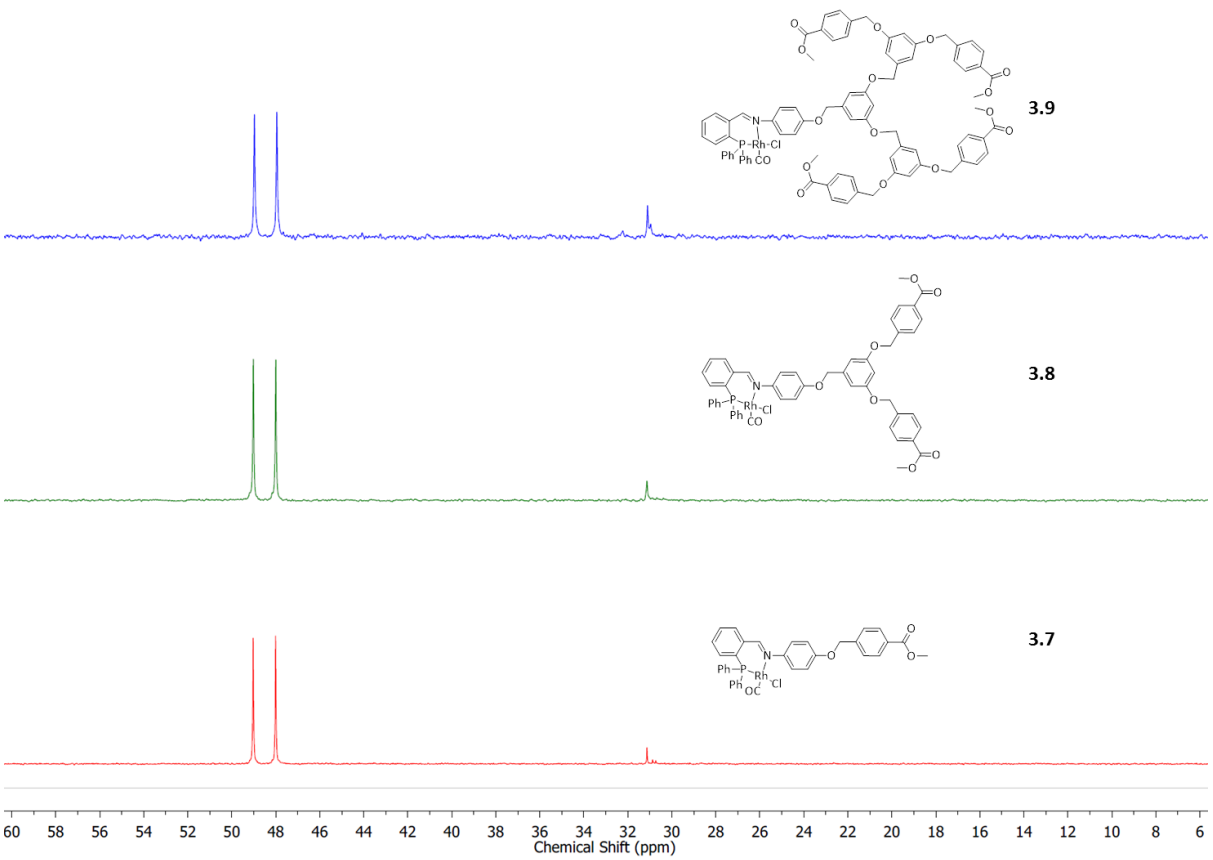

Figure 3.15. *The stacked $^{31}P\{^{1}H\}$ NMR spectra for the rhodium(I) iminophosphine metallodendrons,* ***3.7*** *–* ***3.9.*** *The spectra were recorded in $CDCl_3$.*

3.4.3.2 Infrared Spectroscopy

The infrared spectra of complexes **3.7** – **3.9** displays a shift in the *v*(C=N) absorption band from approximately 1611 cm^{-1} to 1607 – 1609 cm^{-1} (Figure 3.16). This shift to lower wavenumbers supports the coordination of rhodium to the imine nitrogen. A single carbonyl absorption band was observed at 1988, 1986 and 1990 cm^{-1} for complexes **3.7, 3.8,** and **3.9** respectively (Figure 3.16). The wavenumber (1986 – 1990 cm^{-1}) suggests that these are terminal carbonyls, furthermore the occurrence of one absorption band (C≡O) further corroborates the presence of a single isomer in the solid state. The wavenumber region (1986 – 1990 cm^{-1}) is indicative of the *cis* isomer, thus confirming the successful product formation.[46, 48, 49]

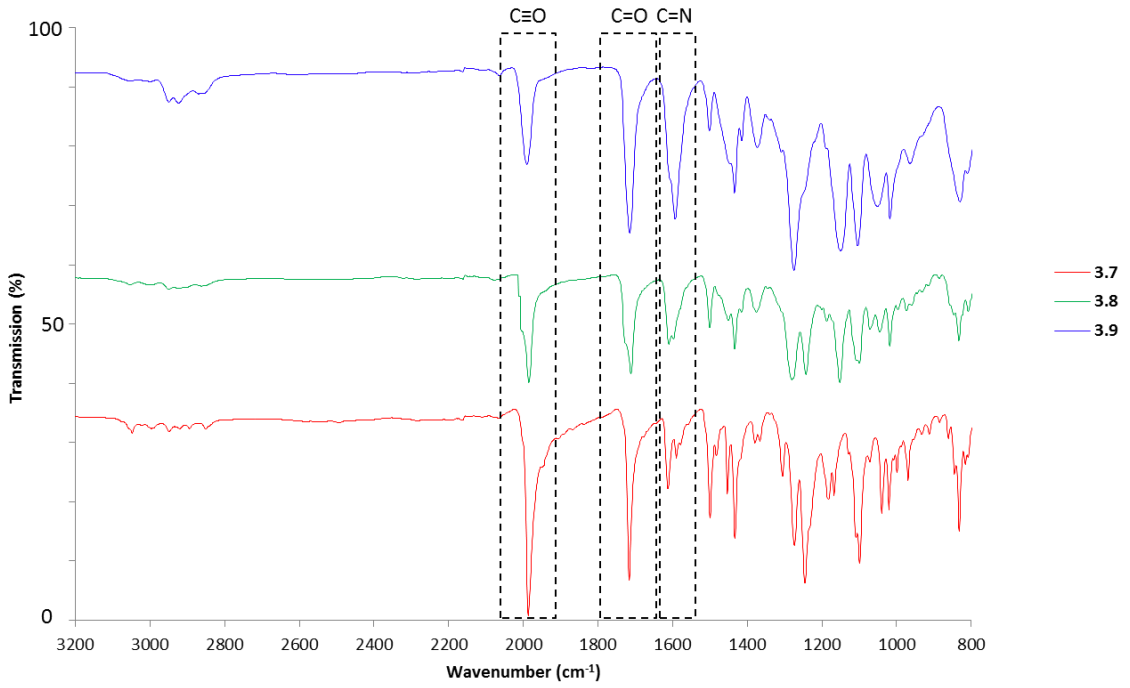

Figure 3.16. *Stacked IR spectra of complexes **3.7** – **3.9.** Importantly, note the shifts of the imine (C=N) absorption bands as well as the introduction of the carbonyl absorption bands (C≡O). The samples were recorded in solid state (ATR).*

3.4.2.3 Mass Spectrometry

HR-ESI mass spectrometry was used to further confirm the structural integrity of the organometallic dendrons **3.7** – **3.9**. The HR-ESI-MS analysis (recorded in the positive mode) of complexes **3.7** – **3.9** yielded $[M\text{-}Cl]^+$ fragments. These are *m/z* 660.0795, 930.1716 and 1470.3429 for complexes **3.7**, **3.8** and **3.9** respectively. This fragmentation pattern is commonly observed for structurally similar *N,P*-iminophosphine Rh(I) organometallic complexes.[46, 47]

3.4.2.4 Single Crystal X-Ray Diffraction (XRD)

The molecular structure of complex **3.7** was confirmed by single crystal X-ray diffraction analysis (Figure 3.17). Single crystals were grown by a slow diffusion of pentane into a concentrated dichloromethane/toluene (*v/v*, 1:1) solution of complex **3.7**.

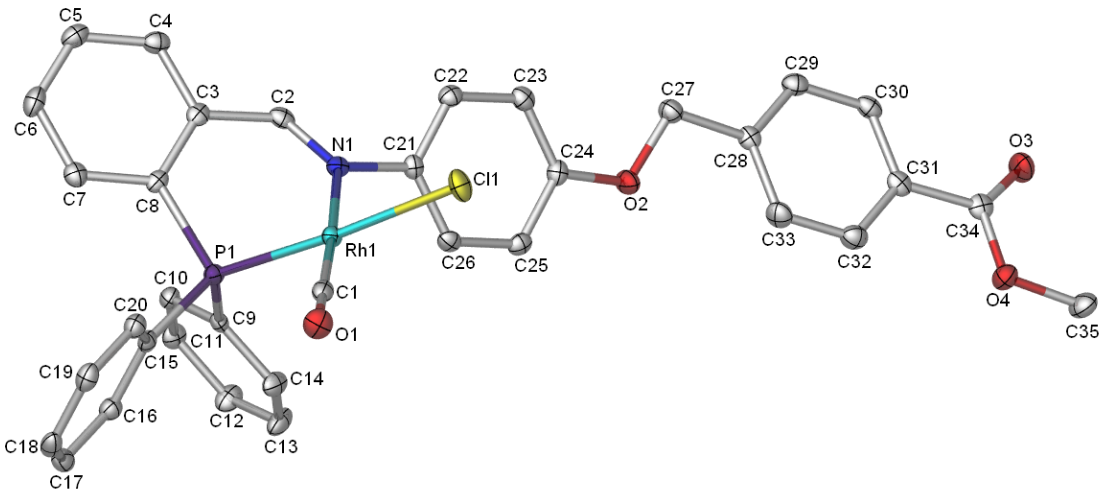

Figure 3.17. *ORTEP representation of complex **3.7**, with thermal ellipsoids at the 50% probability level. Note hydrogen atoms are omitted for clarity. Atoms are labelled for referral in Table 3.4.*

Complex **3.7** crystallizes in a $P2_1/c$ space group with a monoclinic system. A total of 4 molecules per unit cell were observed for complex **3.7**. The bond angles about the metal centre are between 83° – 96 °, which confirms the four-coordinate square-planar geometry around the rhodium centre (Table 3.4). The bond angles between P1-Rh1-Cl1 and N1-Rh1-C1 deviates from the expected 180°, which indicates distortion caused by the six-membered chelate ring about the rhodium atom. More importantly, the molecular structure of complex **3.7** displays the chlorido group *trans* to the phosphorous atom and the terminal carbonyl group *trans* to the imine nitrogen in the solid state. This observation in combination with the IR and NMR data, further confirms the presence of a single isomer, whereby the carbonyl is *cis* to the phosphorous atom.

Table 3.4. *Selected crystallographic information for complex* ***3.7.***

Selected Bond Lengths	**Interatomic distances (Å)**
Rh1-N1	2.119(2)
Rh1-P1	2.2020(8)
Rh1-Cl1	2.3892(8)
Rh1-C1	1.820(3)
N1-C2	1.291(4)
C1-O1	1.149(3)
Selected Bond Angles	**Angles (°)**
N1-Rh1-P1	83.60(6)
N1-Rh1-Cl1	90.84(6)
C1-Rh1-Cl1	89.5(1)
C1-Rh1-P1	96.0(1)
P1-Rh1-Cl1	174.35(3)
N1-Rh1-C1	176.1(1)

The geometry, bond length and angles are comparable to structurally similar *N,P*-iminophosphine Rh(I) complexes.[46, 48, 49] The full crystallographic data and structure refinement parameters of complex **3.7** can be found in Table 5.2, Chapter 5.

The characterisation data in Chapter 3 supports the successful synthesis of the proposed rhodium(I) dendrons. The correlation between the characterisation data and proposed structures allowed for the catalytic study of these complexes in the hydroformylation of olefins, which is described in Chapter 4.

3.5 Overall Summary

A series of new *N,O*-salicylaldimine and *N,P*-iminophosphine rhodium(I) organometallic dendrons **3.1** – **3.9** were successfully synthesized. The complexes were afforded in excellent yields (79 – 99 %). All complexes were characterised using an array of analytical and spectroscopic techniques. Complexes **3.1** – **3.9** were characterised using NMR (^{1}H, ^{13}C{^{1}H}, ^{31}P{^{1}H}, HSQC, COSY, HMBC), IR spectroscopy, elemental analysis and mass spectrometry (electron impact, electron spray ionisation, matrix-assisted laser desorption ionisation - time of flight), which confirmed the formation of the desired products. Single crystals of complexes **3.1**, **3.4** and **3.7** were analysed by X-ray diffraction. The formation of the six-membered rhodacycles and bidentate co-ordination mode was further confirmed in the solid state by single crystal analysis. The analytical and spectroscopic data correlated well with the proposed structures (**3.1** – **3.9**).

3.6 References

1. E. Buhleier, W. Wehner and F. Vögtle, *Chem. Informationsdienst*, 1978, **9**.
2. G. I. Dzhardimalieva and I. E. Uflyand, *Dalton Trans.*, 2017, **46**, 10139-10176.
3. J. Yang, Q. Zhang, H. Chang and Y. Cheng, *Chem. Rev*, 2015, **115**, 5274-5300.
4. A. Carlmark, C. Hawker, A. Hult and M. Malkoch, *Chem. Soc. Rev.*, 2009, **38**, 352-362.
5. M. A. Mintzer and M. W. Grinstaff, *Chem. Soc. Rev.*, 2011, **40**, 173-190.
6. A. W. Bosman, H. M. Janssen and E. W. Meijer, *Chem. Rev.*, 1999, **99**, 1665-1688.
7. D. Astruc, E. Boisselier and C. Ornelas, *Chem. Rev*, 2010, **110**, 1857-1959.
8. G. R. Newkome, F. Cardullo, E. C. Constable, C. N. Moorefield and A. M. W. C. Thompson, *J. Chem. Soc., Chem. Commun.*, 1993, 925-927.
9. S. Campagna, G. Denti, S. Serroni, M. Ciano and V. Balzani, *Inorg. Chem.*, 1991, **30**, 3728.
10. D. A. Tomalia, *Aldrichim. Acta*, 2004, **37**, 39-57.
11. I. Cuadrado, M. Morán, C. M. Casado, B. Alonso and J. Losada, *Coord. Chem. Rev.*, 1999, **193**, 395-445.
12. A. Berger, R. J. K. Gebbink and G. van Koten, in *Dendrimer Catalysis*, Springer, 2006, pp. 1-38.

13. A.-M. Caminade, A. Ouali, R. Laurent, C.-O. Turrin and J.-P. Majoral, *Coord. Chem. Rev.*, 2016, **308**, 478-497.
14. A. M. Caminade, R. Laurent and J. P. Majoral, *Adv Drug Deliv Rev*, 2005, **57**, 2130-2146.
15. A.-M. Caminade, R. Laurent, B. Delavaux-Nicot and J.-P. Majoral, *New J. Chem.*, 2012, **36**, 217-226.
16. M. C. Parrott, E. B. Marchington, J. F. Valliant and A. Adronov, *J. Am. Chem. Soc.*, 2005, **127**, 12081.
17. A. Sánchez-Méndez, E. de Jesús, J. C. Flores and P. Gómez-Sal, *Eur. J. Inorg. Chem.*, 2010, **2010**, 141-151.
18. T. Lozano-Cruz, P. Ortega, B. Batanero, J. L. Copa-Patino, J. Soliveri, F. J. de la Mata and R. Gomez, *Dalton Trans.*, 2015, **44**, 19294-19304.
19. D. Astruc and F. Chardac, *Chem. Rev*, 2001, **101**, 2991-3023.
20. R. S. Bagul and N. Jayaraman, *Inorg. Chim. Acta*, 2014, **409**, 34-52.
21. S. C. Bourque, F. Maltais, W. Xiao, O. Tardif, H. Alper, P. Arya and L. E. Manzer, *J. Am. Chem. Soc.*, 1999, **121**, 3035-3038.
22. P. Arya, N. V. Rao, J. Singkhonrat, H. Alper, S. C. Bourque and L. E. Manzer, *J. Org. Chem.*, 2000, **65**, 1881-1885.
23. P. Arya, P. Gautam, N. Venugopal Rao, H. Alper, S. C. Bourque and L. E. Manzer, *J. Am. Chem. Soc.*, 2001, **123**, 2889-2890.
24. S.-M. Lu and H. Alper, *J. Am. Chem. Soc.*, 2003, **125**, 13126-13131.
25. L. c. Ropartz, R. E. Morris, D. F. Foster and D. J. Cole-Hamilton, *J. Mol. Catal. A: Chem*, 2002, **182**, 99-105.
26. E. B. Hager, B. C. Makhubela and G. S. Smith, *Dalton Trans.*, 2012, **41**, 13927-13935.
27. G. Giordano, R. H. Crabtree, R. M. Heintz, D. Forster and D. E. Morris, in *Inorg. Synth.*, ed. R. J. Angelici, John Wiley & Sons, Inc., 1990, vol. 28, pp. 88-90.
28. J. Chatt and L. M. Venanzi, *J. Chem. Soc.*, 1957, 4735-4741.
29. P. Govender, A. K. Renfrew, C. M. Clavel, P. J. Dyson, B. Therrien and G. S. Smith, *Dalton Trans.*, 2011, **40**, 1158-1167.
30. C. Janiak, A.-C. Chamayou, A. K. M. Royhan Uddin, M. Uddin, K. S. Hagen and M. Enamullah, *Dalton Trans.*, 2009, **38**, 3698-3709.
31. T. Stringer, PhD thesis, University of Cape Town, 2014.

32. S. Siangwata, S. Chulu, C. L. Oliver and G. S. Smith, *Appl. Organomet. Chem.*, 2017, **31**, e3593-n/a.
33. L. C. Matsinha, S. F. Mapolie and G. S. Smith, *Dalton Trans.*, 2015, **44**, 1240-1248.
34. J. F. G. A. Jansen, E. M. E. d. B.-v. d. Berg and E. W. Meijer, *Science*, 1994, **266**, 1226-1269.
35. V. Diachenko, M. J. Page, M. R. Gatus, M. Bhadbhade and B. A. Messerle, *Organometallics*, 2015, **34**, 4543-4552.
36. D. J. Wink and B. T. Creagan, *J. Am. Chem. Soc.*, 1990, **112**, 8585-8586.
37. S. Fallis, G. K. Anderson and N. P. Rath, *Organometallics*, 1991, **10**, 3180-3184.
38. B. D. Vineyard, W. S. Knowles, M. J. Sabacky, G. L. Bachman and D. J. Weinkauff, *J. Am. Chem. Soc.*, 1977, **99**, 5946-5952.
39. A. R. Chianese, X. Li, M. C. Janzen, J. W. Faller and R. H. Crabtree, *Organometallics*, 2003, **22**, 1663-1667.
40. W. I. Dzik, C. Creusen, R. de Gelder, T. P. J. Peters, J. M. M. Smits and B. de Bruin, *Organometallics*, 2010, **29**, 1629-1641.
41. C. Köcher and W. A. Herrmann, *J. Organomet. Chem.*, 1997, **532**, 261-265.
42. C. Joubert and S. F. Mapolie, unpublished work.
43. B. T. Heaton, C. Jacob and J. T. Sampanthar, *J. Chem. Soc., Dalton Trans.*, 1998, **27**, 1403-1410.
44. P. Govender, S. Ngubane, B. Therrien and G. S. Smith, *J. Organomet. Chem.*, 2017, **848**, 281-287.
45. A.-J. Deeming and P. Sharratt, *J. Organomet. Chem.*, 1975, **99**, 447-453.
46. B. C. Makhubela, A. Jardine and G. S. Smith, *Green Chem.*, 2012, **14**, 338-347.
47. N. Antonels, MSc dissertation, University of Cape Town, 2010.
48. L. Maqeda, B. C. E. Makhubela and G. S. Smith, *Polyhedron*, 2015, **91**, 128-135.
49. N. Antonels, B. Therrien, J. R. Moss and G. Smith, *Inorg. Chem. Commun.*, 2009, **12**, 716-719.

Chapter 4

The Catalytic Evaluation of Rh(I) *N,O*-salicylaldimine And *N,P*-iminophosphine Metallodendrons In The Hydroformylation of Olefins

4.1 Introduction

The daily worldwide consumption of crude oil was estimated to be eighty-nine million barrels in 2013.[1] The dependence on fossil fuels as a fuel source is a worldwide concern, as these non-renewable sources are depleting at an alarming rate.[1] The increased population growth correlates with the increased fossil-fuel consumption and subsequent increased greenhouse gas emissions.[1] Increased greenhouse gas emissions is known to strongly contribute to Global Warming and Climate Change.[2-4] To combat these challenges, a paradigm shift is required with respect to fossil fuels, one innovative alternative is the use of renewable sources of fuel, namely biofuels.[1, 5] In this panorama, the utilisation of biofuels from citrus waste and plant-seed waste is highly beneficial, due to its renewability, lower greenhouse gas emission and the low-sulfur content.[1] The low sulfur content is particularly enticing, as one of the drawbacks in fossil fuels is sulfur poisons.[6-8] Sulfur is known to deactivate catalysts,[9-11] moreover, the combustion of sulfur in fossil fuels to form sulfur dioxide is directly proportional to the increase in acid rain occurrences.[1, 12, 13]

One of the most abundant plant sources globally is citrus fruit, which produces 88 million tonnes per year.[1, 14] Limonene and citronellal are the major components in lemon and

orange oils (88 – 95%). These terpenes are obtained by the distillation of trifoliate citrus peel oils (obtained from citrus-peel waste).[1] Citrus waste are popular feedstocks used in fragrance,[14-16] agrochemical,[17, 18] food,[14, 19] pharmacological,[14, 18, 20] paint[14] and cosmetic fields.[1, 21] Such bio-based materials can be modified to higher-value products by suitable catalytic reactions. With respect to South Africa, millions of tonnes of citrus/plant-seed waste are generated from the agricultural industry.[22] Therefore, by functionalising this low-value biomass to higher value products with atom-economic catalytic process, this approach is enticing to industry as it makes use of multiple Green Chemistry principles.[22]

South Africa has an abundance of substrates for the hydroformylation reaction, these include olefins from the Fischer-Tropsch process at SASOL, triolein from vegetable oil industries in KwaZulu-Natal/Gauteng and limonene from the citrus industries in the Western Cape (Table 4.1).[23-25] From an economical and environmental viewpoint, the functionalisation of these short and long chain olefins could lead to molecules with extended applications (Table 4.1).

Table 4.1. *Selected olefins and their applications post-hydroformylation.*

Substrate	Application of the Product After Hydroformylation
1-Octene	Plasticizer,[25] Fragrance[14, 17, 26, 27]
Styrene	Pharmaceutical[26, 28-32]
7-Tetradecene	Surfactant[33]
Methyl oleate	Polymers, Lubricants, Plasticizers, Paints, Urethane Foams.[34 35]
Triolein	Biodiesel[5, 36-38]
R-Citronellal	Fragrance,[14, 16, 17, 27] Pharmaceuticals[18, 31]
D-Limonene	Fragrance,[14, 17, 27] Pharmaceuticals[15, 18, 31, 39] Waste Valorization[1]

The abundance of short chain olefins from the Fischer-Tropsch processes at SASOL result in the olefins being easily accessible and available at relatively low cost.[25] However, longer

chain carbons are highly desired (>C_8, Flory-Schulz carbon chain spectrum) as these are predominantly used in cosmetic, plasticiser and detergent streams (Table 4.1).[25] The transformation of low-value short chain olefins by functionalisation using syngas to higher value products, forms part of the programme of the National Research Foundation (NRF) centre of Excellence in Catalysis (c*change) and South African Department of Science and Technology (DST), (Scheme 4.1).[25]

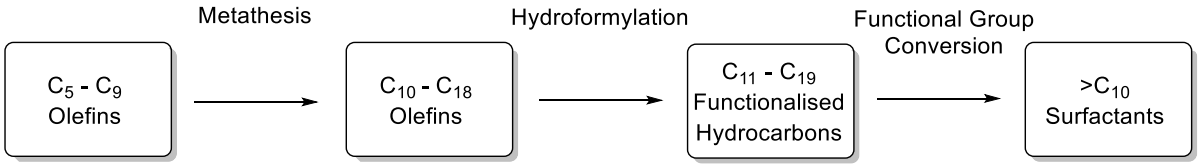

Scheme 4.1. *The proposed reaction pathway for the conversion of low-value short chain olefins to higher-value surfactants.*

Although the functionalisation of synthetically-produced olefins is well reported, there is a lack of literature on the modification of biomass-based olefins.[5, 22] One popular method for the functionalisation of biomass is bacterial fermentation.[1, 19, 22] In context of citrus waste, the high toxicity of *D*-limonene to bacteria inhibits the product formation; hence this pathway is not viable.[1, 19] One less explored method is the use of transition-metal catalytic processes to functionalise biomass.

The hydroformylation reaction, also known as the "Oxo process", is one of the most important industrial processes as it is estimated to produce 10 million tonnes of aldehydes annually.[40] The hydroformylation reaction is the transition metal catalysed addition of carbon monoxide and hydrogen gas to olefins resulting in the formation of aldehydes (Scheme 4.2).[41] The homogeneity of the reaction allows for superior activity and selectivity in comparison to the heterogeneous counterpart; however the separation of the catalyst and product is much more facile in the latter process.[41, 42] One means of overcoming this drawback is to immobilise the complex onto a dendritic support to facilitate this separation.[43-45] Once anchored to dendrimers, these can be effectively separated by ultrafiltration or membrane technology.[46] Dendrimers can aid in the stabilisation of the

metal complex, by virtue of the microenvironment imparted by the dendritic architecture.[45, 47]

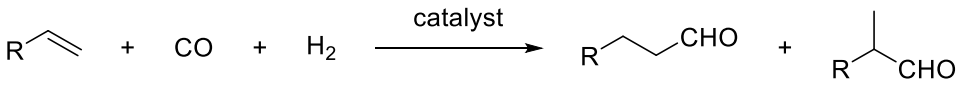

R = Aromatic or Alkyl group

Scheme 4.2. *Hydroformylation of terminal olefins to yield linear and branched aldehydes.*

As an extension to our previous studies, this work is aimed at evaluating the effect of the dendron size on the hydroformylation reaction, using 1-octene as the model substrate. Herein, we report on the catalytic evaluation of mononuclear Rh(I) dendrons (**3.1** - **3.9**) as catalyst precursors in the hydroformylation of olefins. The complexes tested vary in electronic properties, steric characteristics and dendron size. The influences of various donor atoms were investigated using the G_0-analogues (**3.1, 3.4** and **3.7**).

4.2 Results and Discussion

4.2.1 Catalyst Optimisation

The preliminary catalytic evaluation was conducted using complex **3.4** (Figure 4.1) and 1-octene as the model substrate, to obtain the optimised conditions with respect to temperature, pressure and time. These parameters were also conducted at the optimised conditions for similar *N,O*-salicylaldimine Rh(I) catalyst precursors to allow for comparison.[48, 49]

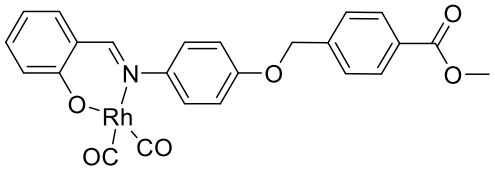

Figure 4.1. *Structure of the catalyst precursor (**3.4**), which was utilised in the catalyst optimisation experiments for the hydroformylation of 1-octene.*

The pressure was varied between 20, 30 and 40 bar (Table 4.2). Furthermore the temperature was varied at 55 °C, 75 °C and 95 °C to obtain a comprehensive optimisation

study for complex **3.4**. Note that these optimisation experiments were not aimed at identifying conditions for quantitative conversion, but rather to identify conditions which gave both excellent conversions and the best *n:iso* ratio. One of the motivations for reaction optimisation is to obtain the best product selectivity, with the mildest conditions possible. This is inherently in line with Green Chemistry principles.

4.2.2 Effect on conversion and catalytic activity

At fixed temperature (Entries 4 – 6 and 7 – 9, Table 4.2, *vide infra*), an increase in pressure results in a general increase in conversion at temperatures 75 °C (entries 4 – 6) and 95 °C (entries 7 – 9). It is understood that the increased CO pressure results in increased CO concentration in solution.[50, 51] The vacant site of the $HRh(CO)L_2$ species (L denotes the appropriate ligand) is occupied by an additional CO, which limits the isomerisation and accelerates the CO migration step.[50, 51] This process results in much faster conversion of the olefin to aldehydes, and this trend is observed for catalyst **3.4** (Table 4.2).[50, 51]

An increase in activity[†] is observed with an increase in both pressure and temperature (Figure 4.2). Notably at 55 °C, low conversions and activity were obtained. This implies that much more energy (higher temperature) is required for activation of the alkene and subsequent hydroformylation. With respect to substrate conversion and catalyst activity, temperatures above 75 °C and pressures above 30 bar were identified as suitable conditions for the hydroformylation of 1-octene.

[†] Turnover frequency is referred to as the catalyst activity [(mmol of aldehydes/mmol of Rh)]/time.

Table 4.2. *The catalyst optimisation results with respect to the effect of temperature and pressure of the catalyst precursor* ***3.4****.*

Entry	Temperature (^{o}C)	Pressure (bar)	Conversion (%)	Aldehydes (%)	Iso-Octenes (%)	*n:iso*	TOF (h^{-1})
1	55	20	10.77	63.95	36.05	2.14	43
2	55	30	20.97	77.67	22.33	1.67	99
3	55	40	7.85	60.70	39.30	1.58	30
4	75	20	50.38	62.13	37.87	2.54	200
5	75	30	99.19	86.44	13.56	1.25	536
6	75	40	99.64	98.61	1.39	1.20	591
7	95	20	96.82	84.98	15.02	0.61	512
8	95	30	99.65	91.99	8.01	0.88	573
9	95	40	100.00	100.00	0.00	0.77	625

The reactor was loaded with toluene (5 mL), 1-octene (0.805 g, 7.175 mmol), internal standard *n*-decane (0.204 mg, 1.435 mmol) and Rh-metal loading (2.87 x 10^{-3} mmol). The reactor was purged with nitrogen three times, followed by purging thrice with syngas. TOF = (mmol of aldehydes/mmol of Rh)/time. Catalyst to substrate ratio utilised was (1:2500). The samples were analysed using GC-FID. Reactions were conducted for 4 hours.

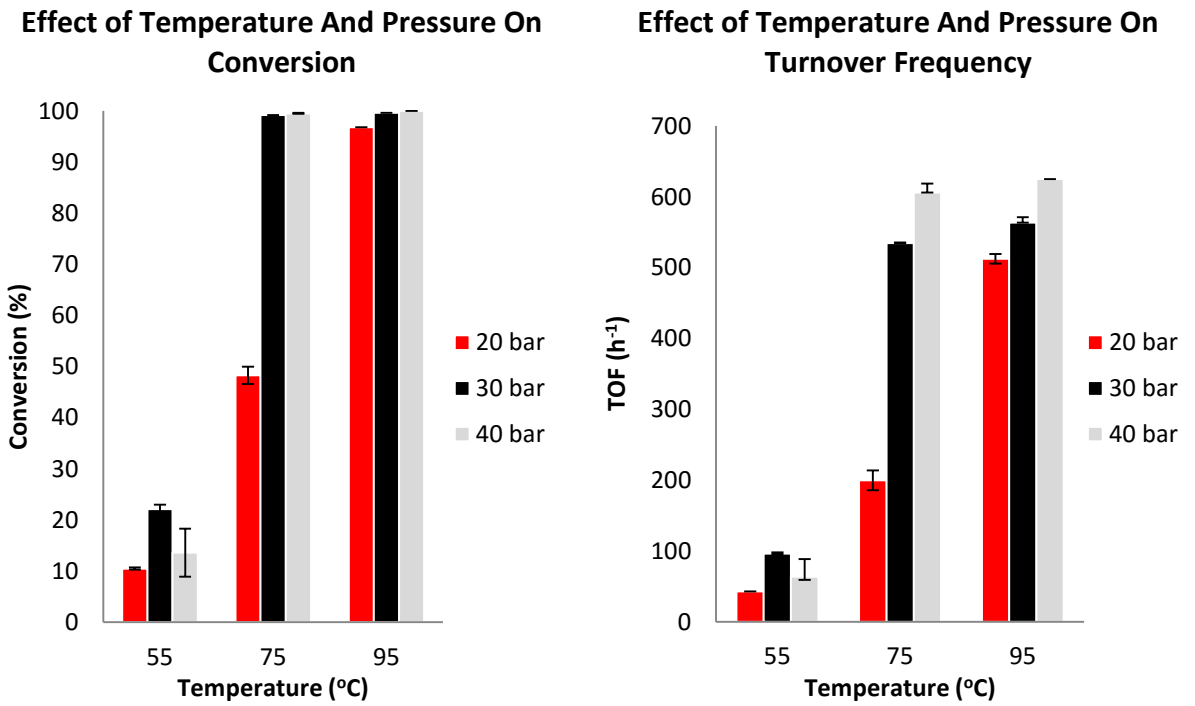

Figure 4.2. *Graphical representation of the conversion and activity as a function of pressure and temperature for catalyst* ***3.4****.*

4.2.3 Effect on chemoselectivity

The catalyst precursor **3.4** displays excellent chemoselectivity at higher pressures and temperatures (Figure 4.3). Based on theoretical calculations by Haumann *et al.* the hydroformylation of internal olefins has a higher activation energy barrier, hence these require more energy for the hydroformylation to occur.[33, 52] This phenomenon is in line with observations for complex **3.4**, as an increase in temperature resulted in better chemoselectivity, as the internal olefins are converted *via* hydroformylation to *iso*-aldehydes. As discussed previously, higher syngas pressures often favour hydroformylation over isomerisation of the olefinic substrate.[33] This is observed at both 75 °C and 95 °C as a function of increasing pressure (Figure 4.3).[33] The increased percentage of *iso*-alkenes at low pressures and temperatures are often observed for structurally similar hydroformylation precursors.[48, 49] The isomerisation behaviour can be attributed to either the lower CO pressure which results in the $HRh(CO)L_2$ possessing a vacant site, and subsequently promotes isomerisation. Additionally, the formation of a different catalytic species at lower pressures may occur. One form is attributed to the formation of rhodium nanoparticles which are known to catalyse the isomerisation of olefins.[43, 53] Mercury drop experiments have been performed on this catalyst. This is discussed later in this chapter.

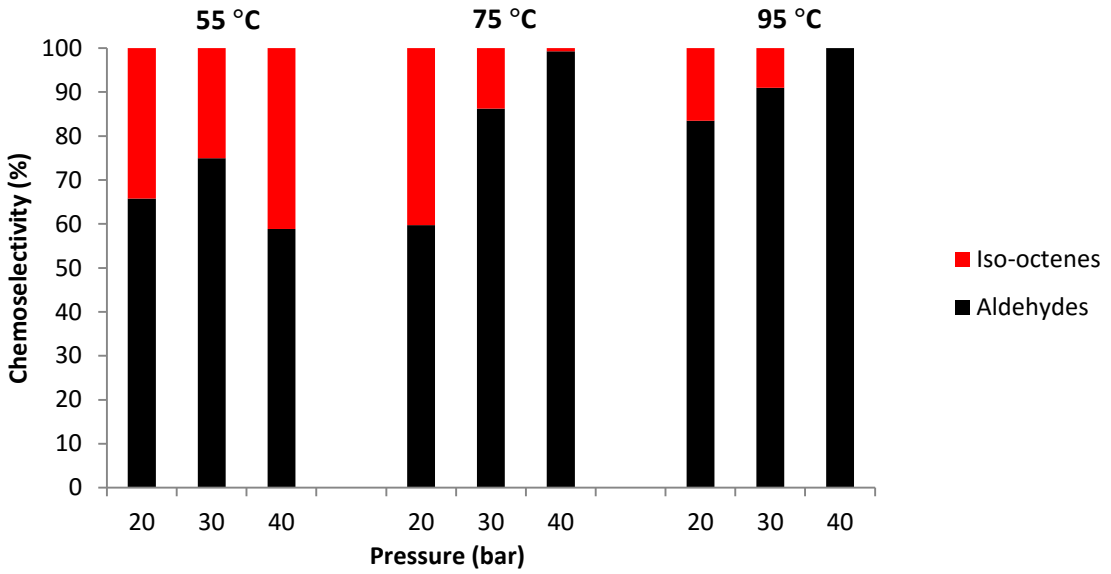

Figure 4.3. *Graphical representation of the chemoselectivity when evaluated using complex* ***3.4****.*

4.2.4 Effect on regioselectivity

The regioselectivity of the hydroformylation of 1-octene is based on the formation of either linear (nonanal) or branched (2-methyl octanal, 2-ethyl heptanal and 2-propyl hexanal) aldehydes. The mechanism (Scheme 1.2, Chapter 1) shows that the hydride can insert according to two different approaches. The *anti*-Markovnikov addition to the terminal olefin yields linear products. Contrastingly, the Markovnikov addition to the internal olefin results in the formation of branched aldehydes. The regioselectivity is predominantly governed by steric crowding enforced by the ligand.[26]

The catalyst precursor **3.4** displays moderate regioselectivity at the tested temperatures and pressures (Figure 4.4). Note that the regioselectivity is maintained across the pressures tested at 55 °C and 75 °C, which suggests that the active species is the same at both temperatures tested for the specific reaction times. When comparing temperatures at 75 °C and 95 °C, it is noted that the percentage of branched aldehydes increases, which ultimately lowers the *n:iso* ratio. One postulation is that the formation of the tetracarbonyl rhodium species $[Rh(CO)_4]^+$ at higher pressures, could influence the selectivity of the catalyst.[54] Hence based on this observation, the pressure and temperature which gives quantitative conversion and the best *n:iso* ratio was 30 bar and 75 °C. This result correlates with the optimised hydroformylation conditions for similar complexes.[43, 54]

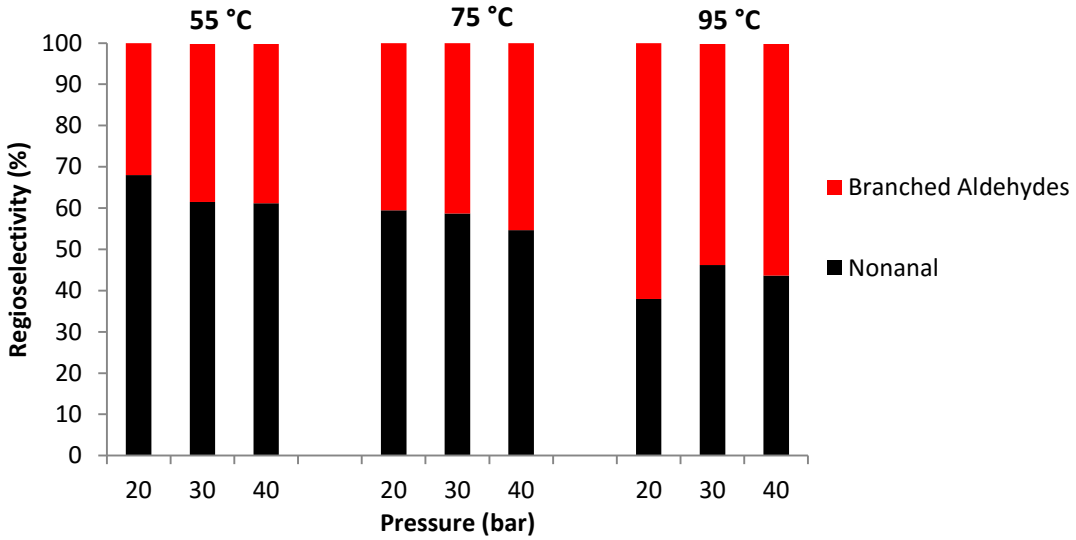

Figure 4.4. *Graphical representation of the regioselectivity when evaluated using complex* ***3.4****.*

4.3 Feedstock Variation

Having identified the optimised conditions as 75 °C and 30 bar, we aimed to explore an array of synthetic and naturally occurring olefins, and subsequently tested these in the hydroformylation reaction (Figure 4.5 and Table 4.3).

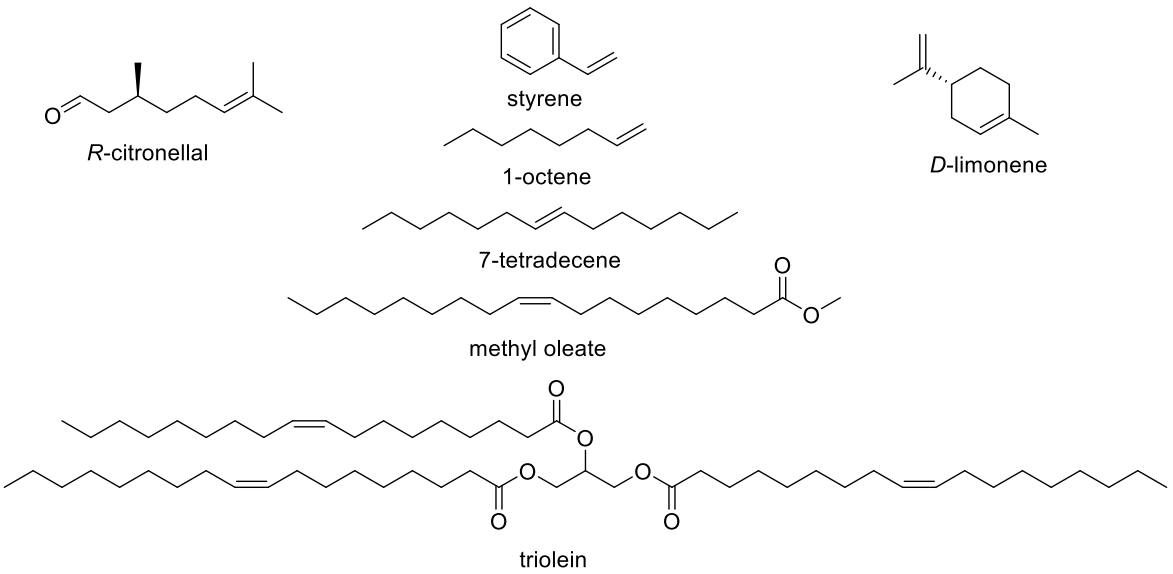

Figure 4.5. *Selected olefins applied in the hydroformylation reaction.*

Table 4.3. *Hydroformylation results using various terminal and internal olefins to using catalyst **3.4***

Entry	Substrate	Conversion (%)	Aldehydes (%)	Linear Aldehydes (%)	Branched Aldehydes (%)	*Iso*-alkenes (%)
1	Styrene	100	100	38.81	61.19	-
2	1-Octene	86.14	86.14	55.56	44.44	13.86
	Substrate	**Conversion (%)**	**Aldehydes (%)**	**Major Branched Aldehydes (%)**	**Minor Branched Aldehydes (%)**	***Iso*-alkenes (%)**
3	7-Tetradecene	73.00	99.99	85.22	14.78	-
4	Methyl Oleate	77.76	99.99	93.09	6.91	-
5	Triolein	51.57	99.99	97.71	2.29	-
6	*D*-Limonene	90.00	99.00	99.00	1.00	-
7	*R*-Citronellal	24.00	79.17	-	-	20.83

The reactor was loaded with toluene (5 mL), substrate (0.574 mmol) and Rh-metal loading (2.87×10^{-3} mmol for entries 1 and 2, 35.88×10^{-3} for entries 3–7). The reactor was purged with nitrogen three times, followed by purging thrice with syngas. The samples were analysed using GC-FID and/or ^{1}H NMR spectroscopy. Conversion is referred to as olefins (includes *iso*-olefins) to aldehydes exclusively. Reactions were conducted for 4 hours.

4.3.1 Styrene and 1-Octene

The model catalyst precursor (**3.4**) was tested using conventional substrates, namely 1-octene and styrene to compare with structurally similar complexes in literature.[26, 32, 48, 49, 54, 55] The catalyst precursor **3.4** is active in the hydroformylation of both 1-octene and styrene. The catalyst conversion and regioselectivity obtained for complex **3.4** is analogous to structurally similar *N,O*-salicylaldimine Rh(I) complexes.[48, 49, 54] The complex displays excellent conversion for 1-octene and styrene after 4 hours. The regioselectivity of complex **3.4** is moderate for styrene (*n:iso* - 0.63) and 1-octene (*n:iso* – 1.24). More importantly, one cannot compare the selectivity of these substrates as their proposed

mechanism of coordination is different in the hydroformylation cycle (Scheme 4.3).[56] Therefore it is necessary to evaluate the hydroformylation activity for both substrates.

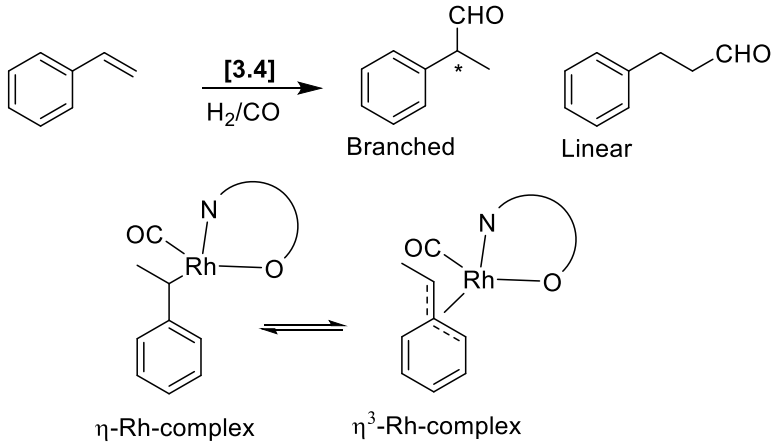

Scheme 4.3. *Proposed mechanism of coordination of the rhodium N,O-bidentate catalyst, which accounts for the regioselectivity towards branched products. Note the modes of coordination for the η-Rh-complex and the η³-Rh-complex.* [56]

4.3.2 7-Tetradecene, Methyl Oleate and Triolein

Complex **3.4** was tested against selected internal olefins, as the hydroformylation of 7-tetadecene (1-octene post metathesis product), methyl oleate and triolein may result in access to a new class of Guerbet-type surfactants, precursors for polyamide monomers and biodiesel respectively.[25, 37, 57, 58] The catalyst precursor **3.4** is active in the hydroformylation of internal olefins, namely 7-tetradecene, methyl oleate and triolein (Table 4.3). The hydroformylation of these internal olefins yields branched products exclusively; however isomerisation may occur to yield various branched products (*iso*-aldehyde and *iso*-alkenes) as displayed in Scheme 4.4.

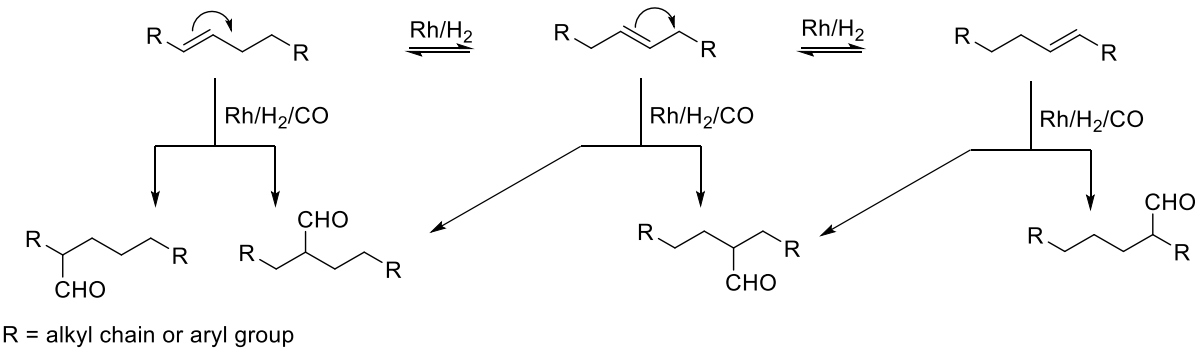

Scheme 4.4. *The tandem isomerisation-hydroformylation pathway under hydroformylation conditions.*

The results for the hydroformylation of 7-tetradecene, methyl oleate and triolein are extremely promising, as conversions ranged between 51 – 77 %. This is unexpected due to the longer reaction times often required to hydroformylate long-chain internal olefins.[33, 52] The regioselectivity for the major branched product (entries 3 – 6, Table 4.3) was obtained between 85 – 98%. These results indicate that the isomerisation of long-chain internal olefins is less favoured under the hydroformylation conditions tested (75 °C, 30 bar, 4 hours). This observation is particularly useful for tandem-catalytic reactions due to the good conversion and excellent regioselectivity observed. To the best of our knowledge this is the first report of the hydroformylation of 7-tetradecene, methyl oleate and triolein using bidentate *N,O*-salicylaldimine Rh(I) complexes.

4.3.3 D-Limonene and R-Citronellal

The catalyst precursor **3.4** is active in the hydroformylation of *D*-Limonene and *R*-Citronellal. Impressively, excellent conversion is observed for *D*-Limonene which is analogous to similar Rh(I) precursors in literature.[15] Notably conversions for these substrates are identified as olefin (including isomerisation products where applicable) to aldehydes exclusively. Interestingly for *D*-Limonene, the hydroformylation of the cyclic olefin was not observed, which indicates that the catalyst is highly selective to the terminal olefin. The conversion for *R*-Citronellal is low as expected, due to the bulky nature of the dimethyl moiety of *R*-citronellal (Scheme 4.5). The order of hydroformylation reactivity is consistent with the specific rates of terminal *vs* internal *vs* branched internal olefins.[33] In the context of this work, the order of hydroformylation reactivity is listed below (Scheme 4.5).

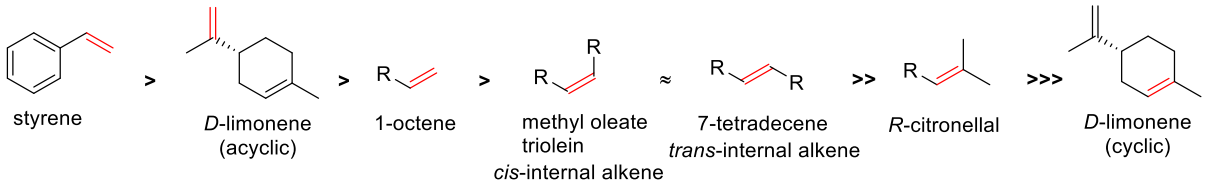

Scheme 4.5. *The order of hydroformylation reactivity at 75°C, 30 bar, 4 hours for the selected olefins with respect to complex* ***3.4****.*

4.4 Catalyst Comparison With Respect To Donor Atoms, Co-Ligands And Dendron Size

The optimised conditions (Section 4.2) and feedstock variation (Section 4.3) have been successfully established. The effect of donor atoms, co-ligands and dendron size were compared in the hydroformylation of 1-octene. Note that complexes **3.1** – **3.9** are neutral Rh(I) catalyst precursors, which allows for comparison across the dendron series (Figure 4.6). The results with respect to chemoselectivity, regioselectivity and catalyst performance are discussed below (Table 4.4, *vide infra*). Note that to the best of our knowledge this is the first report on the use of Fréchet metallodendrons in the hydroformylation reaction.

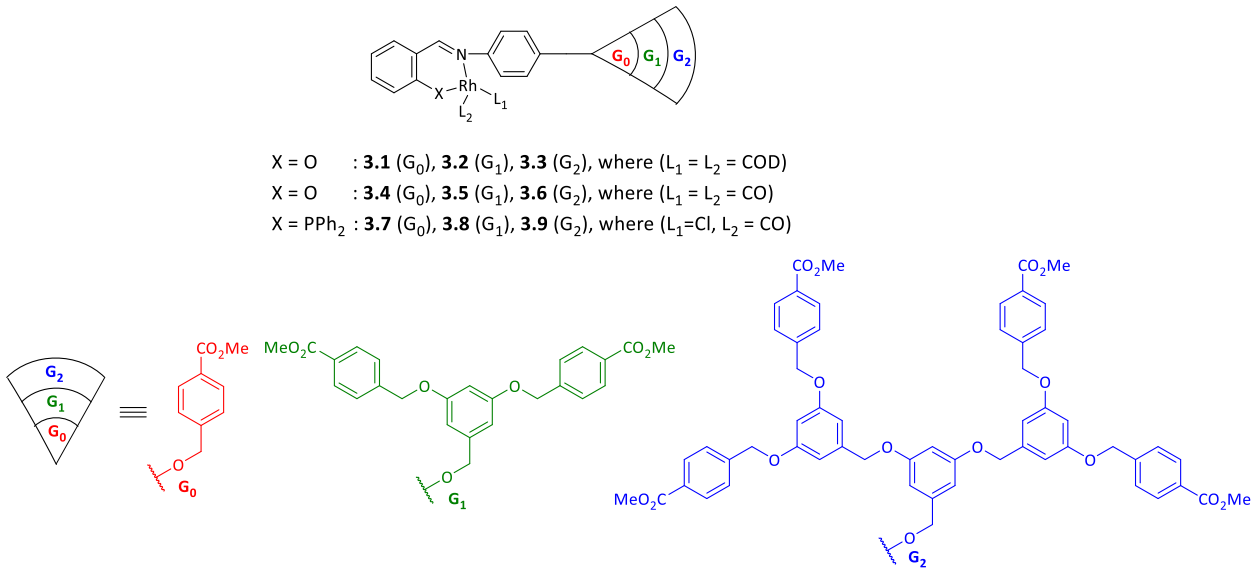

Figure 4.6. *The rhodium(I) organometallic dendrons,* ***3.1*** *–* ***3.9*** *used as catalyst precursors in the hydroformylation of 1-octene.*

4.4.1 Effect of Donor Atoms

Catalyst Performance

Generally, the *N,O*-salicylaldimine complexes (**3.1** – **3.6**) are superior than the *N,P*-iminophosphine complexes (**3.7** – **3.9**) with respect to activity under the tested hydroformylation conditions (Table 4.4). This implies that the *N,P*-iminophosphine Rh(I) complexes (**3.7** – **3.9**) may require an induction period, whereby more energy and/or time is required to reach the activated species and consequently hydroformylate the respective olefins. This induction period is often attributed to the diffusion of syngas in the reaction solvent and subsequent coordination of H_2 and CO to the rhodium site of complexes **3.7** – **3.9**.[59] Furthermore, complexes **3.7** – **3.9** contain bulky phenyl groups on the phosphine atom, which could hinder the coordination CO and H_2 to rhodium.[59] For complexes **3.7** – **3.9**, the rhodium ion is bonded to a chloride ligand, thus upon higher pressures of syngas, hydrogen chloride is formed, which may temporarily inhibit the hydroformylation of the substrate. This was observed in Wilkinson's study on Rh(I) halide aryl-phosphines used for the hydroformylation of various olefins.[60] This induction period is often observed for structurally similar *N,P*-iminophosphine Rh(I) complexes.[60-63] Furthermore as noted in Chapter 3, the oxidation of the *N,P*-iminophosphine complexes **3.7** – **3.9** is observed with

time, which may contribute to the deactivation of the catalyst and subsequent lower catalyst performance observed, however further investigation is required to understand this phenomenon.

Table 4.4. *The effect of dendron size, donor atoms and co-ligands (**3.1** – **3.9**) evaluated using the optimum conditions for the hydroformylation of 1-octene.*

	Conversion (%)	Total Ald. (%)	Total *Iso*-oct. (%)	Linear Ald. (%)	*Iso*-Ald. (%)	*n:iso*	TOF (h^{-1})
3.1	99.27	88.63	11.37	52.81	47.19	1.12	550
3.2	98.98	87.12	12.88	58.28	41.72	1.39	539
3.3	99.30	92.79	7.21	51.83	48.17	1.08	576
3.4	99.28	91.50	8.50	51.77	48.23	1.07	568
3.5	78.04	66.09	33.91	67.34	32.66	2.06	322
3.6	99.25	95.46	4.54	53.60	46.40	1.16	592
3.7	4.56	78.77	21.23	66.90	33.10	2.02	22
3.8	4.95	76.09	23.91	67.51	32.49	2.08	24
3.9	7.56	79.59	20.41	64.07	35.93	1.78	38

The reactor was loaded with toluene (5 mL), 1-octene (0.805 g, 7.175 mmol), internal standard *n*-decane (0.204 mg, 1.435 mmol) and Rh-metal loading (2.87 x 10^{-3} mmol). The reactor was purged with nitrogen three times, followed by purging thrice with syngas. TOF = (mmol of aldehydes/mmol of Rh)/time. Catalyst to substrate ratio utilised was (1:2500). The samples were analysed using GC-FID. Reactions were conducted for 4 hours.

Chemoselectivity

Complexes **3.1** – **3.6** display superior chemoselectivity towards aldehydes in comparison to complexes **3.7** – **3.9**. The chemoselectivity towards aldehydes for complexes **3.1** – **3.9** are comparable for structurally similar complexes in literature.[48, 49, 54] Note that the isomerisation reaction competes with the hydroformylation reaction. Generally, the isomerisation of alkenes increases with an increase in temperature and decrease in syngas pressure. Theoretically, the catalytic system has a higher free energy of activation, as a result the lower pressure allows the complex to possess a vacant site, which is favourable for isomerisation.[63]

Regioselectivity

As expected, complexes **3.7** – **3.9** favoured the formation of nonanal in comparison to complexes **3.1** – **3.6** (*n:iso* ratio of 2.08 vs 1.39 respectively). The hydroformylation precursors **3.7** – **3.9** possess bulky phosphine substituents, which imparts steric crowding around the metal centre and limits the isomerisation and/or alkene insertion under the conditions tested. The effect of monodentate phosphines in catalysis was initially discovered by Tolman and co-workers (Tolman cone angles, Scheme 4.6).[25, 64] This characteristic is defined as the apex angle of a cylindrical cone, which is centred at 2.28 Å from the centre of the phosphorous atom.[64] However Casey and Whiteker posed insight into bidentate systems and defined the natural bite angle (β_n) as the preferred chelation angle of the metal complex (Scheme 4.6).[64] These bidentate chelating systems with wider bite angles favours higher *n:iso* ratios, due to the preferred equatorial-equatorial (*ee*) coordinated mode as imparted by steric constraints.[31, 32, 34] Hence for this reason complexes **3.7** – **3.9** display enhanced regioselectivity in comparison to that of the *N,O*-salicylaldimine complexes (**3.1** – **3.6**).[64] Interestingly, no hydroformylation of 4-octene to 2-propyl-hexanal was observed for complexes **3.7** – **3.9**. This evidence further demonstrates the steric-crowding observed for complexes **3.7** – **3.9**, which is observed for structurally similar bidentate phosphines in literature.[65-67]

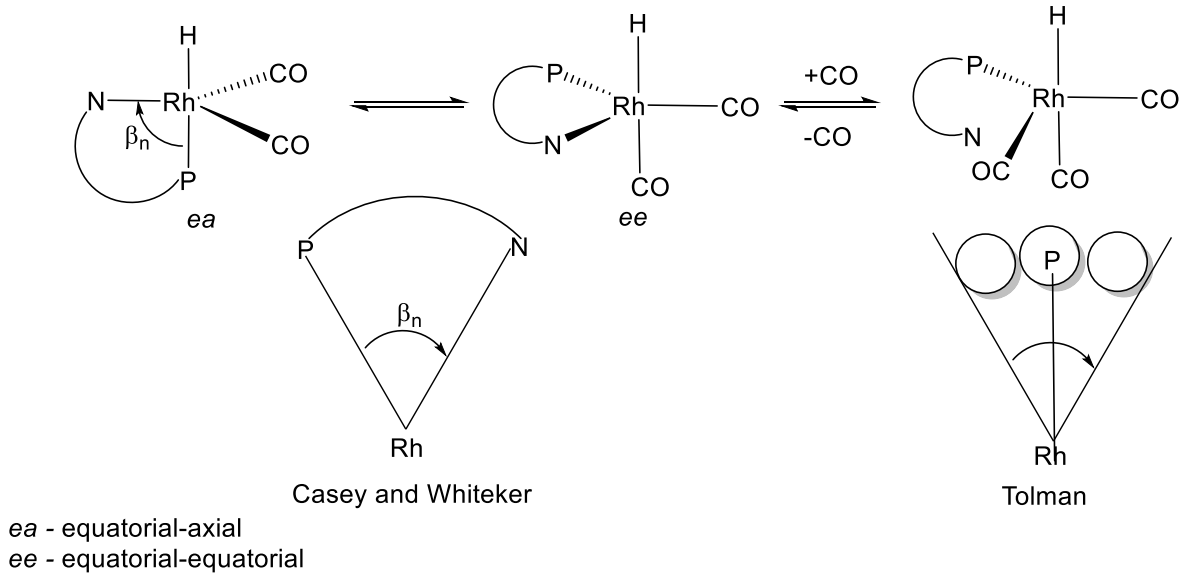

Scheme 4.6. *The influence of the size of the ligand on the regioselectivity of the hydroformylation reaction, as denoted by Tolman, Casey and Whiteker.*[64]

4.4.2 Effect of Co-Ligand in N,O-salicylaldimine Rh(I) complexes

Catalyst Performance

The co-ligand was varied in the *N,O*-salicylaldimine Rh(I) complexes from 1,5-cyclooctadiene (**3.1** – **3.3**) to the dicarbonyl-based complexes (**3.4** – **3.6**). The catalyst precursors **3.4** – **3.6** display superior turnover frequencies in comparison to complexes **3.1** – **3.3**. In the hydroformylation reaction, 1,5-cyclooctadiene is displaced under hydroformylation conditions resulting as either the dicarbonyl or carbonyl hydride species.[68] In the dicarbonyl case (**3.4** – **3.6**), this process is absent, which theoretically results in a shorter time to form the active species.[68] This postulation is in accordance with the observed results. However further studies are required to understand the *N,O*-salicylaldimine catalyst precursors under hydroformylation conditions.

Chemoselectivity and Regioselectivity

The chemoselectivity and regioselectivity of the hydroformylation precursors **3.1** – **3.6** are analogous as expected. Generally when comparing the complexes (**3.1** *vs* **3.4**, **3.3** *vs* **3.6**), slight differences in the chemoselectivity and regioselectivity (± 3%) are observed for these complexes; however the chemoselectivity and regioselectivity results are within the standard deviation for these experiments.

4.4.3 Effect of dendron size

Catalyst Performance

The conversions of 1-octene across the dendron generations are analogous. In Chapter 2, the respective Schiff-base moiety was immobilised on various dendron generations ($G_0 – G_2$). Notably, no significant changes are observed for the aromatic proton signals of the Schiff-base moiety when comparing the characterisation data for the G_0 (**2.8** and **2.9**), G_1 (**2.10** and **2.11**) and G_2 (**2.12** and **2.13**) dendrons. Furthermore the dendron is not a conjugated system, thus it does not affect the electronics of the catalyst system. For these reasons, the activity is comparable for the G_0, G_1 and G_2 Rh(I) dendrons **3.1** - **3.9**. The effects are generally steric and/or they are potentially due to the back-folding of the dendrimer species in solution.[63, 69-71] These results are encouraging and attests to the integrity of the catalytic tests performed (Figure 4.7). A peculiar observation is the much lower conversion observed for complex **3.5** (G_1). One reason is that the complex could initially be forming a bridging carbonyl species. This was not observed in solid or solution state at room temperature (Chapter 3.3.2.2), however the complex may behave differently under hydroformylation conditions. It is known from literature that bridging carbonyls are catalytically inert species in carbonylation reactions. Thus, some of the catalyst may be converted into the bridging carbonyl species, which correlates to the lower conversion observed for catalyst precursor **3.5**.[72, 73] Further investigation is required to understand this trend, but is beyond the scope of this project.

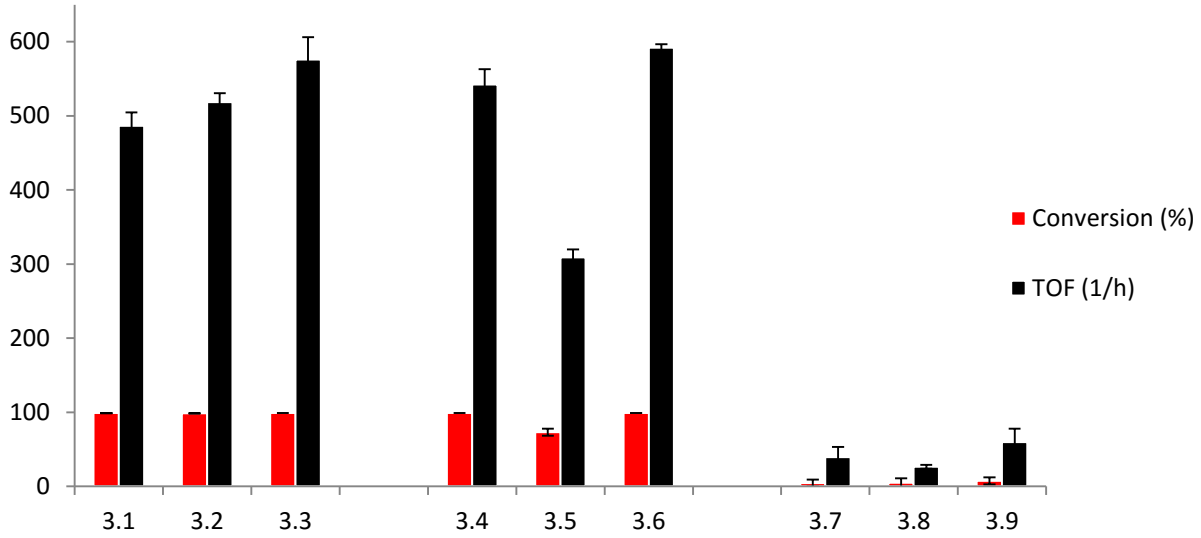

Figure 4.7. *Catalyst efficiency as a function of dendron size **3.1** – **3.9**. Note the catalytic efficiency is described as substrate conversion (red) and turnover frequency (black).*

Chemoselectivity and Regioselectivity

Generally across the generation size (G_0, G_1, G_2) there is an increase in the chemoselectivity to form aldehydes for the hydroformylation precursors. This may be attributed to the bulkier nature (steric-effect) of the dendrons, which limits the isomerisation from terminal to internal alkenes. In both complexes **3.2** and **3.5** (G_1), a drop in the activity is observed. However, this drop in the 1st generation species is often observed for dendrimers. These are described in literature for similar dendritic catalysts applied in the hydroformylation reaction.[74, 75] A general trend observed across the dendron series (G_0 – G_2) is that the regioselectivity is consistent (**3.1** – **3.6** and **3.7** – **3.9**). One reason is that the dendron is presumed to be too far from the catalytic centre to impact on the regioselectivity of the hydroformylation reaction (Figure 4.8). Furthermore, the electronics is similar around the metal centre, which is reflected in the hydroformylation results.

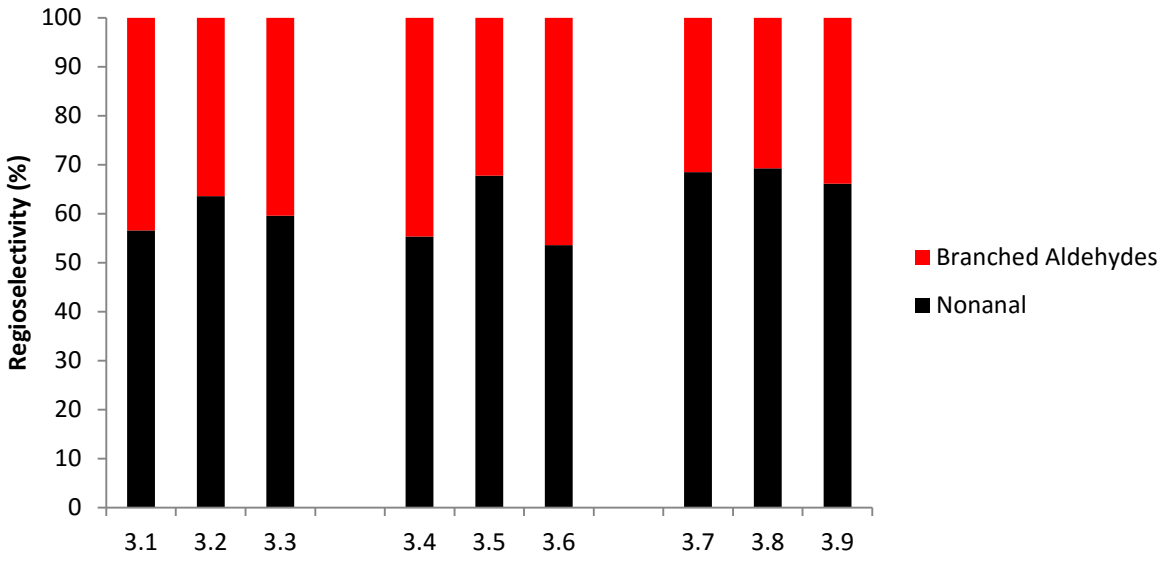

Figure 4.8. *The effect of the dendron size for complexes* ***3.1*** *–* ***3.9*** *on the regioselectivity for the hydroformylation of 1-octene.*

4.5 Selectivity as a function of time

The chemoselectivity and regioselectivity of the Rh(I) complexes (**3.1, 3.4** and **3.7**) were evaluated at various times (Figure 4.9). This was conducted using the optimised conditions 75 °C and 30 bar. The precursors were evaluated at 1 hour, 2 hours, 4 hours and 8 hours respectively. A general trend is observed whereby after 1 hour the chemoselectivity ranged between 53 – 60% for complexes **3.1, 3.4** and **3.7**. An increase in the chemoselectivity is observed which ranged between 69 – 79% for the complexes (**3.1, 3.4** and **3.7**) after 2 hours and ranged between 73 – 100% after 8 hours. Hence the chemoselectivity towards aldehydes increases as a function of time for catalysts **3.1, 3.4** and **3.7**. This observation indicates that the isomerisation products decrease as a function of time and consequently being hydroformylated to branched aldehydes. This observation is confirmed when evaluating the regioselectivity as a function of time. The *n:iso* ratio decreases as a function of time, further providing evidence that the *iso*-octenes are being hydroformylated to *iso*-aldehydes at longer reaction times.

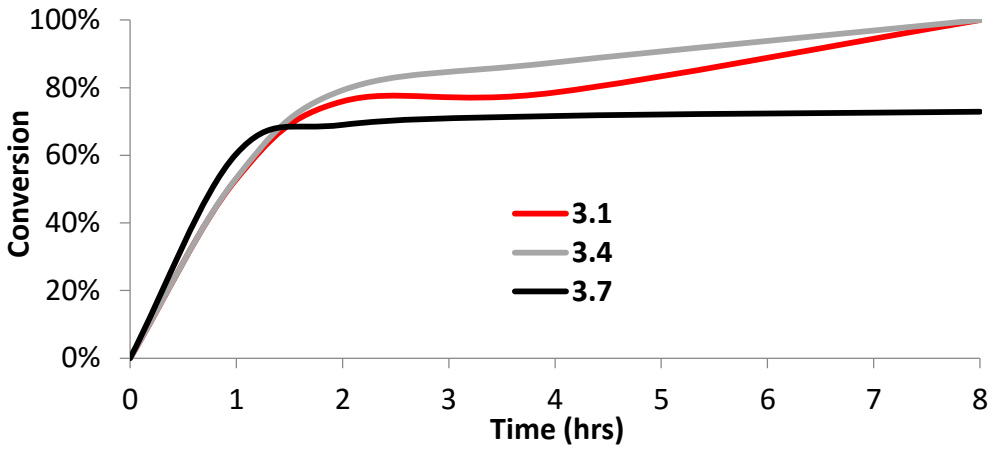

Figure 4.9. *The chemoselectivity of complex **3.1**, **3.4** and **3.7** as a function of time. The reactor was loaded with toluene (5 mL), 1-octene (0.805 g, 7.175 mmol), Rh-metal loading (2.87 x 10^{-3} mmol). The reactor was purged with nitrogen three times, followed by purging thrice with syngas. TOF = (mmol of aldehydes/mmol of Rh)/time. The samples were analysed using GC-FID.*

4.6 Mercury poisoning experiments

A useful method for differentiating between homogeneous and heterogeneous catalysis is mercury drop experiments.[42, 76-79] If nanoparticles are formed in solution, the introduction of mercury results in the formation of an amalgam between mercury and the metal-nanoparticles.[48] This amalgam is not active in the hydroformylation reaction, thus poisoning of the catalytic system results in a drop in the catalytic activity if nanoparticles were present.[48]

The reactions were performed using the temperature (75 °C), time (2 hours for **3.1** and **3.4** *vs* 8 hours for **3.7**) and pressure (30 bar) in the presence of mercury (Figure 4.9). A drop in conversion is observed for the G_0 compounds **3.1, 3.4** and **3.7**. This suggests that the conversion is attributed to a combination of heterogeneous and homogeneous catalysis. Complex **3.7** displays a lower conversion for the mercury drop experiments in comparison to **3.1** and **3.4**. This could be attributed to the oxidation of the phosphorous ligand in solution (as discussed in Chapter 3). The formation and accumulation of colloidal particles are often associated with the increase in the rate of isomerisation; this is consistent with results obtained in section 4.5.

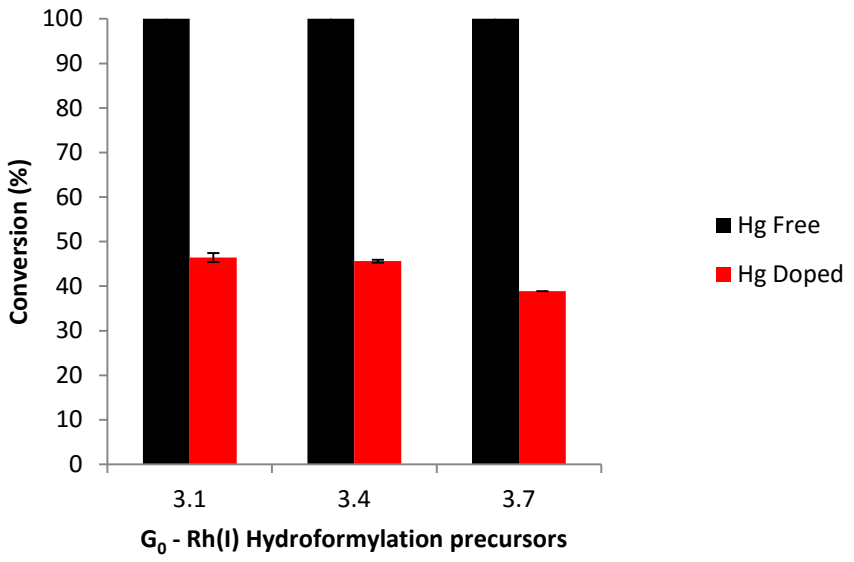

Figure 4.10. *Mercury drop experiments for complexes **3.1, 3.4** and **3.7** respectively. The reactor was loaded with toluene (5 mL), 1-octene (0.805 g, 7.175 mmol), Rh-metal loading (2.87 x 10-3 mmol) and a drop of mercury. The reactions involving **3.1** and **3.4** were run for 2 hours and **3.7** was performed over 8 hours. The reactor was purged with nitrogen three times, followed by purging thrice with syngas. TOF = (mmol of aldehydes/mmol of Rh)/time. The samples were analysed using GC-FID.*

4.7 Overall Summary

A series of Rh(I) mononuclear dendrons **3.1** – **3.9** were evaluated as catalyst precursors in the hydroformylation of 1-octene. The catalyst precursor **3.4** was selected as the model catalyst and the optimised conditions were identified as 75 °C, 30 bar and 4 hours. This precursor **3.4** was evaluated using selected feedstocks, namely 1-octene, styrene, 7-tetradecene, methyl oleate, triolein, *R*-citronellal and *D*-limonene. Complex **3.4** was active in the hydroformylation reaction for all of the substrates. These results are promising and may provide motivation for the application of these catalysts in tandem catalytic processes.

The catalyst precursor **3.1** – **3.6** displays excellent activity, excellent chemoselectivity and moderate regioselectivity for the hydroformylation of 1-octene. The results are comparable to structurally similar complexes in literature. The *N,O*-salicylaldimine catalyst precursors **3.1** – **3.6** display superior activity to the *N,P*-iminophosphine catalyst precursors **3.7** – **3.9** with respect to catalyst activity and chemoselectivity. However the *N,P*-iminophosphine catalyst precursors **3.7** – **3.9** display better regioselectivity than the *N,O*-salicylaldimine

complexes **3.1** – **3.6**. This is due to the larger phenyl substituents for complexes **3.7** – **3.9** which imparts steric crowding around the metal centre. Generally the dicarbonyl catalysts (**3.4** – **3.6**) displayed superior activity than 1,5-cyclooctadiene (**3.1** – **3.3**) catalysts.

The effect of the dendron size displays an increase in the catalytic performance for increased dendron sizes (**3.1** *vs* **3.3**). The larger dendron size could potentially limit the isomerisation towards internal olefins, hence the catalyst activity was much higher for the G_2-dendrons (**3.3, 3.6** and **3.9**). Mercury drop experiments performed on complexes (**3.1, 3.4** and **3.7**) showed significant loss in activity in the presence of mercury. This suggests that a combination of homogeneous and heterogeneous catalysis is responsible for the hydroformylation of these olefins. The addition of excess ligand equivalents could limit the formation of nanoparticles, which ultimately could lead to catalysts which may be recycled and obtain better selectivity.

4.8 References

1. V. Negro, G. Mancini, B. Ruggeri and D. Fino, *Bioresour. Technol.*, 2016, **214**, 806-815.
2. J. F. Mitchell, T. Johns, J. M. Gregory and S. Tett, *Nature*, 1995, **376**, 501-504.
3. T. J. Crowley, *Science*, 2000, **289**, 270-277.
4. J.-R. Petit, J. Jouzel, D. Raynaud, N. I. Barkov, J.-M. Barnola, I. Basile, M. Bender, J. Chappellaz, M. Davis and G. Delaygue, *Nature*, 1999, **399**, 429-436.
5. T. Vanbésien, E. Monflier and F. Hapiot, *Eur. J. Lipid Sci. Technol.*, 2016, **118**, 26-35.
6. H. V. Weiss, M. Koide and E. D. Goldberg, *Science*, 1971, **172**, 261-263.
7. M. S. Reddy and C. Venkataraman, *Atmos. Environ.*, 2002, **36**, 677-697.
8. D. Casagrande, *Spec. Publ. - Geol. Soc. London*, 1987, **32**, 87-105.
9. C. H. Bartholomew, *Appl. Catal., A*, 2001, **212**, 17-60.
10. J. Oudar, *Catal. Rev.: Sci. Eng.*, 1980, **22**, 171-195.
11. J. A. Rodriguez and J. Hrbek, *Acc. Chem. Res.*, 1999, **32**, 719-728.
12. G. E. Likens, C. T. Driscoll and D. C. Buso, *Science*, 1996, **272**, 244.
13. N. M. Johnson, C. T. Driscoll, J. S. Eaton, G. E. Likens and W. H. McDowell, *Geochim. Cosmochim. Acta*, 1981, **45**, 1421-1437.
14. E. V. Gusevskaya, J. Jiménez-Pinto and A. Börner, *ChemCatChem*, 2014, **6**, 382-411.

15. C. G. Vieira, M. C. de Freitas, E. N. dos Santos and E. V. Gusevskaya, *ChemCatChem*, 2012, **4**, 795-801.
16. H. Mimoun, *Chimia*, 1996, **50**, 620-625.
17. G. T. Whiteker and C. J. Cobley, in *Organometallics as Catalysts in the Fine Chemical Industry*, eds. M. Beller and H. U. Blaser, 2012, vol. 42, pp. 35-46.
18. J. L. F. Monteiro and C. O. Veloso, *Top. Catal.*, 2004, **27**, 169-180.
19. K. Fisher and C. A. Phillips, *J. Appl. Microbiol.*, 2006, **101**, 1232-1240.
20. A. Bocco, M.-E. Cuvelier, H. Richard and C. Berset, *J. Agric. Food Chem.*, 1998, **46**, 2123-2129.
21. C. De, R. Saha, S. K. Ghosh, A. Ghosh, K. Mukherjee, S. S. Bhattacharyya and B. Saha, *Res. Chem. Intermed.*, 2013, **39**, 3463-3474.
22. L. A. Pfaltzgraff, E. C. Cooper, V. Budarin and J. H. Clark, *Green Chem.*, 2013, **15**, 307-314.
23. A. Nahman and W. de Lange, *Waste Manage.*, 2013, **33**, 2493-2500.
24. P. Urquhart, *IPM and the citrus industry in South Africa*, International institute for environment and development (IIED). Sustainable agriculture and rural livelihoods programme, 1999.
25. W. L. Peddie, MSc dissertation, Stellenbosch University, 2016.
26. A. van Rooy, E. N. Orij, P. C. Kamer and P. W. van Leeuwen, *Organometallics*, 1995, **14**, 34-43.
27. C. G. Vieira, M. C. de Freitas, K. C. B. de Oliveira, A. de Camargo Faria, E. N. dos Santos and E. V. Gusevskaya, *Catal. Sci. Technol.*, 2015, **5**, 960-966.
28. P. Garner, H. Ü. Kaniskan, J. Hu, W. J. Youngs and M. Panzner, *Org. Lett.*, 2006, **8**, 3647-3650.
29. S. Yu, Y.-m. Chie, Z.-h. Guan, Y. Zou, W. Li and X. Zhang, *Org. Lett.*, 2009, **11**, 241-244.
30. I. del Rio, O. Pamies, P. van Leeuwen and C. Claver, *J. Organomet. Chem.*, 2000, **608**, 115-121.
31. C. Claver, M. Dieguez, O. Pamies and S. Castillon, *Top. Organomet. Chem.*, 2006, **18**, 35-64.
32. E. Boymans, M. Janssen, C. Muller, M. Lutz and D. Vogt, *Dalton Trans.*, 2013, **42**, 137-142.

33. M. Haumann, H. Yildiz, H. Koch and R. Schomäcker, *Appl. Catal., A*, 2002, **236**, 173-178.
34. K. F. Muilwijk, P. C. J. Kamer and P. W. N. M. van Leeuwen, *J. Am. Oil Chem. Soc.*, 1997, **74**, 223-228.
35. G. Fremy, Y. Castanet, R. Grzybek, E. Monflier, A. Mortreux, A. M. Trzeciak and J. J. Ziolkowski, *J. Organomet. Chem.*, 1995, **505**, 11-16.
36. T. Vanbesien, E. Monflier and F. Hapiot, *Green Chem.*, 2016, **18**, 6687-6694.
37. T. Vanbésien, A. Sayede, E. Monflier and F. Hapiot, *Catal. Sci. Technol.*, 2016, **6**, 3064-3073.
38. T. Vanbesien, E. Monflier and F. Hapiot, *Green Chem.*, 2017, **19**, 1940-1948.
39. E. V. Gusevskaya, E. N. dos Santos, R. Augusti, A. d. O. Dias and C. M. Foca, *J. Mol. Catal. A: Chem*, 2000, **152**, 15-24.
40. I. Fleischer, L. Wu, I. Profir, R. Jackstell, R. Franke and M. Beller, *Chem. - Eur. J.*, 2013, **19**, 10589-10594.
41. J. Pospech, I. Fleischer, R. Franke, S. Buchholz and M. Beller, *Angew. Chem., Int. Ed. Engl.*, 2013, **52**, 2852-2872.
42. A. Behr, Y. Brunsch and A. Lux, *Tetrahedron Lett.*, 2012, **53**, 2680-2683.
43. E. B. Hager, B. C. Makhubela and G. S. Smith, *Dalton Trans.*, 2012, **41**, 13927-13935.
44. R. Franke, D. Selent and A. Borner, *Chem. Rev*, 2012, **112**, 5675-5732.
45. S.-M. Lu and H. Alper, *J. Am. Chem. Soc.*, 2003, **125**, 13126-13131.
46. H. P. Dijkstra, G. P. M. van Klink and G. van Koten, *Acc. Chem. Res.*, 2002, **35**, 798-810.
47. A. Berger, R. J. K. Gebbink and G. van Koten, in *Dendrimer Catalysis*, Springer, 2006, pp. 1-38.
48. S. Siangwata, S. Chulu, C. L. Oliver and G. S. Smith, *Appl. Organomet. Chem.*, 2017, **31**, e3593-n/a.
49. L. Maqeda, B. C. E. Makhubela and G. S. Smith, *Polyhedron*, 2015, **91**, 128-135.
50. J. Hjortkjaer, *J. Mol. Catal.*, 1979, **5**, 377-384.
51. P. W. Van Leeuwen and C. Claver, *Rhodium catalyzed hydroformylation*, Kluwer Academic Publishers, New York, 2002.
52. M. Haumann, H. Koch and R. Schomäcker, *Catal. Today*, 2003, **79-80**, 43-49.

53. L. C. Matsinha, P. Malatji, A. T. Hutton, G. A. Venter, S. F. Mapolie and G. S. Smith, *Eur. J. Inorg. Chem.*, 2013, **2013**, 4318-4328.
54. P. Govender, S. Ngubane, B. Therrien and G. S. Smith, *J. Organomet. Chem.*, 2017, **848**, 281-287.
55. S. Paganelli, O. Piccolo, P. Pontini, R. Tassini and V. D. Rathod, *Catal. Today*, 2015, **247**, 64-69.
56. S. Yu, Y.-m. Chie, Z.-h. Guan, Y. Zou, W. Li and X. Zhang, *Org. Lett.*, 2008, **11**, 241-244.
57. A. J. Vorholt, S. Immohr, K. A. Ostrowski, S. Fuchs and A. Behr, *Eur. J. Lipid Sci. Technol.*, 2017, **119**, 1600211-n/a.
58. A. Behr, T. Seidensticker and A. J. Vorholt, *Eur. J. Lipid Sci. Technol.*, 2014, **116**, 477-485.
59. B. C. Makhubela, A. Jardine and G. S. Smith, *Green Chem.*, 2012, **14**, 338-347.
60. D. Evans, J. A. Osborn and G. Wilkinson, *J. Chem. Soc. A*, 1968, 3133.
61. L. Maqeda, MSc dissertation, University of Cape Town, 2014.
62. B. C. Makhubela, PhD thesis, University of Cape Town, 2012.
63. N. Antonels, MSc dissertation, University of Cape Town, 2010.
64. K. M. Mokheseng, MSc dissertation, University of the Free State, 2005.
65. Q. R. Peng, Y. Yang, C. J. Wang, X. L. Liao and Y. Z. Yuan, *Catal. Lett.*, 2003, **88**, 219-225.
66. L. c. Ropartz, R. E. Morris, D. F. Foster and D. J. Cole-Hamilton, *J. Mol. Catal. A: Chem*, 2002, **182**, 99-105.
67. P. Wehman, H. M. A. van Donge, A. Hagos, P. C. J. Kamer and P. W. N. M. van Leeuwen, *J. Organomet. Chem.*, 1997, **535**, 183-193.
68. C. Joubert and S. F. Mapolie, unpublished work.
69. E. de Jesus and J. C. Flores, *Ind. Eng. Chem. Res.*, 2008, **47**, 7968-7981.
70. D. A. Tomalia, *Aldrichim. Acta*, 2004, **37**, 39-57.
71. D. A. Tomalia, A. M. Naylor and W. A. Goddard, *Angew. Chem., Int. Ed.*, 1990, **29**, 138-175.
72. W. I. Dzik, C. Creusen, R. de Gelder, T. P. J. Peters, J. M. M. Smits and B. de Bruin, *Organometallics*, 2010, **29**, 1629-1641.
73. B. T. Heaton, C. Jacob and J. T. Sampanthar, *J. Chem. Soc., Dalton Trans.*, 1998, **0**, 1403-1410.

74. P. Arya, P. Gautam, N. Venugopal Rao, H. Alper, S. C. Bourque and L. E. Manzer, *J. Am. Chem. Soc.*, 2001, **123**, 2889-2890.

75. P. Arya, N. V. Rao, J. Singkhonrat, H. Alper, S. C. Bourque and L. E. Manzer, *J. Org. Chem.*, 2000, **65**, 1881-1885.

76. L. C. Matsinha, S. F. Mapolie and G. S. Smith, *Dalton Trans.*, 2015, **44**, 1240-1248.

77. M. Guerrero, N. T. T. Chau, S. Noel, A. Denicourt-Nowicki, F. Hapiot, A. Roucoux, E. Monflier and K. Philippot, *Curr. Org. Chem.*, 2013, **17**, 364-399.

78. P. Lara, O. Rivada-Wheelaghan, S. Conejero, R. Poteau, K. Philippot and B. Chaudret, *Angew. Chem., Int. Ed.*, 2011, **50**, 12080-12084.

79. C. Louis and D. Astruc, *Nanoparticles and Catalysis*, 2008.

Chapter 5

Experimental

5.1 General Details

5.1.1 Chemicals and General Methods

All reagents were purchased from commercial suppliers (KIMIX, Sigma-Aldrich, Merck and Acros Organics) and used without further purification unless otherwise stated. Rhodium(III) trichloride trihydrate was purchased from Heraeus SA. The rhodium chloro-carbonyl dimer[1] $[Rh(\mu\text{-}Cl)(CO)_2]_2$ and the rhodium chloro-1,5-cyclooctadiene dimer[2] $[Rh(\mu\text{-}Cl)(\eta^2\text{:}\eta^2\text{-}COD)]_2$ were prepared by means of published methods. Solvents were of analytical grade and dried over molecular sieves. Compounds were dried under vacuum. All reactions were carried out under an argon atmosphere using standard Schlenk line techniques unless otherwise stated. In cases where phosphines reagents were used, solvents were degassed utilising at least three freeze-thaw-pump cycles. Reaction progress was monitored using thin-layer chromatography (TLC) on pre-coated silica-gel F_{254} plates in a suitable solvent system. Column chromatography was conducted using 60 Å silica gel (70 – 230 mesh ASTM).

5.1.2 Spectroscopic and Analytical Methods

Nuclear magnetic resonance (NMR) spectra were recorded on either a Bruker Topsin GmbH 400 plus (^{1}H: 400.22 MHz; $^{13}C\{^1H\}$: 100.65 MHz; $^{31}P\{^1H\}$: 162.01 MHz) or a Varian Mercury 300 (^{1}H: 300.08 MHz; $^{13}C\{^1H\}$: 75.46 MHz; $^{31}P\{^1H\}$: 121.47 MHz) spectrometer. These were equipped with a Bruker Biospin GmbH casing and sample injector at 30 °C. Chemical shifts for ^{1}H and $^{13}C\{^1H\}$ NMR were reported using tetramethylsilane (TMS) as the internal standard and $^{31}P\{^1H\}$ NMR spectra were measured relative to H_3PO_4 (85%) as the external standard. Coupling constants are reported in Hz and chemical shifts are reported in ppm.

Infrared (IR) absorptions were measured on a Perkin-Elmer Spectrum 100 FT-IR spectrometer using Attenuated Total Reflectance Infrared spectroscopy (ATR-IR).

Electron impact mass spectrometry (EI-MS) was conducted using a JEOL GCMateII mass spectrometer. Low resolution and high resolution (HR) electrospray ionisation mass spectrometry (ESI-MS) was carried out on a Waters API Quattro mass spectrometer, with scans being conducted in the positive mode. Matrix assisted laser desorption time-of-flight (MALDI-TOF) mass spectra were carried out at the Université d' Artois – Faculté des Sciences Jean Perrin on a Bruker Daltronics Ultraflex 2 equipped with a nitrogen laser and operated at an accelerating voltage of 25 kV. The matrix utilised was either 2,5-dihydroxybenzoic acid (6.5 mM) or 3-aminoquinoline (6.5 mM).

Elemental analysis (C, H, N) were performed using a Fissions EA 110 CHNS apparatus or an Elementar Vario EL Cube Analyser. Melting Points were determined using a Büchi melting point apparatus B-540 and are uncorrected.

5.2 Fréchet dendrons (2.1 – 2.5)

*5.2.1 Methyl (4-bromomethyl)benzoate[3] (**2.1**)*

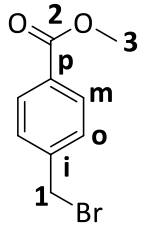

4-Bromomethylbenzoic acid (99.9 mg, 0.465 mmol, 1.00 eq.) was added to a stirring solution of freshly distilled methanol (9.41 mL, 23.3 mmol, 50.0 eq.). To this, a solution of concentrated sulfuric acid (0.280 mL, 0.525 mmol, 1.10 eq.) in methanol was added dropwise, and the mixture was refluxed for 5 hours. The reaction mixture was concentrated under reduced pressure to afford a brown residue. Ice water (10 mL) was carefully added to the flask to quench the sulfuric acid. The resultant mixture was filtered and washed with 3 x 10 mL of ice water. The filtrate was extracted using a diethyl ether: ethyl acetate (1:1) solution. The combined organic fractions dried over anhydrous sodium sulfate. The drying agent was removed by filtration and the filtrate was collected. The filtrate was dried *in vacuo* to afford resulting yellow oil **2.1**.

Yield: 97 mg (91%). **IR (ATR, cm^{-1}):** *v* = 1716 (sharp, medium, C=O), 1276 (sharp, strong, C-O). **^{1}H NMR (400 MHz, $CDCl_3$):** δ 8.01 (d, $^{3}J_{HH}$ = 8.5 Hz, 2H, H_m), 7.45 (d, $^{3}J_{HH}$ = 8.2 Hz, 2H, H_o), 4.49 (s, 2H, H_1), 3.91 (s, 3H, H_3). **^{13}C{^{1}H} NMR (101 MHz, $CDCl_3$):** δ 166.64 (s, C_2), 142.76 (s, C_p), 130.26 (s, C_i), 130.21 (s, C_m), 129.14 (s, C_o), 52.31 (s, C_1), 32.30 (s, C_3). **Elemental Analysis** for $C_9H_9O_2Br$ (227.9730): C, 47.19; H, 3.96; Found C, 47.26; H, 3.96%. **EI-MS (m/z):** 229.8969 [M^{81}]$^{+}$, 227.9025 [M^{79}]$^{+}$, 148.9635 [M-Br]$^{+}$.

*5.2.2 G_1-COOMe-OH dendron[4] (**2.2**)*

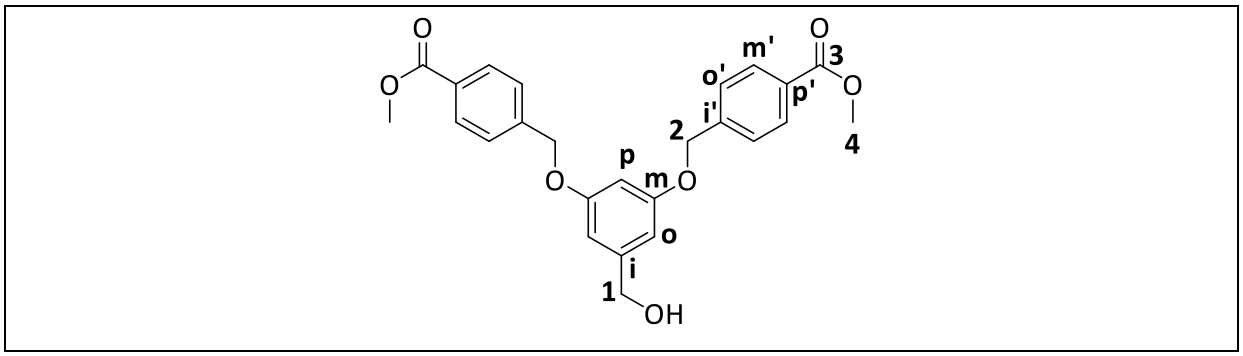

A mixture of 3,5-dihydroxybenzyl alcohol (1.60 g, 11.4 mmol, 1.00 eq.), potassium carbonate (3.94 g, 28.5 mmol, 2.50 eq.) and 18-crown-ether (0.605 g, 2.28 mmol, 0.200 eq.) in dry acetone (250 mL) was refluxed for 1 hour. To this, a solution of methyl (4-bromomethyl)benzoate, **2.1** (5.36 g, 23.4 mmol, 2.05 eq.) in anhydrous acetone (100 mL) was added dropwise. The resultant mixture was further refluxed for an additional 23 hours. The mixture was cooled to room temperature and evaporated to dryness under reduced pressure. The residue was partitioned between water (100 mL) and dichloromethane (100 mL), and the aqueous layer was extracted with dichloromethane (3 x 100 mL). The combined organic extracts were washed with a brine solution, and consequently dried using anhydrous magnesium sulfate. The drying agent was removed by filtration and the filtrate was collected. The filtrate was reduced to yield a brown residue which was purified by means of flash column chromatography. The column was eluted using ethyl acetate: petroleum ether (20 : 80, *v*/*v*) solution, increasing the ethyl acetate to 100%. The solvent was removed under reduced pressure to yield the product, **2.2**, as a white powder.

Yield: 4.28 g (86%). **IR (ATR, cm^{-1}):** *v* = 3508 (broad, weak, O-H), 1712 (sharp, strong, C=O). **^{1}H NMR (400 MHz, $CDCl_3$):** δ 8.06 (d, $^3J_{HH}$ = 8.4 Hz, 4H, $H_{m'}$), 7.49 (d, $^3J_{HH}$ = 8.4 Hz, 4H, $H_{o'}$), 6.64 (d, $^4J_{HH}$ = 2.3 Hz, 2H, H_o), 6.53 (t, $^4J_{HH}$ = 2.3 Hz, 1H, H_p), 5.11 (s, 4H, H_2), 4.64 (s, 2H, H_1), 3.94 (s, 6H, H_4). **^{13}C{^{1}H} NMR (101 MHz, $CDCl_3$):** 166.64 (s, C_3), 159.72 (s, C_m), 143.57 (s, C_i), 141.85 (s, $C_{i'}$), 129.70 (s, $C_{m'}$), 129.57 (s, $C_{p'}$), 126.76 (s, $C_{o'}$), 105.76 (s, C_o), 101.21 (s, C_P), 69.24 (s, C_2), 64.93 (s, C_1), 51.93 (s, C_4). **Elemental Analysis** for $C_{25}H_{24}O_7$ (436.1522): C, 68.80; H, 5.54; Found C, 69.24; H, 5.71%. **EI-MS (m/z):** 436.1629 $[M]^+$. **Melting Point**: 83.51 – 85.0 °C. (no lit. MP reported)

*5.2.3 G_1-COOMe-Br dendron[4] (**2.3**)*

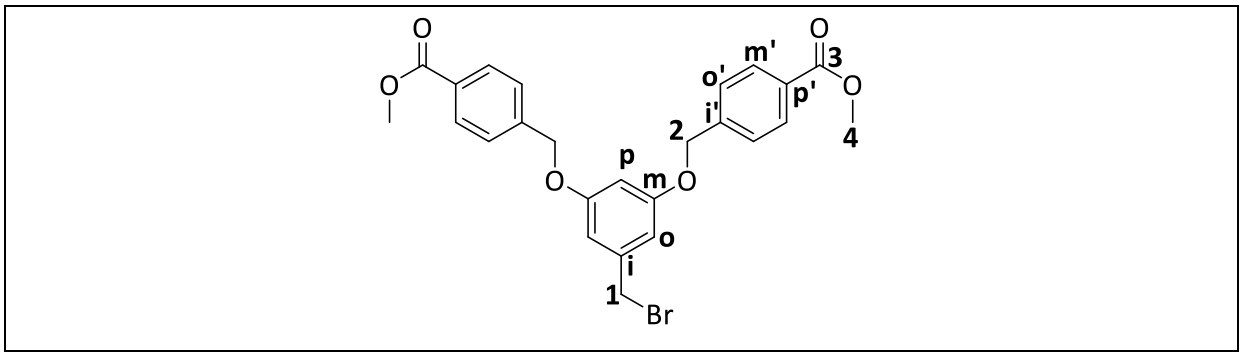

The G_1-COOMe-OH dendron, **2.2** (87.4 mg, 0.200 mmol, 1.00 eq.) was stirred in a minimum amount of dry toluene (3 mL) under an argon atmosphere at room temperature. To this, tetrabromomethane (100 mg, 0.302, 1.52 eq.) was added to the reaction vessel. Triphenylphosphine (78.7 mg, 0.300 mmol, 1.50 eq.) was added neat and the reaction was stirred at room temperature for 0.5 hours. The reaction mixture was poured into water (20 mL) and extracted with dichloromethane (3 x 20 mL). The combined extracts were dried using anhydrous magnesium sulfate. The drying agent was removed by filtration and the filtrate was collected, and evaporated to dryness to yield a yellow residue. The residue was dry-loaded with silica and subjected to flash column chromatography utilising a solvent system of 50% ethyl acetate: petroleum ether (*v/v*). The product, **2.3**, was isolated as a white powder.

Yield: 92 mg (92%). **IR (ATR, cm^{-1}):** *v* = 1712 (sharp, strong, C=O). **^{1}H NMR (300 MHz, $CDCl_3$):** δ 8.03 (d, $^3J_{HH}$ = 8.4 Hz, 4H, $H_{m'}$), 7.45 (d, $^3J_{HH}$ = 8.5 Hz, 4H, $H_{o'}$), 6.61 (d, $^4J_{HH}$ = 2.2 Hz, 2H, H_o), 6.49 (t, $^4J_{HH}$ = 2.2 Hz, 1H, H_p), 5.06 (s, 4H, H_2), 4.37 (s, 2H, H_1), 3.90 (s, 6H, H_4). **^{13}C{^{1}H} NMR (101 MHz, $CDCl_3$):** δ 166.90 (s, C_3), 159.93 (s, C_6), 141.88 (s, C_m), 140.17 (s, $C_{i'}$), 130.04 (s, $C_{m'}$), 129.97 (s, C_i), 127.12 (s, $C_{o'}$), 108.51 (s, C_o), 102.39 (s, C_p), 69.63 (s, C_2), 52.26 (s, C_1), 33.42 (s, C_4). **Elemental Analysis** for $C_{25}H_{23}O_6Br$ (499.3570): C, 60.13; H, 4.64; Found: C, 60.20; H, 4.87%. **EI-MS (m/z):** 499.9609 $[M^{79}]^+$, 497.9704 $[M^{81}]^+$. **Melting Point**: 129.1 – 130.6 °C. (no lit. MP reported)

5.2.4 G_2-COOMe-OH dendron[4] (***2.4***)

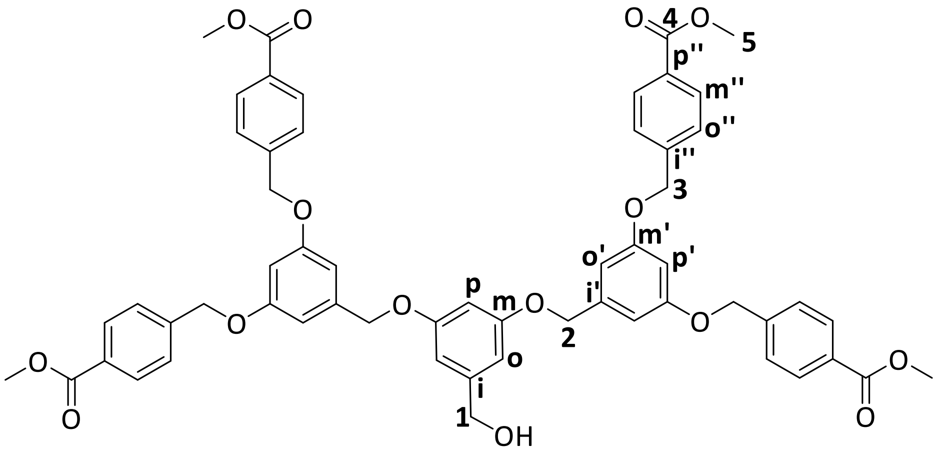

A mixture of 3,5-dihydroxybenzyl alcohol (80.0 mg, 0.570 mmol, 1.00 eq.), potassium carbonate (197 mg, 1.43 mmol, 2.50 eq.) and 18-crown-ether (60.4 mg, 0.228 mmol, 0.400 eq.) in dry acetone (5 mL) was refluxed for 1 hour. To this, a solution of the G_1-COOMe-Br dendrimer, **2.3** (585 mg, 1.17 mmol, 2.00 eq.) in anhydrous acetone (45 mL) was added dropwise. The resultant mixture was refluxed for an additional 23 hours. The mixture was cooled to room temperature and evaporated to dryness under reduced pressure. The residue was partitioned between water (8 mL) and dichloromethane (8 mL), and the aqueous layer was extracted with dichloromethane (3 x 8 mL). The combined organic extracts were washed with a brine solution, and consequently dried using anhydrous magnesium sulfate. The drying agent was removed by filtration and the filtrate was collected. The filtrate was concentrated to a residue and purified by column chromatography. The column was eluted using ethyl acetate: petroleum ether (20: 80, *v*/*v*) solution, increasing the ethyl acetate to 100%. The solvent was removed under reduced pressure to yield the product, **2.4**, as a white powder.

Yield: 486 mg (87%). **IR (ATR, cm^{-1}):** v = 3508 (broad, weak, O-H), 1712 (sharp, strong, C=O). **^{1}H NMR (300 MHz, $CDCl_3$):** δ 8.03 (d, $^3J_{HH}$ = 8.4 Hz, 8H, $H_{m''}$), 7.46 (d, $^3J_{HH}$ = 8.4 Hz, 8H, $H_{o''}$), 6.65 (d, $^4J_{HH}$ = 2.2 Hz, 4H, $H_{o'}$), 6.56 (d, $^4J_{HH}$ = 2.2 Hz, 2H, H_o), 6.53 (t, $^4J_{HH}$ = 2.2 Hz, 2H, $H_{p'}$), 6.45 (t, $^4J_{HH}$ = 2.2 Hz, 1H, H_p), 5.09 (s, 8H, H_3), 4.96 (s, 4H, H_2), 4.60 (s, 2H, H_1), 3.92 (s, 12H, H_5). **$^{13}C\{^1H\}$ NMR (101 MHz, $CDCl_3$):** δ 166.97 (s, C_4), 160.12 (s, C_m), 160.04 (s, $C_{m'}$), 143.74 (s, $C_{i''}$), 142.09 (s, C_i), 139.76 (s, $C_{i'}$), 130.04 (s, $C_{m''}$), 129.90 (s, $C_{p''}$), 127.13 (s, $C_{o''}$), 106.59 (s, $C_{o'}$), 105.90 (s, C_o), 101.87 (s, $C_{p'}$), 101.38 (s, C_p), 69.94 (s, C_2), 69.62 (s, C_3), 65.33 (s, C_1), 52.28 (s,

C_5). **Elemental Analysis** for $C_{57}H_{52}O_{15}$ (976.3306): C, 70.07; H, 5.36; Found: C, 69.59; H, 5.60%. **MALDI-TOF-MS (m/z):** 999.4570 $[M + Na]^+$. **Melting Point**: 117.4 – 119.1 °C. (no lit. MP reported)

*5.2.5 G_2-COOMe-Br dendron[4] (**2.5**)*

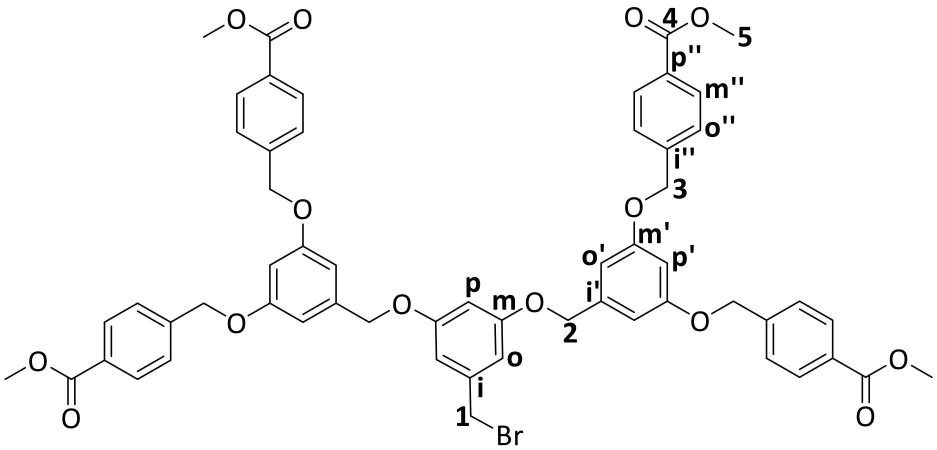

The G_2-COOMe-OH dendron, **2.4** (400 mg, 0.409 mmol, 1.00 eq.) was stirred in a minimum amount of dry toluene (12 mL). To this, tetrabromomethane (353 mg, 1.03 mmol, 2.60 eq.) was added to the reaction vessel. Triphenylphosphine (269 mg, 1.02 mmol, 2.50 eq.) was added neat and the reaction was stirred at room temperature under argon for 0.5 hours. The reaction mixture was poured into water and extracted with dichloromethane (3 x 30 mL). The combined extracts were washed with a saturated brine solution and dried using anhydrous magnesium sulfate. The drying agent was removed by filtration and the filtrate was collected. The organic extracts were evaporated to dryness and the residue was triturated with anhydrous methanol, filtered and washed with diethyl ether to yield the product, **2.5**, as a white powder.

Yield: 410 mg (96%). **IR (ATR, cm^{-1}):** v = 1712 (sharp, strong, C=O). **^{1}H NMR (400 MHz, CDCl$_3$):** δ 8.06 (d, $^3J_{HH}$ = 8.4 Hz, 8H, $H_{m''}$), 7.49 (d, $^3J_{HH}$ = 8.4 Hz, 8H, $H_{o''}$), 6.68 (d, $^4J_{HH}$ = 2.2 Hz, 4H, $H_{o'}$), 6.62 (d, $^4J_{HH}$ = 2.2 Hz, 2H, H_o), 6.56 (t, $^4J_{HH}$ = 2.2 Hz, 2H, $H_{p'}$), 6.50 (t, $^4J_{HH}$ = 2.2 Hz, 1H, $H_{p'}$), 5.12 (s, 8H, H_3), 4.98 (s, 4H, H_2), 4.42 (s, 2H, H_1), 3.94 (s, 12H, H_5). **^{13}C{^{1}H} NMR (101 MHz, CDCl$_3$):** δ 166.79 (s, C_4), 159.92 (s, C_m), 159.90 (s, $C_{m'}$), 141.90 (s, $C_{i''}$), 139.85 (s, C_i), 139.33 (s, $C_{i'}$), 129.90 (s, $C_{m''}$), 129.79 (s, $C_{p''}$), 126.98 (s, $C_{o''}$), 108.25 (s, $C_{o'}$), 106.53 (s, C_o), 102.22 (s, $C_{p'}$), 101.77 (s, C_p), 69.91 (s, C_2), 69.49 (s, C_3), 52.13 (s, C_1), 33.48 (s, C_5). **Elemental Analysis**

for $C_{57}H_{51}O_{14}Br$ (1038.2462): C, 65.83; H, 4.94; Found: C, 65.98; H, 5.25%. **MALDI-TOF-MS (+ve) (m/z):** 1061.2448 $[^{79}M+Na]^+$,1063.2401 $[^{81}M+Na]^+$. **Melting Point**: 121.9 – 123.4 °C. (no lit. MP reported)

5.3 Aryl Schiff Bases (2.6 and 2.7)

*5.3.1 (E)-N-(p-hydroxy)phenylsalicylaldimine[5] (**2.6**)*

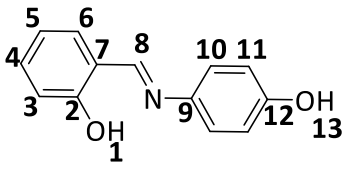

4-Aminophenol (103 mg, 0.942 mmol, 1.00 eq.) was dissolved in hot ethanol (2 mL) and stirred in a reaction flask loaded with a stirrer bar under aerobic conditions. To this, a solution of salicylaldehyde (115 mg, 0.942 mmol, 1.00 eq.) in ethanol (2 mL) was added dropwise, which resulted in the colour change from beige to orange solution. The mixture was refluxed for 4 hours. Upon completion of the reaction as indicated by TLC analysis, the solvent was removed *in vacuo* to yield an orange powder. The powder was dissolved in a minimum amount of chloroform and recrystallized *via* a slow evaporation of chloroform. The orange crystals were filtered and washed with cold petroleum ether, to yield the product (**2.6**) as orange block-like crystals.

Yield: 184 mg (94%). **IR (ATR, cm^{-1}):** *v* = 3380 (broad, weak, O-H), 1615 (sharp, medium, C=N). **^{1}H NMR (400 MHz, $CDCl_3$)**: δ 8.59 (s, 1H, H_8), 7.39 – 7.31 (m, 2H, H_5 and H_3), 7.24 – 7.17 (m, 2H, H_{10}), 7.02 (d, $^3J_{HH}$ = 7.6 Hz, 1H, H_6), 6.96 – 6.90 (m, 1H, H_4), 6.91 – 6.85 (m, 2H, H_{11}).**^{13}C{^{1}H} NMR (101 MHz, $CDCl_3$):** δ 161.29 (s, C_2), 160.70 (s, C_8), 155.23 (s, C_{12}), 141.78 (s, C_9), 132.93 (s, C_4), 132.13 (s, C_6), 122.62 (s, C_{10}), 119.60 (s, C_7), 119.19 (s, C_5), 117.41 (s, C_3), 116.41 (s, C_{11}). **Elemental Analysis** for $C_{13}H_{11}NO_2$ (213.0790): C, 73.23; H, 5.20; N, 6.57; Found C, 72.87; H, 5.14; N, 6.30%. **EI-MS (m/z):** 213.0120 $[M]^+$. **Melting Point**: 139.6 – 140.2°C (literature MP: 141 – 142 °C).[5]

*5.3.1 (E)-4-((2-(diphenylphosphanyl)benzylidene)amino)phenol[6] (**2.7**)*

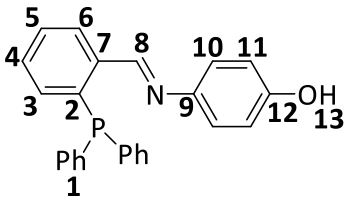

2-Diphenylphosphinobenzaldehyde (381 mg, 1.31 mmol, 1.00 eq.) was loaded to a Schlenk flask equipped with a stirrer bar. Ethanol (15 mL) was degassed by three freeze-thaw-pump cycles and transferred to the Schlenk flask containing 2-diphenylphosphinobenzaldehyde *via* cannulation. To this, a solution of 4-aminophenol (150 mg, 1.38 mmol, 1.05 eq.) in hot ethanol (8 mL) was added dropwise. The resultant mixture was refluxed for 4 hours. The reaction was monitored by TLC and $^{31}P\{^{1}H\}$ NMR spectroscopy. Upon full consumption of the aldehyde, as indicated by $^{31}P\{^{1}H\}$ NMR spectroscopy, the solution was concentrated *in vacuo* and cooled at 0 °C for 3 hours. A pale yellow powder (**2.7**) precipitated out of solution, and was filtered.

Yield: 404 mg (81%). **IR (ATR, cm^{-1}):** *v* = 3016 (broad, weak, O-H), 1615 (sharp, medium, C=N). **^{1}H NMR (300 MHz, $CDCl_3$):** δ 9.08 (d, $^{4}J_{HP}$ = 5.2 Hz, 1H, H_8), 8.18 (ddd, $^{3}J_{HH}$ = 7.7, $^{4}J_{HP}$ = 3.9, $^{4}J_{HH}$ = 1.3 Hz, 1H, H_6), 7.44 (m, 1H, H_3), 7.37 – 7.29 (m, 11H, H_1 and H_4), 6.96 – 6.92 (m, 1H, H_5), 6.89 (d, $^{3}J_{HH}$ = 8.8 Hz, 2H, H_{11}), 6.75 (d, $^{3}J_{HH}$ = 8.8 Hz, 2H, H_{10}). **$^{13}C\{^{1}H\}$ NMR (151 MHz, $CDCl_3$):** δ 156.88 (d, $^{3}J_{CP}$ = 21.8 Hz, C_8), 154.27 (s, C_{12}), 144.93 (s, C_9), 139.64 (d, $^{2}J_{CP}$ = 16.8 Hz, C_2), 138.37 (d, $^{1}J_{CP}$ = 20.3 Hz, C_1), 136.70 (d, $^{2}J_{CP}$ = 10.0 Hz, C_7), 134.05 (d, $^{1}J_{CP}$ = 20.0 Hz, C_1), 133.53 (s, C_5) 130.47 (s, C_1), 128.88 (s, C_1), 128.82 (s, C_4), 128.59 (d, $^{2}J_{CP}$ = 7.2 Hz, C_3), 127.93 (d, $^{3}J_{CP}$ = 3.8 Hz, C_6), 122.42 (s, C_{10}), 115.75 (s, C_{11}). **$^{31}P\{^{1}H\}$ NMR (162 MHz, $CDCl_3$):** -13.24 (s). **Elemental Analysis** for $C_{25}H_{20}NOP$ (381.1283): C, 78.73; H, 5.29; N, 3.67; Found C, 78.22; H, 5.48; N, 3.13%. **EI-MS (m/z):** 381.0023 $[M]^+$. **Melting Point**: 187.6 – 188.6 °C. (no lit. MP reported)

5.4 *N,O*-salicylaldimine and *N,P*-iminophosphine ligand precursors (2.8 – 2.13)

General Method

Compound **2.6** or **2.7** (1.0 – 2.0 eq.), potassium carbonate (1.0 – 2 eq.) and 18-crown-ether (0.2 eq.) was dissolved in anhydrous acetone (30 mL) and refluxed for 1 hour. To this, a solution of **2.1, 2.3** or **2.5** (1 eq.) in dry acetone (20 mL) was added dropwise. The resultant mixture was further refluxed for an additional 23 hours. The mixture was cooled to room temperature and evaporated to dryness under reduced pressure. The residue was partitioned between water (10 mL) and dichloromethane (10 mL), and the aqueous layer was extracted with dichloromethane (3 x 10 mL). The organic fractions were combined and collected. The combined organic fractions were dried using anhydrous magnesium sulfate. After removal of the drying agent by filtration, the solvent was removed to yield a brown residue. The crude product was purified as outlined in the following text for the respective ligands **2.8** – **2.13**.

*5.4.1 G_0-COOMe-N,O-salicylaldimine ligand (**2.8**)*

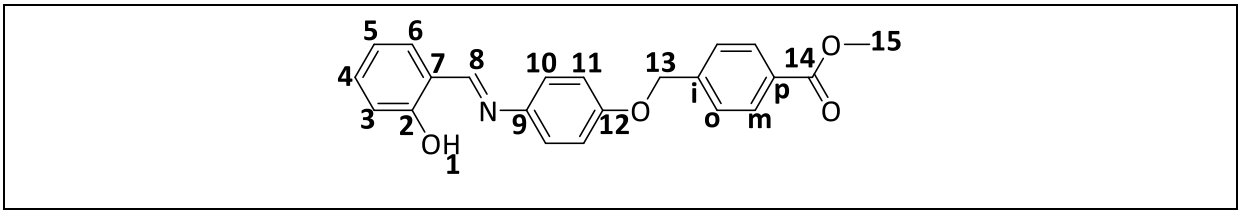

Compound **2.6** (60.1 mg, 0.281 mmol, 1.00 eq.), potassium carbonate (39.2 mg, 0.281 mmol, 1.00 eq.), 18-crown-ether (15.2 mg, 0.0561 mmol, 0.200 eq.) and compound **2.1** (65.0 mg, 0.281 mmol, 1.00 eq.) were reacted in acetone. The residue was dissolved in a minimum amount of chloroform and was kept at 5 ^{o}C for 24 hours. The resultant crystals were filtered and washed with cold chloroform. The product (**2.8**) was identified as a yellow crystalline solid.

Yield: 84 mg (84%). **IR (ATR, cm^{-1}):** *v* = 1720 (sharp, strong, C=O), 1617 (sharp, medium, C=N). **^{1}H NMR (300 MHz, $CDCl_3$):** δ 13.25 (brs, 1H, H_1), 8.53 (s, 1H, H_8), 7.99 (d, $^{3}J_{HH}$ = 8.3 Hz, 2H, H_m), 7.43 (d, $^{3}J_{HH}$ = 8.3 Hz, 2H, H_o), 7.34 – 7.24 (m, 2H, H_5 and H_3), 7.20 (d, $^{3}J_{HH}$ = 9.3 Hz, 2H,

H_{11}), 6.94 (m, 3H, H_{10} and H_6), 6.85 (td, $^3J_{HH}$ = 7.4 Hz, $^4J_{HH}$ = 1.0 Hz, 1H, H_4), 5.07 (s, 2H, H_{13}), 3.85 (s, 3H, H_{15}). **$^{13}C\{^1H\}$ NMR (101 MHz, $CDCl_3$):** δ 166.90 (s, C_{14}), 161.37 (s, C_2), 161.06 (s, C_8), 158.00 (s, C_{12}), 142.42 (s, C_p), 142.23 (s, C_7), 132.95 (s, C_5), 132.17 (s, C_3), 130.22 (s, C_9), 130.12 (s, C_m), 127.14 (s, C_o), 122.52 (s, C_{11}), 119.67 (s, C_i), 119.14 (s, C_4), 117.44 (s, C_6), 116.03 (s, C_{10}), 70.08 (s, C_{13}), 52.15 (s, C_{15}). **Elemental Analysis** for $C_{22}H_{19}NO_4$ (361.1314): C, 73.12; H, 5.30; N, 3.88; Found C, 72.94; H, 5.27; N, 3.60%. **EI-MS (m/z):** 361.1263 $[M]^+$, 212.0207 $[C_{13}H_{10}NO_2]^+$. **Melting Point**: 159.9 – 162.6 °C.

*5.4.2 G_0-COOMe-N,P-iminophosphine ligand (**2.9**)*

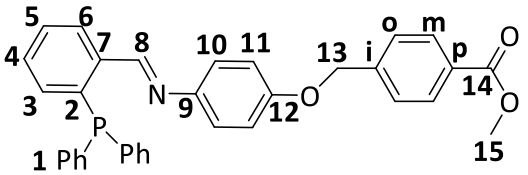

Compound **2.7** (500 mg, 1.31 mmol, 2.00 eq.), potassium carbonate (226 mg, 1.64 mmol, 1.00 eq.), 18-crown-ether (15.0 mg, 0.056 mmol, 0.200 eq.) and compound **2.1** (150 mg, 0.656 mmol, 1.00 eq.) were reacted in degassed anhydrous acetone. The residue was dissolved in chloroform and precipitated with petroleum ether. The resultant crystalline solids were filtered and washed with cold chloroform to yield the product (**2.9**) as a yellow crystalline solid.

Yield: 330 mg (95%). **IR (ATR, cm^{-1}):** 1720 (sharp, strong, C=O), 1613 (sharp, medium, C=N). **^1H NMR (300 MHz, $CDCl_3$):** δ 9.11 (d, $^4J_{HP}$ = 5.2 Hz, 1H, H_8), 8.22 (ddd,$^3J_{HH}$ = 7.7, $^4J_{HP}$ = 3.9, $^4J_{HH}$ = 1.2 Hz, 1H, H_6), 8.08 (d, $^3J_{HH}$ = 8.4 Hz, 2H, H_m), 7.52 (d, $^3J_{HH}$ = 8.4 Hz, 2H, H_o), 7.45 (dd, $^3J_{HH}$ = 7.7 Hz, $^4J_{HH}$ = 0.72 Hz, 1H, H_5), 7.41 – 7.29 (m, 11H, H_1 and H_4), 7.01 – 6.88 (m, 5H, H_3, H_{10} and H_{11}), 5.13 (s, 2H, H_{13}), 3.95 (s, 3H, H_{15}). **$^{13}C\{^1H\}$ NMR (101 MHz, $CDCl_3$):** 166.95 (s, C_{14}), 157.30 (d, $^3J_{CP}$ = 21.7 Hz, C_8), 157.20, (s, C_{12}), 157.17 (s, C_p), 145.26 (s, C_9), 142.35 (s, C_i), 139.57 (d, $^1J_{CP}$ = 16.8 Hz, C_2), 138.46 (d, $^1J_{CP}$ = 20.0 Hz, C_1), 136.70 (d, $^2J_{CP}$ = 9.6 Hz, C_7), 134.20 (d, $^2J_{CP}$ = 20.0 Hz, C_1), 133.71 (s, C_5), 130.76 (s, C_1), 130.02 (s, C_o), 129.08 (s, C_3), 129.03(s, C_4), 128.78 (d, $^2J_{CP}$ = 7.2 Hz, C_1), 128.11 (d, $^3J_{CP}$ = 3.9 Hz, C_6), 127.08 (s, C_m), 122.50 (s, C_{11}),115.40 (s, C_{10}), 69.73 (s, C_{13}), 52.24 (s, C_{15}).**$^{31}P\{^1H\}$ NMR (162 MHz, $CDCl_3$):** -13.25 (s). **Elemental Analysis** for $C_{34}H_{28}NO_3P$ (529.1807): C, 77.11; H, 5.33; N, 2.64; Found: C, 76.88; H, 5.00; N, 2.26%. **EI-MS (m/z):** 529.0436 $[M]^+$. **Melting Point**: 131.4 – 132.9 °C.

*5.4.3 G_1-COOMe-N,O-salicylaldimine ligand (**2.10**)*

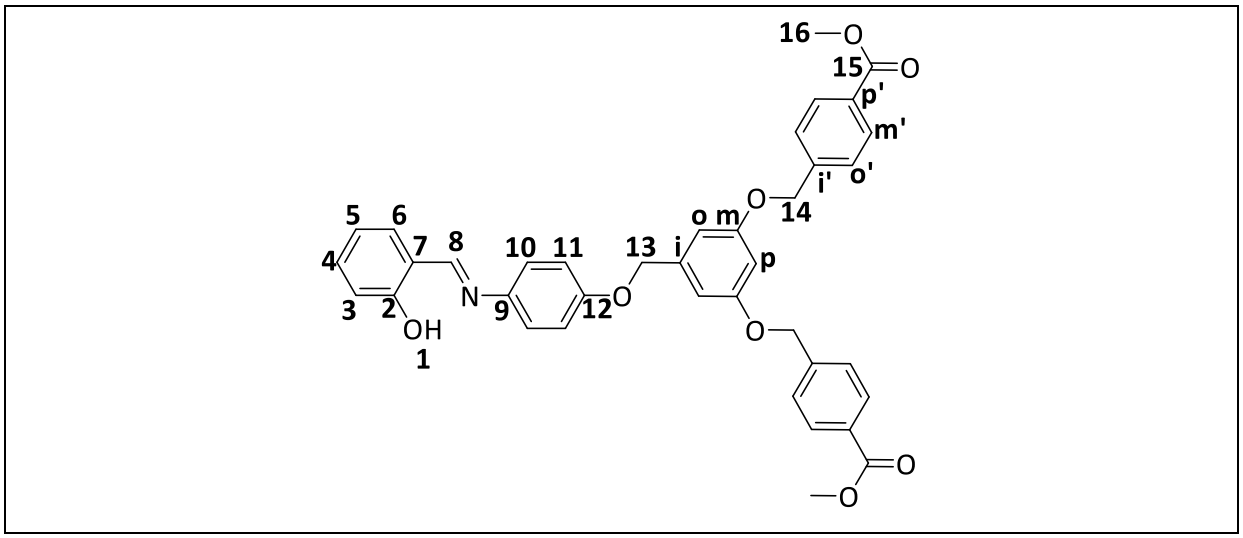

Compound **2.6** (200.0 mg, 0.938 mmol, 2.00 eq.), potassium carbonate (97.22 mg, 0.703 mmol, 1.10 eq.), 18-crown-ether (37 mg, 0.141 mmol, 0.300 eq.) and compound **2.3** (234 mg, 0.469 mmol, 1.00 eq.) were reacted in anhydrous acetone. The crude product was suspended in methanol, filtered and washed with diethyl ether to yield the product (**2.10**) as a pale yellow solid.

Yield: 257 mg (86%). **IR (ATR, cm^{-1}):** *v* = 1720 (sharp, strong, C=O), 1617 (sharp, medium, C=N). **^{1}H NMR (300 MHz, $CDCl_3$):** δ 13.26 (brs, 1H, H_1), 8.51 (s, 1H, H_8), 7.96 (d, $^3J_{HH}$ = 8.4 Hz, 4H, $H_{m'}$), 7.39 (d, $^3J_{HH}$ = 8.4 Hz, 4H, $H_{o'}$), 7.33 – 7.21 (m, 2H, H_5 and H_3), 7.16 (d, $^3J_{HH}$ = 8.8 Hz, 2H, H_{10}), 6.98 – 6.78 (m, 4H, H_{11},H_6 and H_4), 6.59 (d, $^4J_{HH}$ = 2.2 Hz, 2H, H_o), 6.46 (t,$^4J_{HH}$ = 2.2 Hz, 1H, H_p), 5.02 (s, 4H, H_{14}), 4.93 (s, 2H, H_{13}), 3.83 (s, 6H, H_{16}). **^{13}C{^{1}H} NMR (101 MHz, $CDCl_3$):** δ 165.77 (s, C_{15}), 160.01 (s, C_7), 159.66 (s, C_8), 158.92 (s, C_2) 156.77 (s, $C_{p'}$), 140.88 (s, $C_{i'}$), 140.72 (s, C_{12}), 138.52 (s, C_m), 131.74 (s, C_3), 130.99 (s, C_5), 128.88 (s, $C_{m'}$), 128.78 (s, C_i), 125.96 (s, $C_{o'}$), 121.30 (s, C_{10}), 118.36 (s, C_4), 117.98 (s, C_9), 116.16 (s, C_6), 114.61 (s, C_{11}), 105.45 (s, C_o), 100.71 (s, C_p), 69.04 (s, C_{13}), 68.46 (s, C_{14}), 51.12 (s, C_{16}). **Elemental Analysis** for $C_{38}H_{33}NO_8 \cdot H_2O$ (631.2206): C, 70.25; H, 5.43; N, 2.16; Found: C, 70.45; H, 5.06; N, 1.80%. **ESI-MS (m/z, +ve mode):** 632.2280 $[M+H]^+$. **Melting Point**: 131.7 – 134.7 °C.

*5.4.4 G_1-COOMe-N,P-iminophosphine ligand (**2.11**)*

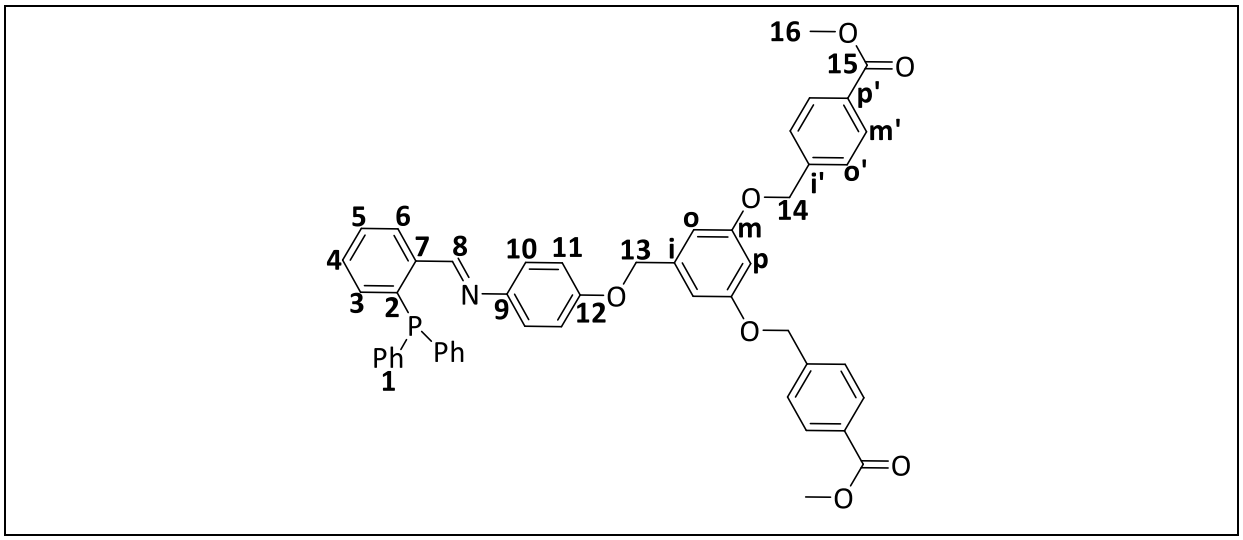

Compound **2.7** (500 mg, 1.31 mmol, 2.00 eq.), potassium carbonate (227 mg, 1.64 mmol, 2.50 eq.), 18-crown-ether (43.3 mg, 0.163 mmol, 0.200 eq.) and compound **2.3** (65 mg, 0.281 mmol, 1.00 eq.) were reacted in degassed anhydrous acetone. The residue was dissolved in chloroform and precipitated with petroleum ether. The residue was triturated with diethyl ether, filtered and dried *in vacuo* to yield the product (**2.11**) as a yellow powder.

Yield: 456 mg (87%). **IR (ATR, cm^{-1}):** *v* = 1714 (sharp, strong, C=O), 1611 (sharp, medium, C=N). **^{1}H NMR (400 MHz, $CDCl_3$):** δ 9.09 (d, $^4J_{HP}$ = 5.2 Hz, 1H, H_8), 8.20 (ddd,$^3J_{HH}$ = 7.7 Hz, $^4J_{HP}$ = 3.3 Hz, $^4J_{HH}$ = 1.5 Hz, 1H, H_6), 8.05 (d, $^3J_{HH}$ = 8.2 Hz, 4H, $H_{m'}$), 7.52 – 7.41 (m, 5H, $H_{o'}$ and H_3), 7.38 – 7.28 (m, 11H, H_1 and H_4), 6.95 (m, 3H, H_5 and H_{11}), 6.88 (d, $^3J_{HH}$ = 8.8 Hz, 2H, H_{10}), 6.67 (d, $^4J_{HH}$ = 2.0 Hz, 2H, H_o), 6.54 (t, $^4J_{HH}$ = 2.0 Hz, 1H, H_p), 5.10 (s, 4H, H_{14}), 4.98 (s, 2H, H_{13}), 3.92 (s, 6H, H_{16}). **^{13}C{^{1}H} NMR (101 MHz, $CDCl_3$):** δ 166.94 (s, C_{15}), 160.07 (s, C_m), 157.80 – 156.65 (C_{12}, C_8), 145.17 (s, $C_{p'}$), 142.10 (s, C_9), 139.93 (s, $C_{i'}$), 139.76 (s, C_2), 138.45 (d, $^1J_{CP}$ = 19.9 Hz, C_1), 136.76 (d, $^2J_{CP}$ = 9.7 Hz, C_7), 134.21 (d, $^2J_{CP}$ = 20.0 Hz, C_1), 133.73 (s, C_5), 130.73 (s, C_1), 130.04 (s, $C_{m'}$), 129.95 (s, C_3), 129.09 (s, C_4), 129.03 (s, C_i), 128.79 (d, $^3J_{CP}$ = 7.1 Hz, C_1), 128.12 (d, $^3J_{CP}$ = 3.8 Hz, C_6), 127.14 (s, $C_{o'}$), 122.47 (s, C_{11}), 115.44 (s, C_{10}), 106.65 (s, C_o), 101.85 (s, C_p), 70.20 (s, C_{14}), 69.65 (s, C_{13}), 52.25 (s, C_{16}).**^{31}P{^{1}H} NMR (162 MHz, $CDCl_3$):** -13.26 (s). **Elemental Analysis** for $C_{50}H_{42}NO_7P{\cdot}1.5\ H_2O$ (799.2699): C, 72.63; H, 5.49; N, 1.69; Found: C, 72.32; H, 5.31; N, 3.25%. **MALDI-TOF-MS (+ve) (m/z):** 800.2130 $[M + H]^+$. **Melting Point**: 132.4 – 134.4 °C.

*5.4.5 G_2-COOMe-N,O-salicylaldimine ligand (**2.12**)*

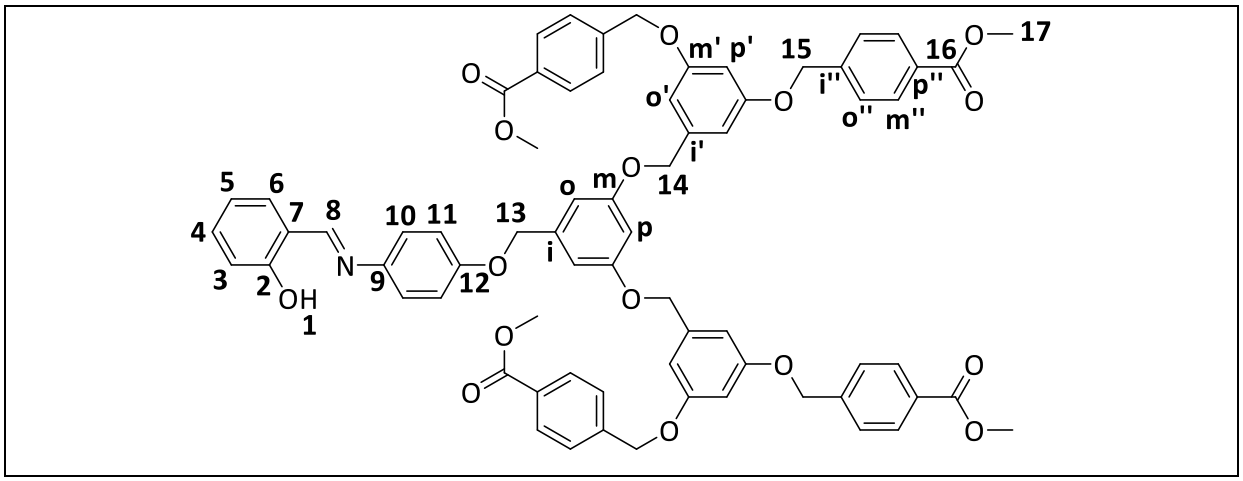

Compound **2.6** (40.7 mg, 0.191 mmol, 2.00 eq.), potassium carbonate (20.0 mg, 0.143 mmol, 1.50 eq.), 18-crown-ether (6.31 mg, 0.0239 mmol, 0.250 eq.) and compound **2.5** (100 mg, 0.0954 mmol, 1.00 eq.) were reacted in anhydrous acetone. The crude product was triturated with methanol, filtered and washed with diethyl ether to yield the product (**2.12**) as a pale yellow powder.

Yield: 95 mg (86%). **IR (ATR, cm^{-1}):** *v* = 1716 (sharp, strong, C=O), 1617 (sharp, medium, C=N). **^{1}H NMR (300 MHz, $CDCl_3$):** δ 13.26 (brs, 1H, H_1) 8.49 (s, 1H, H_8), 7.95 (d, $^3J_{HH}$ = 8.1 Hz, 8H, $H_{m''}$), 7.39 (d, $^3J_{HH}$ = 8.0 Hz, 8H, $H_{o''}$), 7.27 (m, 2H, H_6 and H_4), 7.16 (d, $^3J_{HH}$ = 9.0 Hz, 2H, H_{11}), 6.92 (m, 4H, H_{10}, H_5, H_3), 6.58 (s, 6H, H_o and $H_{o'}$), 6.46 (s, 3H, H_p and $H_{p'}$), 5.01 (s, 8H, H_{15}), 4.94 (s, 2H, H_{14}), 4.90 (s, 4H, H_{13}), 3.84 (s, 12H, H_{17}). **^{13}C{^{1}H} NMR (101 MHz, $CDCl_3$):** δ 166.87 (s, C_{16}), 161.12 (s, C_7), 160.71 (s, C_8), 160.14 (s, C_2), 160.02 (s, $C_{p''}$), 157.96 (s, $C_{i''}$), 142.01 (s, C_m), 141.78 (s, $C_{m'}$), 139.61 (s, C_{12}), 139.46 (s, C_i), 132.84 (s, $C_{i'}$), 132.11 (s, C_6), 129.99 (s, C_4), 129.88 (s, $C_{m''}$), 127.08 (s, $C_{o''}$), 122.42 (s, C_{11}), 119.46 (s, C_q), 119.10 (s, C_5), 117.27 (s, C_3), 115.73 (s, C_{10}), 106.62 (s, C_o), 106.47 (s, $C_{o'}$), 101.77 (s, C_p and $C_{o'}$), 70.25 (s, C_{13}), 69.98 (s, C_{14}), 69.56 (s, C_{15}), 52.23 (s, C_{17}). **Elemental Analysis** for $C_{70}H_{61}NO_{16}\cdot 3H_2O$ (1171.3990): C, 68.56; H, 5.51; N, 1.14; Found: C, 68.39; H, 5.13; N, 1.28%. **MALDI-TOF-MS (m/z, +ve mode):** 1172.5930 $[M + H]^+$. **Melting Point**: 130.3 – 133.5 °C.

*5.4.6 G_2-COOMe-N,P-iminophosphine ligand (**2.13**)*

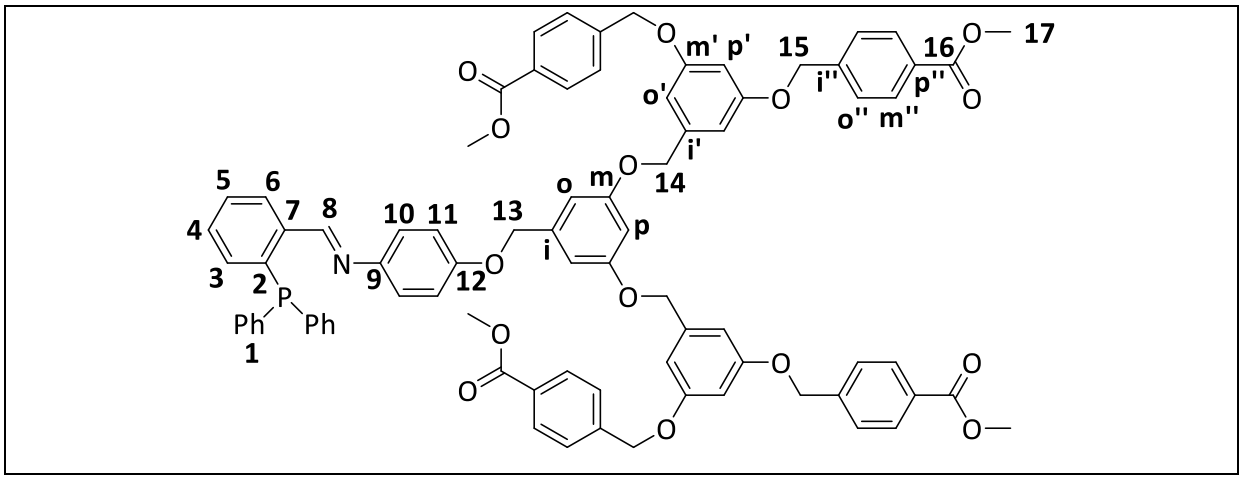

Compound **2.7** (75.0 mg, 0.198 mmol, 2.00 eq.), potassium carbonate (34.2 mg, 0.247 mmol, 2.50 eq.), 18-crown-ether (6.54 mg, 0.0248 mmol, 0.250 eq.) and compound **2.5** (103 mg, 0.100 mmol, 1.00 eq.) were reacted in degassed anhydrous acetone. The residue was triturated with anhydrous methanol, filtered and dried *in vacuo* to yield the product (**2.13**) as a pale yellow powder.

Yield: 117 mg (88%). **IR (ATR, cm^{-1}):** *v* = 1714 (sharp, strong, C=O), 1611 (sharp, medium, C=N). **^{1}H NMR (400 MHz, $CDCl_3$):** δ 9.08 (d, $^4J_{HP}$ = 5.2 Hz, 1H, H_8), 8.18 (ddd,$^3J_{HH}$ = 7.8, $^4J_{HP}$ = 3.9, $^4J_{HH}$ = 1.1 Hz, 1H, H_6), 8.03 (d, $^3J_{HH}$ = 8.2 Hz, 8H, $H_{m''}$), 7.50 – 7.41 (m, 9H, $H_{o''}$ and H_3), 7.37 – 7.28 (m, 11H, H_3 and H_1), 6.96 – 6.85 (m, 5H, H_5, H_{10} and H_{11}), 6.66 (d, $^4J_{HH}$ = 2.0 Hz, 4H, $H_{o'}$), 6.64 (d, $^4J_{HH}$ = 2.0 Hz, 2H, H_o), 6.53 (t, $^4J_{HH}$ = 2.0 Hz, 2H, $H_{p'}$), 6.51 (t, $^4J_{HH}$ = 2.0 Hz, 1H, H_p), 5.09 (s, 8H, H_{15}), 4.97 (s, 6H, H_{14} and H_{13}), 3.91 (s, 12H, H_{17}). **^{13}C{^{1}H} NMR (101 MHz, $CDCl_3$):** δ 166.92 (s, C_{16}), 160.17 (s, $C_{m'}$), 160.07 (s, C_m), 157.36 - 156.97 (m, C_{12} and C_8), 145.11 (s, $C_{p''}$), 142.09 (s, C_9), 139.75 (s, $C_{i''}$), 139.69 (s, C_2), 138.45 (d, $^1J_{CP}$ = 20.0 Hz, C_1), 136.77 (d, $^2J_{CP}$ = 9.6 Hz, C_7), 134.20 (d, $^2J_{CP}$ = 20.0 Hz, C_1), 133.74 (s, C_5), 130.73 (s, C_1), 130.04 (s, $C_{m''}$), 129.94 (s, C_3), 129.09 (s, C_4), 129.03 (brs, C_i and $C_{i''}$), 128.79 (d, $^3J_{CP}$ = 7.2 Hz, C_1), 128.14 (s, C_6), 127.13 (s, $C_{o''}$), 122.47 (s, C_{11}), 115.44 (s, C_{10}), 106.69 (s, $C_{o'}$), 106.52 (s, C_o), 101.91 (s, $C_{p'}$), 101.79 (s, C_p), 70.29 (s, C_{13}), 70.05 (s, C_{14}), 69.64 (s, C_{15}), 52.24 (s, C_{17}). **^{31}P{^{1}H} NMR (162 MHz, $CDCl_3$):** -13.29 (s). **Elemental Analysis** for $C_{82}H_{70}NO_{15}P{\cdot}4H_2O$ (1339.4483): C, 71.29; H, 5.69; N, 1.01; Found: C, 71.13; H, 5.77; N, 0.68%. **MALDI-TOF-MS (+ve) (m/z):** 1340.4801 $[M + H]^+$. **Melting Point**: 130.3 – 133.5 °C.

5.5 Rhodium(I) 1,5-Cyclooctadiene *N,O*-salicylaldimine Organometallic Dendrons (3.1 – 3.3)

General Method

A solution of triethylamine (1 – 1.2 eq.) in dichloromethane (10 mL) was added dropwise to a stirring solution of compound **2.8, 2.10** or **2.12** (1 eq.) in dichloromethane (20 mL). The solution was stirred for 1 hour at 25 °C. $[Rh(\mu\text{-}Cl)(\eta^2\text{:}\eta^2\text{-}COD)]_2$ (0.50 – 0.55 eq.), dissolved in dichloromethane (5 mL), was subsequently added and the reaction mixture was stirred for an additional 3 hours. The solution was then washed with water (3 x 10 mL) in a separating funnel to remove the ammonium chloride formed. The aqueous layer was extracted with dichloromethane (3 x 10 mL). The combined organic extracts were dried using magnesium sulfate. The drying agent was removed by filtration and the filtrate was collected and evaporated to dryness. The residue was taken up in a minimum amount of chloroform, to which petroleum ether was added to precipitate the desired complex.

*5.5.1 G_0-N,O-COOMe Rh(COD) complex (**3.1**)*

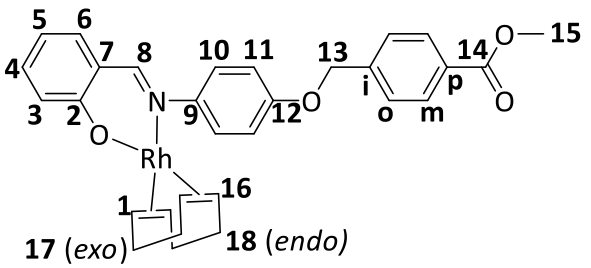

Compound **2.8** (506 mg, 1.40 mmol, 1.00 eq.) and triethylamine (142 mg, 1.40 mmol, 1.00 eq.) were reacted with $[Rh(\mu\text{-}Cl)(\eta^2\text{:}\eta^2\text{-}COD)]_2$ (346 mg, 0.700 mmol, 0.500 eq.). Complex **3.1** was isolated as a yellow crystalline solid.

Yield: 704 mg (88%). **IR (ATR, cm^{-1}):** *v* = 2833 (broad, weak, C-H_{COD}), 1716 (sharp, strong, C=O), 1609 (sharp, medium, C=N). **^{1}H NMR (300 MHz, $CDCl_3$):** δ 8.07 (d, $^3J_{HH}$ = 8.3 Hz, 2H, H_m), 7.97 (d, $^3J_{RhH}$ = 1.7 Hz, 1H, H_8), 7.50 (d, $^3J_{HH}$ = 8.3 Hz, 2H, H_o), 7.34 (td, $^3J_{HH}$ = 8.6 Hz, $^4J_{HH}$ = 1.7 Hz, 1H, H_3), 7.15 (dd, $^3J_{HH}$ = 8.0, $^4J_{HH}$ = 1.7 Hz, 1H, H_5), 6.99 – 6.91 (m, 5H, H_6, H_{10} and H_{11}), 6.56 (td, $^3J_{HH}$ = 8.6 Hz, $^4J_{HH}$ = 1.1 Hz, 1H, H_4), 5.14 (s, 2H, H_{13}), 4.60 (m, 2H, H_1), 3.93 (s, 3H, H_{15}), 3.23 (m, 2H, H_{16}), 2.38 (m, 4H, H_{18}), 1.81 (m, 4H, H_{17}). **^{13}C{^{1}H} NMR (101 MHz, $CDCl_3$):**

167.29 (s, C_{14}), 166.91 (s, C_2), 166.19 (s, C_8), 156.76 (s, C_{12}), 146.72 (s, C_7), 142.23 (s, C_p), 135.58 (s, C_5), 135.34 (s, C_3), 130.24 (s, C_m), 130.12 (s, C_o), 127.18 (s, C_{10}), 124.49 (s, C_6), 122.30 (s, C_9), 118.91 (s, C_i), 115.05 (s, C_{11}), 114.79 (s, C_4), 84.90 (d, $^1J_{RhC}$ = 12.3 Hz, C_1), 73.02 (d, $^1J_{RhC}$ = 14.1 Hz, C_{16}), 70.12 (s, C_{13}), 52.17 (s, C_{15}), 31.59 (s, C_{18}), 29.20 (s, C_{17}). **Elemental Analysis** for $C_{30}H_{30}NO_4Rh{\cdot}1.5H_2O$ (571.1230): C, 60.21; H, 5.56; N, 2.34; Found: C, 59.94; H, 5.23; N, 1.93%. **EI-MS (m/z):** 571.0999 $[M]^+$, 212.0335 $[M\text{-}Rh\text{-}COD]^+$. **Melting Point**: Decomposes with melting, onset occurs at 242.6 °C.

*5.5.2 G_1-N,O-COOMe Rh(COD) complex (**3.2**)*

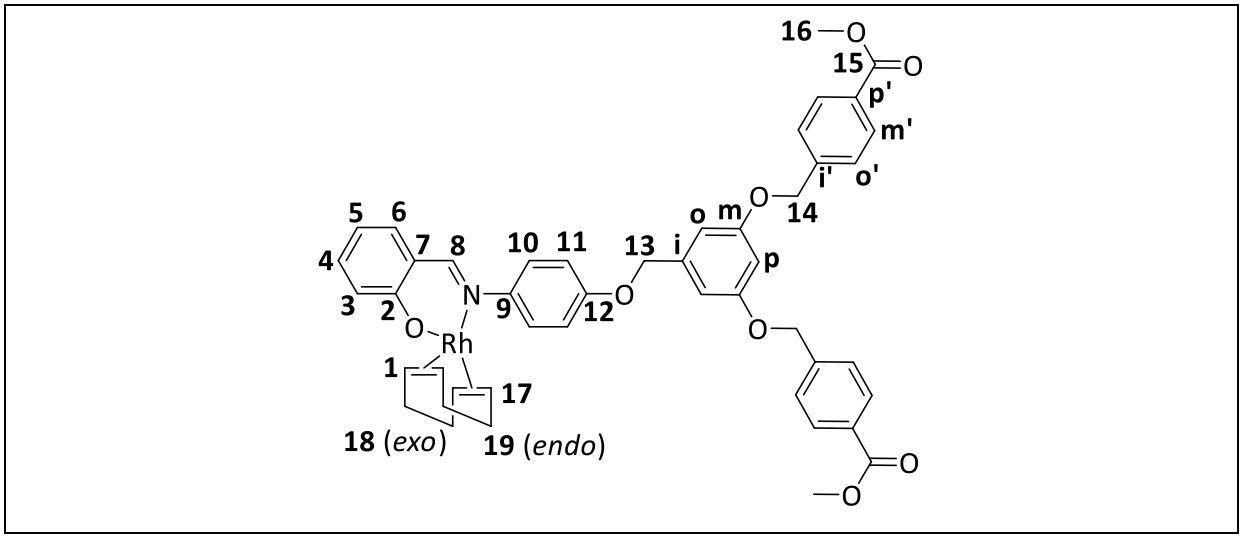

Compound **2.10** (50 mg, 0.0594 mmol, 1.00 eq.) and triethylamine (33.6 mg, 0.332 mmol, 1.05 eq.) were reacted with $[Rh(\mu\text{-}Cl)(\eta^2{:}\eta^2\text{-}COD)]_2$ (78.1 mg, 0.138 mmol, 0.510 eq.). Complex **3.2** was isolated as a yellow powder.

Yield: 229 mg (86%). **IR (ATR, cm^{-1}):** *v* = 2833 (broad, weak, C-H_{COD}), 1710 (sharp, strong, C=O), 1605 (sharp, medium, C=N). **^{1}H NMR (300 MHz, $CDCl_3$):** δ 8.05 (d, $^3J_{HH}$ = 8.3 Hz, 4H, $H_{m'}$), 7.97 (d, $^3J_{RhH}$ = 1.5 Hz, 1H, H_8), 7.48 (d, $^3J_{HH}$ = 8.3 Hz, 4H, $H_{o'}$), 7.34 (ddd, $^3J_{HH}$ = 8.6, $^3J_{HH}$ = 6.9, $^4J_{HH}$ = 1.7 Hz, 1H, H_3), 7.15 (dd, $^3J_{HH}$ = 8.0, $^4J_{HH}$ = 1.6 Hz, 1H, H_5), 7.01 – 6.83 (m, 5H, H_{10}, H_{11} and H_6), 6.67 (d, $^4J_{HH}$ = 2.1 Hz, 2H, H_o), 6.61 – 6.50 (m, 2H, H_p and H_4), 5.11 (s, 4H, H_{14}), 4.98 (s, 2H, H_{13}), 4.59 (s, 2H, H_1), 3.92 (brs, 6H, H_{16}), 3.23 (brs, 2H, H_{17}), 2.37 (brs, 4H, H_{18}), 1.94 – 1.68 (m, 4H, H_{17}). **^{13}C{^{1}H} NMR (101 MHz, $CDCl_3$):** δ 166.99 (s, C_{15}), 166.94 (s, C_2), 166.17 (s, C_8), 160.10 (s, C_m), 156.69 (s, C_{12}), 146.25 (s, C_7), 142.03 (s, $C_{i'}$), 142.17 (s, $C_{p'}$), 139.65 (s, C_i), 135.62 (s, C_5), 135.35 (s, C_3), 130.07 (s, $C_{m'}$), 129.99 (s, $C_{o'}$), 127.15 (s, C_{10}),

124.39 (s, C_6), 122.17 (s, C_9), 114.85 (s, C_{11}), 114.73 (s, C_4), 106.74 (s, C_o), 101.86 (s, C_p), 84.84 (d, $^1J_{RhC}$ = 12.0 Hz, C_1), 73.05 (d, $^1J_{RhC}$ = 14.1 Hz, C_{17}), 70.24 (s, C_{13}), 69.66 (s, C_{14}), 52.31 (s, C_{16}), 31.52 (s, C_{19}), 29.17 (s, C_{18}). **Elemental Analysis** for $C_{46}H_{44}NO_8Rh{\cdot}1.5H_2O$ (841.2122): C, 63.60; H, 5.45; N, 1.61; Found: C, 63.96; H, 5.17; N, 1.66%. **HR-ESI-MS (m/z, +ve mode):** 632.2287 $[M\text{-}Rh\text{-}COD]^+$. **Melting Point**: Decomposes with melting, onset occurs at 241.1 °C.

*5.5.3 G_2-N,O-COOMe Rh(COD) complex (**3.3**)*

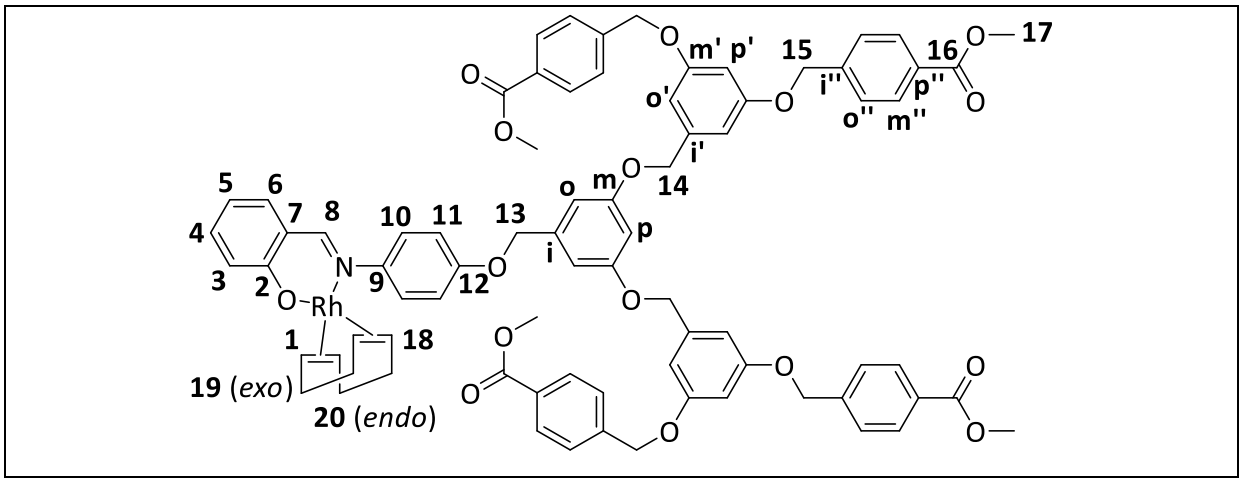

Compound **2.12** (80.0 mg, 0.0682 mmol, 1.00 eq.) and triethylamine (8.29 mg, 0.0819 mmol, 1.20 eq.) were reacted with $[Rh(\mu\text{-}Cl)(\eta^2{:}\eta^2\text{-}COD)]_2$ (18.5 mg, 0.0375 mmol, 0.554 eq.). Complex **3.3** was isolated as a yellow powder.

Yield: 37 mg (79%). **IR (ATR, cm^{-1}):** *v* = 1716 (sharp, strong, C=O), 1607 (sharp, medium, C=N). **^{1}H NMR (400 MHz, $CDCl_3$):** δ 8.03 (d, $^3J_{HH}$ = 8.2 Hz, 8H, $H_{m''}$), 7.96 (s, 1H, H_8), 7.46 (d, $^3J_{HH}$ = 8.2 Hz, 8H, $H_{o''}$), 7.33 (ddd, $^3J_{HH}$ = 8.6, $^3J_{HH}$ = 6.9, $^4J_{HH}$ = 1.8 Hz, 1H, H_3), 7.13 (dd, $^3J_{HH}$ = 8.0, $^4J_{HH}$ = 1.7 Hz, 1H, H_5), 6.93 (m, 5H, H_{10}, H_{11} and H_6), 6.66 (m, 6H, H_o and $H_{o'}$), 6.61 – 6.47 (m, 4H, H_p, $H_{p'}$ and H_4), 5.09 (s, 8H, H_{15}), 4.97 (s, 6H, H_{13} and H_{14}), 4.59 (brs, 2H, H_1), 3.91 (s, 12H, H_{17}), 3.23 (brs, 2H, H_{18}), 2.39 (m, 4H, H_{20}), 1.80 (m, 4H, H_{19}). **^{13}C{^{1}H} NMR (101 MHz, $CDCl_3$):** δ 166.94 (s, C_{16}), 166.89 (s, C_2), 166.13 (s, C_8), 160.15 (s, $C_{m'}$), 160.04 (s, C_m), 156.71 (s, C_{12}), 146.18 (s, C_7), 142.00 (s, $C_{i''}$), 139.58 (s, C_i), 139.50 (s, $C_{i'}$), 139.42 (s, $C_{p''}$), 135.59 (s, C_5), 135.31 (s, C_3), 130.02 (s, $C_{m''}$), 129.91 (s, $C_{o''}$), 127.10 (s, C_{10}), 124.35 (s, C_6), 122.12 (s, C_9), 114.81 (s, C_{11}), 114.70 (s, C_4), 106.67 (s, C_o), 106.60 (s, $C_{o'}$), 101.78 (s, C_p), 101.72 (s, $C_{p'}$), 84.79 (d, $^1J_{RhC}$ = 12.1 Hz, C_1), 73.01 (d, $^1J_{RhC}$ = 13.9 Hz, C_{18}), 70.30 (s, C_{13}), 70.00 (s, C_{14}), 69.59 (s, C_{15}), 52.25 (s, C_{17}), 31.48 (s, C_{20}), 29.13 (s, C_{19}). **Elemental Analysis** for $C_{78}H_{72}NO_{16}Rh$

(1381.3906): C, 67.77; H, 5.25; N, 1.10; Found: C, 68.02; H, 4.88; N, 0.72; %. **MALDI-TOF-MS (+ve mode, m/z):** 1382.5970 $[M+H]^+$, 1278.5550 $[M\text{-}COD]^+$, 1172.5660 $[M\text{-}Rh\text{-}COD]^+$. **Melting Point**: Decomposes with melting, onset occurs at 192.0 °C.

5.6 Rhodium(I) Dicarbonyl *N,O*-salicylaldimine Organometallic Dendrons (3.4 – 3.6)

General Method

The rhodium COD precursor (**3.1 – 3.3**) was dissolved in 15 mL of dichloromethane. Carbon monoxide gas (1 bar) was bubbled through the solution for 0.5 hours. The solvent was removed under reduced pressure, and the product was dried *in vacuo*. The crude product was dissolved in a minimum amount of DCM, to which petroleum ether was added to precipitate the crude product. The crude product was triturated with pentane (to remove the displaced 1,5-cyclooctadiene) to yield the desired complex.

5.6.1 G_0-N,O-COOMe $Rh(CO)_2$ complex (3.4)

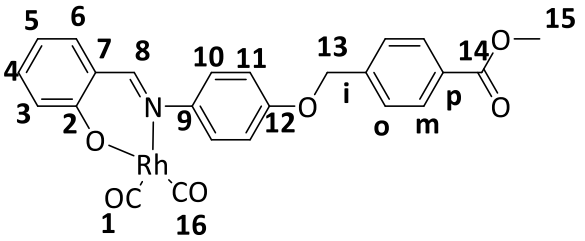

Complex **3.1** (50.0 mg, 0.0880 mmol) was reacted with carbon monoxide to afford complex **3.4** as an orange crystalline solid.

Yield: 45 mg (99 %). **IR (ATR, cm^{-1}):** *v* = 2067 (sharp, strong, C≡O), 1996 (sharp, strong, C≡O), 1714 (sharp, strong, C=O), 1609 (sharp, strong, C=N). **^{1}H NMR (300 MHz, $CDCl_3$):** δ 8.17 (d, $^3J_{RHH}$ = 1.6 Hz, 1H, H_8), 8.09 (d, $^3J_{HH}$ = 8.2 Hz, 2H, H_m), 7.53 (d, $^3J_{HH}$ = 8.2 Hz, 2H, H_o), 7.51 – 7.39 (m, 1H, H_3), 7.27 (m, 3H, H_5 and H_{11}), 7.12 (appd, $^3J_{HH}$ = 8.6 Hz, 1H, H_6), 7.01 (d, $^3J_{HH}$ = 8.8 Hz, 2H, H_{10}), 6.73 (appt, $^3J_{HH}$ = 7.3 Hz, 1H, H_4), 5.18 (s, 2H, H_{13}), 3.95 (s, 3H, H_{15}). **^{13}C{^{1}H} NMR (101 MHz, $CDCl_3$):** δ 184.35 (d, $^2J_{RhC}$ = 65.5 Hz, C_1), 183.66 (d, $^2J_{RhC}$ = 64.3 Hz, C_{16}), 166.89 (s, C_{14}), 165.70 (s, C_8), 164.65 (s, C_2), 157.31 (s, C_7), 152.06 (s, C_{12}), 141.87 (s, C_i), 136.07 (s, C_5), 135.45 (s, C_3), 130.06 (s, C_m), 130.00 (s, C_9), 127.13 (s, C_o), 124.45 (s, C_{11}), 121.85 (s, C_6),

118.38 (s, C_p), 116.36 (s, C_4), 115.15 (s, C_{10}), 69.85 (s, C_{13}), 52.27 (s, C_{15}). **Elemental Analysis** for $C_{24}H_{18}NO_6Rh{\cdot}2H_2O$ (519.0189): C, 51.91; H, 3.99; N, 2.52; Found: C, 52.27; H, 3.51; N, 2.22%. **HR-ESI-MS (m/z):** 520.0323 $[M]^+$, 464.0416 $[M\text{-}(CO)_2]^+$, 362.1433 $[M\text{-}Rh\text{-}(CO)_2]^+$. **Melting Point**: Decomposes with melting, onset occurs at 198.9 °C.

5.6.2 G_1-N,O-COOMe $Rh(CO)_2$ complex (3.5)

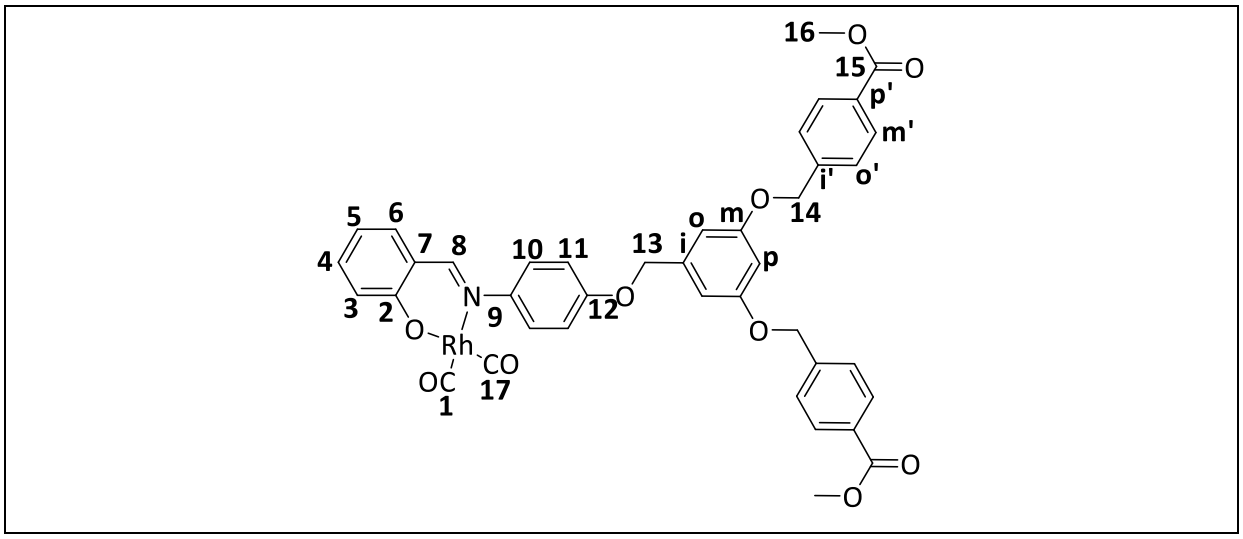

Complex **3.2** (132 mg, 0.157 mmol) was reacted with carbon monoxide to afford complex **3.5** as a red powder.

Yield: 117 mg, (95%). **IR (ATR, cm^{-1}):** *v* = 2071 (sharp, strong, C≡O), 2011 (sharp, strong, C≡O), 1714 (sharp, strong, C=O), 1611 (sharp, strong, C=N). **^{1}H NMR (400 MHz, $CDCl_3$):** δ 8.18 (d, $^3J_{RhH}$ = 1.7 Hz, 1H, H_8), 8.08 (d, $^3J_{HH}$ = 8.3 Hz, 4H, $H_{m'}$), 7.51 (d, $^3J_{HH}$ = 8.3 Hz, 4H, $H_{o'}$), 7.49 – 7.43 (m, 1H, H_3), 7.32 – 7.21 (m, 3H, H_5 and H_{11}), 7.13 (appd, $^3J_{HH}$ = 8.6 Hz, 1H, H_6), 6.98 (d, $^3J_{HH}$ = 8.8 Hz, 2H, H_{10}), 6.78 – 6.68 (m, 3H, H_o and H_4), 6.58 (t, $^4J_{HH}$ = 2.2 Hz, 1H, H_p), 5.13 (s, 4H, H_{14}), 5.06 (s, 2H, H_{13}), 3.94 (s, 6H, H_{16}).**^{13}C{^{1}H} NMR (101 MHz, $CDCl_3$):** δ 184.25 (d, $^2J_{RhC}$ = 69.9 Hz, C_1), 183.56 (d, $^2J_{RhC}$ = 68.8 Hz, C_{17}), 166.78 (s, C_{15}), 165.58 (s, C_8), 164.53 (s, C_2), 159.97 (s, C_7), 157.33 (s, C_{12}), 151.82 (s, C_m), 141.89 (s, $C_{i'}$), 139.34 (s, C_i), 135.95 (s, C_5), 135.34 (s, C_3), 129.92 (s, $C_{m'}$), 129.82 (s, C_9), 126.99 (s, $C_{o'}$), 124.28 (s, C_{11}), 121.73 (s, C_6), 118.28 (s, $C_{p'}$), 116.25 (s, C_4), 115.00 (s, C_{10}), 106.51 (s, C_o), 101.76 (s, C_p), 70.14 (s, C_{13}), 69.49 (s, C_{14}), 52.26 (s, C_{16}). **Elemental Analysis** for $C_{40}H_{32}NO_{10}Rh$ (789.1081): C, 60.85; H, 4.09; N, 1.77; Found: C, 60.82; H, 4.00; N, 1.67%. **HR-ESI-MS (m/z):** 790.1157 $[M]^+$, 734.1209

$[M\text{-}(CO)_2]^+$, 632.2277 $[M\text{-}Rh\text{-}(CO)_2]^+$. **Melting Point**: Decomposes with melting, onset occurs at 214 °C.

5.6.3 G_2-N,O-COOMe $Rh(CO)_2$ complex (3.6)

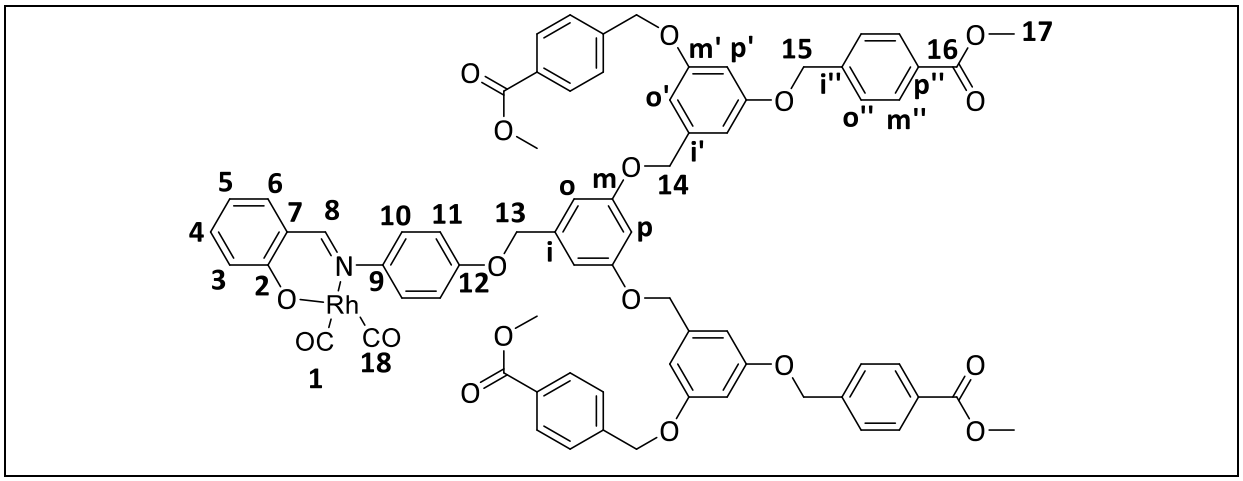

Complex **3.3** (65.0 mg, 0.0470 mmol) was reacted with carbon monoxide to afford complex **3.6** as a pale yellow powder.

Yield: 37 mg (79%). **IR (ATR, cm^{-1}):** *v* = 2071 (sharp, strong, C≡O), 2000 (sharp, strong, C≡O), 1716 (sharp, strong, C=O), 1607 (sharp, medium, C=N). **^{1}H NMR (400 MHz, $CDCl_3$):** δ 8.16 (d, $^3J_{RhH}$ = 1.9 Hz, 1H, H_8), 8.03 (d, $^3J_{HH}$ = 8.5 Hz, 8H, $H_{m''}$), 7.46 (d, $^3J_{HH}$ = 8.6 Hz, 8H, $H_{o''}$), 7.20 (s, 4H, H_3, H_5 and H_{11}, overlap with $CDCl_3$), 7.10 (m, 1H, H_6), 6.97 (d, $^3J_{HH}$ = 7.4, 2H, H_{10}), 6.71 (ddd, $^3J_{HH}$ = 7.9, $^3J_{HH}$ = 6.9, $^4J_{HH}$ = 1.0 Hz, 1H, H_4), 6.66 (m, 6H, H_o and $H_{o'}$), 6.53 (m, 3H, H_p and $H_{p'}$), 5.10 (s, 8H, H_{15}), 5.02 (s, 2H, H_{13}), 4.98 (s, 4H, H_{14}), 3.91 (s, 12H, H_{17}).**^{13}C{^{1}H} NMR (101 MHz, $CDCl_3$):** δ 184.76 (d, $^2J_{RhC}$ = 70.3 Hz, C_1), 183.35 (d, $^2J_{RhC}$ = 69.1 Hz, C_{18}), 166.91 (s, C_{16}), 165.72 (s, C_8), 164.77 (s, C_2), 160.11 (s, C_7), 157.33 (s, C_{12}), 151.97 (s, C_m and $C_{m'}$), 142.05 (s, $C_{i''}$), 139.66 (s, $C_{i'}$), 139.30 (s, C_i), 136.10 (s, C_5), 135.43 (s, C_3), 130.06 (s, $C_{m''}$), 129.99 (s, C_9), 127.13 (s, $C_{o''}$), 127.28 (s, C_{11}), 121.93 (s, C_6), 118.42 (s, $C_{p''}$), 116.38 (s, C_4), 115.20 (s, C_{10}), 106.73 (s, $C_{o'}$), 106.59 (s, C_o), 101.88 (s, C_p and $C_{p'}$), 70.42 (s, C_{13}), 70.07 (s, C_{14}), 69.67 (s, C_{15}), 52.26 (s, C_{17}). **Elemental Analysis** for $C_{72}H_{60}NO_{18}Rh{\cdot}1H_2O$ (1329.2865): C, 64.15; H, 4.64; N, 1.04; Found: 64.33; H, 4.79; N, 0.82%. **HR-ESI-MS (m/z):** 1330.3027 $[M]^+$, 1274.2863 $[M\text{-}(CO)_2]^+$, 1172.4108 $[M\text{-}Rh(CO)_2]^+$. **Melting Point**: Decomposes with melting, onset occurs at 198.0 °C.

5.7 Rhodium(I) Chloro-Carbonyl *N,P*-iminophosphine Organometallic Dendrons (3.7 – 3.9)

General Method

The *N,P*-iminophosphine ligand (**2.9, 2.11** or **2.13**) was stirred in a degassed solution of dichloromethane. To this $[Rh(\mu\text{-}Cl)(CO)_2]_2$ was added which immediately resulted in a colour change of the solution from yellow to red. The reaction was stirred for 1 hour and monitored by TLC analysis. The solution was added to a silica-packed column, and eluted with EtOAc under a flow of argon. The product associated with the bright orange band was collected. The combined fractions were reduced *in vacuo* to yield the desired complex.

5.7.1 G_0-N,P-COOMe RhCl(CO) complex (3.7)

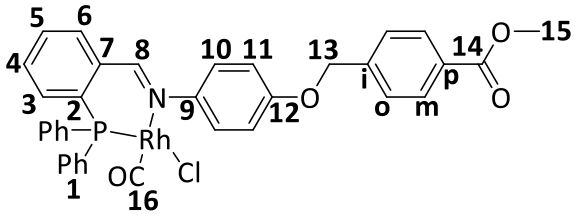

Compound **2.9** (100 mg, 0.189 mmol, 1.00 eq.) was reacted with $[Rh(\mu\text{-}Cl)(CO)_2]_2$ (37.4 mg, 0.0963 mmol, 0.510 eq.). Complex **3.7** was isolated as an orange powder.

Yield: 126 mg (96 %). **IR (ATR, cm^{-1}):** *v* = 1988 (sharp, strong, C≡O), 1720 (sharp, strong, C=O), 1609 (sharp, medium, C=N). **^{1}H NMR (400 MHz, $CDCl_3$):** δ 8.02 – 7.91 (m, 3H, H_8 and H_m), 7.56 – 7.32 (m, 15H, H_1, H_4, H_5, H_6, H_o), 7.21 – 7.16 (m, 2H, H_{11}, overlap with $CDCl_3$), 6.91 (dd, $^3J_{HH}$ = 8.9 Hz, $^3J_{HH}$ 8.5 Hz, 1H, H_3), 6.82 (d, $^3J_{HH}$ = 8.9 Hz, 2H, H_{10}), 5.02 (s, 2H, H_{13}), 3.85 (s, 3H, H_{15}).**^{31}P{^{1}H} NMR (162 MHz, $CDCl_3$):** 48.52 (d, $^1J_{RhP}$ = 165.2 Hz). **Elemental Analysis** for $C_{35}H_{28}NO_4ClPRh$ (695.0500): C, 60.40; H, 4.06; N, 2.01; Found C, 60.03; H, 4.12; N, 1.65%. **HR-ESI-MS (m/z)**: 696.0754 $[M]^+$, 660.0795 $[M\text{-}Cl]^+$. **Melting Point**: Decomposes with melting, onset occurs at 213.6 °C.

5.7.2 G_1-N,P-COOMe RhCl(CO) complex (3.8)

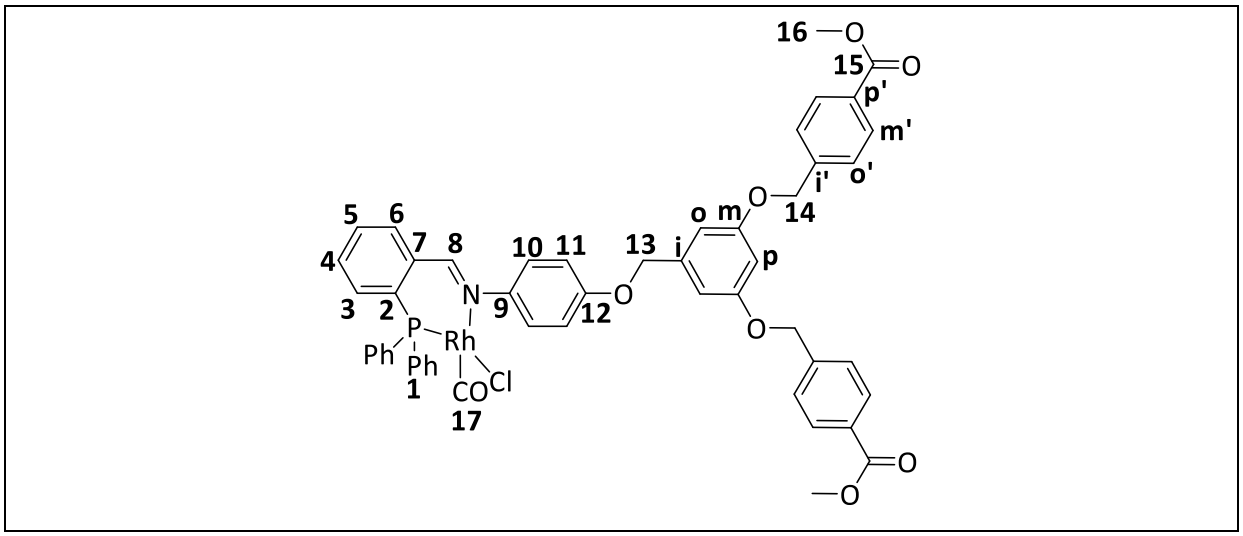

Compound **2.11** (100 mg, 0.125 mmol, 1.00 eq.) was reacted with $[Rh(\mu\text{-}Cl)(CO)_2]_2$ (24.8 mg, 0.0638 mmol, 0.510 eq.). Complex **3.8** was isolated as an orange powder.

Yield: 114 mg (94 %). **IR (ATR, cm^{-1}):** *v* = 1986 (sharp, strong, C≡O), 1720 (sharp, strong, C=O), 1607 (sharp, medium, C=N). **^{1}H NMR (300 MHz, $CDCl_3$):** δ 8.07 (m, 5H, H_8 and $H_{m'}$), 7.53 (m, 17H, H_1, H_4, H_5, H_6, $H_{o'}$), 7.30 (m, 2H, H_{11}, overlap with $CDCl_3$), 7.05 – 6.95 (m, 1H, H_3), 6.89 (d, $^3J_{HH}$ = 8.9 Hz, 2H, H_{10}), 6.67 (d, $^4J_{HH}$ = 2.2 Hz, 2H, H_o), 6.56 (t, $^4J_{HH}$ = 2.2 Hz, 1H, H_p), 5.12 (s, 4H, H_{14}), 4.99 (s, 2H, H_{13}), 3.94 (s, 6H, H_{16}). **^{31}P{^{1}H} NMR (162 MHz, $CDCl_3$):** 48.51 (d, $^1J_{RhP}$ = 165.2 Hz). **Elemental Analysis** for $C_{51}H_{42}NO_8ClPRh\cdot 7H_2O$ (965.1392): C, 56.08; H, 5.17; N, 1.28; Found: C, 56.50; H, 5.55; N, 0.98; %. **HR-ESI-MS (m/z)**: 930.1716 $[M\text{-}Cl]^+$. **Melting Point**: Decomposes with melting, onset occurs at 161.9 °C

5.7.3 G_2-N,P-COOMe RhCl(CO) complex (3.9)

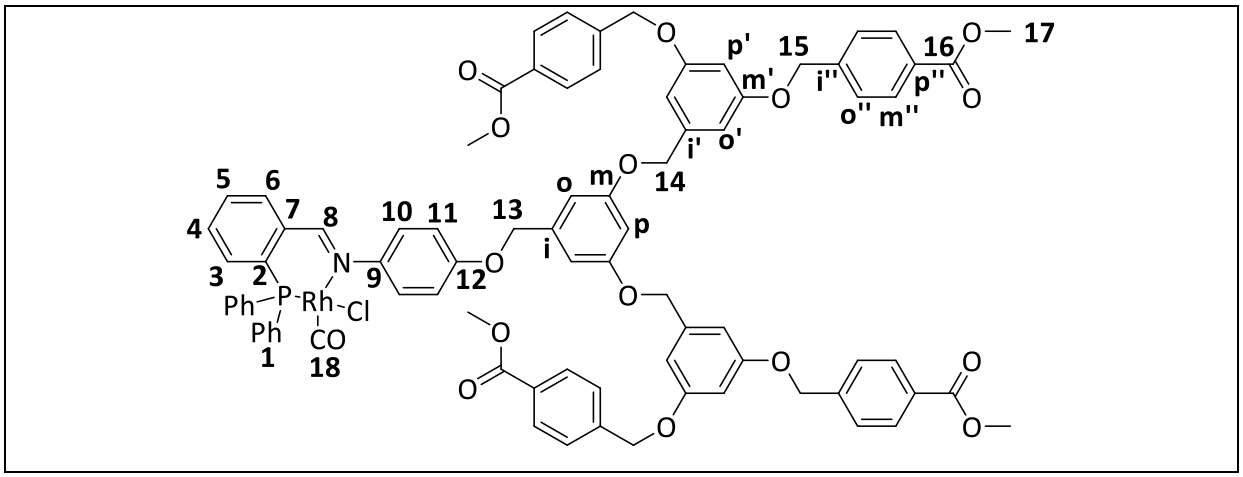

Compound **2.13** (100 mg, 0.0746 mmol, 1.00 eq.) was reacted with $[Rh(\mu\text{-}Cl)(CO)_2]_2$ (15.1 mg, 0.0388 mmol, 0.510 eq.). Complex **3.9** was isolated as an orange amorphous solid.

Yield: 104 mg, (93 %). **IR**: **(ATR, cm^{-1})** 1990 (sharp, strong, C≡O), 1720 (sharp, strong, C=O), 1609 (sharp, medium, C=N). **^{1}H NMR (400 MHz, $CDCl_3$):** δ 8.05 (m, 9H, H_8 and $H_{m''}$), 7.51 (m, 21H, H_1, H_4, H_5, H_6, $H_{o''}$), 7.30 – 7.09 (m, 3H, H_{11} and H_3, overlap with $CDCl_3$), 6.91 (d, $^3J_{HH}$ = 8.9 Hz, 2H, H_{10}) 6.70 – 6.56 (m, 9H, H_p, $H_{p'}$, H_o and $H_{o'}$), 5.12 (s, 8H, H_{15}), 4.99 (s, 6H, H_{13} and H_{14}), 3.94 (s, 12H, H_{17}). **^{31}P{^{1}H} NMR (162 MHz, $CDCl_3$):** 48.46 (d, $^1J_{RhP}$ = 165.2 Hz). **Elemental Analysis** $C_{83}H_{70}NO_{16}ClPRh\cdot 11H_2O$ (1505.3176): C, 58.47; H, 5.44; N, 0.88; Found C, 58.70; H, 5.81; N, 1.03;%. **HR-ESI-MS (m/z)**: 1470.3429 $[M\text{-}Cl]^+$. **Melting Point**: Decomposes with melting, onset occurs at 117.3 °C

5.8 NMR Experiments

5.8.1 Phosphorous stability experiments

Compound **2.9** or **3.1** was dissolved in degassed $CDCl_3$ under aerobic conditions (0.1 mmol/mL). The ^{31}P{^{1}H} NMR was collected at 0, 1, 2, 4, and 8 hour intervals.

To identify the phosphine oxide of the ligand, a solution of **2.9** in dichloromethane was evaporated to a residue under a stream of air. The compound was dried *in vacuo* and analysed using ^{31}P{^{1}H} NMR spectroscopy. The ^{31}P{^{1}H} NMR spectra were recorded on a Bruker Biospin GmbH spectrometer at 162.00 MHz. The phosphine oxide was observed at δ_P 31.26 ppm.

5.9 X-ray Crystallography Methods

Single-crystal X-ray diffraction data (compounds **2.8, 3.1** and **3.4**) were collected using a Bruker Kappa APEX II DUO diffractometer equipped with a graphite-monochromated Mo-Kα radiation (λ = 0.71073 Å). The temperature was controlled by an Oxford Cryostream cooling system (Oxford Cryostat). Cell refinement and data reduction were achieved using the program SAINT.[7] The data were scaled, and absorption correction was accomplished using SADABS.[8] The structure was solved by direct methods by using SHELXS-9733 and refined by full-matrix least-squares methods based on F^2 using SHELXL-9733.[9]

All non-hydrogen atoms were refined anisotropically. All hydrogen atoms (except H_1 for compound **2.8**) were placed in idealised positions and refined in riding models with U_{iso} assigned 1.2 or 1.5 times U_{eq} of their parent atoms and the C-H bond distances were constrained from 0.95 to 0.99 Å.

With respect to compound **2.8**, the hydroxyl hydrogen H_1 was located in the difference electron density map and refined independently. Flack x = 0.182(908) by classical fit to all intensities, 0.673(189) from 1821 selected quotients (Parsons' method). The programs X-Seed, Mercury and POV-Ray were used to produce ORTEP images of compounds **2.8, 3.1** and **3.4**.[8] Selected crystal data and structure refinement properties are provided in Table 5.1 and 5.2.

Table 5.1. *Selected crystal data and structural refinement properties for the ligand* ***2.8.***

	2.8
Empirical Formula	$C_{22}H_{19}NO_4$
Formula weight / g.mol^{-1}	361.38
Crystal system	Orthorhombic
Space group	*Pna*2$_1$
Crystal colour and shape	Colourless block
Crystal size	0.48 x 0.52 x 0.65
a / Å	6.0825(9)
b / Å	7.0656(11)
c / Å	40.788(6)
α / °	90
β / °	90
γ / °	90
V / Å^3	1752.93
Z, Z’	Z: 4 Z’: 0
T / K	173(2)
D_c / g.cm^{-1}	1.369
μ / mm^{-1}	0.095
Reflections used [I> 2s(I)]	4250
R_{int}	36694, 4250, 0.027
Final R indices [I > 2s(I)]	4045
R indices (all data)	0.0350
Goodness-of-fit	1.042
Max, Min Δρ/e Λ^{-3}	-0.20, 0.24

Table 5.2. *Selected crystal data and structural refinement properties for complexes* ***3.1,*** ***3.4*** *and* ***3.7.***

	3.1	**3.4**	**3.7**
Empirical Formula	$C_{30}H_{30}NO_4Rh$	$C_{24}H_{18}NO_6Rh$	$C_{35}H_{28}ClNO_4PRh$
Formula weight / g.mol^{-1}	571.48	519.30	695.91
Crystal system	Monoclinic	Monoclinic	Monoclinic
Space group	$P2_1/c$	$P2_1/c$	$P2_1/n$
Crystal colour and shape	Yellow block	Red block	Red block
Crystal size	0.18 x 0.19 x 0.21	0.09 x 0.14 x 0.19	0.03 x 0.07 x 0.12
a / Å	11.1388(15)	17.7573(17)	13.5854(8)
b / Å	18.327(2)	10.5493(10)	10.4098(6)
c / Å	12.3562(17)	24.617(2)	21.5335(12)
α / °	90	90	90
β / °	102.026(3)	109.528(2)	100.4050(10)
γ / °	90	90	90
V / Å^3	2467.05	4346.17	2995.22
Z, Z’	Z: 4 Z’: 0	Z: 8 Z’: 0	Z: 4 Z’:0
T / K	173(2)	173(2)	100(2)
D_c / g.cm^{-1}	1.539	1.587	1.543
μ / mm^{-1}	0.730	0.827	0.754
Reflections used [I> 2s(I)]	6182	8892	6109
R_{int}	55561, 6182, 0.084	56349, 8892, 0.051	24389, 6109, 0.047
Final R indices [I > 2s(I)]	5006	6624	4484
R indices (all data)	0.0484	0.0647	0.0607
Goodness-of-fit	1.046	1.023	1.021
Max, Min Δρ/e Λ^{-3}	-0.52, 0.49	-0.74, 1.94	-0.58, 0.53

5.10 General Methods for the Hydroformylation Reaction

The hydroformylation reactions were performed in a 90 mL stainless steel pipe reactor equipped with a Teflon-coated magnetic stirrer bar. The reactor was charged with toluene (5 mL), substrate [1-octene and styrene (7.175 mmol), 7-tetradecene, methyl oleate, triolein, *D*-citronellal and *R*-Limonene (0.574 mmol)], internal standard *n*-decane (1.26 mmol for 1-octene and styrene only) and Rh-metal loading (2.87 x 10^{-3} mmol). The pipe reactor was flushed with nitrogen three times, followed by flushing with syngas (1:1, CO: H_2) three times. The reactor was pressurised to the desired pressure and consequently heated to the desired temperature. Samples were collected at the beginning and at the end of each reaction. All reactions were performed in duplicate and are recorded as an average of two identical experiments.

5.10.1 Product analysis by GC-FID for 1-octene and styrene

The hydroformylation samples for 1-octene and styrene were analysed on a Perkin Elmer Clarus 580 GC equipped with a flame-ionisation detector. The products were confirmed in relation to authentic standards for the hydroformylation products of 1-octene (internal-octenes and isomers of nonanal) and styrene (3-phenylpropanal and 2-phenylpropanal).

5.10.2 Product analysis by ^{1}H NMR spectroscopy for 7-tetradecene, methyl oleate, triolein, D-citronellal and R-Limonene

The hydroformylation samples for 7-tetradecene, methyl oleate, triolein, *D*-citronellal and *R*-Limonene were analysed using ^{1}H NMR spectroscopy. Conversion is referred to as total conversion of olefins (substrate and its isomerised products) to aldehydes exclusively. The normalisation factor (*NF*) was determined in relation to 7-tetradecene, methyl oleate, triolein, *D*-citronellal and *R*-limonene (Table 5.3). The method was obtained from Hapiot and co-workers.[10-12]

Table 5.1. *The calculated normalisation factor for 7-tetradecene, methyl oleate, triolein, D-citronellal and R-Limonene.*

Substrate	Normalisation Factor (NF)
7-Tetradecene	0
Methyl oleate	0
Triolein	1 (glycerol proton)
D-Limonene	1 (internal cyclic olefin)
R-Citronellal	0

For the respective substrates (Table 5.3), the number of initial (DB_i) and final (DB_f) double bonds are:

$DB_i = (A_i - NF)/2$, A_i is the peak integration of the olefinic protons before the reaction

$DB_f = (A_f - NF)/2$, A_f is the peak integration of the olefinic protons after the reaction. At the end of the reaction, the conversion is denoted as:

$$\text{Conversion (\%)} = [(DB_i - DB_f)/DB_i] \times 100 = [(A_i - A_f)/(A_i - NF)] \times 100$$

$$\text{Aldehyde Selectivity (\%)} = P_{major}/(P_{major} + P_{minor1} + P_{minor2} + P_{minor3}) \times 100$$

where P_{major} is the integration for the major aldehyde product and P_{minor} denotes the integration for the minor aldehyde product as elucidated from ^{1}H NMR spectroscopy.

5.11.3 Mercury poisoning studies

The hydroformylation reactions were performed in a 90 mL stainless steel pipe reactor equipped with a Teflon-coated magnetic stirrer bar. The reactor was charged with toluene (5 mL), 1-octene (7.175 mmol), internal standard *n*-decane (1.26 mmol), a drop of mercury and Rh-metal loading (2.87×10^{-3} mmol). The pipe reactor was purged with nitrogen three times, followed by purging with syngas (1:1, CO: H_2) three times. The reactor was pressurised to 30 bar and heated to 75 °C. The experiments were conducted for 4 hours (complex **3.1** and **3.4**) and 8 hours (complex **3.7**).

5.11 References

1. A.-J. Deeming and P. Sharratt, *J. Organomet. Chem.*, 1975, **99**, 447-453.
2. J. Chatt and L. M. Venanzi, *J. Chem. Soc.*, 1957, 4735-4741.
3. N. Zydziak, C. M. Preuss, V. Winkler, M. Bruns, C. Hübner and C. Barner-Kowollik, *Macromol. Rapid Commun.*, 2013, **34**, 672-680.
4. C. J. Hawker, K. L. Wooley and J. M. J. Fréchet, *J. Am. Chem. Soc*, 1993, **115**, 4375-4376.
5. S. A. Elroby, S. Aboud, S. G. Aziz and R. Hilal, *J. Struct. Chem.*, 2015, **56**, 414-427.
6. M. Koprowski, R.-M. Sebastian, V. Maraval, M. Zablocka, V. Cadierno, B. Donnadieu, A. Igau, A. Caminade and J.-P. Majoral, *Organometallics*, 2002, **21**, 4680-4687.
7. T. Schulz, K. Meindl, D. Leusser, D. Stern, J. Graf, C. Michaelsen, M. Ruf, G. M. Sheldrick and D. Stalke, *J. Appl. Crystallogr.*, 2009, **42**, 885-891.
8. L. J. Farrugia, *J. Appl. Crystallogr.*, 2012, **45**, 849-854.
9. G. M. Sheldrick, *Acta Crystallogr., Sect. C: Struct. Chem.*, 2015, **71**, 3-8.
10. T. Vanbesien, E. Monflier and F. Hapiot, *Green Chem.*, 2017, **19**, 1940-1948.
11. T. Vanbésien, A. Sayede, E. Monflier and F. Hapiot, *Catal. Sci. Technol.*, 2016, **6**, 3064-3073.
12. T. Vanbesien, E. Monflier and F. Hapiot, *Green Chem.*, 2016, **18**, 6687-6694.

Chapter 6

Conclusion and Future Outlook

6.1 Overall Summary and Conclusions

The primary objectives of this study were to synthesize a series of Fréchet metallodendrons with Schiff-base rhodium(I) complexes at the focal point and characterise these using spectroscopic and analytical techniques, which include NMR spectroscopy (^{1}H, ^{13}C{^{1}H}, ^{31}P{^{1}H}, COSY, HSQC and HMBC), IR spectroscopy, elemental analysis and mass spectrometry (EI, ESI, HR-ESI and MALDI-TOF). The catalyst precursors were evaluated in the hydroformylation of various olefins. To the best of our knowledge the synthesis, characterisation and hydroformylation evaluation of these Schiff-base Rh(I) dendron complexes have not been reported in literature.

A series of Fréchet dendrons (**2.1 – 2.5**) were prepared by template procedures. The dendrons were isolated in high yields and characterised accordingly. The *N,O*-salicylaldimine (**2.6**) and *N,P*-iminophosphine (**2.7**) ligands were prepared by Schiff-base condensation reactions and were isolated in high yields. The respective *N,O*-salicylaldimine and *N,P*-iminophosphine Schiff-bases were immobilised to the appropriate Fréchet dendron (**2.1, 2.3** or **2.5**) to yield a series of Fréchet dendrons with Schiff-bases at the focal point (**2.8 – 2.13**). The Williamson-ether synthesis using the *N,O*-salicylaldimine ligands (**2.8, 2.10** and **2.12**) display 100% regioselectivity, this was confirmed using single-crystal X-ray diffraction for compound **2.8** in the solid state. These ligands (**2.8 – 2.13**) are new and have been fully characterised using various analytical and spectroscopic techniques.

The *N,O*-salicylaldimine ligands (**2.8, 2.10 and 2.12**) were complexed using [Rh(μ-Cl)COD]$_2$ *via* a bridge splitting reaction to afford the neutral PGM complexes **3.1 – 3.3**. The spectroscopic and analytical data revealed the bidentate (*N,O*) co-ordination mode of the metal to the

ligand. The subsequent reaction of complexes **3.1 – 3.3** with carbon monoxide *via* a COD displacement reaction afforded a series of dicarbonyl Rh(I) dendrons (**3.4 – 3.6**). Similarly, the *N,P*-iminophosphine ligands (**2.9, 2.11** and **2.13**) were complexed using $[Rh(\mu\text{-}Cl)(CO)_2]_2$ *via* a bridge splitting reaction to afford complexes **3.7 – 3.9**. The complexes are new and were fully characterised using spectroscopic and analytical techniques. Single crystal XRD was used to confirm the mode of coordination and molecular structures for complexes **3.1**, **3.4** and **3.7** in the solid state.

The catalyst precursors **3.1 – 3.9** were active in the hydroformylation of 1-octene. Complex **3.4** was selected as the model catalyst for which the conditions of temperature and pressure were optimised. The catalyst precursor **3.4** was evaluated at the optimised conditions, 75 °C, 30 bar and 4 hours with a catalyst to substrate ratio of 1:2500. The precursor **3.4** was assessed against various substrates, namely 1-octene, styrene, 7-tetradecene, methyl oleate, triolein, *D*-limonene and *R*-citronellal. Generally, the catalyst precursor **3.4** displays excellent conversion and moderate selectivity for 1-octene and styrene. The conversion for the internal olefins, namely (*E*)-7-tetradecene, methyl oleate (*cis*) and triolein (*cis*) were promising with conversions ranging from 51 – 77%. The regioselectivity for these substrates were between 85 – 98%, more importantly no hydrogenation products were observed, which shows potential for tandem catalysis. The catalyst precursor **3.4** was active in the hydroformylation of *D*-limonene and *R*-citronellal. Excellent conversion and regioselectivity was observed for *D*-Limonene and no hydroformylation was observed for the cyclic olefin, which displays excellent regioselectivity for the catalyst.

The catalyst precursors **3.1 – 3.6** display excellent conversion and chemoselectivity as well as moderate regioselectivity in the hydroformylation of 1-octene. In contrast, the precursors **3.7 – 3.9** display low conversion, good chemoselectivity and good regioselectivity. A slight increase in conversion and chemoselectivity was observed when comparing the Rh(I) COD complexes (**3.1 – 3.3**) to the Rh(I) dicarbonyl complexes (**3.4 – 3.6**). This was expected as the COD ancillary ligand is displaced under hydroformylation conditions. Thus by forming the dicarbonyl species, this process is absent and results in a shorter time to form the active catalyst for complexes **3.4 – 3.6**. The *N,P*-iminophosphine catalysts (**3.7 – 3.9**) displays higher regioselectivity than the *N,O*-salicylaldimine counterpart. This is due to the bulky phosphine

ligand which imparts steric crowding around the metal centre. A general trend across the dendron series (**3.1 – 3.3, 3.4 – 3.6, 3.7 – 3.9**) displays an increase in conversion and chemoselectivity for larger generations, which is potentially due to the bulkier nature of the larger dendron which limits the isomerisation from terminal to internal alkenes. Mercury drop tests were performed for catalysts **3.1, 3.4** and **3.7**, notably a significant drop in conversion was observed, which confirms that the hydroformylation of 1-octene for complexes **3.1, 3.4** and **3.7** is a combination of homogeneous catalysis and catalysis mediated by Rh nanoparticles suspended in solution.

6.2 Future Outlook

6.2.1 Investigating Water-Soluble Fréchet Dendrons.

This study has shown the great scope of Fréchet dendrons applied in the hydroformylation experiments. The improvement towards recyclable catalysts may be possible by the conversion of the methyl-ester terminated Fréchet dendrons to carboxylate terminated Fréchet dendrons. This could improve the aqueous solubility of the complexes, which will allow for testing and recycling of the catalysts under aqueous biphasic conditions (Figure 6.1). This was attempted for the *N,O*-salicylaldimine Fréchet dendron series and the G_0 precursor has been isolated and evaluated as an aqueous biphasic hydroformylation precursor. The compound displays limited aqueous solubility. This was corroborated by the significant drop in activity (51%) for this catalyst upon recycling. One method to inhibit leaching is to add more water-soluble groups on the dendritic scaffold. This was attempted for larger generations (G_1 and G_2), however no product could be isolated. Further studies and troubleshooting is required to optimise this reaction.

6.2.2 Incorporation of bulky groups close to the metal centre.

The experiments in this study have shown that the presence of bulky phenyl groups close to metal centre is essential for high *n:iso* ratios. As reported by Smith and co-workers, the incorporation of bulky tertiary-butyl groups results in an increased nonanal formation.[1, 2] The bulky substituent can be altered to influence the bite angle of the ligands, which could potentially result in higher linear aldehyde formation (Figure 6.1).

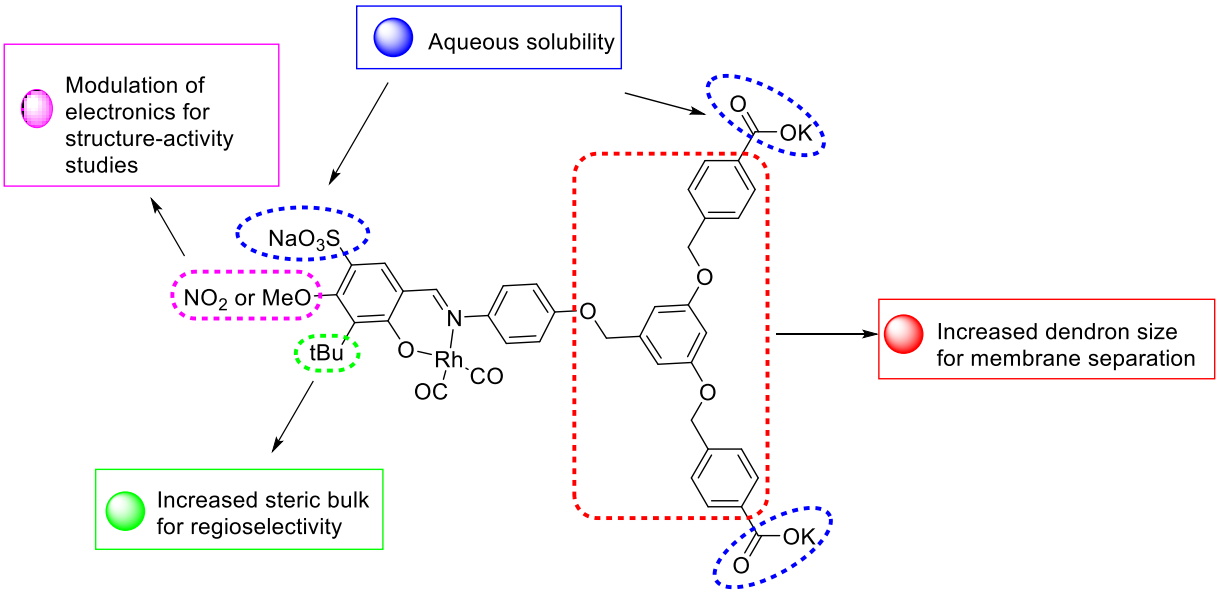

Figure 6.1. *The proposed hydroformylation precursor for modification towards the improvement of these catalysts.*

6.2.3 Investigating higher dendron generations for membrane technology.

The Fréchet dendrons displayed excellent stability in this study, hence higher generations could be constructed (G_3, G_4, and G_5) with insight into separating these homogenous catalyst precursors using membrane technology (Figure 6.1).[3] Various dendritic skeletons can be tested to observe whether these significantly modulate the catalytic activity. Furthermore the introduction of various functional groups on the dendritic surface can allow for metallodendrons with new properties.

6.2.4 Metallodendrimers immobilised on cyclodextrin

An alternative means to introduce aqueous solubility is to immobilise these dendrons with cyclodextrin. There are various reported methods for this immobilisation; these include covalent linking, encapsulation and supramolecular assemblies.[4-10] The use of the covalent method could potentially be the most promising, as the cyclodextrin moiety may increase aqueous solubility, and act as a molecular host for the encapsulation of long-chain olefins in aqueous media. This could combat the challenge of mass transfer limitations encountered in the aqueous hydroformylation of long-chain olefins.

6.2.5 Tandem catalytic processes.

The hydroformylation results of various olefins are discussed in Chapter 4 was extremely promising. Excellent chemoselectivity was observed and this is particularly interesting for tandem catalytic processes. Selected examples include hydroamination, hydroaminomethylation (HAM) and tandem hydroformylation-hydrogenation reactions.[11-13] The HAM of methyl oleate could lead to polymers,[11, 13] the hydroformylation of citronellal in ethanol/triethyl orthoformate could lead to the formation of acetals,[14] HAM of triolein could lead to biodiesel with biocidal properties and the HAM of 7-tetradecene may result in a new class of Guerbet-type surfactants.[12, 15, 16] We have already performed preliminary tests (HAM) for triolein and methyl oleate and the results of extremely promising. We are currently looking at expanding the experiments by focusing on the effects of ligand electronics and stability studies similar complexes reported in this study.

6.3 References

1. L. C. Matsinha, S. F. Mapolie and G. S. Smith, *Dalton Trans.*, 2015, **44**, 1240-1248.
2. E. B. Hager, B. C. Makhubela and G. S. Smith, *Dalton Trans.*, 2012, **41**, 13927-13935.
3. H. P. Dijkstra, G. P. M. van Klink and G. van Koten, *Acc. Chem. Res.*, 2002, **35**, 798-810.
4. M. Elard, J. Denis, M. Ferreira, H. Bricout, D. Landy, S. Tilloy and E. Monflier, *Catal. Today*, 2015, **247**, 47-54.
5. J. Li, Z. Zhou, L. Ma, G. Chen and Q. Li, *Macromolecules*, 2014, **47**, 5739-5748.
6. F. X. Legrand, N. Six, C. Slomianny, H. Bricout, S. Tilloy and E. Monflier, *Adv. Synth. Catal.*, 2011, **353**, 1325-1334.
7. H. Bricout, F. Hapiot, A. Ponchel, S. Tilloy and E. Monflier, *Sustainability*, 2009, **1**, 924-945.
8. M. Mourer, F. Hapiot, E. Monflier and S. Menuel, *Tetrahedron*, 2008, **64**, 7159-7163.
9. F. Hapiot, S. Tilloy and E. Monflier, *Chem. Rev*, 2006, **106**, 767-781.
10. A. R. Khan, P. Forgo, K. J. Stine and V. T. D'Souza, *Chem. Rev*, 1998, **98**, 1977-1996.
11. A. J. Vorholt, S. Immohr, K. A. Ostrowski, S. Fuchs and A. Behr, *Eur. J. Lipid Sci. Technol.*, 2017, **119**, 1600211-n/a.
12. T. Vanbesien, E. Monflier and F. Hapiot, *Green Chem.*, 2017, **19**, 1940-1948.

13. A. Behr, T. Seidensticker and A. J. Vorholt, *Eur. J. Lipid Sci. Technol.*, 2014, **116**, 477-485.
14. H. Mimoun, *Chimia*, 1996, **50**, 620-625.
15. T. Vanbésien, A. Sayede, E. Monflier and F. Hapiot, *Catal. Sci. Technol.*, 2016, **6**, 3064-3073.
16. T. Vanbésien, E. Monflier and F. Hapiot, *Eur. J. Lipid Sci. Technol.*, 2016, **118**, 26-35.